Signal Processing
in
Local Sensor Validation

Sheung Kai Yung

Exeter College, Oxford

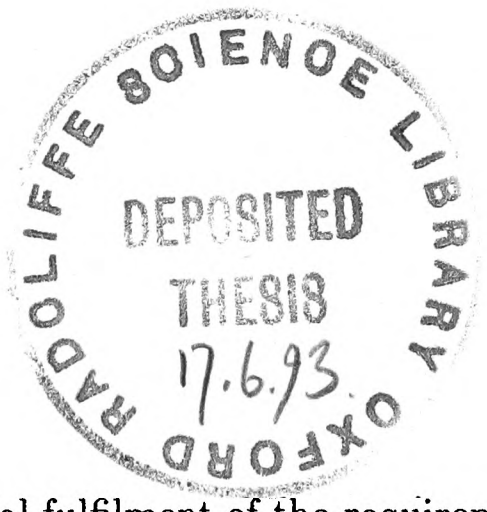

Submitted in partial fulfilment of the requirements for the degree of
Doctor of Philosophy at the University of Oxford.

Michaelmas 1992

Signal Processing in Local Sensor Validation

Sheung Kai Yung
Exeter College, Oxford

Submitted in partial fulfilment of the requirements for the degree of
Doctor of Philosophy at the University of Oxford.

Michaelmas 1992

Abstract

Sensor integrity plays a crucial role in automatic control and system monitoring, both in achieving performance and guaranteeing safety. Conventional approaches in sensor failure detection demand precise process models and abundant central computing power. This thesis describes the development and the evaluation of a novel local sensor validation scheme which is independent of the underlying process and is applicable to a wide variety of sensors.

A signal-based in-situ sensor validation scheme is proposed. Typical sensor failures are classified according to their signal patterns. To avoid the ambiguity between genuine failures and legitimate measurand variations, a pair of decomposition filters are designed to partition the sensor output; and attention is focused on characteristics beyond the measurement signal bandwidth, which is the only essential process-related variable required. In addition, the application of decimating filters is explored, both as a relief to the analog anti-aliasing filter and as an enhancement in signal discretization. An expression is derived relating the oversampling rate and the attainable improvement in signal resolution.

Based on a period of failure-free observation, a whitening filter is identified by modelling the decomposed sensor signal as a stochastic time-series. Significant progress is achieved by a deliberate injection of bandlimited random noise to ensure signal stationarity and to avoid inadmissible leakage of measurement signal into the innovation sequence.

The adopted failure detection strategy is primarily innovation-based. Pertinent sensor signal information is extracted recursively by a collection of efficient and robust signal processing algorithms. Its validity is continuously monitored by statistical tests on which a series of precursory failure alarms are formulated. Any aberration detected is then diagnosed under the supervision of a simple rule-based system.

The practicality, efficacy and flexibility of the proposed scheme are successfully demonstrated by a bench-top thermocouple experiment and extensive synthetic simulations.

To Joyce,

my mother and my father

Acknowledgements

I would like to thank my supervisor, Professor D. W. Clarke, for his guidance and advice throughout the course of this research.

The fruitful and enlightening discussion with many colleagues at Oxford has contributed a lot to this thesis. I am particularly obliged to Coorous Mohtadi-Haghighi, Terence Tsang, Leung Bun Au, Dario Boriani, Bernard Robinson, Dan McMichael, Da Wei Gu, Chris Hinton, Grevin Williams, Kouk-Hun Kim, David Peel and Yousef Al-Assaf.

I am also deeply indebted to Schlumberger Cambridge Research Limited for providing me not only a stimulating and an enjoyable working environment, but also all the essential facilities to complete this thesis. In particular, my sincere thanks are due to Tony Booer, Mike Sheppard, Bertrand Peltier and Richard Meehan for their kind understanding and continuous encouragement.

This research is generously funded by the Croucher Foundation, to whom I am especially grateful. In addition, I would like to take this opportunity to thank the Jardine Foundation for the financial support of my earlier undergraduate studies.

Over the years, I owe so much to my parents. Without their perseverance and many sacrifices, I would not have led my life to the full. I am also truly thankful to Anne and Patrick Lee, Shirley and David Chan and Edwin Yung for their patience and moral support.

Lastly, but most importantly, I would like to express my whole-hearted gratitude to Joyce, who has brought so much happiness into my life. Her ceaseless inspiration, consolation and care are my vital source of support during the production of this thesis.

Contents

List of Figures

List of Tables

List of Assumptions

List of Properties

List of Guidelines

Chapter 1

Introduction

Rapid advances in measurement science not only introduce innovative sensing technology, but also offer low-cost, rugged and reliable sensors compatible with industrial environments [Jordan, 1985]. Sensors are gaining ever-increasing significance in all modern industries [Payne, 1983] and play a crucial role in acquiring prerequisite information for supervision, control, optimization and interpretation. In a typical process plant, instrumentation can account for up to 40% of the capital cost [Barney, 1985]. Representative measurements include temperature, pressure, flow, motion, force, torque, level and chemical properties [Doebelin, 1983; Mylroi and Calvert, 1984; Parr, 1986; Sydenham, 1983].

The technological drive towards the 'manless plant' and high energy-intensive processes demands greater intelligence, availability and reliability of instrumentation. The degree of damage incurred by the loss of a sensor can be substantial, varying according to its function: from the basic cost of maintenance and replacement to a degraded process performance and inferior product quality. In critical situations, a sensor failure may lead to a complete plant shutdown or even human injuries and fatalities. Moreover, health and safety legislation on company liability requires greater assurance that failures can be quickly detected and isolated before endangering the environment and human life. It is therefore both economical and essential to maintain the precision and credibility of the sensor outputs.

Traditionally, the conditions of the instruments are monitored by skillful operators, routinely checking analog dials, digital readings, graphical displays and chart recorders. However, this conservative approach denies the operators the opportunity to focus their attention and expertise on guaranteeing process stability and maximizing production efficiency. The mundane procedure of sensor monitoring inevitably leads to human errors [Lees, 1983]. Furthermore, in the current trend of distributed instrumentation [Brignell,

1986] where hundreds and thousands of sensors are scattered in a vast geographical area, the burden on the operators becomes extremely onerous, if not unmanageable. All these call for a versatile automatic sensor validation scheme which will safeguard the integrity of the measurements.

1.1 Sensor validation

A sensor validation scheme should accommodate a broad spectrum of sensor failures. Primarily, it should fulfil the following two major tasks:

- **Detection** involves discovering any sensor anomaly and malfunction;
- **Diagnosis** seeks to provide a comprehensive analysis of the observed abnormality and is further divided into three functions:
  - *Localization* isolates the faulty sensor in a multi-sensor environment;
  - *Identification* classifies the type and, if feasible, determines the source of the failure;
  - *Estimation* establishes the effects and the severity of the identified aberration.

Expeditious detection and accurate diagnosis of actual, or even impending, sensor failures enable incipient and appropriate remedial actions to be taken, such as rescheduling of maintenance, inhibition of corrupted control loops or initialization of emergency shutdown.

1.2 Review of conventional validation schemes

Fault detection and diagnosis has been a subject of active research in the last two decades, covering not only *sensor*, but also *actuator* and *process* (or *component*) failures. This section highlights the vast variety of developed techniques, which broadly fall into three categories[1]:

- Methods that are independent of the underlying process model (*model-free*),

[1]Or a combination among the three.

- Methods that rely on a quantitative mathematical relationship among the outputs and/or the inputs (*model-based*),
- Methods that utilize a qualitative model in the form of rules and heuristics (*knowledge-based*).

Areas of practical application are summarized in Yung and Clarke [1989, Table 1] and Patton *et al.* [1989, Chapter 1]. In addition, comprehensive overviews of the subject are found in the survey papers by Willsky [1976; 1980], Isermann [1984], Upadhyaya [1985], Basseville [1988], Gertler [1988] and Frank [1990], as well as in the books by Himmelblau [1978], Pau [1981], Basseville and Benveniste [1986] and Patton *et al.* [1989].

1.2.1 Model-free validation

Limit checking is the most widely adopted validation scheme. Individual measurement and its rate of change are directly verified with prescribed thresholds [Isermann, 1984]. The triggering levels are often selected to represent the physical limits imposed by the sensor specification and the process operating conditions.

Fault-tolerance in safety-critical systems, such as aircrafts and nuclear power plants, is typically accomplished by **hardware redundancy**. Identical sensors in at least triplex configuration are compared and failures are isolated by majority voting [Willsky, 1976]. This is sometimes inadmissible when, for example, adding further sensors might exceed the maximum payload of a space mission or weaken the walls of a pressure vessel. Furthermore, hardware redundancy is insensitive to both 'gradual' and 'common-mode' failures.

Over a restricted pass band, redundancy can be generated between dissimilar signals (e.g. between the external input and the measured response). **Band-limiting filters** have been applied to detect failures in a pitch-control system of a fly-by-wire aircraft simulator [Jones and Corbin, 1988] and to monitor hardware and software faults in a control computer [Corbin and Jones, 1990].

Time-series analysis offers a powerful tool in condition monitoring and failure detection. Both non-parametric [Anyakora and Lees, 1973] and parametric [Upadhyaya and Skorska, 1982; Liang and Dornfeld, 1989] techniques have been employed to enhance failure signatures and to monitor parameters such as statistical moments [Martin *et al.*, 1992], zero-crossings [Kitamura and Türkcan, 1985], power spectra [Janik and Isermann,

1990; Mechefske and Mathew, 1992a], higher-order spectra [Sato *et al.*, 1977], cepstra [Lyon, 1987, Chapter 7] and performance-related indices including response times and damping ratios [Upadhyaya and Kerlin, 1978; Upadhyaya and Kitamura, 1981].

Direct mappings between failures modes and available input-output data (or their transforms) can be achieved either by conventional **pattern recognition** algorithms [Mechefske and Mathew, 1992b] or by the more esoteric approach of **artificial neural networks** [Hoskins and Himmelblau, 1988; Naidu *et al.*, 1989; Naidu *et al.*, 1990; Rangwala and Dornfeld, 1990; Hoskins *et al.*, 1991]. Neural network is particularly proficient in accommodating complex nonlinear mappings but its efficacy relies heavily on the representativeness of the calibration data on which the network is trained and the ability of the network to 'generalize' when unforeseen features are encountered.

1.2.2 Model-based validation

Contrary to hardware redundancy, **analytical** (or **functional**) **redundancy** demands an explicit mathematical model of the process which encapsulates the inherent consistency, both static and dynamic, among process inputs and outputs [Chow and Willsky, 1984]. The validation procedure is generally carried out in the central computer where input/output data are readily accessible and is composed of three main steps:

- **Process modelling** in either a transfer function or a state-space framework;
- **Residual generation** to exhibit failure signatures;
- **Hypothesis testing** to detect and isolate anomalies.

Popular validation techniques based on analytical redundancy will be reviewed and references on parameter sensitivity and robustness will be provided.

Parity space

A systematic check on the consistency of redundant information is attained by an orthogonal transformation into the parity space [Ray *et al.*, 1983]. Polenta *et al.* [1988] implemented this residual generation concept in a real-time sensor validation scheme for a research nuclear reactor. Chow and Willsky [1984] further extended the idea to a generalized parity space to cater for both algebraic (*direct redundancy*) and dynamic (*temporal*

redundancy) relationships between inputs and outputs. Based on the process incidence matrix, Gertler and co-workers [Gertler and Luo, 1989; Gertler *et al.*, 1990] modified the parity functions by additional linear transformations to guarantee *isolable* failures.

Failure sensitive filters

The failure sensitive filter pioneered by Beard [1971] and Jones [1973] is primarily a full-order state estimator with the filter gain specially designed whereby the output residual subject to a particular failure is constrained to a fixed direction or a fixed plane. The Beard-Jones filter is only applicable to time-invariant systems and is suboptimal as a state estimator. Recent advances in the design and analysis of failure sensitive filters are available from a geometric perspective [Massoumnia, 1986; Massoumnia *et al.*, 1989] and as an eigenstructure assignment [White and Speyer, 1987]. Min [1989a] utilized a pair of failure sensitive filters to detect and isolate RPM sensor biases in internal combustion engines.

Dedicated observers

Optimal state observers and Kalman filters generate state or output estimation errors as diagnostic residuals. Clark and co-workers introduced the *dedicated observer scheme* with a bank of Luenberger observers [Clark *et al.*, 1975; Clark, 1978a] and the *simplified observer scheme* with a single Luenberger observer in a deterministic case [Clark, 1978b] or a single Kalman filter in a stochastic environment [Clark and Setzer, 1980]. Equipped with a design methodology for *unknown input observers* and an insight into the system structure, Janßen and Frank [1984] established a unified *hierarchical observer scheme* for component failure detection in large complex systems. A more thorough theoretical background was summarized in Frank [1990]. Furthermore, direct failure detection and estimation can be achieved by an explicit inclusion of the failure parameters into the system states. Bellingham and Lees [1977b] presented a method combining state augmentation and model partitioning to detect state bias errors.

Multiple model hypothesis

Failure localization can be facilitated by a parallel bank of filters individually parametrized and optimized for each of the multiple hypothesized failure modes. The filter bank

basically behaves as a simultaneous parameter and state estimator and the hypothesis with the maximum a posteriori probability is nominated as the 'best-fit' model [Willsky, 1980]. Notwithstanding their taxing computational requirements, multiple model techniques have been applied to tube leak detection in a heat exchanger [Vasudeva *et al.*, 1986], sensor validation in a turbine engine [Merrill *et al.*, 1988] and safety monitoring in a chemical reaction [King and Gilles, 1990].

Innovation-based detection

Under the failure-free condition, innovation (output estimation error) generated from an ideal estimator (Luenberger observer, Kalman filter or least squares estimator) driven by the full output vector should be zero-mean and uncorrelated. This provides a foundation for a powerful residual generation scheme which is associated with a number of hypothesis testing procedures:

- **Statistical innovation test**

  Mehra and Peschon [1971] proposed a series of classical statistical tests on the innovation sequence, including a whiteness test, a Gaussian zero-mean test and a chi-squared covariance test. In addition, Halme and Selkäinaho [1984] tackled the dual problem of parameter and state estimation and adopted a Student's t-test and a F-test for a change in mean and a change in variance respectively between two sliding windows. The basic idea was carried through in Bellingham and Lees [1977a] on detecting malfunction in flow loop instrumentation and in Usoro *et al.* [1985] on validating thermocouple outputs in a HVAC[2] system.

- **Generalized Likelihood Ratio** (GLR)

  For each hypothesized failure, the GLR method first computes the maximum likelihood estimates of both the failure magnitude and the failure time from the innovation sequence and then evaluates the log likelihood ratio with respect to a nominal model. Full-blown GLR requires a growing bank of matched filters and the predicted time of failure is, therefore, often constrained within a finite window in practical implementations [Willsky and Jones, 1976; Willsky *et al.*, 1980].

[2]Heating, Ventilation and Air Conditioning.

- **Sequential Probability Ratio Test** (SPRT)
  Much of the computational complexity in GLR lies in the initial maximum likelihood estimations. By specifying the size and the time of failure a priori, SPRT significantly improves the algorithmic efficiency and, under the Gaussian assumption, the log likelihood ratio becomes a straightforward cumulative sum [Chien and Adams, 1976; Yoshimura *et al.*, 1979; Segen and Sanderson, 1980]. Deckert *et al.* [1977] utilized a duplex hardware redundancy structure in a F-8 fly-by-wire aircraft to determine the failure time and to initiate a SPRT algorithm for sensor failure isolation. A comparative study of GLR and SPRT was given in Basseville and Benveniste [1983].

Parameter estimation

Apart from the process state variables and the derived innovation sequence, parameters of the mathematical model also inherit potential failure signatures. On-line parameter tracking requires a reliable, possibly variable, forgetting algorithm in order to maintain the adaptivity of the estimator. Most research to date gears towards the *indirect* approach in which the estimated model parameters are first mapped to a set of physical quantities (e.g. mass, friction and resistance) as diagnostic measures [Isermann, 1984]. Moreover, Ono *et al.* [1987] put forward a technique to identify the failure severity by computing the influence matrix of the diagnostics on the model parameters. An extensive collection of both *direct* and *indirect* tests were developed in McMichael [1988] which explored a broad feature space covering system gains, bandwidths, dead times, d.c. offsets and noise variances.

Robustness

A fundamental limitation in model-based failure detection is its dependence on the precise knowledge of the underlying process and the associated noise statistics. Growing awareness on the adverse effects of unmodelled dynamics in practical applications has led to increasing contributions to robust validation techniques in all the aforementioned areas, such as robust parity space [Chow and Willsky, 1984; Gertler and Luo, 1989; Gertler *et al.*, 1990; Wünnenberg and Frank, 1990], robust Beard-Jones detection filters [Min, 1989b], sensitivity discriminating observers [Frank and Keller, 1980; El Madbouly and

Frank, 1983], unknown input observers [Patton *et al.*, 1986; Ge and Fang, 1988; Frank, 1990], robust threshold selection [Kosut and Walker, 1984; Emami-Naeini *et al.*, 1988] and robust parameter estimation [Kwon and Goodwin, 1990; Wahlberg, 1990].

1.2.3 Knowledge-based validation

Knowledge-based methods complement conventional analytical and algorithmic techniques and offer an opportunity to combine numeric and symbolic models for failure detection and, in particular, fault diagnosis. In complex processes such as batch chemical reactions or power generation, fault diagnosis is a knowledge-intensive exercise based primarily on logical judgement rather than numerical computation [Milne, 1987]. Andow [1985] and Palowitch and Kramer [1985] examined the application of an *expert system* to fault diagnosis in a chemical plant, in an attempt to mimic the deductive reasoning of a process operator.

In general, the knowledge-based validation techniques can be divided into two classes: those based on a collection of inference rules and heuristics (*shallow knowledge*) and those built on a structural and functional model of the fundamental behaviour of system components (*deep knowledge*). Fault dictionary [Koscielny, 1986; Himmelblau, 1978, Section 6.2] and fault diagnostic tree [Cohn and Ott, 1971; Himmelblau, 1978, Section 7.2] are two typical shallow knowledge approaches: the former contains a list of causes and effects while the latter depicts the cause-effect relationships as a series of either-or branches. On the other hand, Leary and Gawthrop [1987] provided a systematic approach to failure detection and localization based on a 'deep' model of the process and a constraint suspension method. Both shallow [Chandrasekaran and Punch III, 1988] and deep [Scarl *et al.*, 1987] knowledge-based methods have been applied to sensor validation.

1.3 Motivations of the thesis

Conventional centralized validation techniques suffer from a number of drawbacks:

- Precise mathematical or knowledge-based models of the process as well as well-characterized external disturbances are required [Kerr, 1989]. These may be extraordinarily complicated to construct and may, even then, have gross errors.

- Since the models are 'tailor-made' and the validation algorithms are 'fine-tuned' for each process, a modification of the underlying system or a transfer of the techniques to a new application is extremely expensive and demands an enormous amount of expertise.

- Including the joint problem of detecting process and sensor failures increases the combinatorial dimension and hence the cost. The monitoring process has to be carried out centrally and this competes for computer power with control, scheduling and optimization activities.

These are the main obstructions to their becoming widely accepted in industry.

The new generation of 'smart' sensors and 'intelligent' transmitters exhibits superior performance to conventional 'dumb' instruments. The employment of embedded microprocessors and digital interfaces offers local computing power and incorporates advanced utilities such as signal compensation, self diagnosis and remote reconfiguration [de Sá, 1988; Favennec, 1987; Howell and Hamilton, 1990]. Commercial applications include pressure transmitters [Bradshaw, 1984], diameter gauges [Bhattacharya, 1988] and temperature sensors [Bradshaw, 1989]. In addition, the technological progress and the standardization of digital Fieldbus provide a set of universal protocols and metrics for reliable bi-directional digital communication between local measurement devices and the central supervisory unit [Jordan *et al.*, 1992; Wood, 1988]. This opens the opportunity for *local sensor validation* as a flexible and cost-effective solution.

1.4 Organization of the thesis

The primary aim of this thesis is to design and evaluate a local sensor validation scheme applicable to a wide variety of sensors and processes. Systematic development of the overall methodology as well as the individual algorithms are documented in detail. In addition, extensive guidelines are provided to facilitate the implementation and the commissioning of the validation scheme. An outline of the thesis is summarized as follows:

Chapter 2 explains the fundamental concepts behind local sensor validation. Typical sensor failure modes, characterized by their specific signal patterns, are identified. Their different behaviour under an open and a closed loop environment is studied and related to the system type number and the closed loop bandwidth. The paradox

of the inability to distinguish between sensor failures and legitimate measurand changes within the signal bandwidth is then highlighted in the frequency domain. A decentralized hierarchical structure of the local sensor validation scheme is proposed in which the activities are divided into three stages — commissioning, learning and tracking.

Chapter 3 addresses various problems encountered in the commissioning and the learning stage. A minimal set of underlying assumptions is laid down testifying the flexibility of the algorithm. Measurement signal bandwidth is defined and its estimation discussed. The application of decimating filters is explored, particularly in its resolution enhancement in digital quantization. After being decomposed, the sensor output is fitted to an appropriate stochastic time-series model to sharpen the ensuing detection methods. The utility of dithering, a controlled injection of random signals, in whitening filter design is also investigated.

Chapter 4 describes the failure detection and diagnosis procedures in the tracking stage. A suite of efficient signal processing algorithms is developed to extract pertinent signal properties, including mean, variance, filtered rate of change and measure of bias. Precursory monitoring and detection are achieved by statistical tests on which a series of failure alarm indicators are formulated. Driven by a simple rule-based system, any detected abnormality is subsequently diagnosed and the failure severity estimated.

Chapter 5 examines aspects of implementation, operation and adaptation in the validation scheme. A brief account on an integrated software package is reported. The feasibility of the proposed validation scheme is verified by a bench-top thermocouple experiment. Particular emphasis is on the description of an exemplary operating sequence. Synthetic simulations are also carried out in an attempt to demonstrate the adaptability of the scheme to both nonstationary measurement noises and bandpass measurement signals.

Chapter 6 draws the conclusion on major issues raised and key results arrived in this thesis and recommends potential areas for further research.

A preliminary overview of the research covered in this thesis has been published in Yung and Clarke [1989].

Chapter 2

A Local Sensor Validation Scheme

2.1 Introduction

As the effective operation of a control or monitoring system depends completely upon the data received from the sensors in the system, any failure leading to inaccurate measurement is undesirable and indeed sometimes intolerable. A faulty sensor will lead to non-optimal estimation and control and this in turn might lead to catastrophic results. For example, in critical cases of nuclear reactor monitoring or aerospace control, the consequence may well be enormous human and economic loss. Even in cases of intrinsically safe industrial processes, undetected faulty sensors in the system could possibly lead to temporary shutdown of the plant; loss of profits and waste of manpower inevitably follow.

The conventional centralized approach in sensor failure detection suffers from its dependence on an accurate and detailed mathematical model of the process. It is therefore expensive to install and any slight alteration of the process may demand significant modification. Sensor validation at a local level provides a cost-effective and flexible alternative. By devolving the intensive toil of sensor signal monitoring to a local level, it relieves the central computing power for control and optimization.

With the above in sight, a detailed investigation into the problems of local sensor validation and an attempt to improve the status quo in this field are worth the efforts from both economic and technical points of view. Before a meaningful examination of the problems in this field could be carried out, it is necessary to have a good understanding of the fundamental concepts concerned. This chapter endeavours to provide a sound support and a favourable background on which further detailed analysis could be carried out. Basic concepts in sensor validation are defined and the blueprints of an innovative sensor validation scheme at a local level are set out.

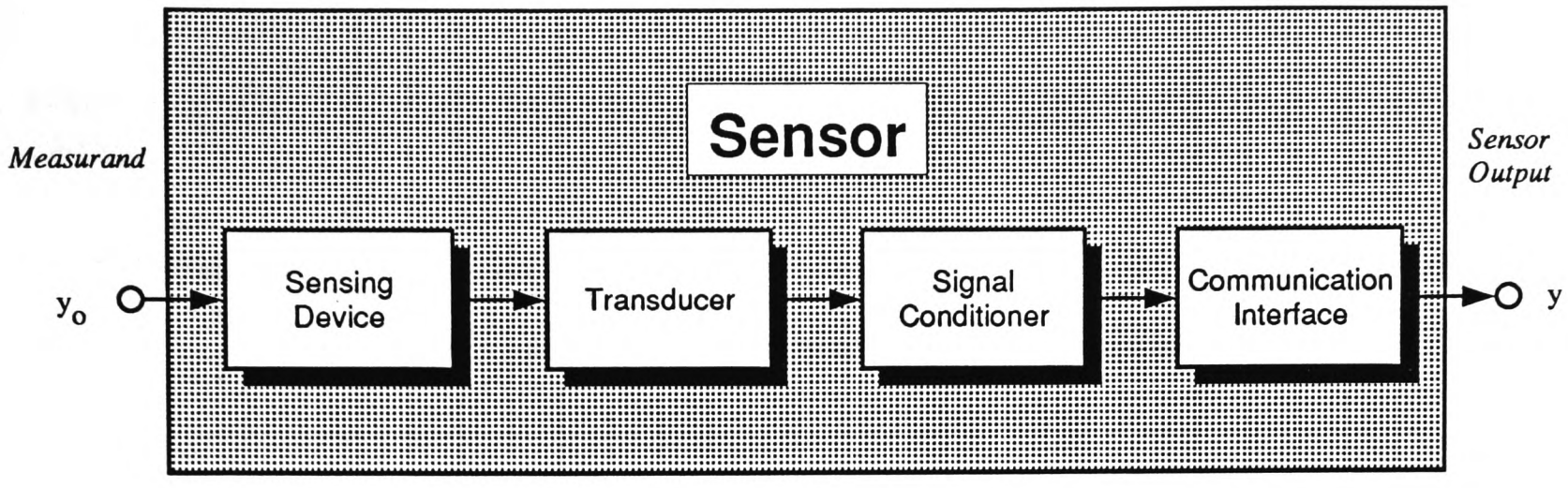

Figure 2.1: A typical sensor system

2.2 Definition of a sensor system

A *sensor* is a device which exploits some physical, chemical or biological phenomena to provide a response to the quantity being measured. The response is often transformed by a *transducer* into a mode (e.g. voltage and current) more convenient for communication, processing and display.

The term *sensor* is used in generality here to represent the *entire* sensor system which comprises of the sensing device, the transducer, the signal conditioner and the necessary communication interface (Figure 2.1). The input to the sensor is the measurand, y_o, which is unknown and the output is the measurement, y, which is usually an electrical signal in an analog form (0 – 10 V or 4 – 20 mA) or in its digital equivalent.

For example, a Type K thermocouple sensor system has the following components:

- The *sensing device* consists of the Chromel / Alumel junction and the thermo-pocket,
- The *transducer* is the Chromel / Alumel cable which converts the temperature at the junction into an electrical voltage difference at the terminal end,
- The *signal conditioner* includes the signal amplifier, the cold-junction compensation and the output linearization,
- The *communication interface* embodies the communication ports and cables, the differential amplifier, the anti-aliasing filter and the analog-to-digital converter.

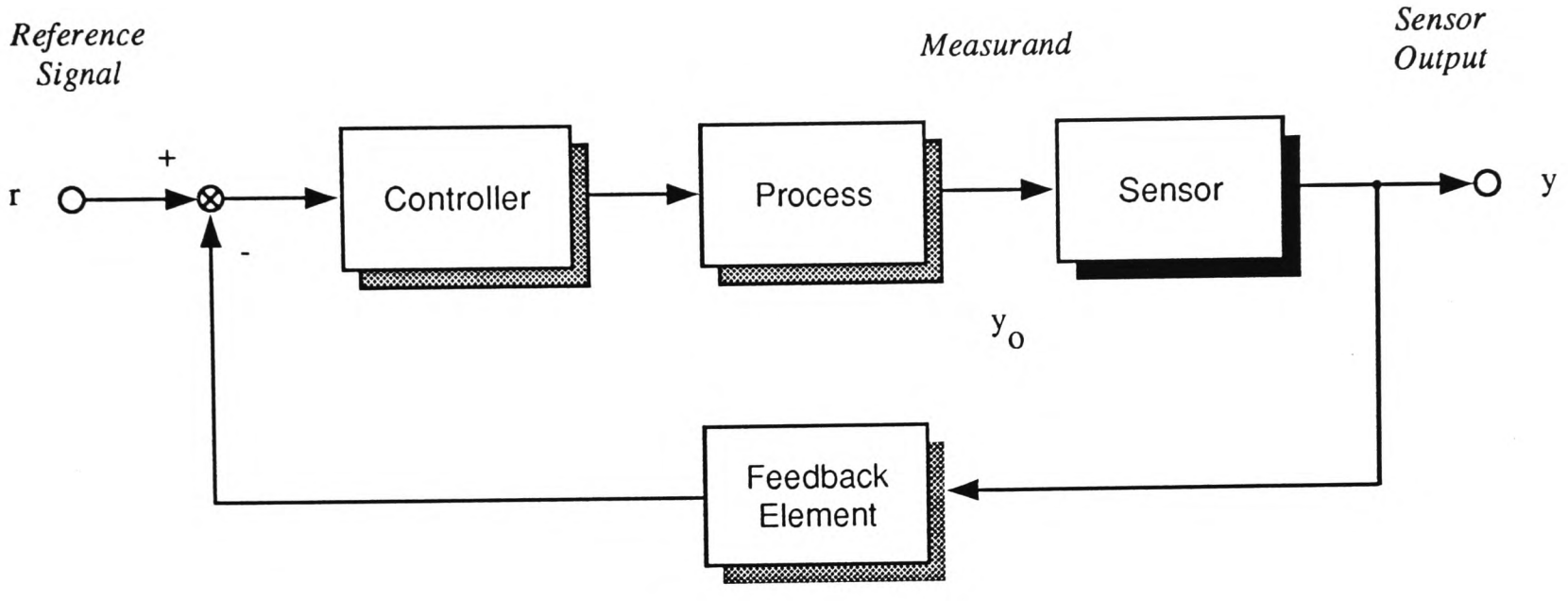

Figure 2.2: A sensor system in a closed loop environment

2.2.1 Sensor systems in open and closed loop environments

A sensor system can be operated either in open loop or closed loop. In an open loop environment, the measurand, y_o, is not affected by the sensor output, y. The sensor system serves primarily as a monitoring instrument. On the other hand, the sensor output in a closed loop environment is fed back to the controller to achieve closed loop regulation on the measurand. A schematic layout of a sensor system operating in closed loop is depicted in Figure 2.2. It should be noted that the measurand in open loop environment may itself be under separate closed loop control. The feedback signal may either be available from another similar instrument or inferred from other physical measurements.

2.3 A model of the sensor output

The development of a model of the sensor output can provide a valuable foundation for any further analysis. While a tailor-made model for a particular sensor and environment has the advantage of precision, it is very much limited in application. In contrast, a general and application-independent model is more versatile and flexible. Its adaptability makes it the most suitable basis for a system non-specific validation scheme.

The sensor output $y(t)$ is composed of two components: the measurement signal $s(t)$

and the measurement noise $n(t)$,

$$y(t) = s(t) + n(t) \tag{2.1}$$

The measurement signal is represented by the output of a 'generalized' process $\mathcal{G}$ driven by arbitrary 'generalized' input $v(t)$,

$$s(t) = \mathcal{G}(v(t)) \tag{2.2}$$

The 'generalized' process incorporates both the dynamics of the process being measured and the sensor itself. It is intentional not to impose any restriction on the linearity and the time-invariant characteristics of the 'generalized' process[1] $\mathcal{G}$. Neither is there any assumption on the stochastic, stationary and ergodic properties of the 'generalized' input signal $v(t)$. The model of the measurement signal $s(t)$ described in Equation 2.2 covers a broad spectrum of applications and can be utilized both in open loop and closed loop environments.

For a *linear*[2] discrete time system,

$$s(t) = \mathcal{G}(q^{-1})\, v(t) \tag{2.3}$$

where $\mathcal{G}(q^{-1})$ is a rational polynomial in the shift operator q^{-1} and $q^{-k}\, v(t) \equiv v(t-k)$. In an open loop environment, $\mathcal{G}(q^{-1})$ represents the process transfer function $G(q^{-1})$ which takes account of the dynamics of the sensor. $v(t)$ is the aggregate input $u(t)$ to the process. This may include the actuator signals and the change in ambient conditions. On the other hand, in a closed loop environment, $\mathcal{G}(q^{-1})$ represents the closed loop transfer function $G_c(q^{-1})$ and $v(t)$ corresponds to the reference signal (or setpoint value) $r(t)$. In summary,

$$\textbf{Open loop} \qquad s(t) = G(q^{-1})\, u(t) \tag{2.4}$$

$$\textbf{Closed loop} \qquad s(t) = G_c(q^{-1})\, r(t) \tag{2.5}$$

Similarly, the measurement noise $n(t)$, which is an unknown stochastic signal, can be described as the output of a 'generalized' noise model $\mathcal{M}$, driven by a white noise process $e(t)$,

$$n(t) = \mathcal{M}(e(t)) \tag{2.6}$$

---

[1] For clarity of explanation and notation, the generalized process $\mathcal{G}$ will often be considered to be a linear or linearized version as in Equation 2.3.

[2] Or a linearized version of a nonlinear process.

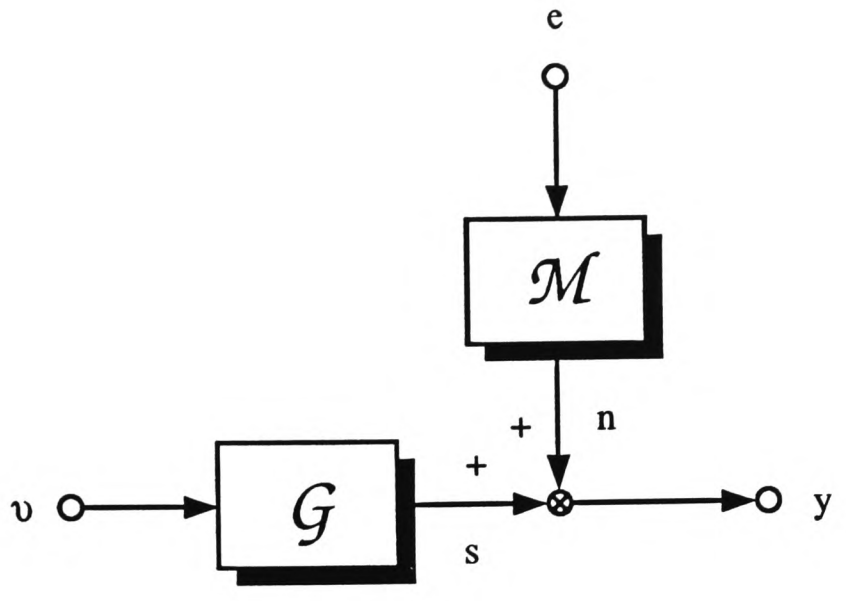

	Open loop	*Closed loop*
$\mathcal{G}$	$G(q^{-1})$	$G_c(q^{-1})$
$\mathcal{M}$	$M(q^{-1})$	$N(q^{-1})$ [a]
$v(t)$	$u(t)$	$r(t)$

[a] As seen at the sensor output, the spectral properties of the measurement noise $n(t)$ will change once feedback is introduced. The relationship between $M(q^{-1})$ and $N(q^{-1})$ will be derived in Section 2.6.1.

Figure 2.3: A model of the sensor output

By the spectral factorization theorem [Åström and Wittenmark, 1984, Section 6.5], if the measurement noise has a rational spectral density function, it can be specified in discrete time by

$$n(t) = M(q^{-1})\, e(t) \tag{2.7}$$

where $M(q^{-1})$ is a rational polynomial in q^{-1}. The overall model of the sensor output is illustrated in Figure 2.3 and can be expressed as

$$y(t) = \mathcal{G}(q^{-1})\, v(t) + M(q^{-1})\, e(t) \tag{2.8}$$

A note on multiple noise sources

Most real processes have more than one noise source acting on the measurement system (e.g. amplifier noise, mechanical vibration and quantization noise). Each can be well represented by a stochastic signal as described in Equation 2.7. The measurement noise can take the form of

$$n(t) = \sum_i M_i(q^{-1})\, e_i(t) \tag{2.9}$$

However, by spectral factorization, all the noise sources can be combined to one single source with equivalent spectral properties. With reference to Equation 2.7 and taking into account that $e_i(t)$ are uncorrelated with variance $\sigma^2_{e_i}$,

$$M(q^{-1})\ M(q)\,\sigma^2_e = \sum_i M_i(q^{-1})\, M_i(q)\,\sigma^2_{e_i} \tag{2.10}$$

where all the zeros and poles of $M(q^{-1})$ are within the unit circle and σ^2_e is the variance of $e(t)$.

2.4 Sensor failure

2.4.1 Definition

Generally speaking, a sensor is declared faulty if the output measurement y gives an incorrect representation of the measurand y_o. However, in practice, it seems vague as to what constitutes a correct or an incorrect representation, especially with the fact that the measurand is unknown. A more specific definition of sensor failure is that the sensor output y exceeds some of the physical limits inherent in the design of the instrument. This is sometimes called a 'hard' failure. Although this definition is commonly adopted, it is very conservative and restrictive and is certainly insufficient for high performance and critical situations.

A more dynamic approach is suggested in Isermann [1984]. A sensor failure is defined as "a non-permitted deviation from the characteristic properties". This includes not only the 'hard' failures but also those 'soft' failures such as an excessive drift as well as an abnormal increase in the output noise level. A code of normal behaviour of the sensor output is required to establish the characteristic properties. This code can either be deduced from the sensor specification and the process information or derived from

the past record of typical sensor behaviour. The problem of forming this code will be addressed in more detail in Chapter 3.

2.4.2 Typical sensor failure modes

Sensor failure can arise from any part of the sensor system. A loose connection in a thermocouple, a blocked orifice plate and a blown-out operational amplifier in a pressure transmitter are all categorized as sensor failures. Tracing down the source of failure cannot be accomplished without a detailed knowledge of all the sensor components and their interactions. Nevertheless, a defective sensor will often exhibit characteristic failure signatures in its output domain. At a local sensor level, it is more productive and efficient for a generic validation scheme to classify sensor failure in terms of the output signal patterns than of the original source of failure.

There is a large variety of measurements carried out in industries: temperature, pressure, flow, motion, level, force, torque, *etc.* Sensor characteristics differ greatly according to their designs and applications. Drawing down a typical set of sensor failure patterns is by no means a trivial task. Basing on Anyakora and Lees [1972] and a collection of sensor failure detection papers, *eight* typical failure modes are considered:

- **Hardover failure** — when the sensor output or its rate of change exceeds some pre-specified thresholds inherent in the design of the instrument and the process being measured.
- **Bias failure** — when there is an abrupt step change in the sensor output (such change takes place much faster than the process allows in its normality).
- **Spike failure** — when an abrupt but transient jump occurs in the sensor output which is much quicker than the process permits.
- **Stuck failure** — when the sensor output holds on to a constant level.
- **Erratic failure** — when there is a significant and persisting change in the measurement noise level.
- **Cyclic failure** — when a sinusoidal or a narrow-band signal appears unexpectedly in the sensor output.

- **Drift failure** — when the sensor output increases or decreases continuously and the change is so slow and gradual that makes it distinguishable from a bias.

- **Nonlinear failure** – when the sensor output exhibits saturation, dead-band or hysteresis behaviour.

Graphical plots of the eight typical failure modes are depicted in Figure 2.4. It has to be noted that the above is by no means an exhaustive list of sensor failure patterns. However, it should have covered most of the cases. The validation scheme presented herein is designed to accommodate additional failure modes without excessive modifications. Furthermore, not every mode of failure will occur in every sensor. For example, a *stuck* failure most commonly occurs in mechanical systems such as a LVDT[3] and a variable-area flowmeter but rarely would it appear in a thermocouple[4]. This should not pose a serious problem to the validation scheme. If it is known *a priori* that some failure modes will be absent in a particular sensor, the validation scheme can either be configured to veto any detection of those failure modes or to disable the relevant detection procedures at onset.

2.5 Sensor failures in an open loop environment

In an open loop environment, the sensor output is connected directly to an acquisition unit, a display module or an alarm system. It is used basically as a monitoring instrument and will not affect the variable it measures. Consequentially, in case of a failure, any of the eight typical failure modes mentioned in Section 2.4.2 will be revealed directly in the sensor output. Except for the hardover failure[5], the other seven failure modes can be divided into *two* main categories:

- Additive failures

- Non-additive failures

[3]LVDT stands for Linear Variable Differential Transformer.

[4]Failure caused by an open circuit, a closed circuit or a defective operational amplifier usually triggers a pull-high or pull-low signal and is considered as a *hardover* or a *bias* failure.

[5]Strictly speaking, hardover failure is not characterized by a particular signal pattern. It concerns primarily with some pre-specified thresholds being exceeded and does not fall into either of the two categories.

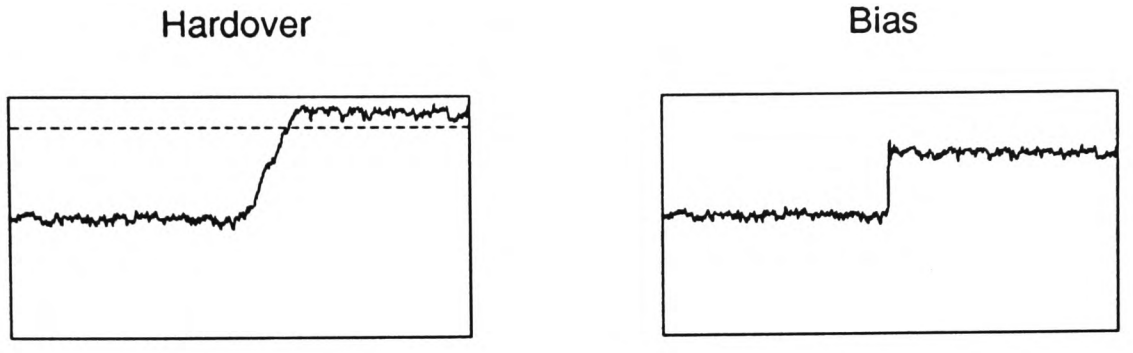

Figure 2.4: Typical sensor failure modes

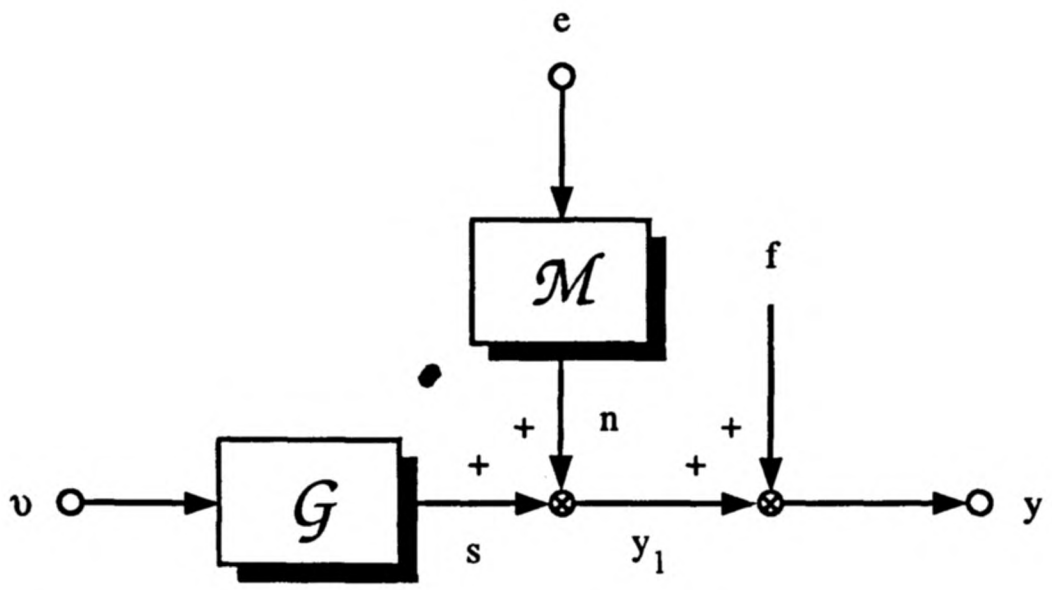

Figure 2.5: An additive sensor failure

2.5.1 Additive failures

In this category, the anomalous sensor output can be expressed as the sum of the legitimate sensor output $y_l(t)$ and a failure signal $f(t)$ as shown in Figure 2.5,

$$y(t) = y_l(t) + f(t) \tag{2.11}$$

The five types of sensor failure modes can be described as:

Bias	$f(t) = \Theta(q^{-1})\,\vartheta_1\,\alpha(t')$	(2.12)
Spike	$f(t) = \Theta(q^{-1})\,\vartheta_1\,\delta(t')$	(2.13)
Erratic	$f(t) = \Theta(q^{-1})\,\vartheta_1\,\bar{e}(t)\,\alpha(t')$	(2.14)
Cyclic	$f(t) = \vartheta_1 \sin(2\pi\vartheta_2(t - t_f) + \vartheta_3)\,\alpha(t')$	(2.15)
Drift[6]	$f(t) = \vartheta_1(t - t_f)\,\alpha(t')$	(2.16)

[6] A *linear* drift is considered here.

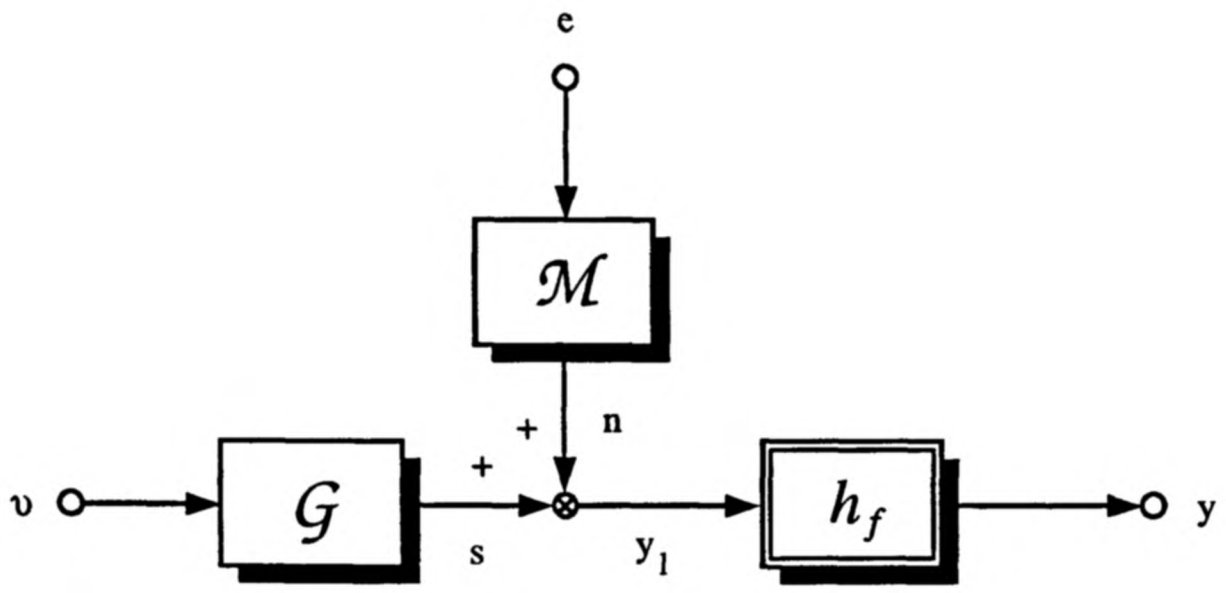

Figure 2.6: A non-additive sensor failure

where $\Theta(q^{-1})$ is the failure signature filter. It is device and failure specific and is usually unknown *a priori*.

ϑ_i is the failure size parameter.

t_f is the time of failure and $t' = t - t_f$.

$\bar{e}(t)$ is a white noise process with unit variance.

$\alpha(t')$ is the Heaviside step function and $\alpha(t') = \begin{cases} 1 & t' \geq 0 \\ 0 & t' < 0 \end{cases}$.

$\delta(t')$ is the Dirac delta function and $\delta(t') = \begin{cases} 1 & t' = 0 \\ 0 & t' \neq 0 \end{cases}$.

2.5.2 Non-additive failures

Not all sensor failures are additive in nature. In particular, the stuck or the nonlinear failure is better presented by a nonlinear function h_f operating on the legitimate sensor output $y_l(t)$ as

$$y(t) = h_f\left(y_l(t)\right) \tag{2.17}$$

This is summarized in Figure 2.6. The two failure modes can be shown as:

Stuck

$$h_f(y_l(t)) = y_{\text{stuck}} \tag{2.18}$$

Nonlinear

Saturation

$$h_f(y_l(t)) = \begin{cases} \underline{y}_{\text{sat}} & y_l < \underline{y}_{\text{sat}} \\ y_l(t) & \underline{y}_{\text{sat}} \leq y_l(t) \leq \bar{y}_{\text{sat}} \\ \bar{y}_{\text{sat}} & y_l(t) > \bar{y}_{\text{sat}} \end{cases} \tag{2.19}$$

Dead-band

$$h_f(y_l(t)) = \begin{cases} y_l(t) - \underline{y}_{\text{db}} & y_l < \underline{y}_{\text{db}} \\ 0 & \underline{y}_{\text{db}} \leq y_l(t) \leq \bar{y}_{\text{db}} \\ y_l(t) - \bar{y}_{\text{db}} & y_l(t) > \bar{y}_{\text{db}} \end{cases} \tag{2.20}$$

where y_{stuck} is a constant.

$\underline{y}_{\text{sat}}$ and $\bar{y}_{\text{sat}}$ are the lower and upper saturation limits respectively.

$\underline{y}_{\text{db}}$ and $\bar{y}_{\text{db}}$ are the lower and upper extremities of the dead-band respectively.

2.6 Sensor failures in a closed loop environment

In contrast to that in an open loop environment, the controller in closed loop regulates the sensor output and tries to keep the output to the setpoint value. It does so in disregard of whether the sensor output accurately represents the measurand. Thus it is not surprising that when a sensor fails, the illegitimate sensor output (i.e. an inaccurate representation of the measurand) will in some way be 'corrected' by the feedback law. As a result, there will not be as apparent a symptom of sensor failure as found in the open loop. This is not to say that sensor failure is not detectable in a closed loop environment but the signal characteristics at the sensor output end which manifest such failure will take a different form. It must be further noted that all the failures possible in an open loop can also be found in a closed loop environment and as in open loop, the seven failure modes[7] could be grouped under additive (Section 2.5.1) and non-additive (Section 2.5.2) failures.

[7]The eight typical failure modes presented in 2.4.2 less the hardover failure.

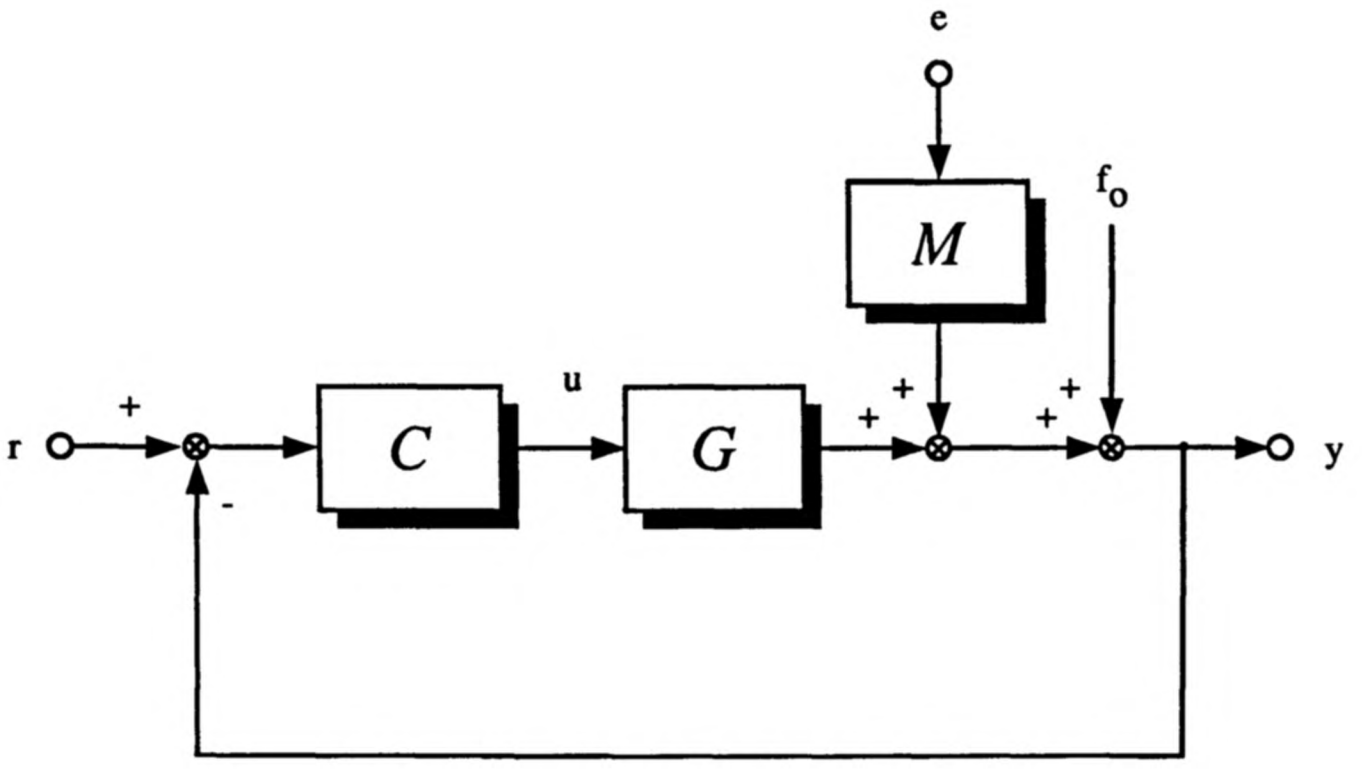

Figure 2.7: Additive sensor failure in a closed loop environment

2.6.1 Analysis of additive failures in a closed loop environment

The differences in signal patterns of the additive failures in the two environments will be highlighted by the investigation of a linear sensor system operating in closed loop (Figure 2.7). The arguments of the transfer functions and those of the signals are intentionally omitted. In this way, the results from this analysis can be applied in both the continuous and discrete time domains.

With reference to Figure 2.7, C is the controller transfer function, r is the reference signal, u is the control signal, and G, M and e are defined as in the open loop case (Equations 2.4 and 2.7). The additive failure described in Equations 2.12 to 2.16 is in this section termed f_o. This is to distinguish it from the actual failure pattern f appearing at the sensor output. The sensor output y is given by

$$y = G\,u + M\,e + f_o \tag{2.21}$$

and the feedback control law is defined as

$$u = C\,(r - y) \tag{2.22}$$

It follows that

$$y = \underbrace{G_c\,r}_{s} + \underbrace{N\,e}_{n} + \underbrace{F\,f_o}_{f} \tag{2.23}$$

where

$$G_c = \frac{\mathcal{C}G}{1+\mathcal{C}G} \tag{2.24}$$

$$F = \frac{1}{1+\mathcal{C}G} \tag{2.25}$$

$$N = \frac{M}{1+\mathcal{C}G} = MF \tag{2.26}$$

G_c is the *closed loop transfer function* while F and N are named the *failure shaping function*[8] and the *noise shaping function* respectively.

The failure signal characteristics in a closed loop environment depend both on the failure shaping function F and the existing additive failure f_o,

$$f = F f_o \tag{2.27}$$

The failure patterns will be transformed by the feedback control action which are summarized in Property 2.1 and 2.2.

Spike, bias and drift failures

Property 2.1 *In a stable linear closed loop environment, the signal pattern of a spike, bias or drift failure depends on the system type number:*

1. *A spike failure retains its original pattern,*
2. *A bias failure retains the original form in a type-0 system and resembles a spike otherwise,*
3. *A drift failure retains the original form in a type-0 system but resembles a bias in a type-1 system and a spike in all other cases.*

In the closed loop environment, the behaviour of spike, bias and drift failures can be more easily elucidated in the continuous time s-domain. If the closed loop transfer function $G_c(s)$ is stable, then the failure transfer function $F(s)$ is also stable because the two transfer functions share the same characteristic polynomial (Equations 2.24 and 2.25). In other words, $F(s)$ may only have zero roots in the numerator but not in the denominator. In particular, if the forward transfer function $\mathcal{C}(s)\,G(s)$ can be expressed as

$$\mathcal{C}(s)\,G(s) = \frac{G'(s)}{s^\kappa} \tag{2.28}$$

[8] In control terminology, F is known as the sensitivity function [D'Azzo and Houpis, 1966, Section 14.2].

where $G'(0)$ is finite and not equal to zero and $\kappa = 0, 1, 2, \ldots$ then

$$F(s) = \frac{s^\kappa}{s^\kappa + G'(s)} \tag{2.29}$$

In control literature, κ is commonly known as the *system type number* [D'Azzo and Houpis, 1966, Section 6.3]. It follows from Equation 2.27 that

$$f(t) = \mathcal{L}^{-1}\{F(s)\, f_o(s)\} \tag{2.30}$$

and $\mathcal{L}^{-1}\{\cdot\}$ is the inverse Laplace Transform operator. From Equations 2.12, 2.13 and 2.16, the Laplace Transform of spike, bias and drift failures are given by

$$\textbf{Spike} \qquad f_o(s) = \vartheta_1 \tag{2.31}$$

$$\textbf{Bias} \qquad f_o(s) = \frac{\vartheta_1}{s} \tag{2.32}$$

$$\textbf{Drift} \qquad f_o(s) = \frac{\vartheta_1}{s^2} \tag{2.33}$$

For clarity, t_f is taken to be 0 and $\Theta(s)$ is assumed to be 1. Property 2.1 then becomes apparent by simply substituting Equations 2.31, 2.32 and 2.33 alternatively into Equation 2.30 with various system type numbers κ.

Example 2.1

This example illustrates the features described in Property 2.1 and highlights the difference in signal patterns of spike, bias and drift failures in closed loop environments with various system type numbers. Three linear closed loop systems with type numbers 0, 1 and 2 are simulated. To avoid unnecessary confusion, no measurement noise is introduced, i.e. $e = 0$. From Equation 2.23, the sensor output is given by

$$y = G_c\, r + F\, f_o \tag{2.34}$$

These systems are designed so that their failure shaping functions F have the same cut-off frequencies. They are summarized as follows:

		System I	*System II*	*System III*
System type number	κ	0	1	2
Forward transfer function	$C(s)\,G(s)$	$\frac{10}{s+1}$	$\frac{21s+121}{s(s+1)}$	$\frac{32s^2+363s+1331}{s^2(s+1)}$
Closed loop transfer function	$G_c(s)$	$\frac{10}{s+11}$	$\frac{21s+121}{(s+11)^2}$	$\frac{32s^2+363s+1331}{(s+11)^3}$
Failure shaping function	$F(s)$	$\frac{s+1}{s+11}$	$\frac{s(s+1)}{(s+11)^2}$	$\frac{s^2(s+1)}{(s+11)^3}$

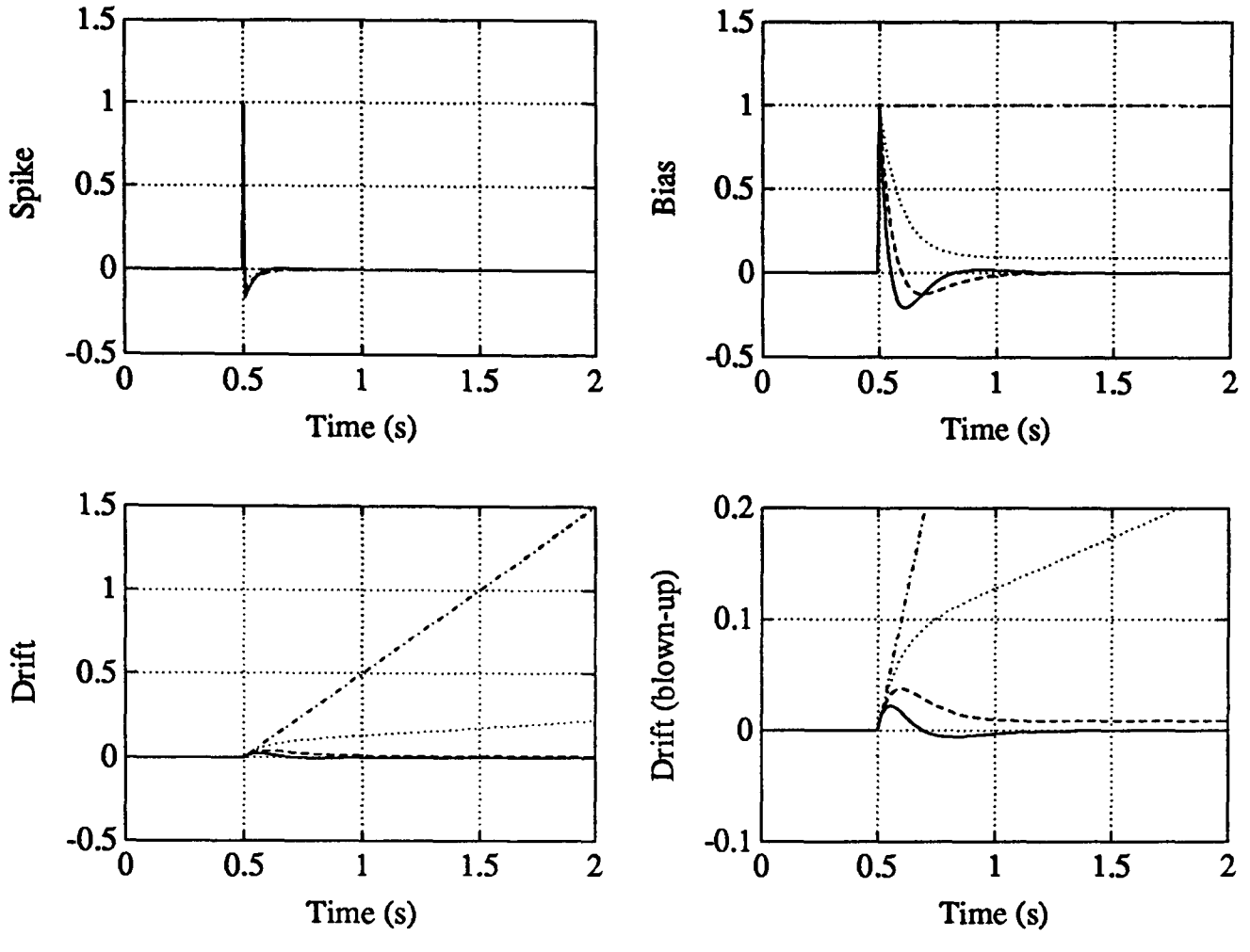

Figure 2.8: Spike, bias and drift failures in closed loop systems with different type numbers (dashdot: open loop, dotted: type-0, dashed: type-1, solid: type-2)

The simulations are sampled at 200 Hz and the reference signal r is kept constant at zero for simplicity. The spike, bias and drift failures are all of unit magnitudes and the drift failure is taken to be linear, i.e. $\vartheta_1 = 1$ in Equations 2.31, 2.32 and 2.33. Failure occurs at 0.5 s in every case. The results are depicted in Figure 2.8 and agree well with Property 2.1.

Erratic and cyclic failures

Property 2.2 *In a 'well-behaved' closed loop environment, the signal pattern of an erratic or cyclic failure depends on the frequency response of the closed loop transfer function:*

1. *Failure signal components at frequencies much higher than the closed loop system bandwidth are retained,*

2. *Failure signal components at frequencies much lower than the closed loop system bandwidth are attenuated.*

The analysis of the signal characteristic of an erratic or cyclic failure in closed loop is

better understood in the frequency domain. For a 'well-behaved' closed loop system,

$$G_c(j\omega) \approx 1 \qquad \text{for small } \omega, \qquad \text{i.e. unity gain at low frequencies} \tag{2.35}$$

$$G_c(j\omega) \approx 0 \qquad \text{for large } \omega, \qquad \text{i.e. roll off at high frequencies} \tag{2.36}$$

From Equations 2.24 and 2.25, it can be easily shown that

$$G_c(j\omega) + F(j\omega) \equiv 1 \qquad \forall\, \omega \tag{2.37}$$

Following the above, it can be inferred that:

$$|F(j\omega)| \approx 0 \qquad \text{for small } \omega \tag{2.38}$$

$$|F(j\omega)| \approx 1 \qquad \text{for large } \omega \tag{2.39}$$

Basically, $F(j\omega)$ acts like a highpass filter with unity gain at high frequencies. The cut-off of the filter centres in the vicinity of the closed loop bandwidth. For a linear noise shaping function, the spectral density of the failure signal $\Phi_f(\omega)$ is shown as

$$\Phi_f(\omega) = |F(j\omega)|^2 \, \Phi_{f_o}(\omega) \tag{2.40}$$

Hence, Property 2.2 follows:

1. The spectral component of $f(t)$ at high frequencies is retained,
2. The spectral component of $f(t)$ at low frequencies is attenuated,
3. The intermediate component depends heavily on the frequency response $F(j\omega)$ and in turn on $G_c(j\omega)$.

Example 2.2

This example demonstrates the effects of the failure shaping function in the frequency domain on erratic and cyclic failures as discussed in Property 2.2. System II (type-1) in Example 2.1 is simulated. Again, the sampling frequency is 200 Hz and both the reference signal r and the measurement noise n are kept at zero throughout. The frequency responses of the closed loop transfer function G_c and the failure shaping function F are shown in Figure 2.9. F acts effectively as a highpass filter and its cut-off frequency is estimated to be 2.77 Hz. The erratic failure and cyclic failure in this example is specified

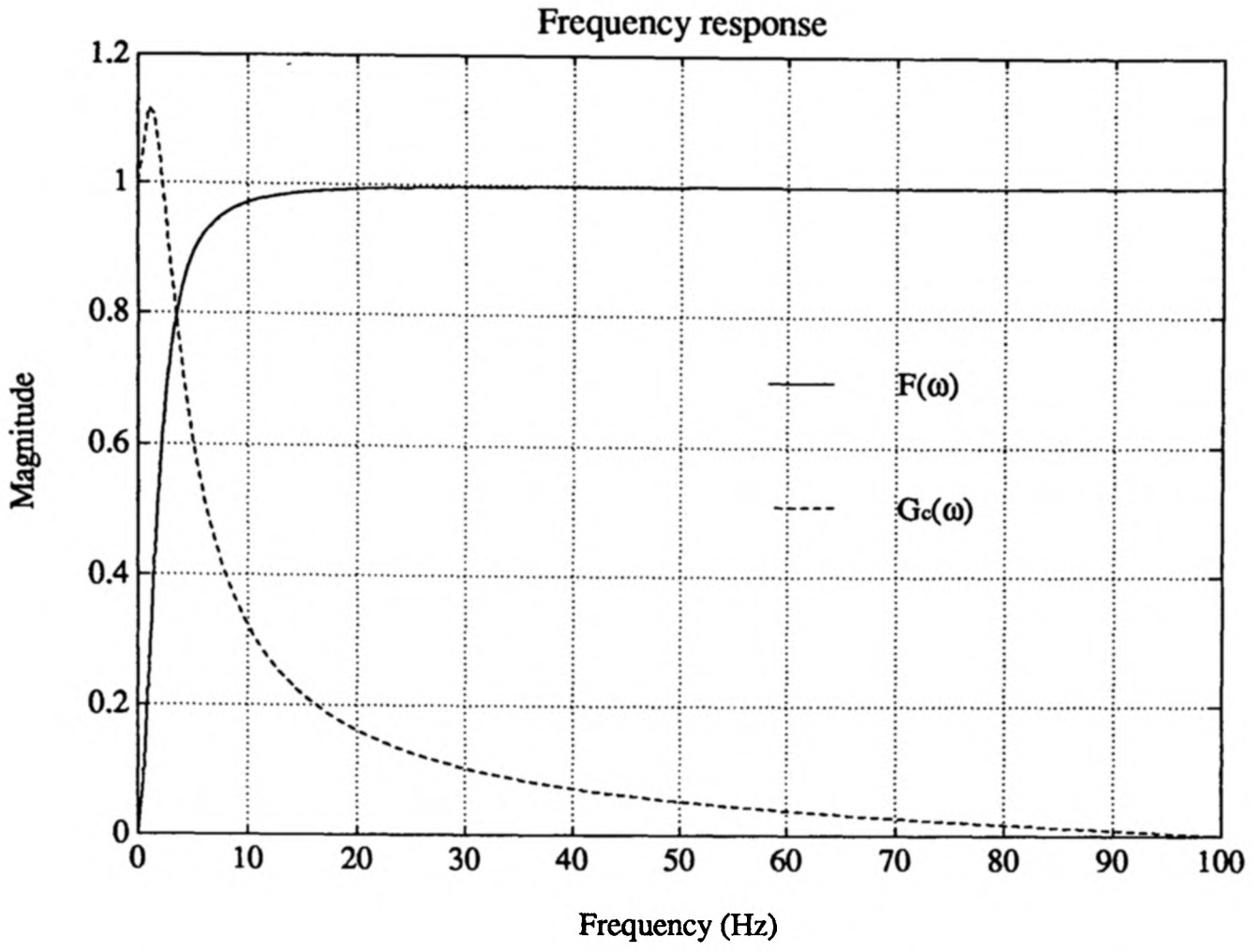

Figure 2.9: Frequency responses of closed loop transfer function and failure shaping function

as

$$\textbf{Erratic} \qquad f_o(t) = \Theta(q^{-1})\,\bar{e}(t) \qquad \sigma_{\bar{e}}^2 = 1 \tag{2.41}$$

$$\textbf{Cyclic} \qquad f_o(t) = \sin(2\pi f_c t) \tag{2.42}$$

In each mode, a low frequency failure and a high frequency failure are simulated separately. In the low frequency failures, the cyclic frequency f_c is 1 Hz whilst the erratic failure signature filter $\Theta(q^{-1})$ is chosen to be a second order Butterworth lowpass filter with cut-off frequency at 1 Hz. On the other hand, f_c is set to 5 Hz and $\Theta(q^{-1})$ to 1 (i.e. a all-pass filter) in the high frequency failure cases. All failures take place at 0.5 s and the sensor outputs are given in Figure 2.10. It is clear that the low frequency failures are significantly suppressed in both cases whereas the high frequency failure signals remain more or less unchanged. The variances of the sensor outputs under erratic failures and the amplitudes of the cyclic failure signatures are summarized as follows:

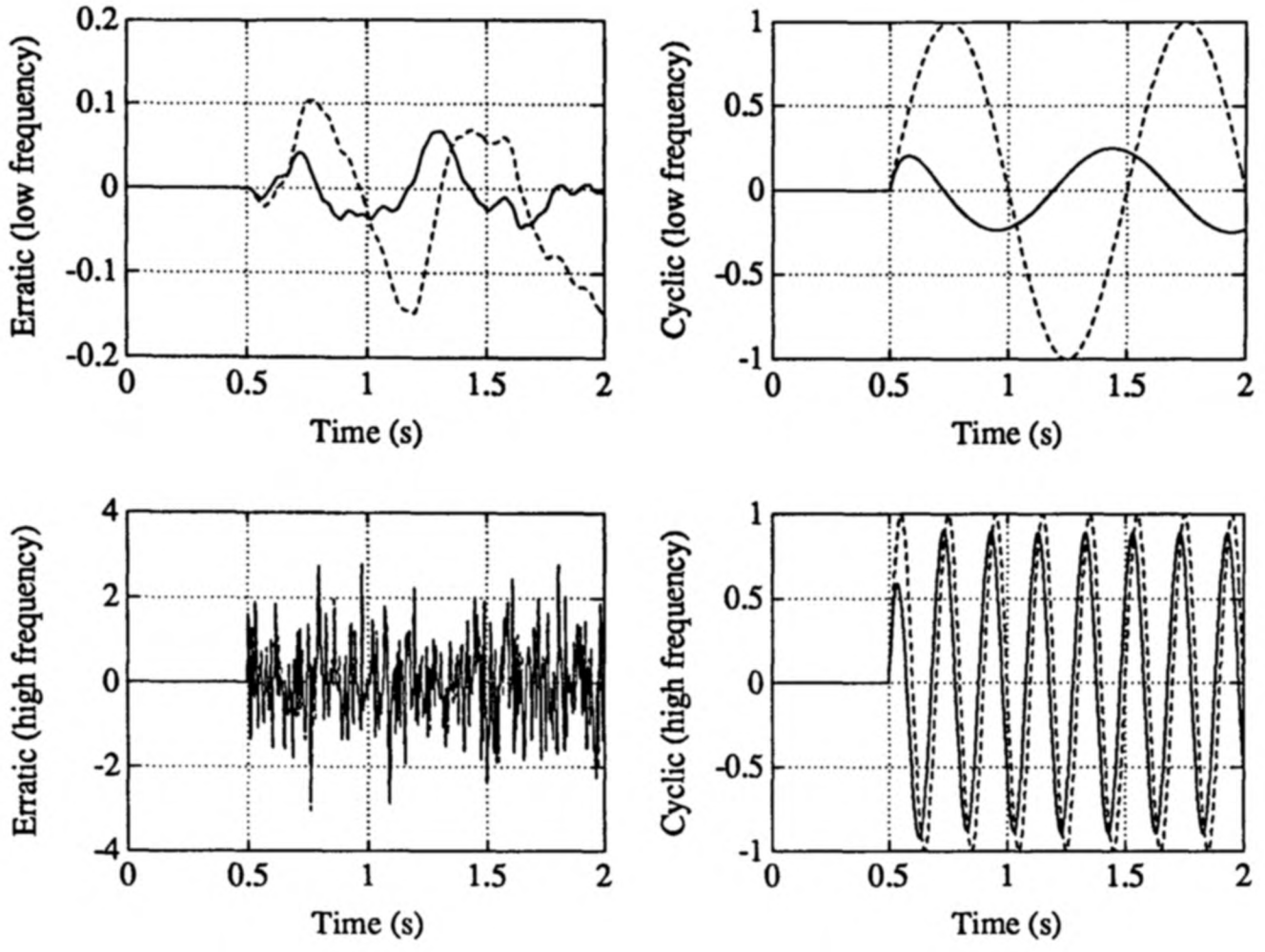

Figure 2.10: Erratic and cyclic failures in a closed loop system (dashed: open loop, solid: closed loop)

		Open loop	*Closed loop*
Erratic	(low frequency)	5.79×10^{-3}	0.78×10^{-3}
	(high frequency)	1.01	0.98
Cyclic	(low frequency)	1.00	0.25
	(high frequency)	1.00	0.92

2.6.2 Comments on non-additive failures in a closed loop environment

Due to the presence of the nonlinear function h_f in non-additive sensor failures (Equations 2.18 to 2.20), it is futile to carry out the analysis with linear system theories. It is obvious that a controller designed for a healthy sensor will not be able to eliminate the effects of these failures totally. The following guidelines are formulated to illustrate some non-additive failure patterns in closed loop:

1. A sensor with a stuck failure will hold on to a fixed value irrespective of any control action.

2. In case of a saturation failure, if the setpoint exceeds the saturation level, the sensor output will stick prematurely at the saturation level despite the efforts of the controller to drive it towards the setpoint value. The sensor will appear to be suffering from a stuck failure until the setpoint is changed to a level within the linear region.

2.6.3 Observations on sensor failures in closed loop

The sensor failure signal characteristics in a closed loop environment are a subset of those found in open loop. Thus, a process independent validation scheme sufficient for detection of failures in open loop can certainly cope in a closed loop environment.

However, as the failure patterns in closed loop may be transformed, a local validation scheme at the sensor end cannot ascertain whether a spike failure detected is actually caused by a spike, a bias or a drift. Further analysis has to be carried out at a higher level, for example, by inspecting the properties of the control signals.

2.7 A perspective of sensor validation in the frequency domain

The primary and fundamental problem in sensor validation is to distinguish sensor failure $f(t)$ from the legitimate sensor output $y_l(t)$ which is composed of the unknown signal $s(t)$ and the stochastic measurement noise $n(t)$. The conventional approach to this problem has the major drawback of requiring an accurate estimate of the legitimate sensor output. It is suggested that a system non-specific local validation scheme which approaches the problem in the frequency domain is a better solution with greater flexibility in application.

2.7.1 The conventional centralized approach

An accurate estimate of the legitimate sensor output $\hat{y}_l(t)$ is a necessary prerequisite for the operation of the centralized approach. The decision on whether there is a sensor

failure is made by comparing the actual output $y(t)$ with $\hat{y}_l(t)$. The prime difficulty of this lies on the reliability and complexity of the computation of $\hat{y}_l(t)$. Currently, there are two main methods to estimate the legitimate sensor output:

1. **Kalman filter / Luenberger observer / input-output modelling**
   [Bellingham and Lees, 1977b; Clark, 1978b; Clark and Setzer, 1980; El Madbouly and Frank, 1983; Janßen and Frank, 1984]
   The computation of $\hat{y}_l(t)$ is based on the estimate of the states of the system. This requires a detailed mathematical model which can be extraordinarily complicated to construct and even then may have gross error. The requisite of having complete real-time information of input signals confines its application to processes under closed loop control.

2. **Hardware / analytical redundancy**
   [Chow and Willsky, 1984; Deckert *et al.*, 1977; Frank, 1990; Polenta *et al.*, 1988]
   The estimate $\hat{y}_l(t)$ is inferred from the measurement of redundant sensors. Except for hardware redundancy, this approach demands an exact relationship among the redundant information. The working out of such relationships can be both costly and complicated in sophisticated and advanced processes. Furthermore, redundant information may not always be available. This approach cannot work in a standalone sensor system and therefore its application is limited.

2.7.2 System non-specific local validation

In realization of the mentioned problems of the conventional approaches, the development of a system non-specific local validation method which can operate without redundant sensor information is called for. The main objective is to construct a cost-effective and flexible scheme which could be adopted into different types of processes relatively easily. As discussed in Section 2.7.1, it is uneconomical to obtain the estimate $\hat{y}_l(t)$ at every sampling instant and this becomes even more onerous at the local level. It is suggested that taking an alternative perspective of sensor validation in the frequency domain is most enlightening and is very beneficial to the design of the new scheme.

In most chemical and other process industries, the measurement signal $s(t)$ is often bandlimited by the process but the measurement noise $n(t)$ covers a much wider frequency band. Any change in the measurement output $y(t)$ within the signal bandwidth caused by

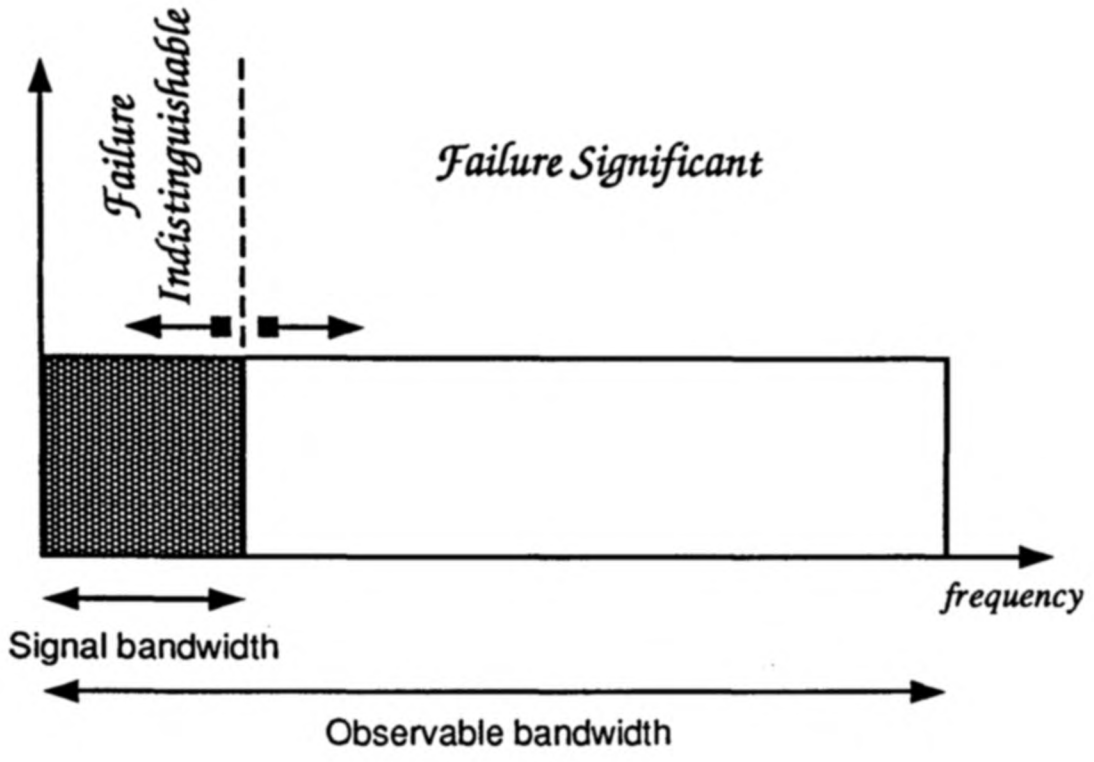

Figure 2.11: Perspective of sensor validation in the frequency domain

a sensor failure is *inherently* indistinguishable from the legitimate change of the measurand without *a priori* assumptions. Therefore, the validation scheme should concentrate in monitoring the output outside the signal bandwidth (Figure 2.11). This will reduce the rate of false alarm caused by the confusion of genuine sensor failure with legitimate change in sensor output.

As in all other sensor validation algorithms, it is assumed that the measurement noise $n(t)$ is fairly stationary. Any unanticipated change in the characteristics of $n(t)$ is considered to be a failure. A more detailed elucidation of the characteristics and problems of the validation scheme is to follow.

2.8 Characteristics of local sensor validation scheme

Sensor validation is at the lowest level of a hierarchical fault detection system (Figure 2.12). For the benefit of the overall efficiency, the local validation scheme should not be *competitive* with the higher level. It should rather be *cooperative* and *complementary*. It should provide prompt, accurate and adequate information to the level above when the sensor fails so that appropriate remedial actions can be carried out. This may include scheduling of maintenance or 'graceful' degradation of the control loop. In brief, the local sensor validation scheme should be:

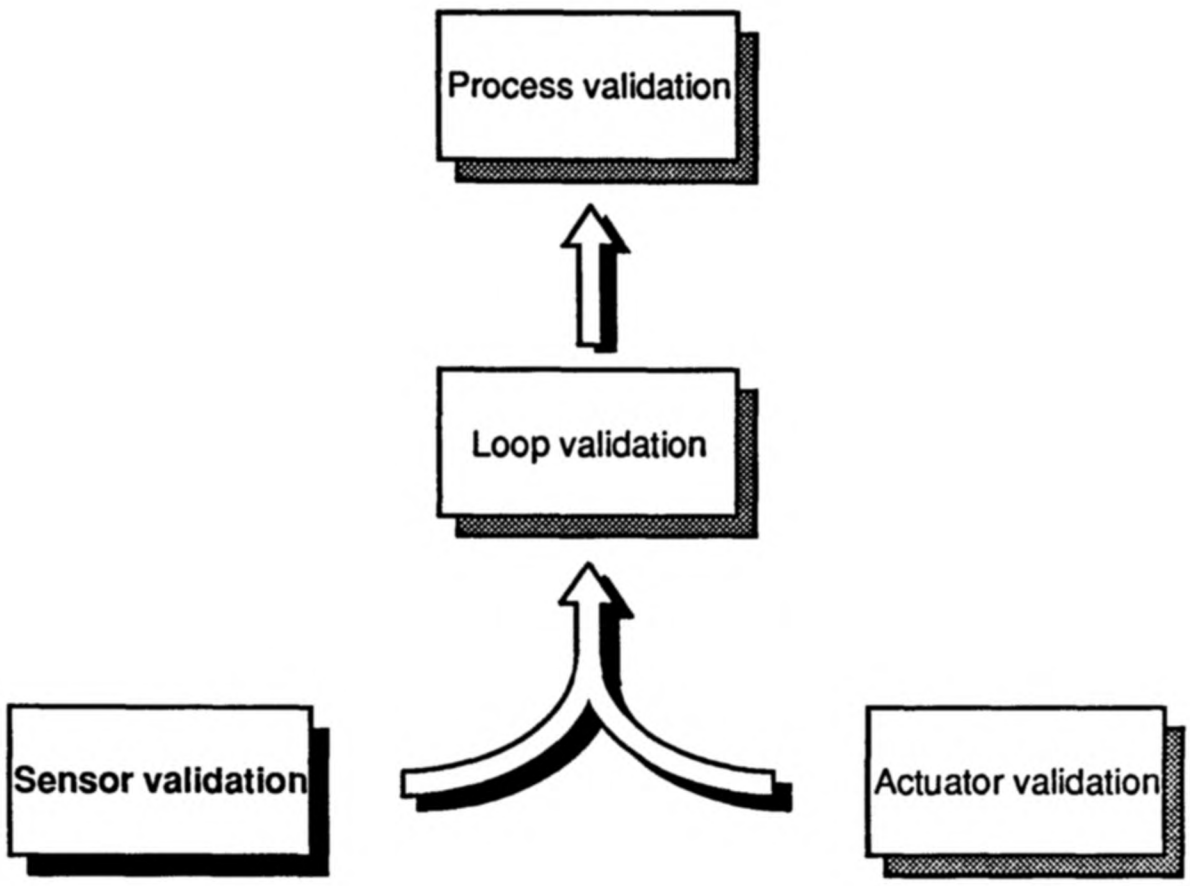

Figure 2.12: A hierarchical fault detection system

- **Comprehensive** — capable of detecting and diagnosing various modes of sensor failure,
- **Portable** — applicable to a wide range of sensors,
- **Simple** — able to be carried out at the sensor end,
- **Expeditious** — making prompt detection and diagnosis,
- **Reliable** — providing accurate detection and reducing the false alarm rate to minimal,
- **Process independent** — free from the requirement of developing a detailed process model.

There are two major hurdles in the development of the local sensor validation scheme:

1. Due to safety reasons, the power supply to a sensor has to be limited. Consequentially, the computation ability may be small.
2. The information readily accessible locally by the validation scheme is restricted to the measurement output $y(t)$.

The first hurdle can be overcome by applying simple signal processing techniques to the detection methods. Inevitably, some 'optimalities' attained in centralized detection methods have to be sacrificed. Nonetheless, a prompt response from a simple detection procedure is sometimes more appreciated. With the second hurdle in mind, additional information should be acquired as a redress to the problem. This includes both sensor specific information like the operating range and the response time as well as process related knowledge such as the system bandwidth and the process noise level. In a nutshell:

> *With only the sensor output y available, and allowing for some prior knowledge of the sensor and its operating environment, a sensor validation scheme is to detect various possible sensor failure modes expeditiously. The scheme should provide the following information: the time, the mode and the size of failure.*

2.9 A decentralized hierarchical approach

The local sensor validation scheme is divided into three stages: the commissioning stage, the learning stage and the tracking stage. A similar structure was utilized by Upadhyaya and Skorska [1984] in their data-driven detection method and McMichael [1988] in his centralized fault detection scheme. Functions performed in each stage include:

1. **Commissioning stage**

   Prior knowledge of sensor specification, operating conditions and signal patterns for each failure modes are either supplied by the process engineer or extracted from an inbuilt knowledge base. This information is essential for the subsequent fault detection and diagnosis. Sensor signal should be well-conditioned and have adequate resolution. The bandwidth of the measurement signal is then estimated and the sampling frequency is selected accordingly. Finally, a suitable decomposition algorithm is configured to partition the sensor output into a signal and a noise component.

2. **Learning stage**

   Based on a suitable decomposition algorithm and an assumed 'error-free' observation of sensor output over a specified period, a simple time-series model is selected to represent the 'healthy' sensor. Identification techniques are employed to estimate

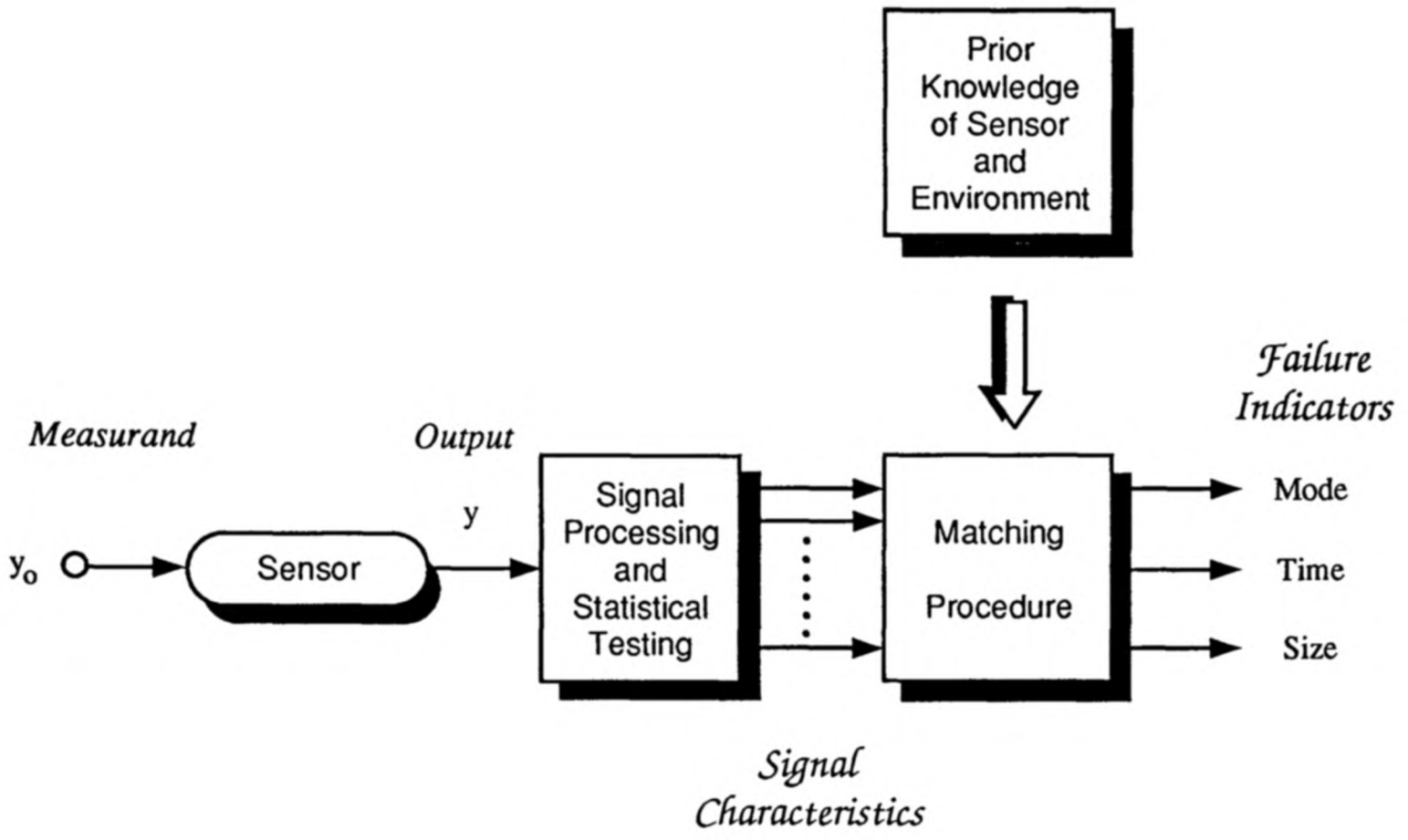

Figure 2.13: Architecture of the local sensor validation scheme

the unknown parameters on-line and the model is tested for validity. Statistical and spectral properties of the measurement are also computed as a reference.

3. **Tracking stage**

   A predominantly innovation-based technique is employed [Kailath, 1970; Mehra and Peschon, 1971]. An inverse filter (based on the model parameters estimated during the learning stage) generates the innovation sequence, from which the characteristics of sensor failures are captured using simple signal processing techniques. Together with the prior knowledge acquired during the commissioning stage, the signal patterns extracted are matched with the proposed failure modes for diagnosis. This is illustrated in Figure 2.13.

The tracking stage is further divided into two phases:

1. **Ordinary phase**

   This corresponds to the normal operation during which minimal signal processing and testing algorithms are applied to monitor the sensor behaviour. Any detected abnormality will switch the validation scheme to the alert phase. The signal process-

ing procedures employed includes mean, variance, rate of change and a measure of bias. A set of failure alarm indicators is installed to provide the basis for subsequent failure identification.

2. **Alert phase**

   This is initiated if any aberration in the sensor signal is detected during the ordinary phase. Depending on the nature of the aberration, and on the prior knowledge acquired in the commissioning stage, additional signal processing and testing procedures are called in, if necessary, to determine the state of the failure mode indicator.

The main reason for dividing the tracking stage into two phases is that sensor failures are rare in occurrence, and it is extremely uneconomical and indeed unnecessary to employ an individual algorithm to monitor each and every possible failure mode. The proposed approach requires only a small amount of processing power in the ordinary phase and consequently, failures can be detected promptly. In the alert phase, extra computing power can be scheduled for the increase in demand. A schematic diagram of the hierarchical validation scheme is shown in Figure 2.14.

2.10 Conclusions

This chapter sets out to explore the many concepts and problems in sensor validation. With fundamental concepts, such as sensor systems and sensor failures, defined, it proceeds to set down a system non-specific model of the sensor output and examine in detail the different failure patterns in open loop and closed loop environments. A study of the sensor failure characteristics leads to the drawing up of eight typical sensor failure modes. All these contribute to provide a firm groundwork for the construction of a novel sensor validation scheme which is innovative in both its approach to and the tackling of the sensor failure detection problem. The successful development of such a scheme will offer a cheaper, simpler and application independent alternative to the conventional centralized approach. This is beneficial not only to new applications, but can also be useful in established processes where the conventional method has been installed and a detailed process model has already been developed. The new scheme can improve the status quo by acting as a filter and a hierarchical system can be developed where all the sensors will usually be monitored locally. If any irregularity is detected, the conventional scheme

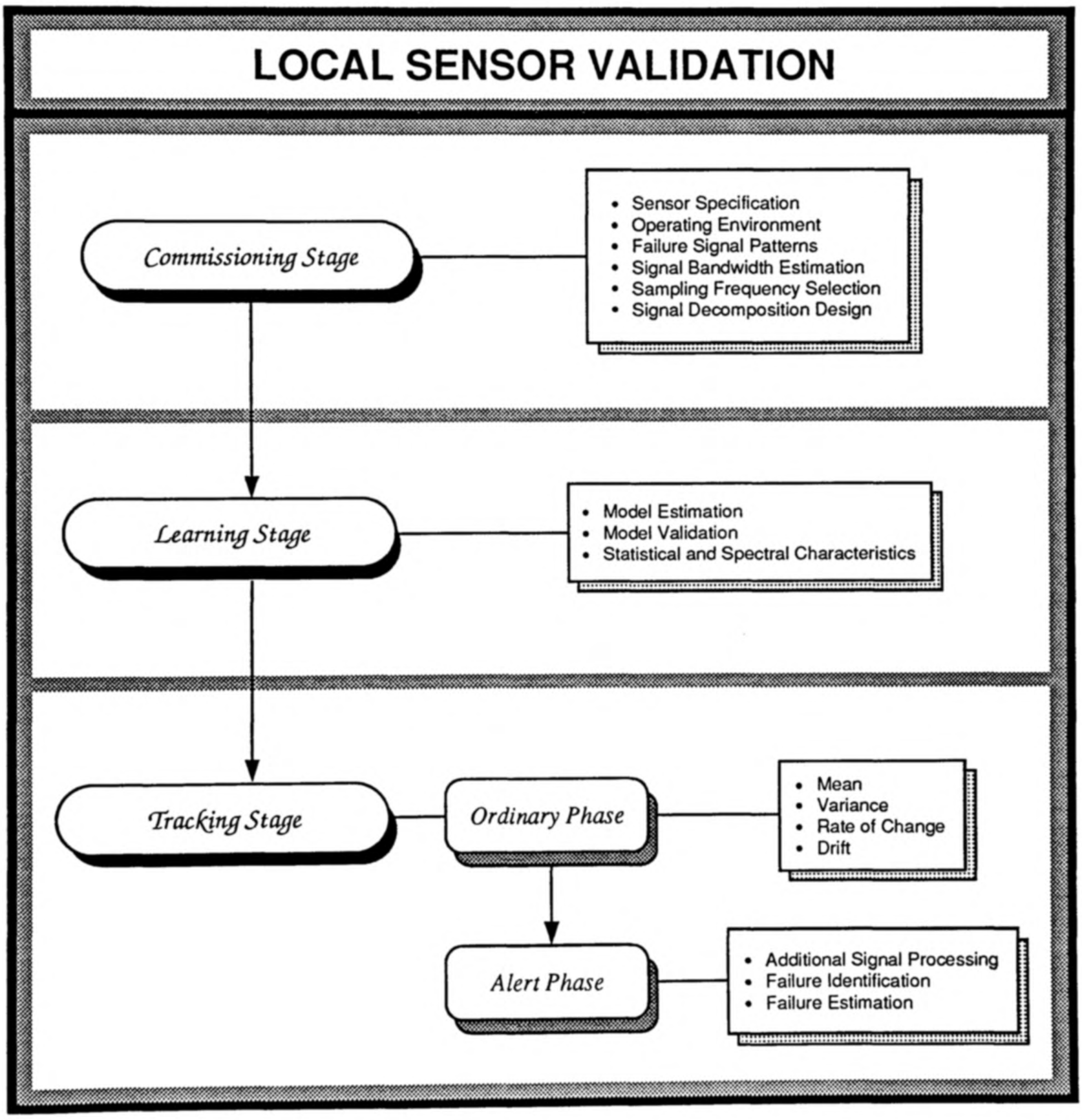

Figure 2.14: Hierarchical structure of the local sensor validation scheme

can be triggered off to obtain optimal information on the failure. In this way, for most of the time, the monitoring could be done locally and a large proportion of the central computing power can be spared for other tasks.

With all the merits of this new scheme in mind, it is now appropriate to inquire into the prerequisites necessary for its successful development. The followings are the essentials that should be borne in mind:

1. Although an exact detailed model of the process is not necessary, the knowledge about the frequency band at which the signal is dominating will be very useful. This is generally known to the process engineer or can be estimated without incurring much costs.

2. In order that the validation scheme can monitor signal characteristics outside the signal bandwidth, the sensor output must be sampled at a much higher frequency than the signal bandwidth.

3. In a closed loop system, the controller at a higher level usually has to be run at a much slower rate than the validation scheme because:

   - control, scheduling and optimization activities are computationally more taxing,
   - sampling too fast often leads to nonminimum phase behaviour [Åström and Wittenmark, 1984, Section 3.6].

   Therefore, a proper method to decrease the sampling rate at the interface has to be designed.

4. Raw sensor output has to be decomposed so that only the components outside the signal bandwidth are used for validation.

5. The behaviour of the stationary measurement noise should be 'learned' in an initial stage to provide a baseline model.

6. Signal processing techniques are required to extract various failure patterns.

7. Alarm indicators have to be designed to signify failures detected.

The first five points will be discussed in Chapter 3 while the last two will be dealt with in detail in Chapter 4.

Chapter 3

The Commissioning Stage and the Learning Stage

3.1 Introduction

Validating sensor signals at a local level is by no means straightforward and 'problem-free'. A number of hurdles, as highlighted in Chapter 2, have to be overcome. Additional knowledge (both sensor and process specific) has to be acquired in the commissioning stage to supplement the scarcity of locally accessible information and to facilitate the subsequent modelling, detection and diagnostic processes. Measurement signal bandwidth is one of the vital piece of knowledge to be acquired. In order to eliminate the confusion between an actual sensor failure and a legitimate change of the measurand, it is suggested that the local sensor validation scheme should focus only on signal characteristics outside the bandwidth. In view of this, an appropriate definition and a step-by-step estimation procedure of the signal bandwidth will have to be laid down.

An effective validation scheme which monitors high frequency signal behaviour demands well-conditioned sensor output to be sampled at a rate comparatively higher than the signal bandwidth. A few practical issues may arise: such as stringent specification on the analog anti-aliasing filter, inadequate resolution on the analog-to-digital converter and interfacing of information flow between the sensor validation scheme and the next higher level which operates at a lower rate. The application of decimating filters is proposed as a solution to all these problems.

Furthermore, sensor validation beyond the signal bandwidth necessitates the raw sensor output to be decomposed into a signal-dominant and a noise-dominant component. Various classical approaches, such as Wiener filtering, are reviewed and fundamental prop-

erties of a pair of infinite impulse response decomposition filters are formulated.

As to the learning stage, the key objective is to obtain a baseline model of the normal sensor characteristics. In contrast to the computationally extensive mathematical models employed in conventional centralized fault detection schemes, a simple and versatile stochastic time-series model is adopted. Practical implementation of model estimation techniques is examined and statistical testings on model adequacy are discussed.

It is submitted that the combination of signal decomposition and modelling is not without difficulty, especially when there is a severely nonstationary measurement signal. An innovative solution with the injection of artificial random signals, known here as 'dither', is to be investigated.

As a brief summary, Sections 3.2 to 3.7 in this chapter discuss the various tasks carried out in the commissioning stage while Sections 3.8 to 3.11 address the problems encountered in the learning stage.

3.2 Knowledge acquisition

Without any external support, the information readily accessible to the local sensor validation scheme is limited solely to the unprocessed sensor output $y(t)$. This single piece of information is inadequate to implement an effective validation procedure. More information is required to formulate a code of normal behaviour of the sensor output (Section 2.4.1) and to sharpen the detection algorithms. Basically, the additional information can be categorized into two parts: *sensor-specific* and *process-specific*:

- **Sensor-specific knowledge**
  - Sensor specification (e.g. output limits, maximum rate of change, dynamic range and response time/bandwidth);
  - Linearity of the sensor output;
  - Measurement noise characteristics;
  - Probable failure modes and their associated signal patterns;
  - Significance of each failure mode (loss severity) and the probability of occurrence (MTBF – mean time between failures) [IEEE, 1981].

- **Process-specific knowledge**
  - Operating conditions (e.g. measurand ranges);
  - Process dynamics (e.g. time constants, bandwidths);
  - Energy and the spectral features of the generalized input v (Section 2.3);
  - Properties of the process disturbance.

Sensor-specific data are provided by the manufacturers and can be stored *a priori* in an embedded memory. On the other hand, process dependent information is to be supplied by the process/instrument engineers during the installation of the sensor and after each major process modification.

In addition, a number of assumptions are laid down for subsequent analyses and discussions. Further assumptions will be stated hereafter where appropriate.

Assumption 3.1 *The measurement signal is assumed to be bandlimited.*
Most industrial processes have inherent lowpass filtering characteristics and hence the signal to be measured, $s(t)$, is usually confined in a frequency band. Sensor output $y(t)$ beyond this frequency band is dominated by the measurement noise $n(t)$.

Assumption 3.2 *The measurement noise is assumed to be reasonably stationary.*
Any unanticipated departure from the nominal noise level is considered to be a failure. This may be due to improper installation or an unacceptable degradation in sensor performance [Anyakora and Lees, 1973]. For example, a poor attachment of a strain gauge to its substratum or a prolonged exposure of a thermocouple outside its operating range will alter the noise characteristics in the measurement.

Assumption 3.3 *The measurement noise is assumed to cover a much wider frequency band than the measurement signal.*
The measurement noise is in many cases taken to be an idealized white noise process which has a flat spectrum with an 'infinite' bandwidth.

Assumption 3.4 *The measurement noise is assumed to be uncorrelated with the measurement signal.*
Under normal condition, the measurement noise can be considered to be a stochastic signal independent of the measurement signal. The adopted model of the sensor output, as

illustrated in Figure 2.3, ensures that the assumption still holds when applied in a closed loop environment since the reference signal (but not the control signal), in most cases, is uncorrelated with the measurement noise

Assumption 3.5 *All other actuators and process equipments are assumed to be fault-free.*

Any non-permitted sensor output behaviour caused by a faulty equipment or a process disturbance is locally declared as a sensor failure. It is up to a higher level in the hierarchy (Figure 2.12) to discriminate between an actuator/process breakdown and a genuine sensor failure.

3.3 Measurement signal bandwidth

As explained in Assumption 3.1, the measurement signal $s(t)$ is usually bandlimited by the process. Validating sensor output within the signal bandwidth based on the restrictive information available at a local level is profoundly difficult. The results can also be misleading as the change in sensor output caused by a failure is inherently indiscernible from legitimate signal variations. It is suggested that an efficient local sensor validation scheme should focus on sensor outputs outside the signal bandwidth (Section 2.7.2) and an estimate of the measurement signal bandwidth is therefore a *sine qua non* for its successful development and application.

3.3.1 Definition of the measurement signal bandwidth

One major problem in the signal bandwidth estimation is the nonstationary nature of the measurement signal $s(t)$ given by Equation 2.3

$$s(t) = \mathcal{G}(q^{-1})\, v(t) \tag{3.1}$$

The nonstationary characteristic can either be attributed to a time-varying generalized process $\mathcal{G}(q^{-1})$ or, more likely, to a nonstationary generalized input signal $v(t)$. For instance, in a closed loop environment (Equation 2.5), $\mathcal{G}(q^{-1})$ is represented by the closed loop transfer function $G_c(q^{-1})$ which would be time-varying if either the control algorithm is adaptive or the process itself is not time-invariant; $v(t)$ is represented by the reference signal $r(t)$ which would typically be a nonstationary step sequence.

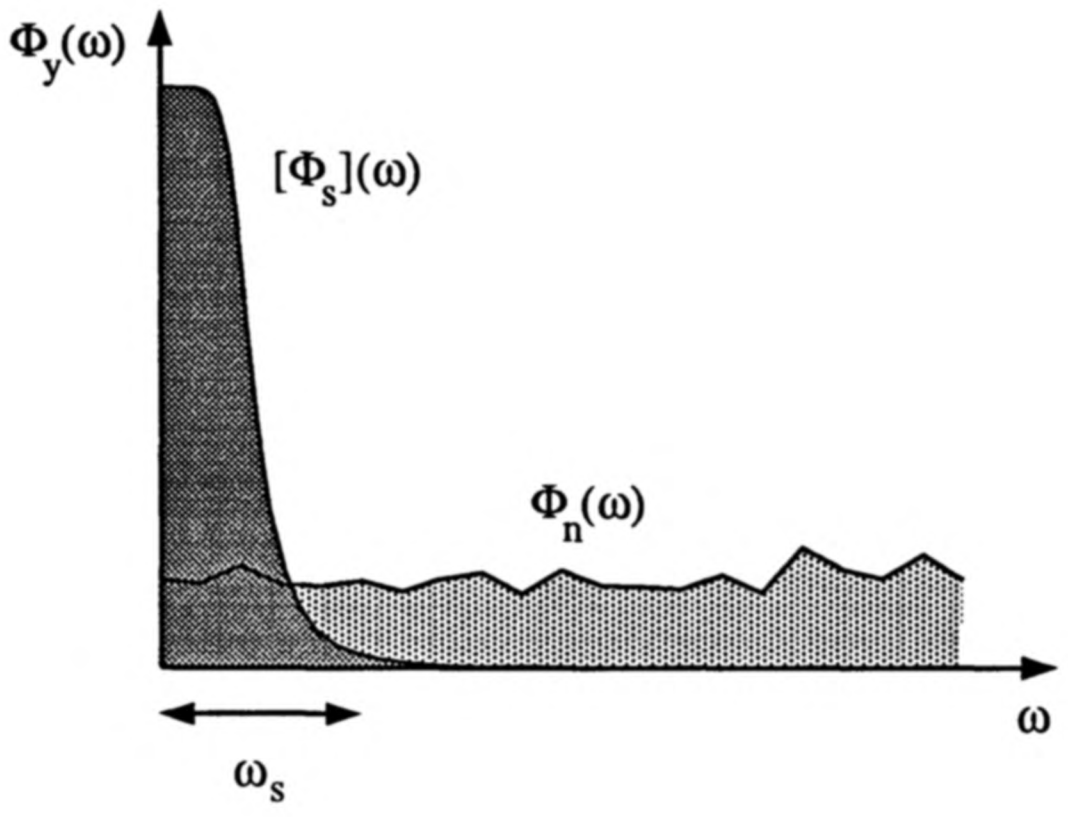

Figure 3.1: Spectral characteristics of the measurement signal and noise

Conventional spectral analysis assumes stationarity of the signal which is inadequate for this application. A worst case analysis[1] is adopted and the upper bound of the measurement signal spectra $[\Phi_s](\omega)$ is defined as

$$[\Phi_s](\omega) \geq \Phi_s(\omega, t) \qquad \forall \ \omega \text{ and } t \tag{3.2}$$

As discussed in Assumptions 3.1 and 3.3, the measurement signal is bandlimited whilst the measurement noise covers a wide frequency band. For the following analyses, it is further assumed that the measurement signal $s(t)$ has a lowpass filtered characteristic and is confined to a low frequency band as depicted in Figure 3.1.

Assumption 3.6 *The measurement signal is assumed to be confined to a low frequency band.*

On the basis of the above assumption, the measurement signal bandwidth ω_s is defined as the 'lowest' frequency where the power spectrum of the measurement noise $\Phi_n(\omega)$ is 'significantly' larger than the upper bound of the measurement signal spectra $[\Phi_s](\omega)$. As

[1]Formal analysis of nonstationary signals can be carried out in a frequency-time representation [Bendat and Piersol, 1986, Chapter 12].

a rule of thumb, ω_s can be taken to be[2]

$$\omega_s = \{\omega_s : \Phi_n(\omega) \geq 10\,[\Phi_s](\omega) \qquad \forall \omega > \omega_s\} \tag{3.3}$$

and there does not exist a lower frequency ω ($< \omega_s$) which satisfies Equation 3.3. Therefore, ω_s depends both on $\Phi_n(\omega)$ and $[\Phi_s](\omega)$, and from Equation 3.1, $[\Phi_s](\omega)$ depends on $\mathcal{G}$ and $\Phi_v(\omega)$.

In practice, detailed individual expressions of $\mathcal{G}$, $\Phi_v(\omega)$ and $\Phi_n(\omega)$ are seldom available and their evaluation hardly feasible and economical. Nevertheless, the process engineer can often provide a reasonable guess of the measurement signal bandwidth. If not, ω_s can be estimated based on the following information[3]:

- Process gain $\mathcal{G}_o$,
- Process bandwidth ω_B,
- Process rate of roll-off at high frequencies ℓ,
- 'Worst' input spectrum $[\Phi_v](\omega)$, and
- Strength of the measurement noise σ_n^2.

These will be discussed in more detail in Sections 3.3.2 to 3.3.6.

3.3.2 Estimation of the process gain

In the continuous time domain, a generalized process[4] $\mathcal{G}(s)$ can be expressed as

$$\mathcal{G}(s) = \frac{\mathcal{G}_o \prod_{i=1}^{nz'} \left(1 - \frac{s}{z_i}\right)}{s^{\mu} \prod_{i=1}^{np'} \left(1 - \frac{s}{p_i}\right)} \qquad z_i,\, p_i \neq 0 \quad \forall i \tag{3.4}$$

---

[2]The factor of 10 should be considered as a guideline rather than a definitive rule. In general, as the factor becomes larger, the rate of false alarm caused by legitimate signal changes will be reduced but the sampling frequency has to be raised.

[3]If the process is nonstationary, the process-related variables ($\mathcal{G}_o$, ω_B and ℓ) should be evaluated from the 'worst' $\mathcal{G}$, i.e. the one that covers the widest frequency band.

[4]For a *stable* generalized process, $\mu \leq 0$ and $Re[p_i] < 0 \quad \forall i$.
For a *minimum phase* process, $\mu \geq 0$ and $Re[z_i] < 0 \quad \forall i$.

and its frequency response $\mathcal{G}(j\omega)$ as

$$\mathcal{G}(j\omega) = \frac{\mathcal{G}_o \prod_{i=1}^{nz'} \left(1 - \frac{j\omega}{z_i}\right)}{(j\omega)^\mu \prod_{i=1}^{np'} \left(1 - \frac{j\omega}{p_i}\right)} \tag{3.5}$$

The indices nz' and np' are given by

$$\begin{cases} nz' = nz \\ np' = np - \mu \end{cases} \quad \text{if } \mu \geq 0 \tag{3.6}$$

$$\begin{cases} nz' = nz + \mu \\ np' = np \end{cases} \quad \text{if } \mu < 0 \tag{3.7}$$

where nz and np are the total number of zeros and the total number of poles of $\mathcal{G}(s)$ respectively. $\mathcal{G}_o$ is defined here as the process gain. The typical value of μ in an open loop environment ($\mathcal{G} = G$) is 0, 1 or 2 whereas in closed loop ($\mathcal{G} = G_c$) μ is often designed to be 0.

When $\mu = 0$, $\mathcal{G}_o$ is in fact the steady state or d.c. gain of the process. By far the most common procedure to estimate the steady state gain is a step response test: if the output changes by Δy in response to a step input of Δv, $\mathcal{G}_o = \frac{\Delta y}{\Delta v}$. Note that in a closed loop environment, if the system type number (Property 2.1) is larger than zero, $\mathcal{G}_o$ is guaranteed to be unity.

A more versatile approach to estimate $\mathcal{G}_o$ for $\mu > 0$ is by means of the bode plot of $\mathcal{G}$ (refer to Section 3.3.3 for techniques to approximate $\mathcal{G}(j\omega)$ from both the frequency and the time domains). At low frequencies where $\omega \ll \min(|z_1|, \ldots, |z_{nz'}|, |p_1|, \ldots, |p_{np'}|)$,

$$|\mathcal{G}(j\omega)| \simeq \frac{\mathcal{G}_o}{\omega^\mu} \tag{3.8}$$

and taking the logarithm

$$20 \log_{10} |\mathcal{G}(j\omega)| \simeq 20 \log_{10} \mathcal{G}_o - 20\mu \log_{10} \omega \tag{3.9}$$

In a plot of $20 \log_{10} |\mathcal{G}(j\omega)|$ against $\log_{10} \omega$ (Figures 3.2), the slope of the curve at low frequencies approaches -20μ dB/decade and the interpolation of this low-frequency curve intersects the horizontal axis ($20 \log_{10} |\mathcal{G}(j\omega)| = 0$) at $\omega = \sqrt[\mu]{\mathcal{G}_o}$.

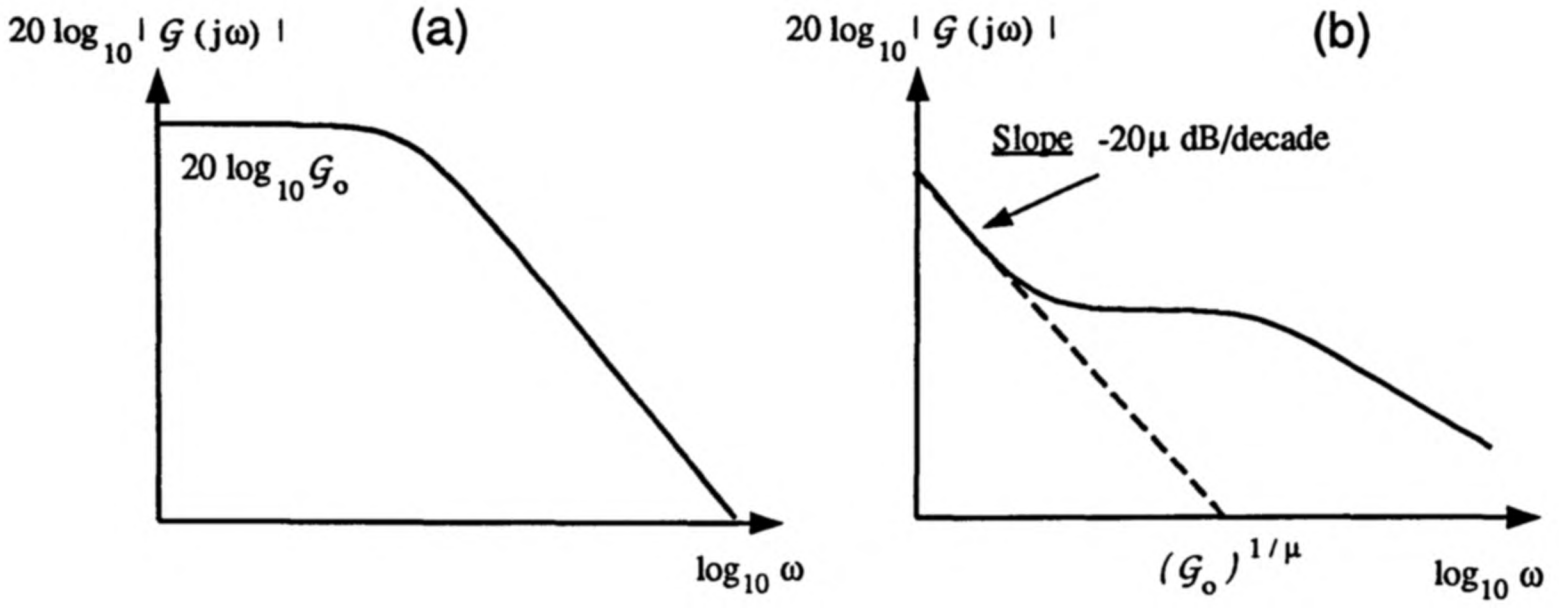

Figure 3.2: Bode plots of $\mathcal{G}$: (a) $\mu = 0$, (b) $\mu > 0$

3.3.3 Estimation of the process bandwidth

Based on Assumption 3.6, the bandwidth of a process in the continuous time domain[5] $\mathcal{G}(s)$ is defined as ω_B such that [Power and Simpson, 1978]

$$|\mathcal{G}(j\omega_B)| = \frac{1}{\sqrt{2}}\mathcal{G}_o \tag{3.10}$$

and

$$|\mathcal{G}(j\omega)| < |\mathcal{G}(j\omega_B)| \qquad \forall\omega > \omega_B \tag{3.11}$$

where $\mathcal{G}_o$ is the process gain as defined in Section 3.3.2. ω_B is also known as the 3 dB point.

Methods for estimating the process bandwidth are widely available in literature. Highlights of various techniques are summarized as follows:

1. *Mathematical modelling*

   In certain applications, a detailed transfer function of the process $\mathcal{G}(s)$ is available via physical modelling. The bandwidth ω_B can then either be solved analytically from Equation 3.10 or be estimated graphically from the bode plot of $\mathcal{G}$;

2. *Spectral (frequency-domain) analysis*

   The frequency response of the process $\mathcal{G}(j\omega)$, and hence its bandwidth ω_B, can be evaluated by injecting a test signal $v(t)$ with a known spectrum $\Phi_v(\omega)$ into the

[5] In discrete time, simply substitute s by q^{-1}, and $j\omega$ by $e^{-j\omega T_m}$ (T_m is the sampling period).

system [Söderström and Stoica, 1989, Chapter 3]. $\mathcal{G}(j\omega)$ is then estimated by the ratio of the cross spectrum between the output and input signals, $\Phi_{yv}(\omega)$, to the spectrum of the test signal $\Phi_v(\omega)$. Typical examples of the test input include a series of sinusoids, a PRBS[6] and a white noise process.

3. *Transient (time-domain) analysis*
   A crude estimate of the process bandwidth ω_B can be obtained from the step or impulse response[7] of a variety of processes: a first order system [D'Azzo and Houpis, 1966, Section 20.3], a second order overdamped system with significantly different time constants [D'Azzo and Houpis, 1966, Section 20.3] and a second order underdamped system with a resonant peak [Power and Simpson, 1978]. In addition, the Guillemin's procedure [Raven, 1961, Appendix III] provides a numerical/graphical technique to approximate the frequency response of an arbitrary system from its step response, and through which the process bandwidth can be inferred.

3.3.4 Estimation of the rate of roll-off

The frequency responses of most industrial processes roll off at high frequencies (Assumption 3.1). In the continuous time domain, this is characterized by the fact that the number of poles, np, in the transfer function $\mathcal{G}(s)$ exceeds the number of zeros, nz, The rate of roll-off at high frequencies is dictated by the difference[8] ℓ given by

$$\ell = np - nz \tag{3.12}$$

$$= np' - nz' + \mu \tag{3.13}$$

From Equation 3.5, the amplitude of $\mathcal{G}(j\omega)$ at high frequencies ($\omega \gg \max(|z_1|, \ldots, |z_{nz'}|, |p_1|, \ldots, |p_{np'}|)$) is given by

$$|\mathcal{G}(j\omega)| \simeq \frac{\mathcal{G}_o}{\omega^\ell} \left(\frac{\prod_{i=1}^{np'} p_i}{\prod_{i=1}^{nz'} z_i} \right) \tag{3.14}$$

ℓ can be estimated either from the physics of the process or by interpreting the bode plot of $\mathcal{G}$ at high frequencies which rolls off at a rate of 20ℓ dB/decade or 6ℓ dB/octave. In the

[6]Pseudo-Random Binary Sequence.

[7]The Fourier Transform of an impulse response of a process is equivalent to its frequency response.

[8]ℓ is also termed 'pole excess' [Åström and Wittenmark, 1984, Section 3.4].

event that all the above mentioned methods are unsuccessful, a conservative estimate of ℓ should be taken to be 1.

3.3.5 Estimation of the input spectrum

As discussed in Section 2.3, the generalized input $v(t)$ may not necessarily be stationary and ergodic. It may be a time-varying stochastic disturbance acting on the process or it may be a nonstationary staircase-type reference input in a closed loop environment. In the context of measurement signal bandwidth estimation (Equation 3.2), the spectrum of the 'worst' input (i.e. the one that dominates the measurement noise for the widest bandwidth) is of particular interest. Despite the large variety of input signals, most fall within two categories:

- **White noise input**

  Most stochastic disturbances can be adequately modelled as white noise processes. In an open loop environment where the measurand is unknown, the generalized input is often considered as

  $$v(t) = e(t) + \bar{v} \tag{3.15}$$

  $\bar{v}$ is the mean level of the input and $e(t)$ is a white noise process. The variance of $e(t)$ may be time-varying and the 'worst' input spectrum is

  $$[\Phi_v^e](\omega) = (\sigma_e^2)_m \qquad \forall\omega \tag{3.16}$$

  where $(\sigma_e^2)_m$ is the maximum expected variance of $e(t)$.

- **Step input**

  In a closed loop environment, the generalized input is represented by the reference signal which generally is a sequence of step inputs. For a step of size Δv,

  $$v(t) = \Delta v\, \alpha(t) \tag{3.17}$$

  $\alpha(t)$ is the Heaviside step function as defined in Section 2.5.1. The maximum expected step change, $(\Delta v)_m$, is utilized to estimate the 'worst' input spectrum, which is given by

  $$[\Phi_v^s](\omega) = \frac{(\Delta v)_m^2}{\omega^2} \tag{3.18}$$

The superscripts e and s in $[\Phi_v]$ denotes the 'worst' input spectrum for a white noise input and a step input respectively.

3.3.6 Estimation of the measurement noise level

In practice, it is found that the spectrum of the measurement noise $\Phi_n(\omega)$ is fairly uniform over a relatively wide frequency band (Assumption 3.3). In the limit, n is considered to be a white noise process and $\Phi_n(\omega)$ is fixed at the variance σ_n^2 over all frequencies. Assuming n to be a white noise, σ_n^2 can be derived from the output spectrum $\Phi_y(\omega)$ either at sufficiently high frequencies where the measurement output is dominated by noise or by anchoring the measurand at a constant level. Based on the peak-to-peak output value r_n, an estimate of the standard deviation of Gaussian white noise is given in Goff [1966]:

$$\sigma_n \simeq \frac{r_n}{8} \tag{3.19}$$

where the measurand is either assumed to be held constant or its low frequency variations removed. More details on the critical values of the range (or peak-to-peak value) of a sample from a Gaussian distribution are tabulated in Owen [1962, Section 6.1].

3.3.7 Estimation of the high-frequency gain

For a linear generalized process $\mathcal{G}$, the upper bound of the measurement signal spectrum $[\Phi_s](\omega)$ is given by

$$[\Phi_s](\omega) = |\mathcal{G}(j\omega)|^2 \; [\Phi_v](\omega) \tag{3.20}$$

Equation 3.14 implies that the amplitude of the process transfer function at high frequencies depends not only on the process gain $\mathcal{G}_o$ and the rate of roll-off ℓ, but also on the exact values of all the zeros and poles, which are rarely available. Nonetheless, under certain assumptions, an estimate of $|\mathcal{G}(j\omega)|$ can be expressed as a function of $\mathcal{G}_o$, ℓ and the process bandwidth ω_B.

Assumption 3.7 *The process bandwidth ω_B (in $rads^{-1}$) is much larger than the maximum absolute value of all the zeros and poles.*

Using the 3 dB point (Equation 3.10) as a reference and if Assumption 3.7 holds, the gain of the process at high frequencies ($\zeta\omega_B \gg \max(|z_1|, \ldots, |z_{nz'}|, |p_1|, \ldots, |p_{np'}|)$) can be written as

$$|\mathcal{G}(j\zeta\omega_B)| \simeq \frac{\mathcal{G}_o}{\sqrt{2}\,\zeta^\ell} \tag{3.21}$$

Note that at the 3 dB point ($\zeta = 1$), $|\mathcal{G}(j\omega_B)| = \frac{\mathcal{G}_o}{\sqrt{2}}$ and the gain rolls off at a rate of 20ℓ dB/decade. In general, the validity of Assumption 3.7 will be more likely if ℓ is small and zeros are present with magnitudes smaller than those of the poles.

If there are good reasons to rebut Assumption 3.7, another point in the bode diagram, $|\mathcal{G}(j\omega_h)|$, has to be selected instead to act as the reference where ω_h is much larger than the maximum absolute value of all the zeros and poles. The gain can then be rewritten as

$$|\mathcal{G}(j\zeta\omega_h)| \simeq \frac{|\mathcal{G}(j\omega_h)|}{\zeta^\ell} \tag{3.22}$$

3.3.8 Estimation of the measurement signal bandwidth

From the definition in Equation 3.3, the measurement bandwidth ω_s depends both on the upper bound of the measurement signal spectrum $[\Phi_s](\omega)$ and the measurement noise spectrum $\Phi_n(\omega)$. Techniques to estimate the various properties of $\mathcal{G}$ ($\mathcal{G}_o$, ω_B and ℓ), the 'worst' input spectrum $[\Phi_v](\omega)$ and the strength of measurement noise σ_n^2 are discussed in Sections 3.3.2 to 3.3.6. In addition, if Assumption 3.7 is satisfied, Equation 3.21 will provide an estimate of the gain of the process at high frequencies.

Consider the two typical input signals examined in Section 3.3.5 — a white noise input (Equations 3.15 and 3.16) and a step input (Equations 3.17 and 3.18), two corresponding dimensionless measures of signal-to-noise ratio are defined as follows:

$$\textbf{White noise input} \qquad \mathcal{R}_e = \frac{\mathcal{G}_o^2\,(\sigma_e^2)_m}{\sigma_n^2} \tag{3.23}$$

$$\textbf{Step input} \qquad \mathcal{R}_s = \frac{\mathcal{G}_o^2\,(\Delta v)_m^2}{\sigma_n^2} \tag{3.24}$$

where $\mathcal{G}_o$ is the process gain and σ_n^2 is the measurement noise level as discussed in Section 3.3.6. A guideline to select an estimate of the measurement signal bandwidth ω_s based on ω_B, ℓ and the signal-to-noise ratio ($\mathcal{R}_e$ or $\mathcal{R}_s$) can be formulated as:

Guideline 3.1 *If Assumptions 3.1, 3.3, 3.6 and 3.7 hold, the measurement signal bandwidth as defined in Equation 3.3 can be estimated to be*

$$\omega_s = \zeta\,\omega_B \tag{3.25}$$

where the multiplicative factor ζ is defined accordingly for the two typical input signals as:

$$\textbf{White noise input} \qquad \zeta = (5\,\mathcal{R}_e)^{\frac{1}{2\ell}} \tag{3.26}$$

$$\textbf{Step input} \qquad \zeta = \left(\frac{5\,\mathcal{R}_s}{\omega_B^2}\right)^{\frac{1}{2(\ell+1)}} \tag{3.27}$$

Adopting the equality condition in the definition of the measurement signal bandwidth (Equation 3.3), and combining with Equations 3.20 and 3.21, it can be shown that

$$\sigma_n^2 = \frac{5\,\mathcal{G}_o^2}{\zeta^{2\ell}}\,[\Phi_v](\zeta\omega_B) \tag{3.28}$$

where $\omega_s = \zeta\,\omega_B$ as in Equation 3.25. Consider the two typical input signals:

- **White noise input** — substituting Equations 3.16 and 3.23 into Equation 3.28 would lead to Equation 3.26.
- **Step input** — similarly, substituting Equations 3.18 and 3.24 into Equation 3.28 would result in Equation 3.27.

In addition, several points are worth noting here:

1. ω_B in Equation 3.27 must be expressed in $\mathrm{rad\,s^{-1}}$.
2. The inequality constraint in the definition of ω_s (Equation 3.3) will automatically be satisfied for the two input signals if Assumption 3.7 holds and $\zeta \geq 1$. Assumption 3.7 implies that the amplitude of the frequency response, $|\mathcal{G}(j\omega)|$, is a monotonic decreasing function for frequencies above the process bandwidth ($\omega \geq \omega_B$) if $\ell \geq 1$ (Assumption 3.6).
3. Guideline 3.1 will still provide a crude estimate of ω_s if Assumption 3.7 is violated. Alternatively, ω_s can be estimated by following a similar procedure using Equation 3.22 instead of Equation 3.21.
4. For input signals not belonging to any of the two typical categories, an estimate of ω_s can be obtained by substituting the specific $[\Phi_v](\zeta\omega_B)$ into Equation 3.28 and solving for ζ.
5. In some open loop environments or critical processes where the generalized input v is not under free manipulation, comprehensive tests are prohibited and the entire set of the required information ($\mathcal{G}_o$, ω_B, ℓ, $[\Phi_v](\omega)$ and σ_n^2) may not be available. Then, the measurement signal bandwidth ω_s has to be estimated from representative spectra of the measurement output, $\Phi_y(\omega)$, by inspecting the 'break-off' points from

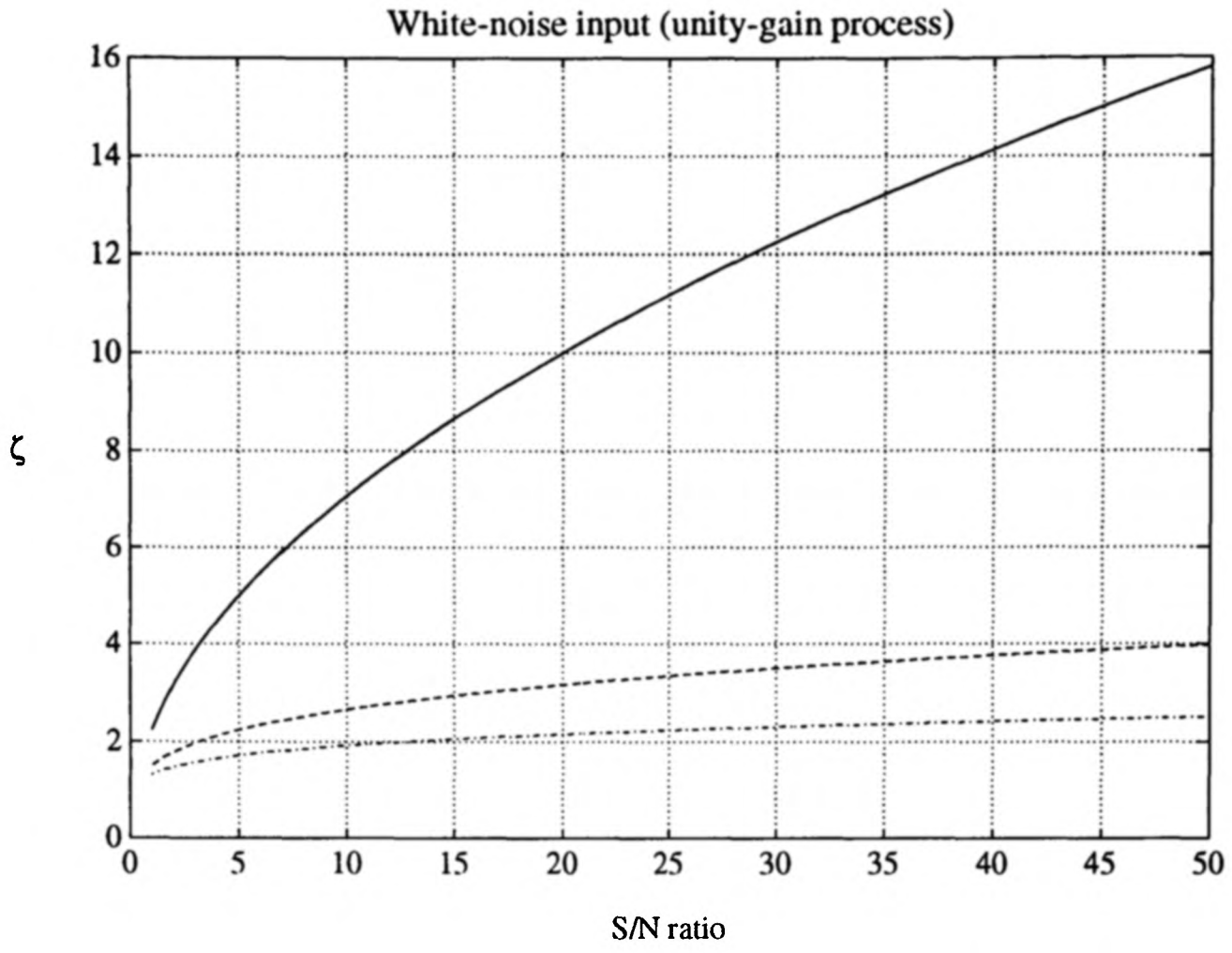

Figure 3.3: Estimation of the measurement signal bandwidth with white noise input (solid: $\ell = 1$, dashed: $\ell = 2$, dashdot: $\ell = 3$)

the relatively constant measurement noise level at high frequencies. A safety factor can be introduced if more exciting inputs are expected.

Example 3.1

Consider a generalized process $\mathcal{G}$ subject to stochastic white noise input (Equation 3.15). From Equation 3.26 in Guideline 3.1, the measurement signal bandwidth can be estimated to be $\omega_s = \zeta\,\omega_B$ where

$$\zeta = (5\,\mathcal{R}_e)^{\frac{1}{2\ell}} \tag{3.29}$$

A plot of ζ versus the signal-to-noise ratio $\mathcal{R}_e$ defined in Equation 3.23 for $\ell = 1$, 2 and 3 is depicted in Figure 3.3.

Suppose $\mathcal{R}_e = 10$, the estimated measurement signal bandwidth is given by

ℓ	1	2	3
ω_s	$7.1\,\omega_B$	$2.7\,\omega_B$	$1.9\,\omega_B$

(3.30)

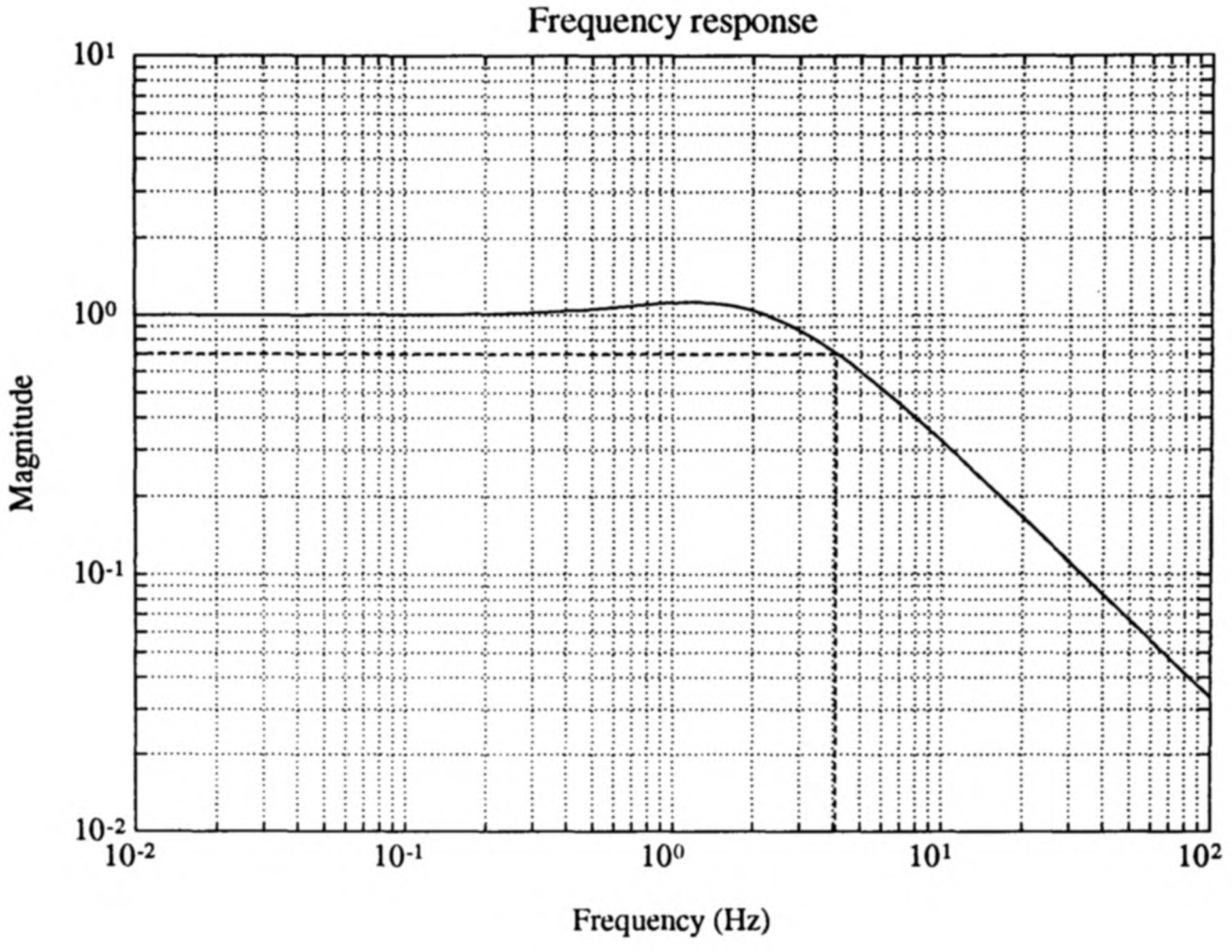

Figure 3.4: Bode plot of $\mathcal{G}$ defined in Equation 3.31

Example 3.2

Consider again System II in Example 2.1 in which the closed loop transfer function is given by

$$\mathcal{G}(s) = \frac{21s + 121}{(s+11)^2} \tag{3.31}$$

A bode plot of $\mathcal{G}$ is illustrated in Figure 3.4 and the process bandwidth ω_B is estimated to be 4.08 Hz (25.64 rads^{-1}). It is apparent that $\mathcal{G}_o = 1$ (unity gain) and $\ell = 1$ (one zero and two poles). From Equation 3.27 in Guideline 3.1, assuming the generalized process is subject to staircase-type inputs with a maximum step change of $(\Delta v)_m$, the measurement signal bandwidth can be estimated to be $\omega_s = \zeta\,\omega_B$ where

$$\zeta = \left(\frac{5\,\mathcal{R}_s}{(2\,\pi\,4.08)^2}\right)^{\frac{1}{4}} \tag{3.32}$$

A plot of ζ versus the signal-to-noise ratio $\mathcal{R}_s$ defined in Equation 3.24 is shown in Figure 3.5.

Suppose the noise level $\sigma_n^2 = 10^{-4}$ and $(\Delta v)_m = 1$. Then[9], $\mathcal{R}_s = 10^4$ and the measurement signal bandwidth can be estimated from Figure 3.5 as $\omega_s = 2.95\,\omega_B$.

[9] $\mathcal{R}_s$ is generally orders of magnitude greater than $\mathcal{R}_\epsilon$ because of their respective definitions.

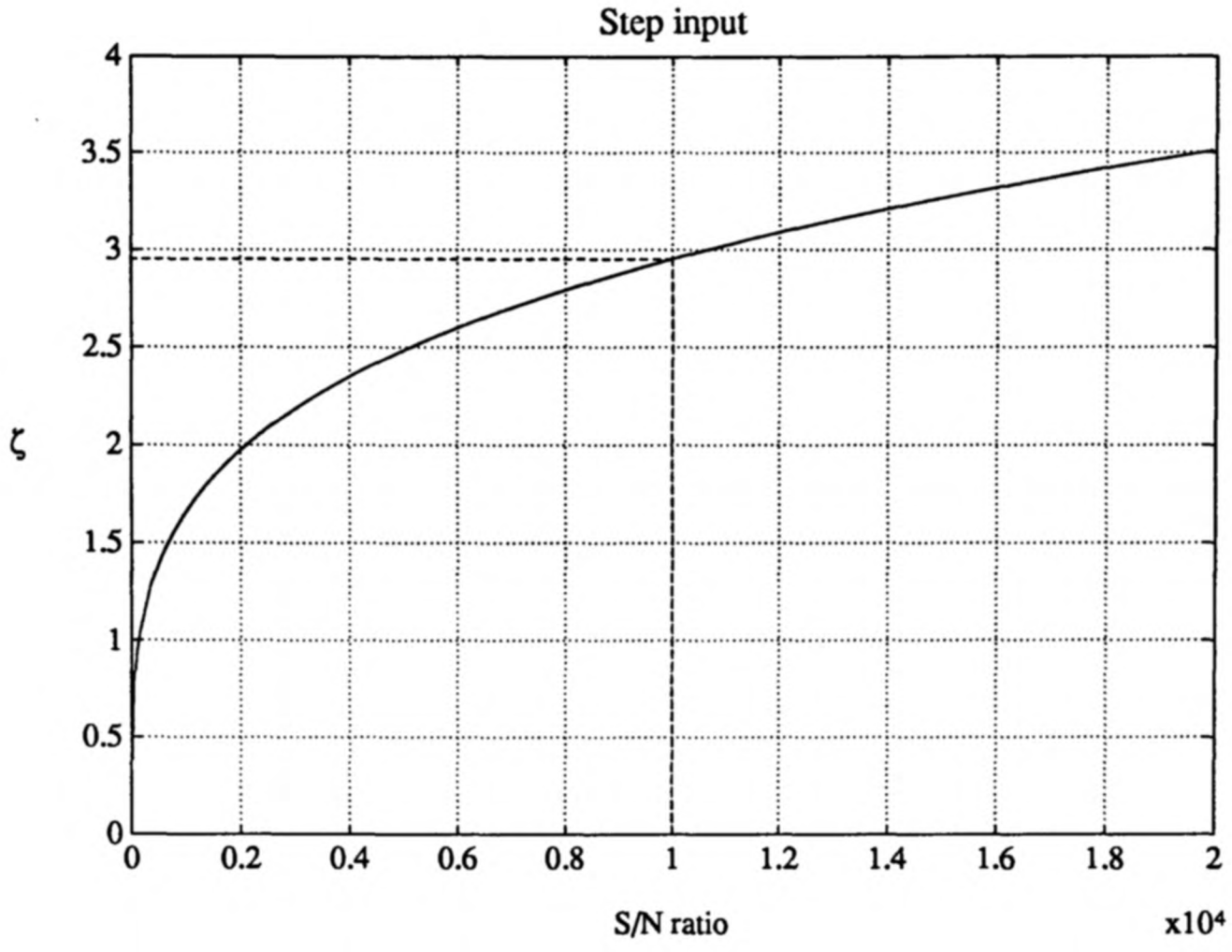

Figure 3.5: Estimation of the measurement signal bandwidth with step input

3.4 Sensor signal conditioning and acquisition

Before being validated in a digital processor, the sensor output has to be properly conditioned and converted into its digital equivalent. Sensor signal conditioning and digitization are commonplaces in communication, speech analysis, signal processing, control and instrumentation. A brief overview is highlighted in this section. More detail references can be found in Barney [1985], Doebelin [1983], Jones [1977], Mylroi [1984], Parr [1986] and Sydenham [1983].

Amplification Transducers with low output levels, such as thermocouples and strain gauge bridges (e.g. load cells, accelerometers) should be amplified to levels compatible with industrial standards in data conversion and communication (i.e. 0 – 10 V or 4 – 20 mA).

Compensation Parasitic defects in sensors should be corrected to eliminate offsets and drifts, e.g. cold junction compensation in thermocouples, as well as removal of temperature and static pressure effects in differential pressure transmitters [Brignell and Dorey, 1983; Brignell, 1987].

Linearization Inherent nonlinearities in sensor measurement should be appropriately removed. This can be achieved either in the analog or the digital domain. A few of the well-known techniques are as follows:

- Direct inversion of a known nonlinear function (e.g. square root extraction in an orifice flowmeter [Doebelin, 1983, Section 2.7]);
- Curve fitting (e.g. 5th order polynomial fitting to the thermocouple output [Metrabyte, 1986, Section 8]);
- Calibration lookup table (e.g. linearization of an electro-optical pressure sensor from calibration data stored at a local PROM[10] [Doebelin, 1983, Sections 6.4 and 10.9]).

Anti-aliasing filter An essential, though often overlooked, prerequisite for successful digitization is a good design of the analog anti-aliasing filter to suppress signal components above the Nyquist frequency. A simple RC network[11] is generally sufficient [Clarke, 1983]. For an application with stringent requirements, a customized active filter chip can be employed [Tsang, 1989]. Nevertheless, at low sampling frequencies, the passive components become unreliable and the performance of the filter deteriorates. Alternative techniques using digital filtering will be presented in Section 3.6.2.

Analog-to-digital conversion Digitization of analog signal will inevitably introduce quantization errors. Inadequate resolution will degrade the performance of any validation scheme. Methods of increasing the resolution of an analog-to-digital converter will be discussed in Section 3.6.3.

Calibration Digital sensor output should be scaled to an appropriate engineering or scientific unit for convenient manipulation and interpretation.

3.5 Choice of sampling frequency

The selection of a proper sampling rate is of fundamental importance to the success of the local sensor validation scheme. Unfortunately, there is no fixed or universally applicable

[10]PROM means Programmable Read Only Memory.

[11]RC denotes resistor-capacitor.

set of rules. It depends essentially on the purpose of the application and the various constraints therein. The minimal requirement is laid down in the Shannon Sampling Theorem [Bendat and Piersol, 1986, Section 10.3]. It states that if an ideal continuous-time signal is bandlimited by a maximum frequency ω_{max}, the minimum sampling frequency for digitization is given by $2\omega_{max}$ for the signal to be completely reconstructed. Åström [1969] derived the optimal sampling rates for the identification of Gauss-Markov time-series. Moreover, some yardsticks are provided in Åström and Wittenmark [1984, Section 3.7] for choosing sampling periods in closed loop systems under digital control. It is suggested that reasonable sampling periods are $0.25 - 0.5\ T_r$ where T_r is the rise time[12] of the system (for a first order system, this corresponds to a sampling rate of $2 - 4\ \omega_B$ Hz). Clarke [1983] discussed the problems of exceedingly small sampling periods encountered in digital control.

In contrast to a closed loop control system in which the frequency range of interest concentrates at the lower values around the process bandwidth ω_B, the local sensor validation scheme is tuned to monitor signal characteristics beyond the sensor signal bandwidth ω_s (Section 2.7). This immediately necessitates a much faster sampling rate than those suggested above for a closed loop control system. Nevertheless, the validation scheme may need to pass on information at a slower rate to avoid excessive loading at the next higher level. An appropriate technique to achieve this objective will be examined in Section 3.6.1. Generally, a shorter sampling period will lead to a faster failure detection. However, practical constraints, such as computational capabilities, will often impose a cap on the maximum attainable sampling rate. A compromise has to be reached and a rule of thumb for the sampling rate selection is given by

Guideline 3.2 *The sampling rate f_m of the local sensor validation scheme should be*

$$f_m = \frac{\omega_m}{2\pi} > \frac{10\,\omega_s}{\pi} \tag{3.33}$$

where ω_s is the sensor signal bandwidth.

It is straightforward to show that Guideline 3.2 implies that $\omega_s < 0.05\,\omega_m$. For a typical value of $\zeta = 10$ (recall $\omega_s = \zeta\,\omega_B$), $f_m > \frac{100\,\omega_B}{\pi}$, which also implies that the sampling rate of the validation scheme is at least 10 times that suggested for the closed loop digital control system.

[12]Refer to Åström and Wittenmark [1984, Section 6.6] for an explanation of rise time T_r.

3.6 Decimating filter

In Sections 3.4 and 3.5, three practical problems are raised during the commissioning of the local sensor validation scheme, viz.

- suitable interfacing of information flow between the local validation scheme and the next higher level which usually operate at different optimal sampling frequencies (Section 3.5),
- stringent design specification on the analog anti-aliasing filter such as sharp cut-off and low sampling rate (Section 3.4),
- inadequate resolution in the analog-to-digital converter which introduces unacceptably large quantization errors (Section 3.4).

Decimating filter, a popular tool in audio signal processing [van den Enden and Verhoeckx, 1989, Chapter 14], is well posed to tackle all the three problems mentioned above.

3.6.1 Signal downsampling in a multirate system

As discussed in Section 3.5 and Guideline 3.2, the local sensor validation scheme is usually operated at a much faster sampling frequency and any validated sensor output and associated information has to be downsampled to a rate compatible with the next higher level in the hierarchy (e.g. a digital control loop).

Suppose a digital signal $x(t)$ sampled at a rate of Nf_m Hz has to be downsampled by an integral factor[13] N to give an output signal $y(t)$ at a rate of f_m Hz. A tempting approach is simply to take one out of every N samples of $x(t)$ which is basically the operation of a sample rate decreaser [Oppenheim *et al.*, 1983, Section 8.7]. Nonetheless, from Shannon Sampling Theorem, the spectrum of the original signal $\Phi_x(f)$ covers a fundamental interval of $0 \leq f \leq \frac{Nf_m}{2}$ Hz while that of the output $\Phi_y(f)$ covers a narrower band of $0 \leq f \leq \frac{f_m}{2}$ Hz. Any spectral components in $\Phi_x(f)$ for $\frac{f_m}{2} \leq f \leq \frac{Nf_m}{2}$ Hz will be aliased into the output signal. Aliasing can be prevented by cascading a digital filter in front of the sample rate decreaser to cut off frequency components of the input beyond

[13] Downsampling by a rational factor can be achieved by a combination of oversampling and downsampling [van den Enden and Verhoeckx, 1989, Section 9.6].

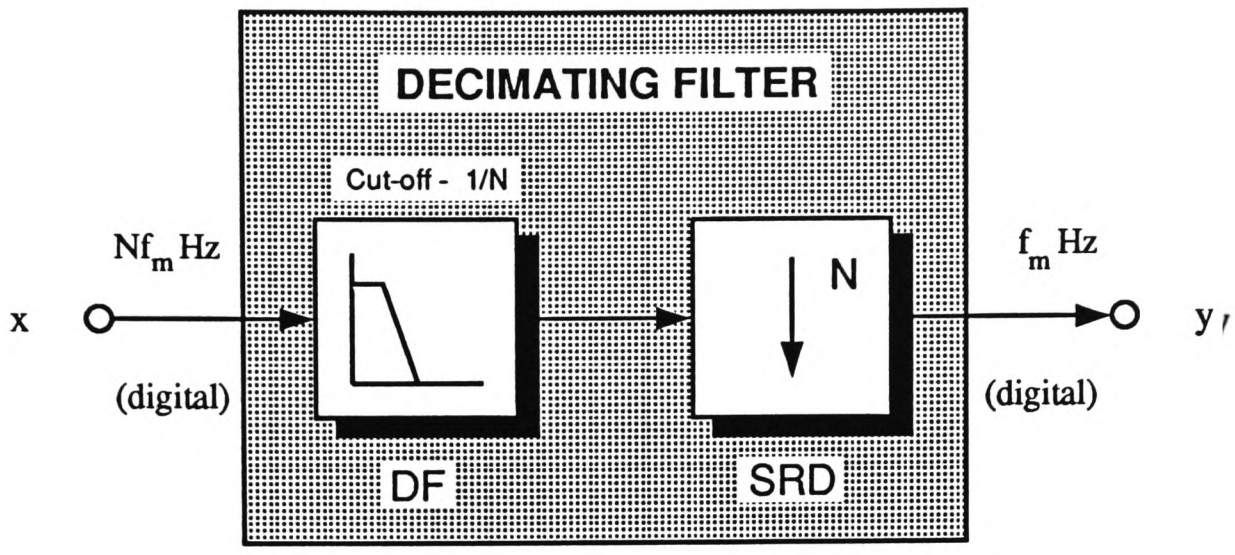

Figure 3.6: A schematic diagram of a decimating filter

$\frac{f_m}{2}$ Hz. The combination of a digital filter (DF) and a sample rate decreaser (SRD) is known as a *decimating filter* [van den Enden and Verhoeckx, 1989, Section 9.2]. A schematic representation of a decimating filter is shown in Figure 3.6. Typically, the digital filter is chosen to be a finite impulse response (FIR) filter which has either symmetric or antisymmetric impulse responses. This class of filters have a special property of exact linear phase characteristics (i.e. signal components at different frequencies are delayed by an identical amount) and thus the filtered signal will not be distorted. However, compared with an infinite impulse response (IIR) filter, FIR filter demands an appreciably higher order to achieve the same specified magnitude response, thereby requiring more storage space for filter coefficients.

3.6.2 Digital versus analog anti-aliasing filter

Anti-aliasing filter is of prime importance in analog-to-digital conversion. The conventional approach is to design an analog lowpass filter to suppress signal components above the Nyquist frequency. However, at low sampling frequencies, analog components become unreliable and the overall filter performance deteriorates. An alternative is to keep a reasonably high sampling rate in the initial digitization stage to alleviate the complication of analog anti-aliasing filter design and then to decimate the digitized signal to the desired sampling frequency. In this way, signals exceeding the ultimate Nyquist frequency are intentionally leaked (but *not* aliased) through the analog-to-digital converter and subsequently removed digitally by the decimating filter, i.e. analog filtering is exchanged for digital filtering. This is motivated by the fact that digital filters not only can meet more

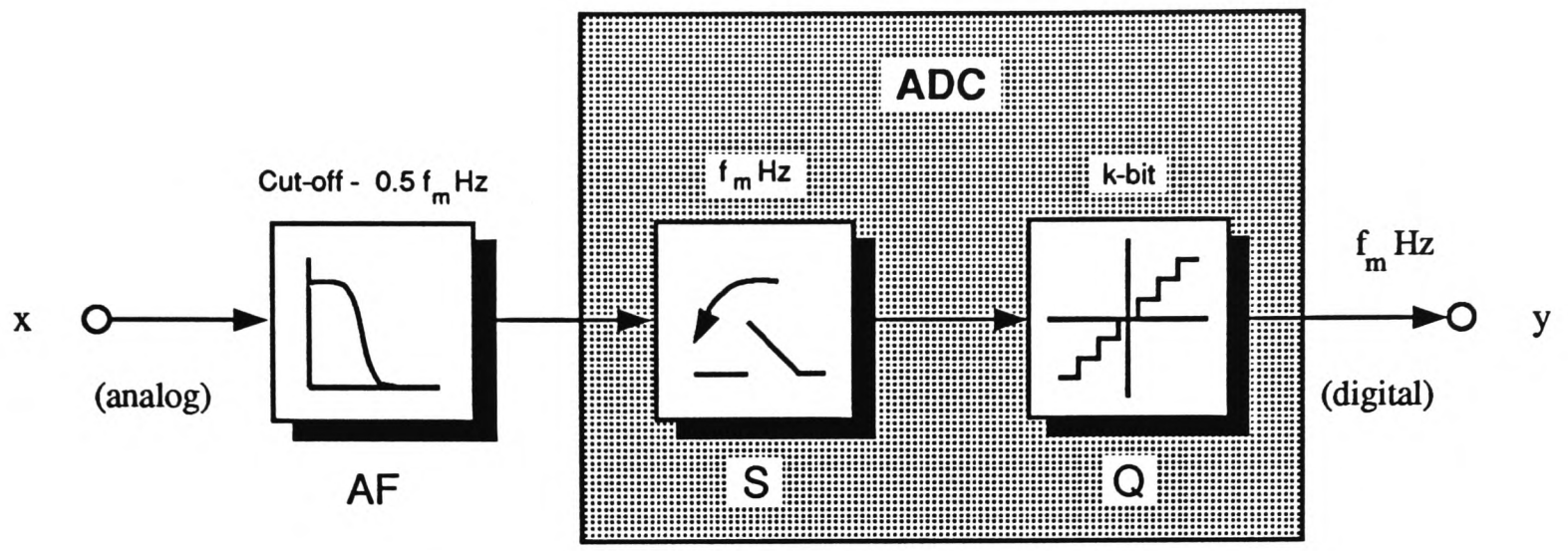

Figure 3.7: Typical setup of analog-to-digital conversion

stringent specification such as narrower transition band and sharper cut-off, but they can also be designed to have a linear phase property which minimizes signal distortion.

3.6.3 Increasing resolution in quantization

Typically, an analog signal is first passed through an analog anti-aliasing filter (AF) before being converted to its digital equivalent in an analog-to-digital converter (ADC). The ADC is composed of a *sampler* (S) to digitize the signal at a prescribed frequency and a *quantizer* (Q) to allocate the values of the signal into discrete levels. A conventional setup of analog-to-digital conversion is depicted in Figure 3.7.

A quantizer is specified primarily by the number of bits of resolution k and its permissible input range $\pm R$. It partitions the input into 2^k discrete levels with a quantization step of

$$\Delta = \frac{2R}{2^k} = \frac{R}{2^{k-1}} \tag{3.34}$$

The finite number of discrete quantized levels inevitably introduces quantization errors in the output. Provided that the input signal does not saturate the quantizer, the quantization process can be regarded as an addition of a stochastic signal ϵ_Q (Figure 3.8). ϵ_Q is the *quantization noise* which is the difference between the discretized output and the original input. In practice, ϵ_Q can generally be assumed to be uncorrelated and uniformly distributed between $\pm\frac{\Delta}{2}$. Its variance provides another quantitative measure on the resolution of the quantizer.

The performance of any validation scheme depends heavily on the quality of the dig-

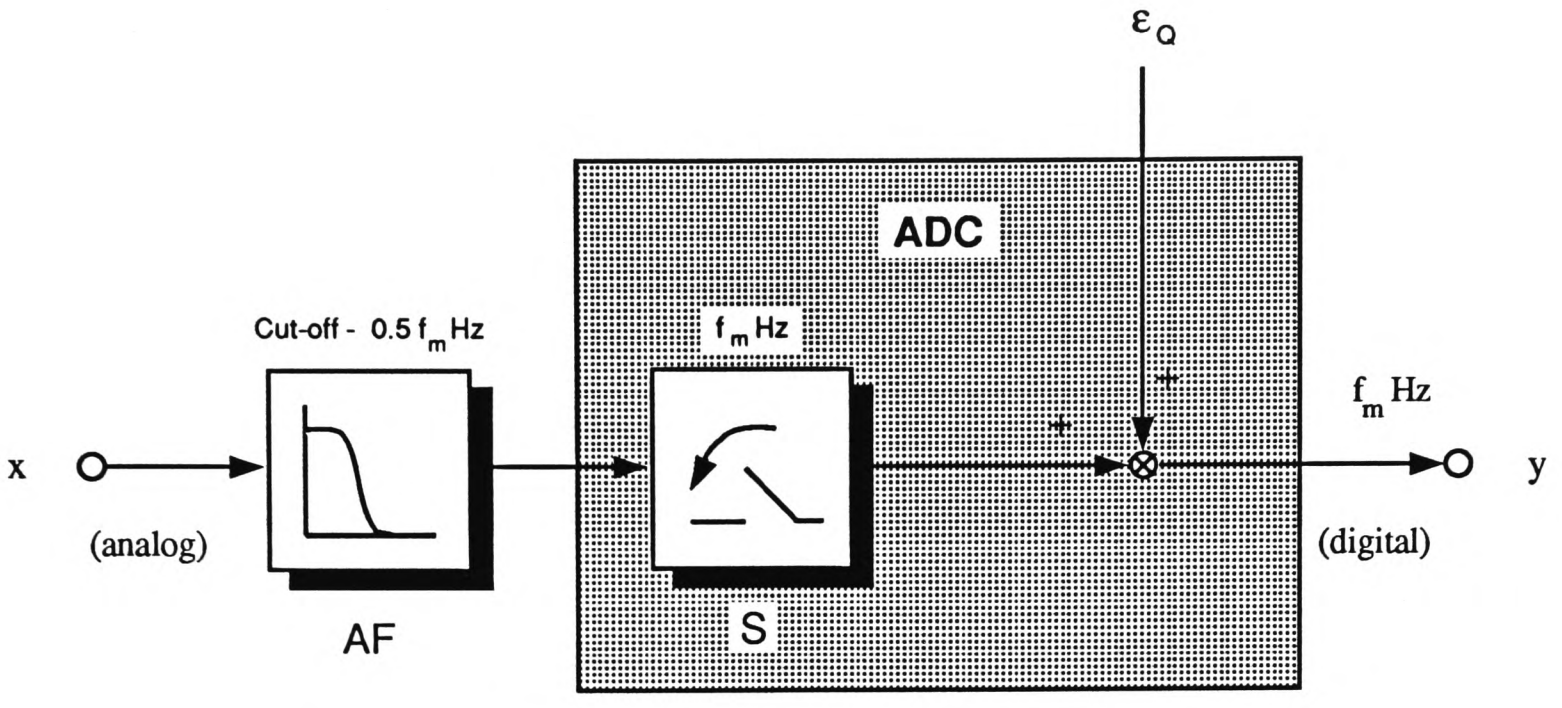

Figure 3.8: Analog-to-digital converter with quantization noise ϵ_Q

itized sensor output and hence adequate resolution is imperative. Several techniques to increase the resolution of the ADC are summarized as follows:

- *Installing a higher resolution ADC*

  The most direct, but also the most expensive, solution is to install a new ADC with more bits ($k' > k$) of resolution. This is a good 'once and for all' answer if the ADC is dedicated to a set of inputs requiring the particular level of resolution. However, this method is uneconomical if the ADC has to be used in a variety of environments and in the majority of cases only a lower resolution (k bits) is necessary.

- *Scaling the input signal (Figure 3.9(a))*

  If the range of the analog input covers only a small subset of the discrete levels in the quantizer, most of the dynamic information of the input will be lost resulting in a coarse digital output with considerable quantization errors. A remedy is to scale up the analog signal $x(t)$ by K where $K = \min\left(\left|\frac{R}{x_{min}}\right|, \left|\frac{R}{x_{max}}\right|\right)$ and to scale down the digital output from the ADC proportionally. The variance of the quantization noise is then effectively reduced by a factor of $\frac{1}{K^2}$. For high precision conversion, this demands a stable analog scaling circuit with accurate trimming. Moreover, this method is not applicable for signals with substantial d.c. offset but minimal variations because the quantizer will be saturated by even a small K.

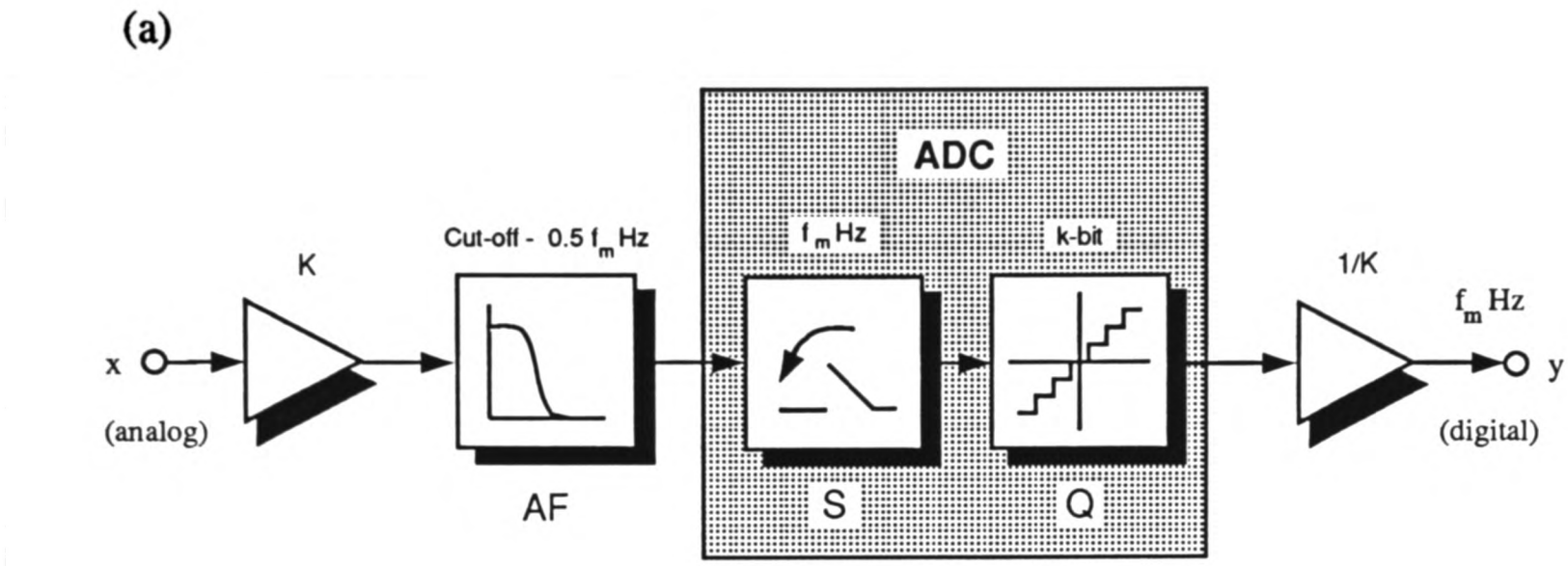

Figure 3.9: Some techniques to increase the resolution of the ADC

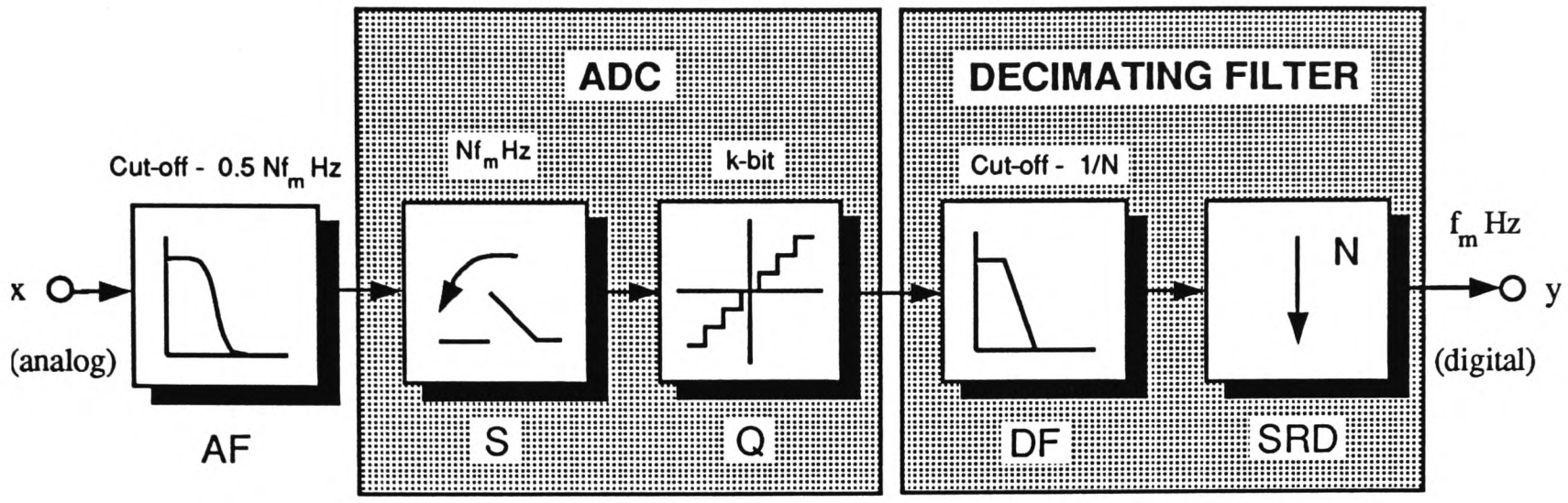

Figure 3.10: Increasing ADC resolution by a decimating filter

- *Scaling the a.c. component of the input (Figure 3.9(b))*
  For input with an ample average value, an alternative is to separate the signal into the d.c. and the a.c. components by appropriate filtering and discretized them individually. Only the a.c. component is scaled in an attempt to increase the resolution of the dynamic information without being saturated by the d.c. offset. However, this introduces additional complications in the analog filter design and in particular, the synchronization of the two filtered components.

An efficient way to enhance the resolution of the ADC is to increase the initial sampling rate intentionally by a factor of N and then downsample the digital signal to the final rate by a *decimating filter* (Figure 3.10). Generally speaking, the faster the initial sampling rate, the more information is available and the better the prediction will be at the downsampling process, and effectively a higher resolution can be achieved. In short, sampling rate, which is seldom a critical criterion in process industries, is traded for resolution. An overwhelming advantage of this approach is that no new hardware (e.g. a better ADC, analog filters or scaling circuits) is required and all additional processing can be carried out digitally in software. It is immune to the d.c. offset problem and the shape of the signal can be preserved (Section 3.6.1). Moreover, it is extremely flexible and can be easily reconfigured to 'any'[14] resolution by varying a single parameter N. The relationship between N and the increase in resolution is discussed in Property 3.1.

[14]See the discussion in Property 3.1.

Property 3.1 *Assuming that the analog input signal to be bandlimited by the Nyquist frequency (defined by the ultimate sampling rate) and the quantization noise of the analog-to-digital converter to be uncorrelated and uniformly distributed, an ideal decimating filter will provide effectively (in a mean square sense) an extra bit of resolution in the digital output signal for every four-fold increase in the initial sampling rate.*

Recall Equation 3.34, the quantization step of a k-bit ADC with an input range of $\pm R$ is given by

$$\Delta = \frac{R}{2^{k-1}} \tag{3.35}$$

Under the assumption that the quantization noise ϵ_Q is uniformly distributed between $-\frac{\Delta}{2}$ and $\frac{\Delta}{2}$, its probability density function $f(\epsilon_Q)$ is $\frac{1}{\Delta}$. Hence, the variance of the quantization noise can be written as

$$\begin{aligned}
\sigma^2_{\epsilon_Q} &= \int_{-\infty}^{\infty} f(\epsilon_Q)\, \epsilon_Q^2\, d\epsilon_Q \\
&= \int_{-\frac{\Delta}{2}}^{\frac{\Delta}{2}} \frac{1}{\Delta}\, \epsilon_Q^2\, d\epsilon_Q \\
&= \frac{\Delta^2}{12} \\
&= \frac{1}{3}\frac{R^2}{2^{2k}}
\end{aligned} \tag{3.36}$$

It has to be noted that the variance of the quantization noise at the ADC output is independent of the initial sampling frequency Nf_m Hz. As ϵ_Q is further assumed to be uncorrelated, its power spectrum $\Phi_{\epsilon_Q}(\omega)$ is constant over the entire fundamental frequency interval of $-\frac{Nf_m}{2}$ Hz to $\frac{Nf_m}{2}$ Hz.

An ideal decimating filter has an ideal lowpass digital filter with an infinitely sharp cut-off at the ultimate Nyquist frequency of $\frac{f_m}{2}$ Hz. Since the original analog signal is assumed to be bandlimited by $\frac{f_m}{2}$ Hz, the digital filter will only suppress the quantization noise ϵ_Q and the spectrum of the filtered noise $\Phi_{\epsilon_{Q_f}}(\omega)$ will then span between $-\frac{f_m}{2}$ Hz and $\frac{f_m}{2}$ Hz. Parseval's Theorem states that the variance of a signal is proportional to the area under the power spectrum. Therefore, the variance of the quantization noise at the decimating filter output is reduced to

$$\sigma^2_{\epsilon_{Q_f}} = \frac{1}{N}\sigma^2_{\epsilon_Q} = \frac{1}{3N}\frac{R^2}{2^{2k}} \tag{3.37}$$

If $N = 4^r$,

$$\sigma^2_{\epsilon_{Q_f}} = \frac{1}{3}\frac{R^2}{2^{2(k+r)}} \tag{3.38}$$

Comparing with Equation 3.36, this is equivalent to the output from a $(k+r)$ bit ADC. It then follows that for every four-fold increase in the initial sampling rate, there is effectively an extra bit of resolution in the digital output.

In practice, there are a few constraints in the actual improvements of resolution:

- The lowpass filter within the decimating filter will not be ideal;
- The quantization noise ϵ_Q will inevitably be correlated if the initial sampling frequency becomes too high;
- There will be no improvement at all if the range of the analog signal is less than the quantization step Δ (analog signal must be scaled).

Hence, Property 3.1 can be considered to be providing an *upper bound* in the increase in ADC resolution by a specified increase in initial sampling rate. The last two constraints can be significantly relaxed by the addition of a small random signal, commonly known as dither[15], to the original analog input [Schuchman, 1964; Wagdy, 1989]. However, there is an associated price to be paid for the implementation of analog summing and dither-generation circuits. A more elaborated type of oversampling filter, known as the *delta-sigma modulator*[16], has become commercially available as a single chip [Agrawal and Shenoi, 1983; Candy and Temes, 1992].

Example 3.3

This simulated example illustrates Property 3.1 and highlights the achievable increase in resolution with a decimating filter. A 'pseudo' analog signal $s(t)$ is simulated by sampling a stochastic signal at 64 Hz. $s(t)$ is normalized by

$$s(t) = \frac{\tilde{s}(t)}{\max(|\tilde{s}(t)|)} \tag{3.39}$$

and the stochastic signal $\tilde{s}(t)$ is given by

$$\tilde{s}(t) = F(q^{-1})\, e(t) \tag{3.40}$$

where $e(t)$ is a random noise uniformly distributed between ± 0.5 and $F(q^{-1})$ is a 6th order Chebyshev lowpass filter with a cut-off frequency at 0.13 Hz (to bandlimit the analog signal). The ultimate sampling rate required is 1 Hz.

[15] Refer to Section 3.11 for a novel application of dithering.

[16] Also known as the sigma-delta modulator.

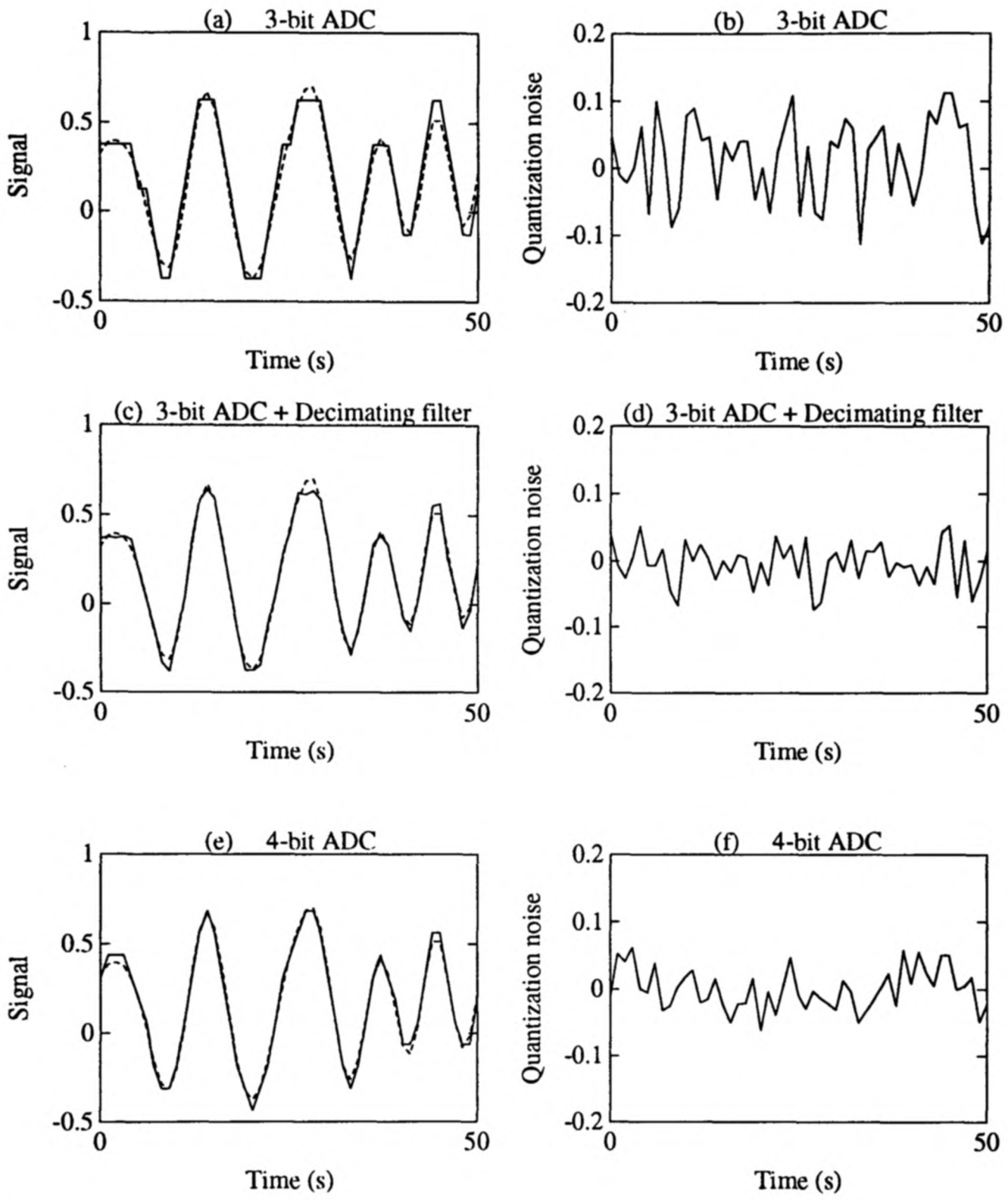

Figure 3.11: Low resolution discretization (original analog signal is represented by a dashed line in (a), (c) and (e))

A low resolution discretization is first carried out so that the quantization effects will be clearly visible in the digital outputs. The analog signal is discretized by a 3-bit ADC (i.e. eight discrete levels) with an input range of ± 1 at both 1 Hz and 4 Hz. For the oversampled (4 Hz) signal, the assigned sampling rate (1 Hz) is restored by a decimating filter with a 400th order symmetric FIR lowpass filter[17]. Both the digitized signals and the quantization noise (the difference between the digital output and the known 'pseudo'

[17]Designed by the classical windowed method [IEEE, 1979, Algorithm 5.2].

analog input[18]) are shown in Figure 3.11(a)–(d). The coarse discrete levels due to the 3-bit ADC are evident in Figure 3.11(a). The combination of oversampling and decimating does improve the discretization process (Figure 3.11(c)) and, as expected, the variance of the quantization noise is down by a factor of 4. The results from a 4-bit ADC are given in Figure 3.11(e) and (f) for comparison.

A more practical 8-bit ADC is employed to demonstrate the increases in the effective resolution for a decimating filter with various oversampling rates. The 'pseudo' analog signal $s(t)$ is initially sampled at N Hz ($N = 1, 4, 16,$ and 64). The variances of the quantization noise are then compared with those from idealized ADCs with various bits of resolution. The results are summarized in Figure 3.12. It is obvious that under favourable conditions, for every four-fold increase in initial sampling rate, there is effectively an extra bit of resolution.

3.7 Sensor signal decomposition

After the analog sensor signal has been properly conditioned and digitized at the appropriate sampling rate, the next crucial procedure is to decompose the sensor output y, based on the estimate of the sensor signal bandwidth ω_s, into *two* components:

$$y = \bar{y} + \tilde{y} \tag{3.41}$$

where $\bar{y}$ consists 'predominantly' of the measurement signal and $\tilde{y}$ of the measurement noise. It is the decomposed signals $\bar{y}$ and $\tilde{y}$ that the subsequent detection scheme primarily monitored. Hence, a well-designed decomposition algorithm is of utmost importance to the success of the local sensor validation scheme.

3.7.1 Optimal filtering

The problem of signal decomposition is encountered in any physical or engineering process involving noisy measurements. In particular, the extraction (or estimation) of the original signal $s(t)$ from a measurement $y(t)$ corrupted by additive noise $n(t)$ has been under active research within the field of '*optimal filtering*'. In summary, the estimate of the signal $\bar{y}$

[18]The delay of 200 samples introduced by the FIR filter has to be taken into account before the computation of the quantization noise.

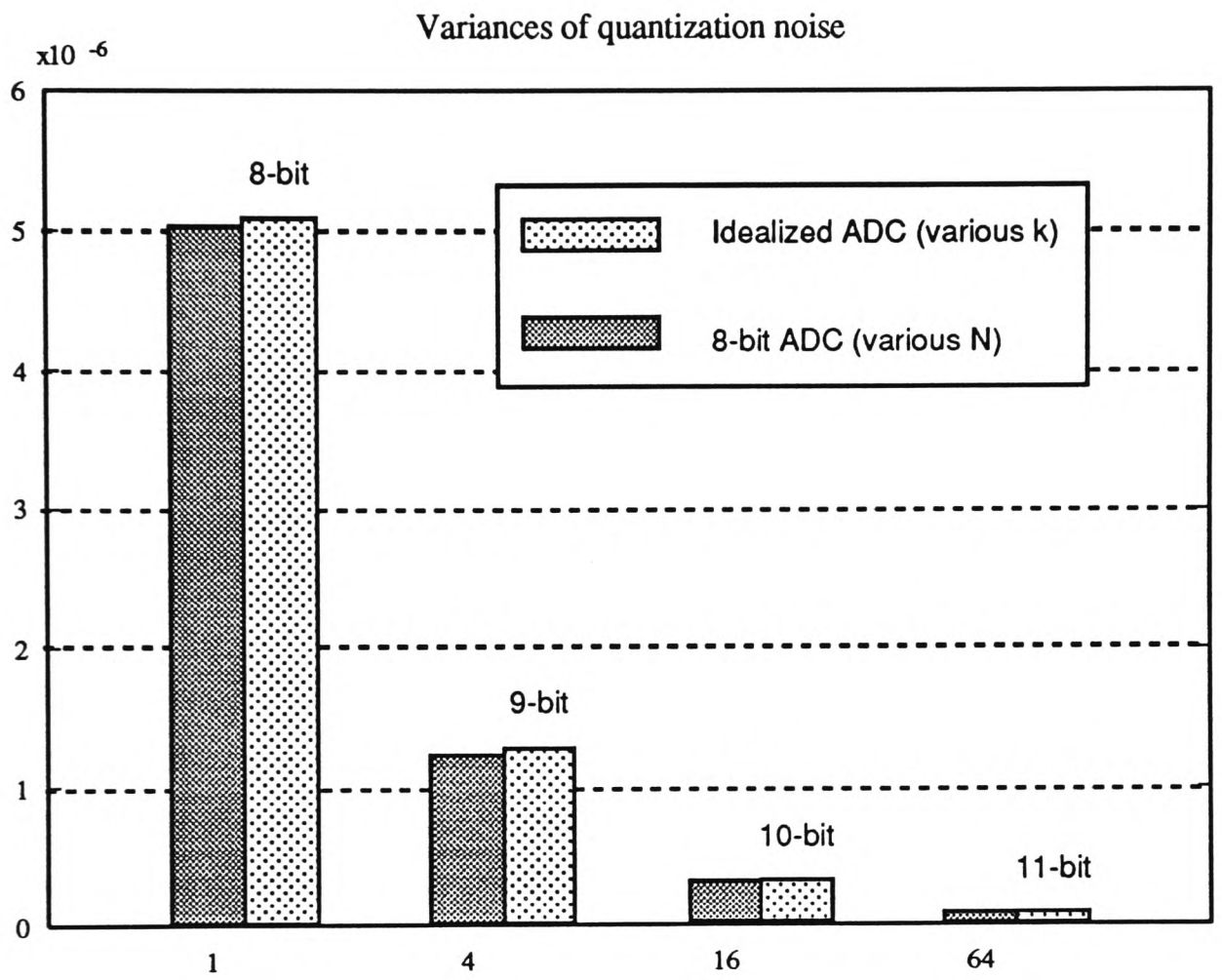

8-bit ADC with decimating filter				
N(Hz)	1	4	16	64
$\sigma^2_{\epsilon_{Q_f}}(10^{-6})$	5.0279	1.2182	0.3043	0.0799
Idealized ADC				
k (bits)	8	9	10	11
$\sigma^2_{\epsilon_Q}(10^{-6})$	5.0863	1.2716	0.3179	0.0795

Figure 3.12: Variances of quantization noise with various initial sampling rates

is taken to be the output of a filter L optimized with respect to a specific criterion and under certain assumptions on $s(t)$ and $n(t)$. Although the design of optimal filters to estimate the noise component receives much less attention in literature, the general idea is very similar. Three classical approaches in optimal filtering are summarized as follows:

- **Matched filter** [Papoulis, 1984, Section 10.5]
  The original signal $s(t)$ is assumed to be known while the noise $n(t)$ is taken to be a stationary random variable with a known spectrum. The filter L is optimized subject to the criterion that the filter output will yield a maximum signal-to-noise ratio.

- **Wiener filter** [Mohanty, 1987, Section 3.10]
  The signal $s(t)$ and the noise $n(t)$ are both assumed to be stationary stochastic signals with known spectra. The optimal filter is then designed to minimize the mean-square output estimation errors.

- **Model-based filter** [Candy, 1986]
  There is a large variety of algorithms under this category depending, among others, on the assumed model of the signal $s(t)$. The model can be in an input-output framework (e.g. the Box-Jenkins filter) or in its state-space equivalent (e.g. the Kalman filter).

All the three signal decomposition methods mentioned above have some shortcomings when applied to local sensor validation: a matched filter is infeasible since the measurement signal $s(t)$ is generally unknown a priori; the design of a Wiener filter is impeded by the unavailability of the exact spectral characteristics of the signal and the noise; and as discussed in Section 2.1, the construction of a detailed input-output (or state space) model is both uneconomical and unreliable which inhibits the applicability of the model-based filters at a local level. Nevertheless, the Wiener filter approach is the most promising among the three. Not only can the spectral features of the signal and the noise be estimated in certain circumstances, but it also contributes valuable insights into the design of non-optimal decomposition filters for general applications.

3.7.2 Signal decomposition by Wiener filtering

The prime objective of a conventional Wiener filter is to acquire an optimal estimate of an unknown signal $s(t)$ from a measurement $y(t)$ corrupted by random noise $n(t)$.

The underlying assumption is that the signal $s(t)$ and the noise $n(t)$ are uncorrelated[19] stationary stochastic signals with known spectra $\Phi_s(\omega)$ and $\Phi_n(\omega)$ respectively. The Wiener filter $L_w(s)$ is designed such that the signal estimate is given by

$$\bar{y}(s) = L_w(s)\, y(s) \tag{3.42}$$

and the mean-square output estimation error $E\left[(\bar{y}(t) - s(t))^2\right]$ is a minimum. The solution is well-known (e.g. [Mohanty, 1987, Section 3.10]) and the optimal filter is usually formulated in the frequency domain as

$$L_w(j\omega) = \frac{\Phi_s(\omega)}{\Phi_s(\omega) + \Phi_n(\omega)} \tag{3.43}$$

In local sensor validation, there is a dual problem of decomposing the noise component as well as the signal component. It is straightforward to show that the optimal filter $H_w(s)$ for the extraction of the noise fraction, known here as the inverse Wiener filter, can be solved in a similar fashion,

$$\tilde{y}(s) = H_w(s)\, y(s) \tag{3.44}$$

where

$$H_w(j\omega) = \frac{\Phi_n(\omega)}{\Phi_s(\omega) + \Phi_n(\omega)} \tag{3.45}$$

The determination of the optimal filters L_w and H_w depends entirely on the exact knowledge of the signal and noise spectra ($\Phi_s(\omega)$ and $\Phi_n(\omega)$) which is rarely available in practice. Nonetheless, adequate estimates of the two spectra can sometimes be found from the spectrum of the measurement output. Since the signal and the noise are assumed to be uncorrelated, the measurement spectrum $\Phi_y(\omega)$ represents the aggregate of the signal and the noise spectra

$$\Phi_y(\omega) = \Phi_s(\omega) + \Phi_n(\omega) \tag{3.46}$$

In many applications, the spectral signature of the signal will stand appreciably above the background noise level at low frequencies (Assumption 3.6). A reasonable curve[20] $\hat{\Phi}_n(\omega)$ can be fitted to the noise-dominant portion (usually at high frequencies above the signal bandwidth ω_s) and extrapolated back into the signal-dominant regime. The difference

[19] The proposed model of the sensor output (Figure 2.3) ensures that the measurement signal and the measurement noise remain uncorrelated even under a closed loop environment (Assumption 3.4).

[20] The noise spectrum is often relatively smoother and can be estimated by a straight line or a low order polynomial.

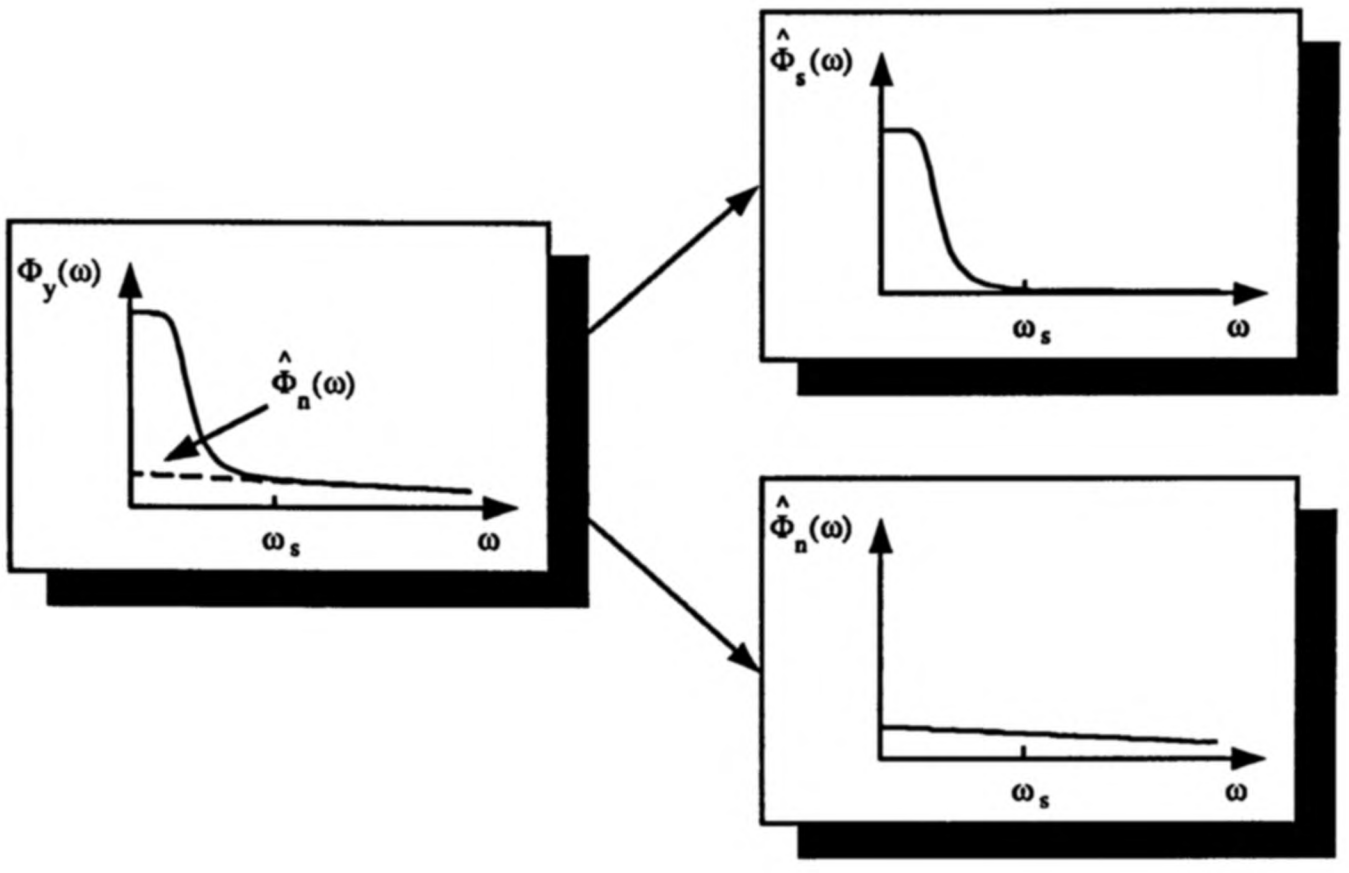

Figure 3.13: Partitioning of the measurement spectrum into the signal and the noise spectra

between the measurement spectrum $\Phi_y(\omega)$ and the estimated noise spectrum $\hat{\Phi}_n(\omega)$ yields the predicted signal spectrum $\hat{\Phi}_s(\omega)$ (Figure 3.13). The optimal Wiener filters can then be evaluated by substituting the two predicted spectra into Equations 3.43 and 3.45.

Finally, two further remarks are worth noting here:

- For local sensor validation, the signal spectrum $\Phi_s(\omega)$ as appeared in Equations 3.43 and 3.45 should be replaced by the upper bound $[\Phi_s](\omega)$ defined in Equation 3.2,
- The standard and the inverse Wiener filter ($L_w(j\omega)$ and $H_w(j\omega)$), as defined in Equations 3.43 and 3.45, are generally *noncausal.* Proper transformations into physically realizable configurations are discussed in Mohanty [1987, Section 3.10].

3.7.3 Signal decomposition by practical filter design

In practice, due to insufficient spectral information on the signal and the noise over the observable bandwidth, a Wiener filter may not always be a viable solution. Non-optimal filters have to be introduced instead to simulate the role of an optimal Wiener filter. The fundamental concern is to isolate the noise-dominant component $\tilde{y}$ from the signal-

dominant component $\bar{y}$ in Equation 3.41 by designing two digital filters, the *signal filter* $L(q^{-1})$ and the *noise filter* $H(q^{-1})$ such that

$$\bar{y}(t) = L(q^{-1})\, y(t) \tag{3.47}$$

and

$$\tilde{y}(t) = H(q^{-1})\, y(t) \tag{3.48}$$

Beneficial insights into the essential properties of the two decomposition filters $L(q^{-1})$ and $H(q^{-1})$ can be acquired by examining the design of a Wiener filter on an idealized system in the continuous-time domain.

Most sensor outputs have a mean level associated with the d.c. information of the measurand. Assuming the measurement signal to be stationary at the moment, $s(t)$ can generically be modelled as

$$s(t) = \bar{s} + \tilde{s}(t) \tag{3.49}$$

where $\bar{s}$ is a constant mean level and $\tilde{s}(t)$ is a zero-mean stochastic signal corresponding to the dynamics of the measurand. The autocorrelation function of $s(t)$ is given by

$$\begin{aligned} R_{ss}(\tau) &= E\left[s(t)\, s(t+\tau)\right] \\ &= \bar{s}^2 + R_{\tilde{s}\tilde{s}}(\tau) \end{aligned} \tag{3.50}$$

and its power spectrum by

$$\begin{aligned} \Phi_s(\omega) &= \mathcal{F}\left\{R_{ss}(\tau)\right\} \\ &= 2\pi\bar{s}^2\bar{\delta}(\omega) + \Phi_{\tilde{s}}(\omega) \end{aligned} \tag{3.51}$$

where $\mathcal{F}\{\cdot\}$ is the Fourier Transform operator and $\bar{\delta}(\omega)$ is a unit impulse at $\omega = 0$. Consider an idealized situation in which the measurement signal is strictly bandlimited by the signal bandwidth ω_s and the measurement noise is a white noise with variance σ_n^2

$$\Phi_{\tilde{s}}(\omega) = \begin{cases} K & |\omega| < \omega_s \\ 0 & |\omega| \geq \omega_s \end{cases} \tag{3.52}$$

$$\Phi_n(\omega) = \sigma_n^2 \qquad \forall\omega \tag{3.53}$$

Substituting back into Equation 3.43 will yield the conventional optimal Wiener solution

$$L_w(j\omega) = \frac{2\pi\bar{s}^2\bar{\delta}(\omega) + \Phi_{\tilde{s}}(\omega)}{2\pi\bar{s}^2\bar{\delta}(\omega) + \Phi_{\tilde{s}}(\omega) + \sigma_n^2}$$

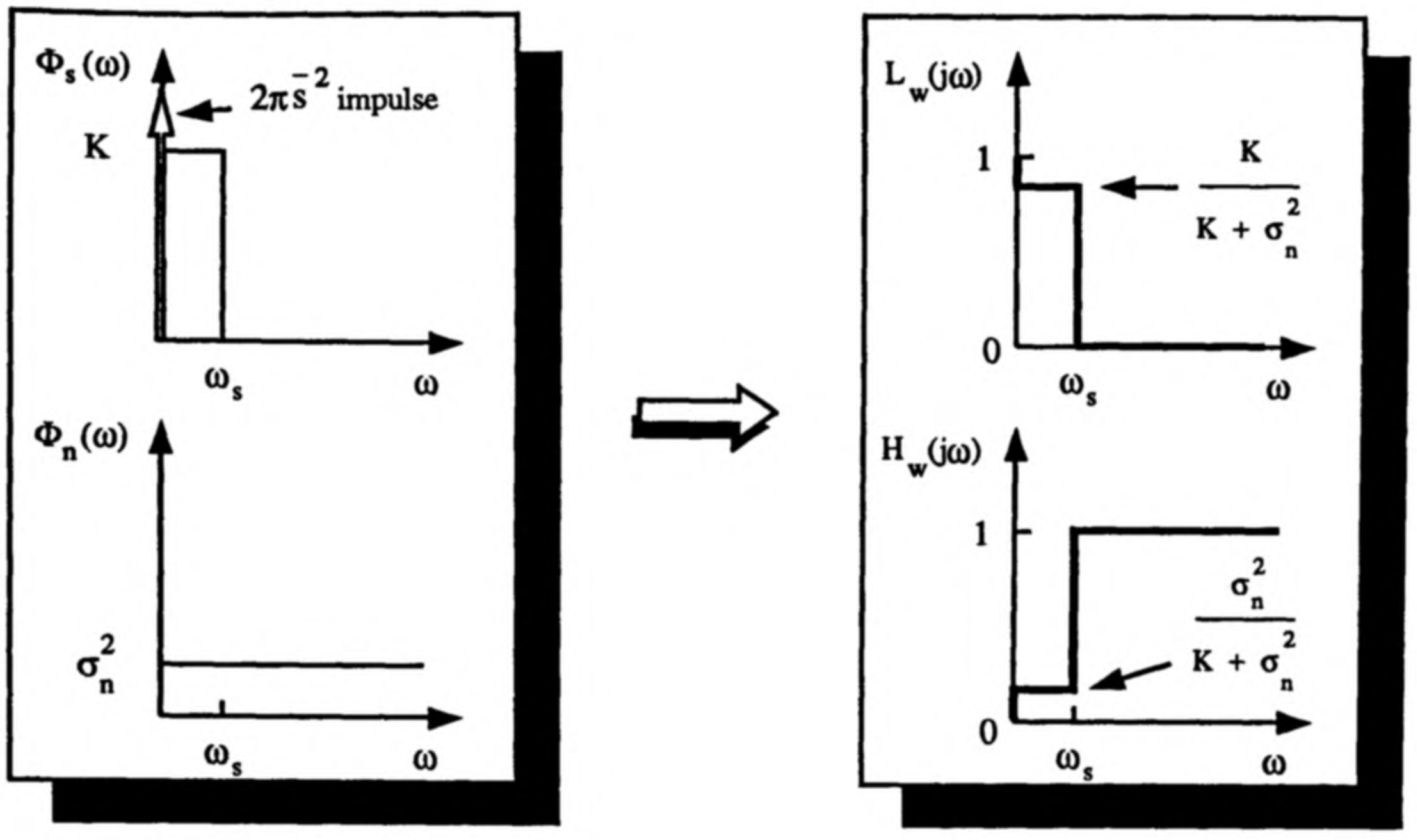

Figure 3.14: Optimal Wiener filters in an idealized situation

$$= \begin{cases} 1 & \omega = 0 \\ \dfrac{K}{K+\sigma_n^2} & 0 < |\omega| < \omega_s \\ 0 & |\omega| \geq \omega_s \end{cases} \tag{3.54}$$

and into Equation 3.45 will give the inverse Wiener filter

$$H_w(j\omega) = \frac{\sigma_n^2}{2\pi\bar{s}^2\bar{\delta}(\omega) + \Phi_{\tilde{s}}(\omega) + \sigma_n^2}$$

$$= \begin{cases} 0 & \omega = 0 \\ \dfrac{\sigma_n^2}{K+\sigma_n^2} & 0 < |\omega| < \omega_s \\ 1 & |\omega| \geq \omega_s \end{cases} \tag{3.55}$$

In a properly commissioned measurement system, $K > \sigma_n^2$. The optimal filter solution is summarized in Figure 3.14.

Properties of decomposition filters

From the above idealized optimal solution, three filter characteristics can be drawn which are common to any decomposition filters.

Guideline 3.3 *Recalling Equations 3.47 and 3.48, the decomposition filters* $L(q^{-1})$ *and* $H(q^{-1})$ *should respectively be a lowpass filter and a highpass filter satisfying the following properties:*

- *Since most measurement signals contain a mean value, the signal filter* $L(q^{-1})$ *should have a unity steady state gain* ($L(1) = 1$) *to track the d.c. level; and the noise filter* $H(q^{-1})$ *should include at least one differentiator* ($H(1) = 0$),
- *For frequencies outside the signal bandwidth* ω_s, $|L(e^{-j\omega T_m})| \simeq 0$ *and* $|H(e^{-j\omega T_m})| \simeq 1$ *where* T_m *is the sampling period,*
- *The optimal gains within* ω_s *should be*

$$|L(e^{-j\omega T_m})| = \frac{\Phi_s(\omega)}{\Phi_s(\omega) + \Phi_n(\omega)} \qquad \textit{and} \qquad |H(e^{-j\omega T_m})| = \frac{\Phi_n(\omega)}{\Phi_s(\omega) + \Phi_n(\omega)}.$$

At frequencies where the signal is much stronger than the noise ($\Phi_s(\omega) \gg \Phi_n(\omega)$), $|L(e^{-j\omega T_m})| \simeq 1$ *and* $|H(e^{-j\omega T_m})| \simeq 0$.

Design of decomposition filters

Filters satisfying Guideline 3.3 can be designed by a variety of techniques (e.g. Parks-McClellan finite impulse response (FIR) filters, Butterworth filters, Chebyshev filters, Elliptic filters and Bessel filters). For signal decomposition in a validation scheme, it is the filter amplitude response which is of additional importance. In particular, adequate signal suppression in the stop band plays a vital role. An infinite impulse response (IIR) filter will generally be able to meet a prescribed amplitude specification with a much lower order and subsequently saves both computational burden and storage requirement. Hence, IIR decomposition filters appear to be a suitable alternative.

Classical IIR filters include the Butterworth, Chebyshev, Elliptic and Bessel filters [Hamming, 1983]. All four can be designed in a lowpass or highpass configuration satisfying the conditions laid down in Guideline 3.3. Briefly, Butterworth filters have a maximally flat response in the pass band, Chebyshev and Elliptic filters provide a steeper cut-off in the expense of some 'ripple' in the pass and/or stop bands and Bessel filters give a 'near-linear' phase characteristics but poorer amplitude response. After the filter type has been finalized, there are two knobs remained to be tuned:

Corner frequency which partitions the pass band and the stop band,

Filter order which primarily controls the rate of cut-off at the corner frequency.

Let the corner frequencies of the signal filter $L(q^{-1})$ and the noise filter $H(q^{-1})$ be ω_L and ω_H respectively. Since the signal bandwidth has been utilized as a cut-off reference, it is natural to assign both corner frequencies to ω_s, i.e.

$$\omega_L = \omega_H = \omega_s \tag{3.56}$$

As for the choice of filter orders n_L and n_H, there is no universally applicable set of rules. The underlying idea is to suppress any undesired signal sufficiently so that

$$\bar{y}(t) = L(q^{-1})\, y(t) \simeq L(q^{-1})\, s(t) \tag{3.57}$$

$$\tilde{y}(t) = H(q^{-1})\, y(t) \simeq H(q^{-1})\, n(t) \tag{3.58}$$

The choice of n_H is of particular importance. Leakage of significant nonstationary measurement signal into $\tilde{y}(t)$ during the *learning stage* will weaken the representativeness of the baseline model (Section 3.8). If this happened during the *tracking stage*, it would generate false alarms and would degrade the performance of the validation scheme. In practice, an order between 1 and 4 has been found to be adequate for this purpose.

Unfortunately, a by-product of signal decomposition is the alteration of the patterns of some failure signals (compared with modification of sensor failure signatures in a closed loop environment discussed in Section 2.6). Cyclic and erratic failures below the signal bandwidth ω_s will be severely subdued in the noise-dominant component $\tilde{y}$ and hence are undetectable (unless the failure signatures are much stronger than the measurement signal). Nevertheless, it is not the goal of the local sensor validation scheme to identify failures within the signal bandwidth as discussed in Section 2.7.2. A more concerned victim is the drift failure. In classical design of digital highpass filters (e.g. Butterworth or Chebyshev filters), the number of difference operators Δ ($\equiv 1 - q^{-1}$) in $H(q^{-1})$ is the same as the filter order n_H. From Guideline 3.3, n_H must at least be one to eliminate the d.c. offset, i.e.

$$H(q^{-1}) = \frac{(1-q^{-1})^{n_H}}{H_d(q^{-1})} = \frac{\Delta^{n_H}}{H_d(q^{-1})} \qquad n_H \geq 1 \tag{3.59}$$

where $H_d(1) \neq 0$. Consider a linear drift failure (a drift of ϑ unit/time) at $t = 0$ in an open loop environment,

$$y(t) = s(t) + n(t) + f(t)$$

where

$$f(t) = \vartheta\, t$$

The noise-dominant component can be estimated as

$$\tilde{y}(t) \simeq H(q^{-1})\, n(t) + \tilde{f}(t)$$

where at steady-state[21], the failure signature $\tilde{f}(t)$ is given by

$$\tilde{f}(t) = \begin{cases} \dfrac{\vartheta\, T_m}{H_d(1)} & n_H = 1 \\ 0 & \text{otherwise} \end{cases} \tag{3.60}$$

For the noise-dominant component to be sensitive to drift failures, n_H has to be kept to one. This does not only impose a severe limitation on the signal suppression capability of the filter $H(q^{-1})$, but since drifts are often gradual (i.e. small ϑ), this also creates a demanding problem in identifying the minute failure signature $\tilde{f}(t)$ from the background noise $H(q^{-1})\, n(t)$. Therefore, it is suggested that the validation scheme should monitor any drifting behaviour from the signal-dominant component $\bar{y}$ instead. To avoid any further confusion, n_H should be chosen to be greater than 1 to eliminate the 'bias' term in $\tilde{y}$ (Equation 3.60) whenever a drift failure is conceivable[22].

In a nutshell, the design of non-optimal decomposition filters can be summed up as follows:

Guideline 3.4 *The decomposition filters $L(q^{-1})$ and $H(q^{-1})$ can be designed as Butterworth (or Chebyshev) lowpass and highpass filters respectively with cut-off frequencies at the signal bandwidth ω_s. If drift failure is a possibility in an open loop or a type-0 closed loop environment, the order of the noise filter $H(q^{-1})$ has to be greater than 1. The orders of the filters have to be selected to achieve adequate suppression within the stop band; further design details can be found in Hamming [Hamming, 1983].*

Example 3.4

A synthetic data set of sensor output in an open loop environment is examined:

$$y(t) = G(q^{-1})\, u(t) + n(t) + f(t) \tag{3.61}$$

[21] Even for $n_H > 1$, a linear drift will still introduce a transient impulse at the time of failure. But since drift is usually fairly slow, i.e. ϑ is very small, the transient will most probably be indistinguishable from the background noise.

[22] Recall from Property 2.1 that in a closed loop environment, a drifting pattern can only be observed in the output of a type-0 system.

The system transfer function $G(q^{-1})$ is simulated as a 2nd order Butterworth lowpass filter with a system bandwidth ω_B of 0.01 Hz. The aggregate input $u(t)$ is composed of three components: a mean level at 0.5, a zero-mean stochastic white noise with variance 2.5×10^{-4}, and a series of step changes (0.05 unit at 250 s, -0.1 unit at 500 s and 0.05 unit at 1000 s). The measurement noise $n(t)$ is taken to be a white noise with variance 2.5×10^{-5}. A linear drift failure $f(t)$ of -0.001 unit/s is initiated at 1500 s. The data is sampled at 1 Hz with a duration of 2000 s.

Based on the above information — $\mathcal{G}_o = 1$, $\omega_B = 0.01$ Hz (i.e. 0.063 rad s^{-1}), $\ell = 2$ and $\mathcal{R}_s = 400$ ($(\Delta v)_m = 0.1$, $\sigma_n^2 = 2.5 \times 10^{-5}$), the signal bandwidth ω_s is estimated to be 0.089 Hz (Equation 3.27). The key objective of this example is to highlight the influence of filter orders on signal suppression and also to investigate the effects of a drift failure on signal decomposition.

Referring to Guideline 3.4, the cut-off frequencies ω_L and ω_H of both the signal filter and the noise filter are chosen to be the signal bandwidth ω_s (0.089 Hz). Firstly, a first-order lowpass and a first-order highpass Butterworth filters are designed as the decomposition filters. The results are shown in Figure 3.15. Both the step changes in the measurement signal and the drifting action are retained in the signal-dominant component $\bar{y}(t)$ and it is clearly evident that some measurement signals are undesirably leaked into the noise-dominant component $\tilde{y}(t)$, especially in the vicinity of the major step change at 500 s. On the other hand, a second order Butterworth noise filter can adequately suppress the measurement signal in this example while the signal filter still provides a similar output in comparison with the first order case (Figure 3.16). As a result of the drift failure at 1500 s, a modest bias has been introduced in $\tilde{y}(t)$ for $n_H = 1$ (mean level of $\tilde{y}(t)$ after failure is -1.72×10^{-3}) but no failure signature has been observed in $\tilde{y}(t)$ when $n_H = 2$ (mean level at 1.39×10^{-5}).

This concludes the *commissioning stage*, in which prior knowledge of the sensor environment is acquired (Section 3.2), the measurement signal bandwidth ω_s is estimated (Section 3.3) and the sampling frequency is selected accordingly (Section 3.5), the sensor signal is then well-conditioned (Section 3.4) and appropriately sampled and digitized (section 3.6); finally, suitable decomposition filters are configured to isolate the signal and the noise components (Section 3.7). All these pave the way for the ensuing *learning stage*.

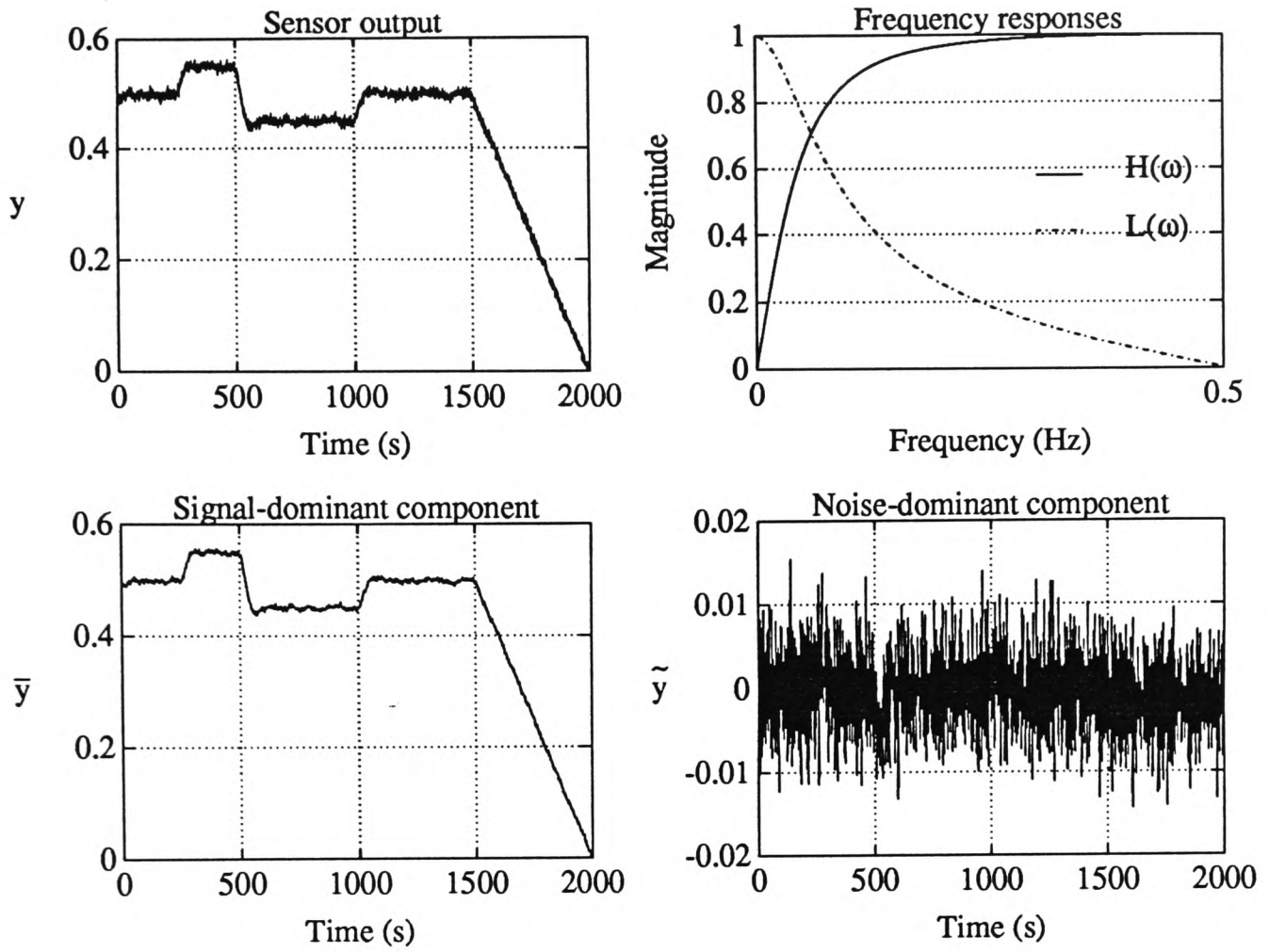

Figure 3.15: Signal decomposition with drift failures ($n_L = n_H = 1$)

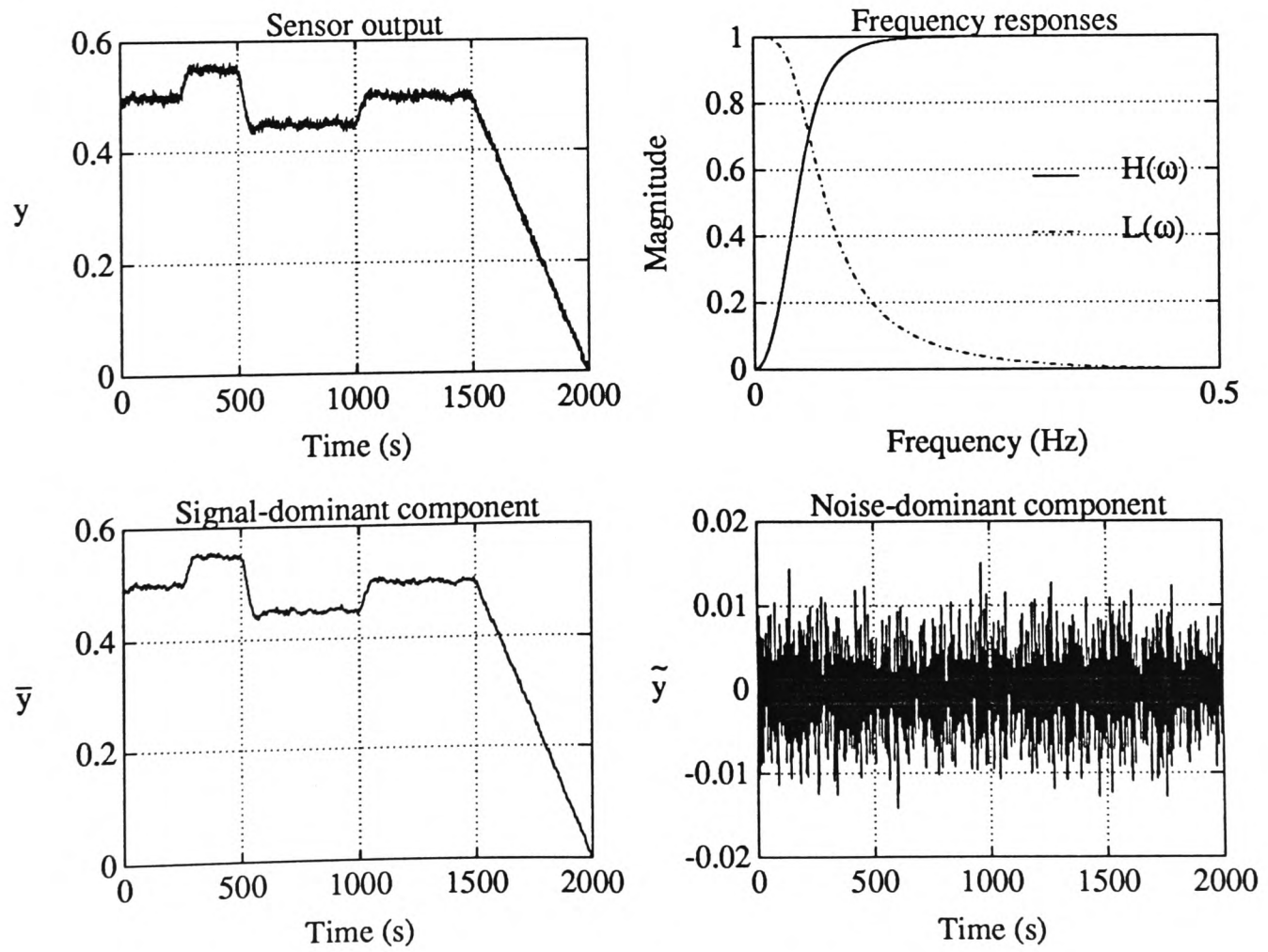

Figure 3.16: Signal decomposition with drift failures ($n_L = n_H = 2$)

3.8 Sensor signal modelling

One of the fundamental tasks in the *learning stage* is to obtain a 'representative' model of a 'good' sensor. Sensor modelling not only provides a standard of normal behaviour of the sensor output, but also sharpens the detection algorithms in the subsequent *tracking stage*. As the local sensor validation scheme is focused on frequency characteristics beyond the signal bandwidth ω_s, it is beneficial to construct a baseline model only on the noise-dominant component $\tilde{y}(t)$ based on an assumed *failure-free* observation of the sensor output. During the learning stage, the following is assumed:

Assumption 3.8 *The sensor is assumed to be under typical operating conditions and be free from any failures in the learning stage.*

Since the learning stage is triggered either after the initial installation or after proper re-commissioning following a major system change, the error-free assumption can often be met.

3.8.1 An ARMA stochastic time-series model

Based on Assumption 3.2, Equation 3.58 and Guideline 3.3, the noise-dominant component can be considered to be a *zero-mean stationary* random process and is well conformed to be modelled as a stochastic time-series. Time-series modelling has been used extensively in forecasting, control and simulation [Box and Jenkins, 1976; Chatfield, 1984; Hannan *et al.*, 1985; Kendall, 1976]. It has been applied to response monitoring of platinum resistance thermometers [Upadhyaya and Kerlin, 1978], stability checking of boiling water reactors from neutron noise sensor data [Upadhyaya and Kitamura, 1981], automatic detection of machine tool wear [Janik and Isermann, 1990; Liang and Dornfeld, 1989], and detection of outliers in sampled data [Tiao, 1985]. On top of Assumptions 3.2, 3.3 and 3.4, an additional assumption on the measurement noise is formulated:

Assumption 3.9 *The measurement noise is assumed to have a rational spectral density function.*

By the *spectral factorization theorem* [Åström and Wittenmark, 1984, Section 6.5], $\tilde{y}(t)$ can be described by an *AutoRegressive Moving-Average* (ARMA) model:

$$A(q^{-1})\,\tilde{y}(t) = C(q^{-1})\,e(t) \tag{3.62}$$

where $e(t)$ is a zero-mean white noise

$$A(q^{-1}) = 1 + a_1 q^{-1} + a_2 q^{-2} + \ldots + a_{na} q^{-na}$$

$$C(q^{-1}) = 1 + c_1 q^{-1} + c_2 q^{-2} + \ldots + c_{nc} q^{-nc}$$

In contrast to the detailed input-output process model required by a conventional centralized detection approach, a much simpler stochastic time-series model is adopted. This helps to widen the applicability of the local sensor validation scheme.

3.8.2 AR versus ARMA modelling

Another popular and more frequently utilized stochastic time-series model is an *autoregressive* (AR) model which can be described as

$$A_{ar}(q^{-1})\,\tilde{y}(t) = e(t) \tag{3.63}$$

i.e. $C(q^{-1}) = 1$ in Equation 3.62. AR model has been widely used in economics, speech processing, vibration analysis and fault detection. Its attractiveness includes:

- Estimation of the unknown AR parameters requires only *linear* optimization. Stable and efficient estimation algorithms exist both for off-line (e.g. Yule-Walker algorithm, Burg algorithm and Levinson-Durbin recursion) and recursive (e.g. recursive least squares and fast lattice filter algorithm) identification [Haykin, 1986; Kay, 1988; Ljung and Söderström, 1983; Marple, 1987];

- AR model is guaranteed to be minimum phase and hence is always invertible;

- Statistical and spectral properties of the signal (e.g. autocorrelation and power spectrum) can be obtained by simple transformations from the AR parameter space through the Yule-Walker equation [Box and Jenkins, 1976, Section 3.2].

Mathematically, any ARMA model can be expressed equivalently by an AR model with infinite order

$$A_{ar}(q^{-1}) = \frac{A(q^{-1})}{C(q^{-1})} = A(q^{-1})\,C^{-1}(q^{-1}) \tag{3.64}$$

If the ARMA model is invertible (or minimum phase), i.e. all the roots of the moving average polynomial $C(q^{-1})$ are within the unit circle, the coefficients of the infinite order 'inverse' polynomial $C^{-1}(q^{-1})$ will decay exponentially to zero. Hence, a 'finite' order AR model can be employed to approximate the ARMA model with reasonable accuracy.

Wahlberg and Ottersten [1986] provides a procedure to transform a high order AR model to a lower ARMA model via model reduction.

Based on Assumption 3.9, the measurement noise $n(t)$ can itself be described by an ARMA process (Equation 2.7)

$$n(t) = M(q^{-1})\, e(t) \tag{3.65}$$

and from the properties of the noise filter $H(q^{-1})$ (Equations 3.58 and 3.59), an infinite-order AR model of the noise-dominant component $\tilde{y}(t)$ can be equated to be

$$A_{ar}(q^{-1}) = \frac{H_d(q^{-1})}{\Delta^{n_H}\, M(q^{-1})} \tag{3.66}$$

The presence of the difference operators Δ in the denominator inhibits convergency when the right hand side is expressed as an infinite series. A finite order AR model is therefore inappropriate. On the other hand, for an explicit ARMA model, Δ can be absorbed into the moving-average polynomial $C(q^{-1})$ and a much lower order model can be constructed.

3.9 Sensor ARMA model estimation

Once the sensor output has been decomposed, the unknown ARMA coefficients of the noise-dominant component $\tilde{y}(t)$ have to be estimated. Parameter estimation is an integral procedure in control and signal processing. Good references that cover a broad spectrum of the subject include Goodwin and Sin [1984], Ljung [1987], Ljung and Söderström [1983] and Söderström and Stoica [1989]. References that specialize in time-series estimation can be found in Box and Jenkins [1976], Kay [1988] and Marple [1987] with the latter two concentrate more on a frequency perspective. Estimation methods specific to ARMA models are discussed in Åström and Mayne [1982], Friedlander [1982], Graupe *et al.* [1975], Li *el al.* [1989] and Peterka [1981].

In general, parameter identification can be divided into two broad categories:

- **Off-line identification** in which a batch of data has to be acquired and stored before the initialization of any parameter estimation procedure. ARMA model[23]

[23] Theoretically, the estimation of an ARMA model can also be achieved by a combination of two linear optimizations and a deconvolution. Firstly, the moving-average polynomial can be estimated from a modified Yule-Walker Equation [Kay, 1988, Section 5.4]. The data are then deconvolved into a pure AR process which can be identified by any method mentioned in Section 3.8.2.

estimation demands *nonlinear* optimization [Box and Jenkins, 1976, Section 7.2] and the data are often passed several times for the estimates to iterate towards the optimal values.

- **Recursive identification** in which the estimates of the unknown model parameters are updated every time when a new observation becomes available. Under favourable conditions, the estimates will also converge asymptotically to the optimal solution.

At a local level, both storage and computational resources are scarce. The huge amount of storage demanded by the off-line approach is prohibitive. Hence, recursive estimation is a more attractive choice. Not only does it require minimal storage, but it also distributes the computational burden uniformly over the acquisition period.

3.9.1 Recursive Gauss-Newton algorithm

A vast variety of recursive identification techniques are available in literature, e.g. least squares, instrumental variables, maximum likelihood and Kalman filtering. Ljung and Söderström [1983] provides a unified framework which is capable of encompassing various recursive estimation methods and they assert that [Ljung and Söderström, 1983, Section 1.5]

> "There is only one recursive identification method. It contains some design variables to be chosen by the user."

Based on a quadratic cost function, many well-known identification techniques can be derived from the recursive Gauss-Newton algorithm [Ljung and Söderström, 1983, Section 3.4] (by selecting a different set of design variables) which is summarized as follows:

ARMA model

Recall from Equation 3.62, the model of the noise-dominant component $\tilde{y}(t)$ is given by

$$A(q^{-1})\,\tilde{y}(t) = C(q^{-1})\,e(t) \tag{3.67}$$

or equivalently in an *equation error* model

$$\tilde{y}(t) = \phi^T(t)\,\theta(t) + e(t) \tag{3.68}$$

where

$$\phi(t) = [-\tilde{y}(t-1) \; -\tilde{y}(t-2) \; \ldots \; -\tilde{y}(t-na) \quad \epsilon(t-1) \, \epsilon(t-2) \; \ldots \; \epsilon(t-nc)]^T$$

$$\theta(t) = [a_1 \, a_2 \; \ldots \; a_{na} \quad c_1 \, c_2 \; \ldots \; c_{nc}]^T$$

$\phi(t)$ and $\theta(t)$ are known as the regressor vector and the parameter vector respectively. $\epsilon(t)$ is an estimate of the unknown stochastic white noise $e(t)$.

Since the noise term $e(t)$ is assumed to be zero-mean, the model for the output prediction is given by

$$\hat{\tilde{y}}(t) = \phi^T(t) \, \hat{\theta}(t) \tag{3.69}$$

where $\hat{x}(t)$ is the estimate of x at time t.

Cost function

The cost function adopted is quadratic

$$V(\theta) = E\left[\frac{1}{2} \epsilon^T(t) \, \epsilon(t)\right] \tag{3.70}$$

and the prediction error $\epsilon(t)$ is given by

$$\epsilon(t) = \tilde{y}(t) - \hat{\tilde{y}}(t) \tag{3.71}$$

Parameter update algorithm

Minimizing the cost function $V(\theta)$ in Equation 3.70 will yield the *recursive Gauss-Newton algorithm*:

$$\tilde{\epsilon}(t) = \tilde{y}(t) - \phi^T(t) \, \hat{\theta}(t-1) \tag{3.72}$$

$$P(t) = \frac{1}{\lambda(t)} \left(P(t-1) - \frac{P(t-1) \, \psi(t) \, \psi^T(t) \, P(t-1)}{\lambda(t) + \psi^T(t) \, P(t-1) \, \psi(t)} \right) \tag{3.73}$$

$$L(t) = \frac{P(t-1) \, \psi(t)}{\lambda(t) + \psi^T(t) \, P(t-1) \, \psi(t)} = P(t) \, \psi(t) \tag{3.74}$$

$$\hat{\theta}(t) = \hat{\theta}(t-1) + L(t) \, \tilde{\epsilon}(t) \tag{3.75}$$

$$\epsilon(t) = \tilde{y}(t) - \phi^T(t) \, \hat{\theta}(t) \tag{3.76}$$

where $\tilde{\epsilon}(t)$ is the a priori prediction error

$\epsilon(t)$ is the a posteriori prediction error

$P(t)$ is generally referred as the covariance matrix

$\lambda(t)$ is the exponential forgetting factor $(0 \leq \lambda(t) \leq 1)$

$\psi(t)$ is the negative innovation gradient vector $\left(\psi(t) = \dfrac{\partial}{\partial \theta} \left(-\epsilon(t)\right)\right)$

Note that $\epsilon(t)$ is also known as the *residuals* or the *innovation sequence*.

3.9.2 Recursive Maximum Likelihood (RML) identification

One technique is to approximate the gradient vector $\psi(t)$ in Equations 3.73 and 3.74 by a filtered version of the regression vector $\phi(t)$ (a prediction error method)

$$\psi(t) = \frac{\phi(t)}{\hat{C}(q^{-1}, t)} \tag{3.77}$$

where $\hat{C}(q^{-1}, t)$ is the current estimate of the moving-average polynomial (i.e. the c-parameters in $\hat{\theta}(t)$). With this particular choice of $\psi(t)$ and if the white noise $e(t)$ in Equation 3.67 is Gaussian, the cost function $V(\theta)$ is equivalent to the negative log likelihood function [Ljung and Söderström, 1983, Section 2.2.3], and minimizing $V(\theta)$ is identical to maximizing the likelihood function. The algorithm is thus termed *Recursive Maximum Likelihood (RML)*.

In order to guarantee convergency, the roots of the estimated moving-average polynomial $\hat{C}(q^{-1}, t)$ must be constrained within the unit circle, i.e. the on-line estimated ARMA model must always be minimum phase. It is therefore imperative to monitor the stability of $\hat{C}(q^{-1}, t)$ in each update and to project the parameter vector $\hat{\theta}(t)$ onto a stable subspace $\mathcal{D}$ if necessary. The parameter update equation (Equation 3.75) has to be modified to

$$\hat{\theta}(t) = \left\| \hat{\theta}(t-1) + L(t)\,\tilde{\epsilon}(t) \right\|_{\mathcal{D}} \tag{3.78}$$

where

$$\mathcal{D} = \{\hat{\theta}(t) : \text{all roots of } \hat{C}(q^{-1}, t) \text{ within the unit circle}\}$$

and

$$\|x\|_{\mathcal{D}} = \begin{cases} x & \text{if } x \in \mathcal{D} \\ \text{projected value in } \mathcal{D} & \text{if } x \notin \mathcal{D} \end{cases}$$

The projection of any 'unstable' roots can be accomplished by an efficient iterative spectral factorization algorithm given in Vostrý [1975].

The RML algorithm is asymptotically efficient and will always converge to a local minimum of the cost function $V(\theta)$, whether or not the *true* system is included in the model structure.

3.9.3 Extended Least Squares (ELS) versus RML

Another popular approach in ARMA model estimation is the pseudolinear regression method in which the gradient vector $\psi(t)$ is directly replaced by the regression vector $\phi(t)$

$$\psi(t) = \phi(t) \tag{3.79}$$

The resulting update equations resemble those in a standard linear least squares regression and the algorithm is named *Extended Least Squares (ELS)*.

Notwithstanding its computational simplicity, ELS does not necessarily converge. If $C_o(q^{-1})$ is the genuine moving-average polynomial, a *sufficient* condition for the algorithm to converge is that $\left(\frac{1}{C_o(q^{-1})} - \frac{1}{2}\right)$ is strictly positive real [Ljung and Söderström, 1983, Section 4.2], i.e.

$$Re\left[\frac{1}{C_o(e^{-j\omega T_m})} - \frac{1}{2}\right] > 0 \qquad \forall\omega \tag{3.80}$$

Furthermore, there is no assurance that the roots of the final estimate of $\hat{C}(q^{-1})$ is within the unit circle and the estimated ARMA model may not be invertible.

Consider a simplified situation in which $n_H = 1$ and $M(q^{-1}) = 1$ in Equation 3.66. The noise-dominant component can be written as

$$H_d(q^{-1})\,\tilde{y}(t) = (1 - q^{-1})\,e(t) \tag{3.81}$$

and hence $C_o(q^{-1}) = 1 - q^{-1}$. It is straightforward to show that

$$Re\left[\frac{1}{C_o(e^{-j\omega T_m})} - \frac{1}{2}\right] = Re\left[-\frac{j\,\cos\frac{\omega}{2}}{2\,\sin\frac{\omega}{2}}\right] = 0$$

which violates the sufficient condition for convergency in Equation 3.80. For sensor model estimation during the learning stage, ELS is not guaranteed to converge and RML is the designated solution despite of the additional requirements of data filtering, stability monitoring and polynomial projection.

3.9.4 Practical notes

A number of practical issues for the success of the sensor ARMA model estimation scheme are highlighted below:

- **Initial values**

  The initial setup of the estimator should only affect the incipient transients and its

effects will fade away as more information becomes available. Without any prior information on the sensor ARMA model, the estimator can be initiated as:

Parameter vector	$\hat{\theta}(0) = 0$
Regression vector	$\phi(0) = 0$
Gradient vector	$\psi(0) = 0$
Covariance matrix	$P(0) = \rho I$

ρ, a measure of the uncertainty on $\hat{\theta}(0)$, should be a large positive number (e.g. 10^5) to accelerate the initial rate of convergence and I is an identity matrix.

- **Forgetting factor**

  The exponential forgetting factor $\lambda(t)$ (Equations 3.73 and 3.74), which lies between 0 and 1, controls the adaptivity of the estimator. With a smaller $\lambda(t)$, more significance is placed on the new information and the estimator is capable of tracking changes in the model. Both fixed and variable forgetting algorithms [Fortescue *et al.*, 1981; Hägglund, 1983; Kulhavý, 1987; Sripada and Fisher, 1987] have been applied to fault detection and adaptive control. For local sensor validation, the adopted formulation ensures that the noise-dominant component $\tilde{y}(t)$ remains stationary during the learning stage and hence $\lambda(t)$ is selected to be 1.

- **Covariance matrix update**

  The successive subtractions in the covariance matrix update (Equation 3.73) when $\lambda(t) = 1$ could lead to problems in round-off errors and numerical instability. This can be improved by employing the normalized Cholesky decomposition and modifying the update equation accordingly based on the Bierman's U-D factorization algorithm [Bierman, 1977; Ljung and Söderström, 1983, Section 6.2].

- **Rate of convergence**

  The convergence of an ARMA model estimation is generally slower when compared with the estimation of a pure AR model. In particular, the presence of differentiators in the moving average polynomial will further aggravate the problem. It has been found in practice that the number of samples required for the RML method to converge is typically in the range of 1000 to 2000 and the autoregressive polynomial $A(q^{-1})$ often converges faster than the moving-average component $C(q^{-1})$. Friedlander [1982] proposed a modified filtering algorithm for the gradient vector $\psi(t)$

(Equation 3.77) not only to increase the rate of convergence but also to simplify stability monitoring.

- **Model order selection**

  The choice of the model orders na and nc requires a compromise between model adequacy and parsimony. Apart from the idealized cases as in pure AR and pure MA processes where the partial autocorrelation and the autocorrelation respectively cut off at the model order [Chatfield, 1984, Section 4], conventional procedures involve the computation of test variables for a range of model orders and the 'best' is selected based on some prescribed criteria [Unbehauen and Göhring, 1974] (e.g. Akaike information criterion and Rissanen minimum description length criterion). Fuchs [1987] presented a statistical test to estimate the order of an ARMA process based on the ranks of Hankel matrices.

  For local sensor validation, the sensor ARMA model can be considered as a sharpening tool[24] rather than a direct basis for failure detection and the requirement for precise model orders is less critical. Hence, an alternative approach is adopted in which an ARMA model with a tentative choice of model orders is first estimated and then validated for its adequacy. With reference to Equation 3.66, the ARMA model should represent an aggregate of the measurement noise process $M(q^{-1})$ as well as the noise filtering action $H(q^{-1})$. A rule of thumb is to choose the orders as $na = nc = n_H + n_M$ where n_H is the order of the noise filter and the additional complexity (n_M) is used to describe the noise spectrum (a value from 1 to 3 is in most cases sufficient)[25]. Model verification will be discussed in the following section.

Example 3.5

To compare the effectiveness of the two recursive identification schemes, Extended Least Squares (ELS) and Recursive Maximum Likelihood (RML), for sensor ARMA model estimation, a simplified sensor system in an open loop environment is studied:

$$y(t) = G(q^{-1})\,u(t) + n(t)$$

[24]The ARMA model can also be considered as a whitening filter 3.11.1.

[25]A larger order n_M will be needed if significant anti-aliasing filtering effects or resonances are observed. In general, an extra order of 2 for every resonance is required.

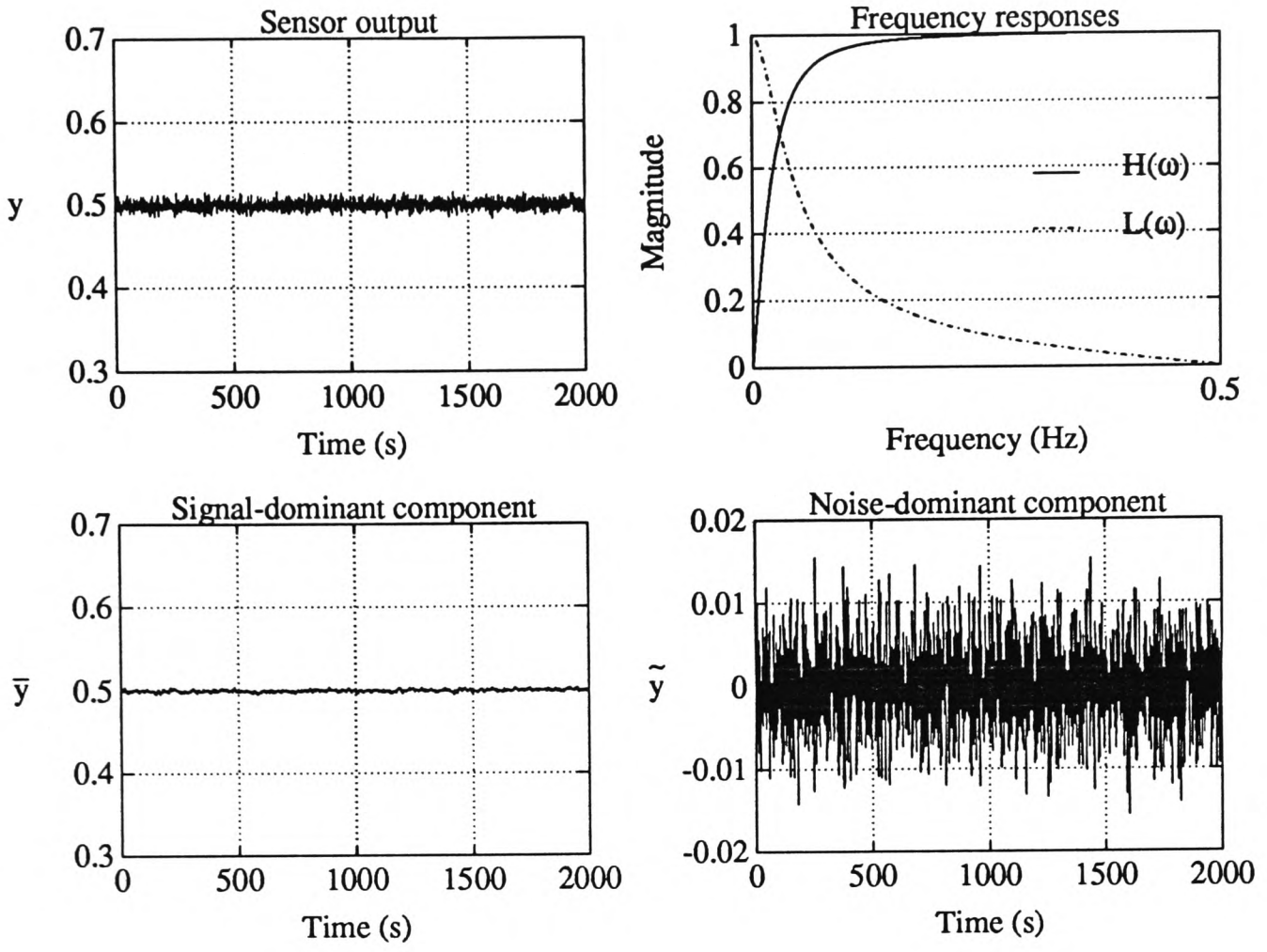

Figure 3.17: Constant sensor output corrupted by white noise

Similar to the setup in Example 3.4, $G(q^{-1})$ is taken to be a 2nd order Butterworth lowpass filter with $\omega_B = 0.01$ Hz and $n(t)$ is a zero-mean white noise with variance 2.5×10^{-5}. For clarity, leakage of the measurement signal into the noise-dominant component is prevented by assigning $u(t)$ to a constant 0.5. The decomposition filters are given by

$$L(q^{-1}) = \frac{0.086\,(1+q^{-1})}{1-0.83q^{-1}}$$

$$H(q^{-1}) = \frac{0.91\,(1-q^{-1})}{1-0.83q^{-1}}$$

which are first order Butterworth lowpass and highpass filters with cut-off frequencies at 0.03 Hz. The signal $y(t)$ is sampled at 1 Hz and the first 2000 s failure-free data are used for the subsequent ARMA model estimation in the learning stage. The original sensor output and the decomposed signals are displayed in Figure 3.17.

For this configuration, the noise-dominant component is just a filtered version of the measurement noise ($\tilde{y}(t) = H(q^{-1})\,n(t)$) and can be written explicitly as an ARMA model

$$A_o(q^{-1})\,\tilde{y}(t) = C_o(q^{-1})\,e(t)$$

where

$$A_o(q^{-1}) = 1 - 0.83q^{-1}$$

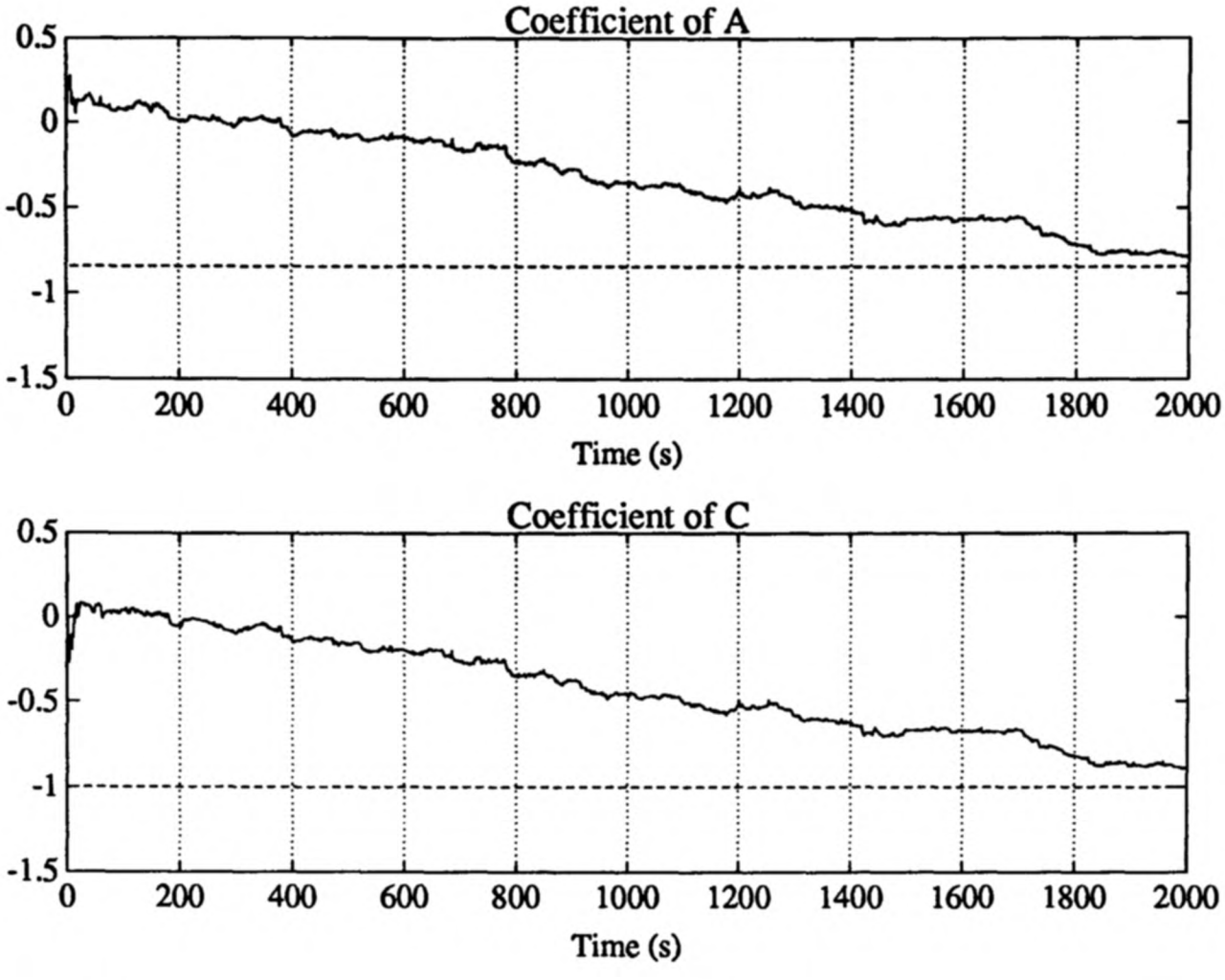

Figure 3.18: ARMA model estimation by ELS (dashed: true value)

$$C_o(q^{-1}) = 1 - q^{-1}$$

It then follows directly from the discussion in Section 3.9.3 that the sufficient convergency condition for ELS (Equation 3.80) has not been met.

An ARMA model ($na = nc = 1$) is then fitted to $\tilde{y}(t)$ and the unknown coefficients are estimated recursively by both the ELS and the RML algorithm. $\hat{\theta}(0)$, $\phi(0)$ and $\psi(0)$ are all set to zero vectors[26] and $P(0)$ is initiated at $10^4\, I$. The estimation results are presented in Figures 3.18 (ELS) and 3.19 (RML). It is clear that the ELS estimates do not converge even after 2000 samples while RML reaches the optimal values after about 1500 samples. The final estimates are given below:

ELS	$\hat{A}(q^{-1}) = 1 - 0.78q^{-1}$	$\hat{C}(q^{-1}) = 1 - 0.89q^{-1}$
RML	$\hat{A}(q^{-1}) = 1 - 0.87q^{-1}$	$\hat{C}(q^{-1}) = 1 - q^{-1}$

This example has shown that, for sensor ARMA model estimation, RML is superior to ELS in both accuracy and efficiency.

---

[26]Without any explicit remark, $\hat{\theta}(0)$, $\phi(0)$ and $\psi(0)$ are always set to zero vectors.

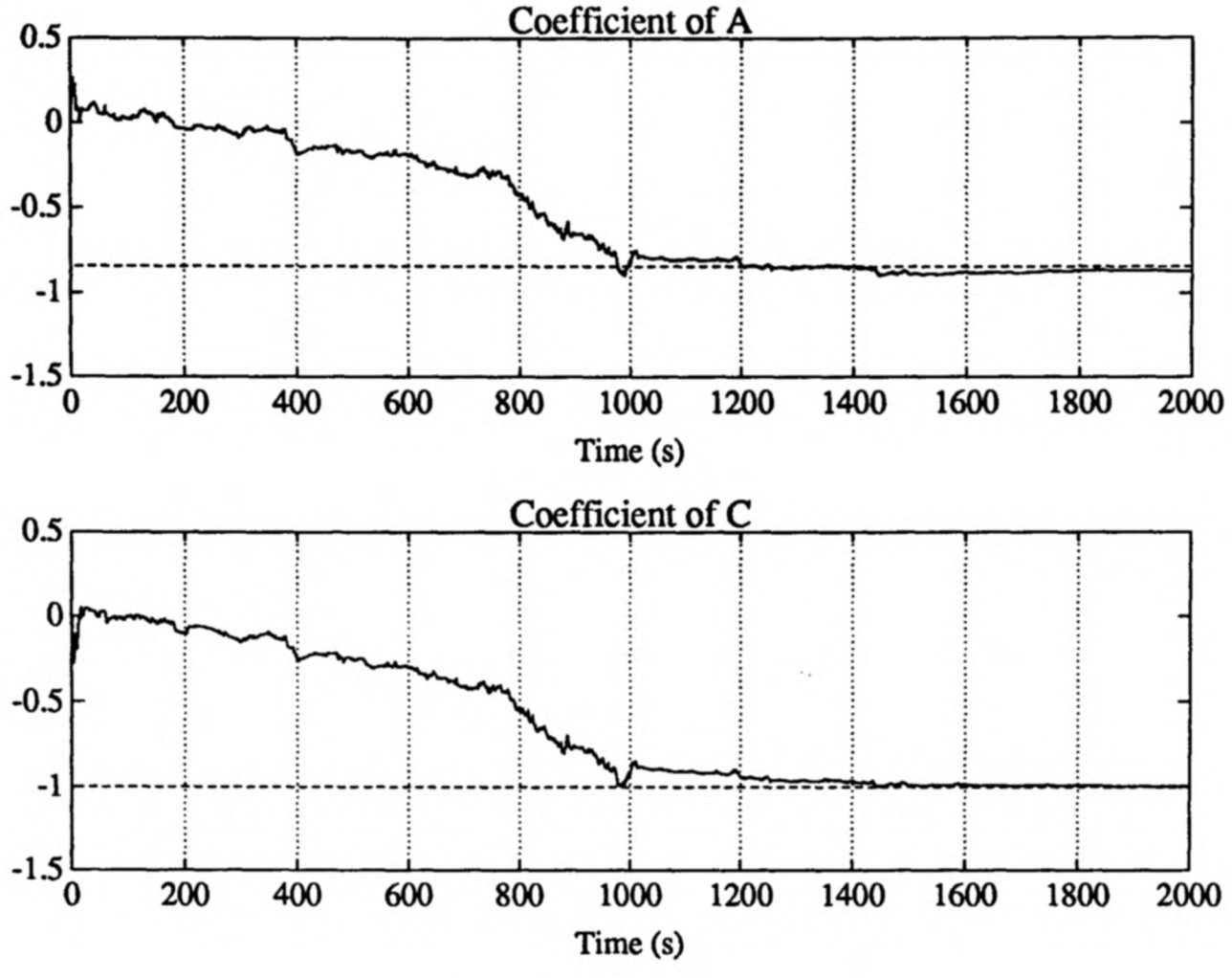

Figure 3.19: ARMA model estimation by RML (dashed: true value)

3.10 Sensor model validation

Prior to its acceptance as a baseline reference in the tracking stage, the sensor ARMA model has to be verified. Under the stationarity (Assumption 3.2) and failure-free (Assumption 3.8) conditions, if the estimated model does indeed adequately represent the noise-dominant process $\tilde{y}(t)$, the *innovation sequence* $\epsilon(t)$ should be a zero-mean white noise with variance σ_ϵ^2 [Boozer and Daniel, 1972; Martin and Stubberud, 1974]. Validation tests based on the innovation are well adapted to models obtained from a prediction error estimation method such as RML [Söderström and Stoica, 1989, Chapter 11]. Model validation is carried out over N samples of the innovation sequence $\{\epsilon(1), \epsilon(2), \ldots, \epsilon(N)\}$ which is generated by

$$\epsilon(t) = \tilde{y}(t) - \phi^T(t)\,\hat{\theta} \tag{3.82}$$

where $\hat{\theta}$ is the final estimate of the parameter vector. Two separate tests are performed: *test of mean* and *test of whiteness*. Additional model verification methods are discussed in Box and Jenkins [1976, Chapter 8] as well as Söderström and Stoica [1989, Chapter 11].

- *Test of mean*

  This tests whether the observed innovation sequence has a zero mean. The sample mean of the innovation is given by

$$\hat{\bar{\epsilon}} = \frac{1}{N}\sum_{k=1}^{N}\epsilon(k) \tag{3.83}$$

  and the 'unbiased' sample variance is

$$\hat{\sigma}_\epsilon^2 = \frac{1}{N-1}\sum_{k=1}^{N}\left(\epsilon(k)-\hat{\bar{\epsilon}}\right)^2 = \left(\frac{1}{N-1}\sum_{k=1}^{N}\epsilon(k)^2\right) - \frac{N}{N-1}\hat{\bar{\epsilon}}^2 \tag{3.84}$$

  Under the null hypothesis (i.e. ϵ is zero-mean), $\hat{\bar{\epsilon}}$ has a Gaussian distribution with a zero mean and a variance equals to $\hat{\sigma}_\epsilon^2/N$ (*Central Limit Theorem*) . Using a 5% significance level test, the null hypothesis is rejected whenever

$$\left|\hat{\bar{\epsilon}}_s\right| = \left|\frac{\sqrt{N}\,\hat{\bar{\epsilon}}}{\hat{\sigma}_\epsilon}\right| > 1.96 \tag{3.85}$$

  $\hat{\bar{\epsilon}}_s$ is termed *standardized innovation mean.*

- *Test of whiteness*

  This checks that the innovation sequence is white (or uncorrelated). The test is based on the sample *autocorrelation* coefficient

$$\hat{R}_{\epsilon\epsilon}(\tau) = \frac{\hat{C}_{\epsilon\epsilon}(\tau)}{\hat{C}_{\epsilon\epsilon}(0)} \tag{3.86}$$

  and the sample autocovariance function is defined as

$$\hat{C}_{\epsilon\epsilon}(\tau) = \frac{1}{N}\sum_{k=\tau+1}^{N}\left(\epsilon(k)-\hat{\bar{\epsilon}}\right)\left(\epsilon(k-\tau)-\hat{\bar{\epsilon}}\right) \tag{3.87}$$

  Under the null hypothesis, $\hat{R}_{\epsilon\epsilon}(\tau)$ is asymptotically uncorrelated and normal with mean zero and variance $1/N$ for $\tau = 1, 2, \ldots, N-1$. Therefore, to accept the sensor ARMA model, not only must $\left|\hat{R}_{\epsilon\epsilon}(\tau)\right|$ lie within $1.96/\sqrt{N}$ for more than 95% and $2.58/\sqrt{N}$ for more than 99%, but it also should not exceed the upper limit by any significant margin.

Example 3.6

This example demonstrates the role of the two tests in validating the adequacy of the estimated sensor ARMA model. The sensor output is simulated at 1 Hz by

$$y(t) = G(q^{-1})\,u(t) + n(t)$$

and $G(q^{-1})$ is a 2nd order Butterworth lowpass filter with a bandwidth of 0.01 Hz. The input $u(t)$ is an uncorrelated random noise with mean 0.5 and variance 2.5×10^{-4} and a resonance is introduced in the measurement noise $n(t)$ by feeding a zero-mean random noise (variance 2.5×10^{-5}) through a bandpass filter (2nd order Butterworth with bandwidth from 0.3 to 0.4 Hz). A pair of second order Butterworth filters are chosen to decompose the signal and the measurement signal bandwidth ω_s is estimated from the sensor output spectrum to be 0.03 Hz. The raw sensor output and the spectra of the decomposed signals are given in Figure 3.20.

ARMA models of $\tilde{y}(t)$, with orders n $(= na = nc)$ varying from 1 to 5, are estimated by the RML algorithm using 2000 samples. The final estimates as well as the corresponding zeros and poles are tabulated below:

n	$\hat{A}(q^{-1})$	(poles)	$\hat{C}(q^{-1})$	(zeros)
1	$1 + 0.19q^{-1}$	-0.19	$1 - 0.52q^{-1}$	0.52
2	$1 + 1.03q^{-1} + 0.59q^{-2}$	$-0.52 \pm 0.57j$	$1 + 0.63q^{-1} - 0.32q^{-2}$	-0.96 0.33
3	$1 + 0.13q^{-1} - 0.23q^{-2}$ $- 0.40q^{-3}$	0.79 $-0.46 \pm 0.54j$	$1 - 0.34q^{-1} - 0.79q^{-2}$ $+ 0.54q^{-3}$	-0.99 $0.67 \pm 0.31j$
4	$1 - 0.81q^{-1} - 0.35q^{-2}$ $- 0.17q^{-3} + 0.41q^{-4}$	$0.88 \pm 0.13j$ $-0.47 \pm 0.55j$	$1 - 1.27q^{-1} - 0.47q^{-2}$ $+ 1.28q^{-3} - 0.49q^{-4}$	-0.99 0.81 $0.73 \pm 0.27j$
5	$1 + 0.060q^{-1} + 0.43q^{-2}$ $- 0.31q^{-3} - 0.11q^{-4}$ $- 0.24q^{-5}$	0.78 $-0.44 \pm 0.54j$ $^{\dagger}0.02 \pm 0.79j$	$1 - 0.41q^{-1} - 0.087q^{-2}$ $+ 0.33q^{-3} - 0.54q^{-4}$ $+ 0.39q^{-5}$	-0.99 $0.69 \pm 0.33j$ $^{\dagger}0.01 \pm 0.82j$

To verify the estimated models, the innovation sequences are generated by Equation 3.82 and tested for zero-mean and whiteness ($N = 2000$). The whiteness tests for $n = 1$ to 4 are depicted[27] in Figure 3.21 and the validation results are summarized as follows:

[27]The whiteness test for $n = 5$ is very similar to that for $n = 3$.

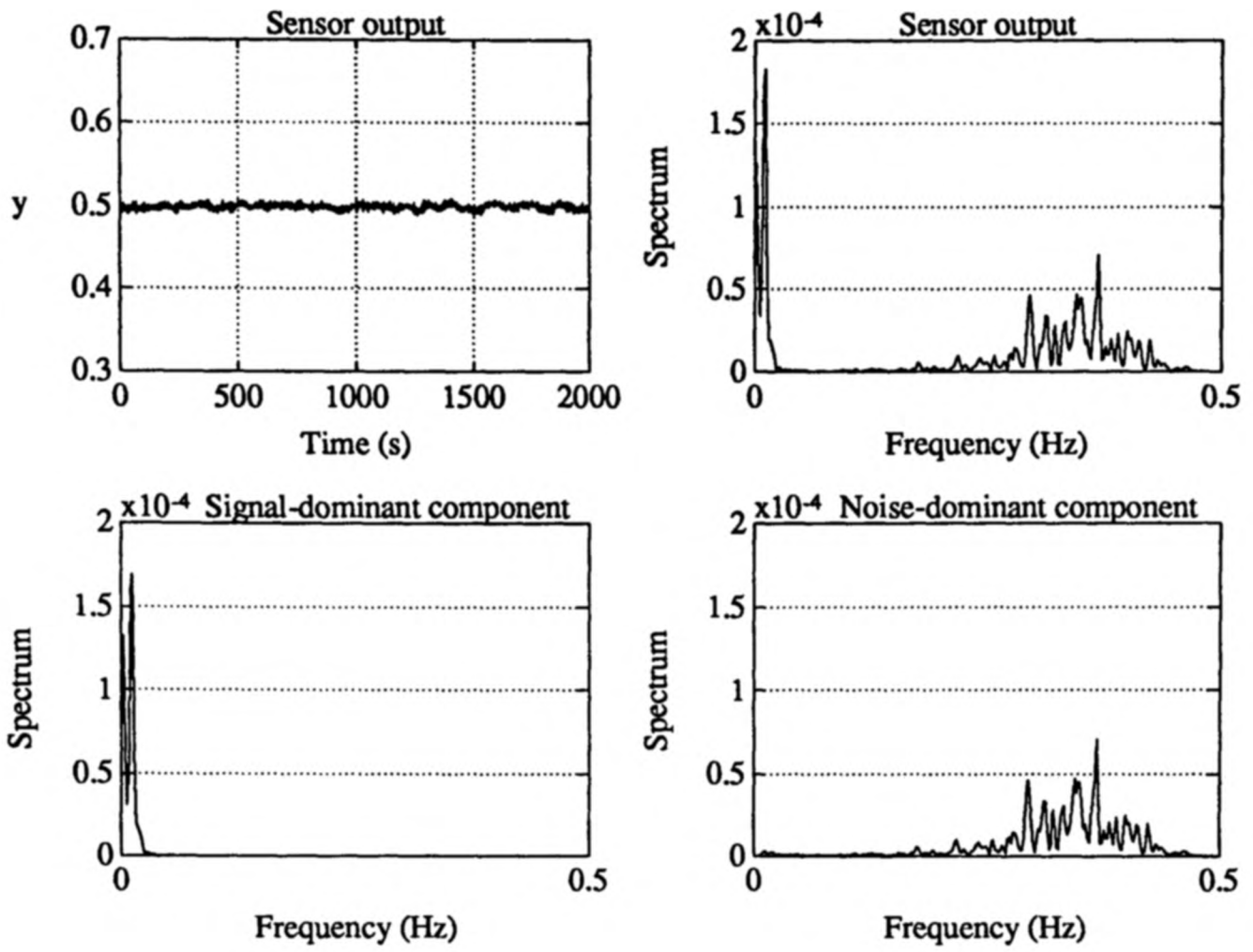

Figure 3.20: Power spectra of the decomposed signals

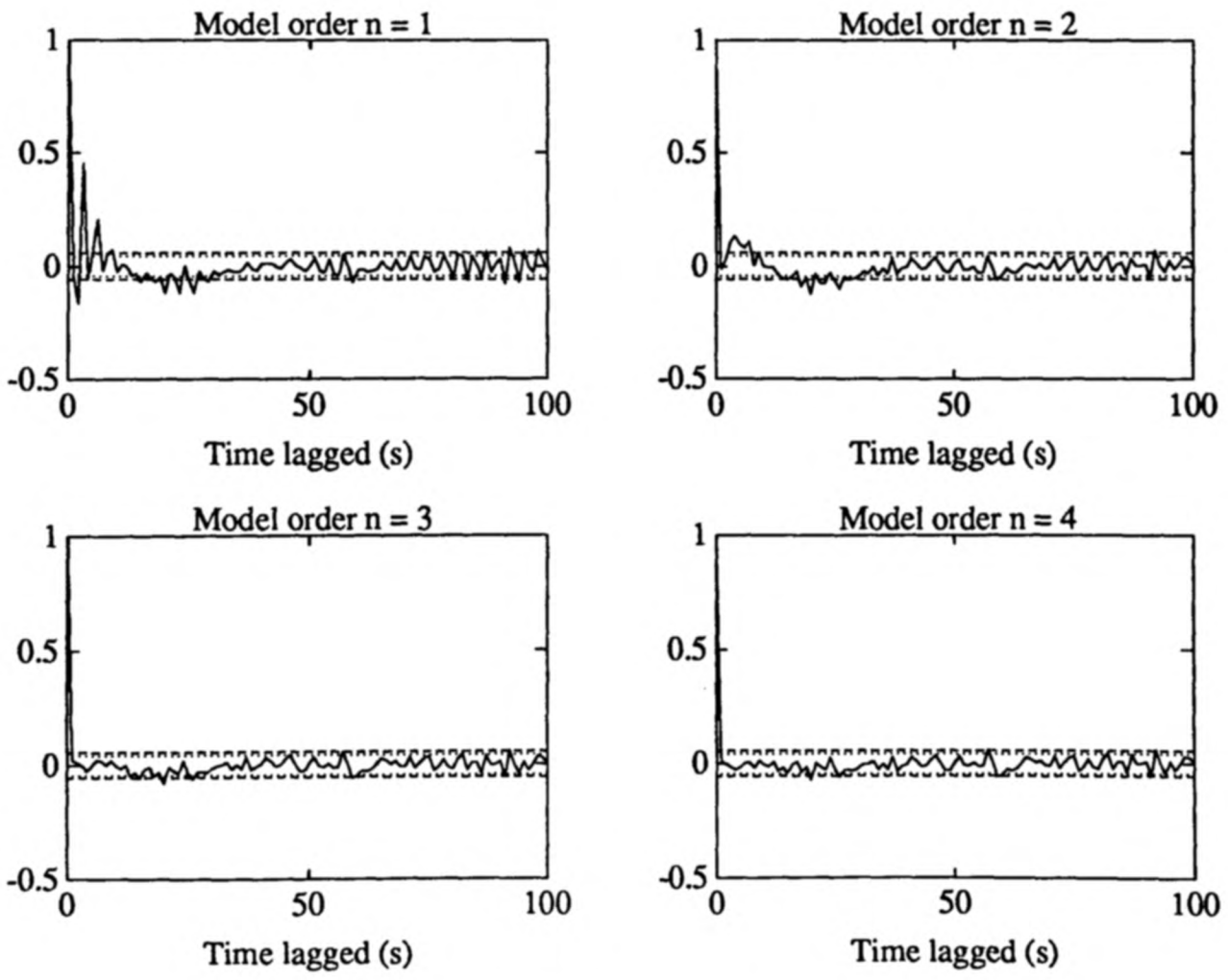

Figure 3.21: Whiteness tests (dotted: 5% limits, dashed: 1% limits)

n	*Test of mean*	*Test of whiteness*	
	Standardized mean (limit: 1.96)	*5% test* (limit: 100)	*1% test* (limit: 20)
1	−0.011 (passed)	132 (failed)	45 (failed)
2	−0.009 (passed)	73 (passed)	22 (failed)
3	−0.022 (passed)	36 (passed)	9 (passed)
4	−0.028 (passed)	29 (passed)	5 (passed)
5	−0.022 (passed)	36 (passed)	9 (passed)

From the discussions in Section 3.9.4, the order of the ARMA model is expected to be greater than two ($n_H = 2$ and $n_M > 0$ due to the resonance in the noise spectrum). Models with $n = 1$ and $n = 2$ do indeed fail the whiteness test and are shown to be inadequate. On the other hand, the near zero-pole cancellation (marked by † in the estimation results) suggests that the fifth order model is likely to be over-parameterized. An ARMA model with $n = 4$ turns out to be the 'best' choice in this example and it agrees with the particular settings in simulation and decomposition ($n_H = 2$ and $n_M = 2$).

3.11 Dither in sensor signal modelling

In most cases, the combination of a sensible design of a pair of decomposition filters and an effective estimation of the ARMA model would successfully partition the measurement signal and the measurement noise. Both the noise-dominant component $\tilde{y}(t)$ and the innovation sequence $\epsilon(t)$ would ideally be independent of the measurement signal and additionally, $\epsilon(t)$ is expected to be a zero-mean white noise process. However, problems may arise if the measurement signal is significantly nonstationary, especially if a representative 'worst-case' of the sensor output is not available in the learning stage due either to practical constraints or to the intrinsic nature of the process (e.g. the generalized input $v(t)$ cannot always be freely manipulated). In these circumstances, sensor ARMA modelling may, on the contrary, induce a substantial leakage of the measurement signal into $\epsilon(t)$, even though the signal appears to be severely suppressed in $\tilde{y}(t)$. The following example highlights the potential complications encountered in the afore-mentioned situations.

Example 3.7

The sensor output is simulated by feeding a white noise with mean 0.2 and variance 2.5×10^{-4} through a 2nd order Butterworth lowpass filter ($\omega_B = 0.01$ Hz). At the same time, it is corrupted by a zero-mean independent random noise with variance 2.5×10^{-5}. It is also known a priori that the measurement signal is subject to nonstationary step changes and the maximum jump $(\Delta v)_m$ is expected to be 0.3 unit. Based on Equation 3.27, the measurement signal bandwidth ω_s is estimated to be 0.13 Hz ($\mathcal{R}_s = 3600$, $\omega_B = 0.01$ Hz and $\ell = 2$). In line with Guideline 3.2, the sampling rate is selected to be 4 Hz and a total duration of 1000 s is studied, in which the first half of the data set (2000 samples) is reserved for the learning stage. Three step changes are initiated (all after the learning stage): 0.1 unit at 625 s, 0.2 unit at 750 s and finally 0.3 unit at 875 s. A pair of 2nd order Butterworth filters (cut-off frequency at ω_s) is utilized to partition the sensor output into $\bar{y}(t)$ and $\tilde{y}(t)$.

During the learning stage, a second order ARMA model of $\tilde{y}(t)$ (i.e. $na = nc = 2$) is identified by the RML algorithm and the final estimates is found to be

$$\begin{aligned} \hat{A}(q^{-1}) &= 1 + 0.23q^{-1} + 0.72q^{-2} \\ \hat{C}(q^{-1}) &= 1 - 0.033q^{-1} - 0.96q^{-2} \end{aligned}$$

Innovation sequence is then generated from Equation 3.82 both during the initial learning stage and the following tracking stage. The sensor output, the decomposed signals and the innovation at the two stages are shown in Figure 3.22. Despite having passed the validation tests in the learning stage as well as the absence of any evidence of measurement signal leakage into $\tilde{y}(t)$ over the entire period, features relating to the legitimate signal step changes undesirably reappear as 'spikes' in the innovation sequence during the tracking stage. This will introduce a serious upset in the innovation-based detection scheme (Section 4.2), leading to false alarms and unnecessary panic.

3.11.1 Sensor ARMA model as a whitening filter

In the commissioning stage and the learning stage, in addition to the design of the decomposition filters $L(q^{-1})$ and $H(q^{-1})$, the sensor ARMA modelling can, in fact, be considered as another exercise in filter design. The objective of the ARMA model estimation is to

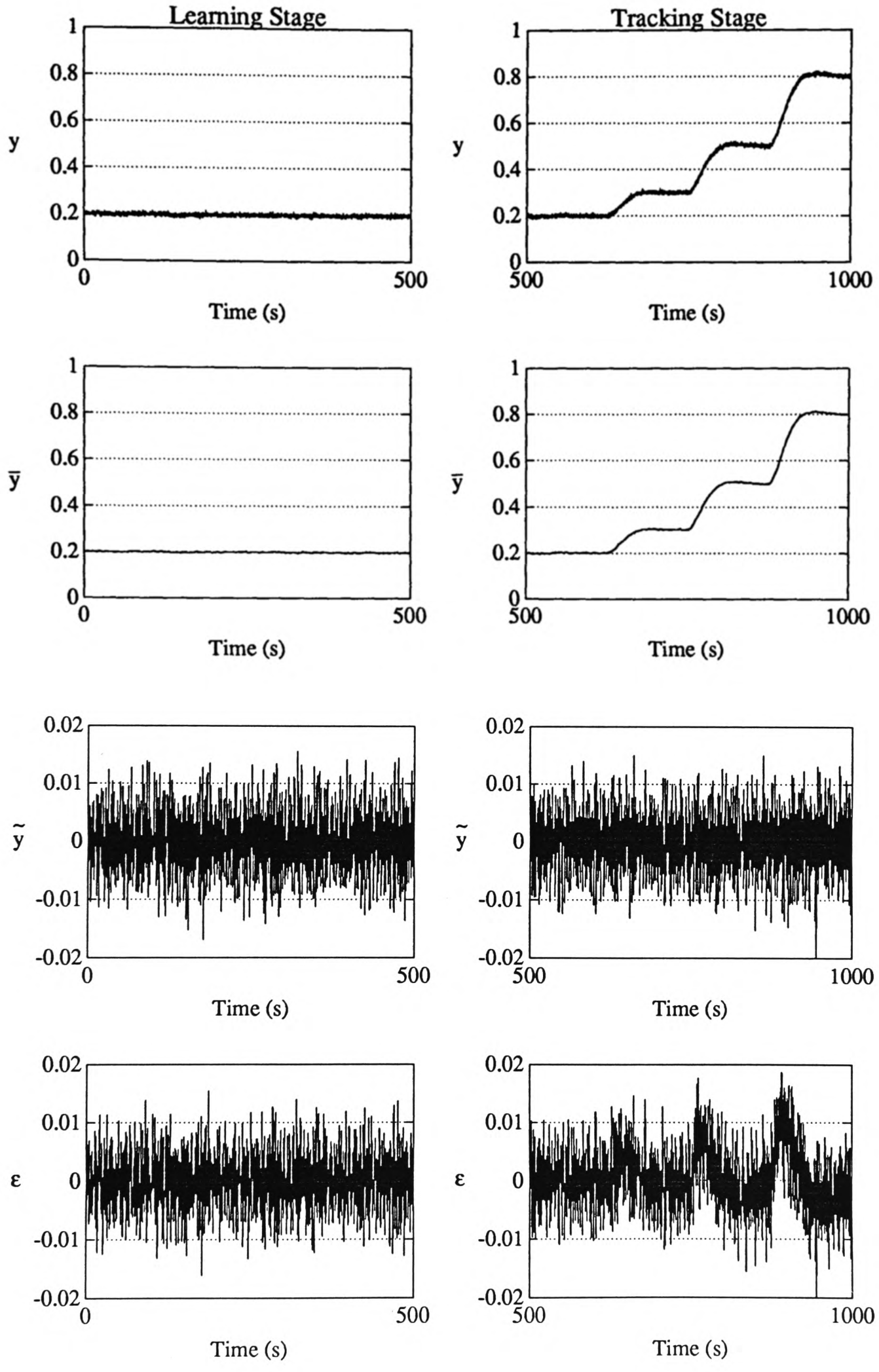

Figure 3.22: Decomposed signals and innovation sequence of a nonstationary sensor output

search for a pair of optimal polynomials $\hat{A}(q^{-1})$ and $\hat{C}(q^{-1})$ such that the innovation sequence $\epsilon(t)$ is a zero-mean white noise and its variance is minimized. It is equivalent to the design of a rational filter

$$\Gamma(q^{-1}) = \frac{\hat{A}(q^{-1})}{\hat{C}(q^{-1})} \tag{3.88}$$

so that its response to the noise-dominant component $\tilde{y}(t)$ will have a flat spectrum. $\Gamma(q^{-1})$ is generally known as a *whitening filter* [Candy, 1988, Chapter 10].

Similar to Equation 3.82, the innovation sequence can be generated by the whitening filter (Equation 3.88) as

$$\epsilon(t) = \Gamma(q^{-1})\,\tilde{y}(t) \tag{3.89}$$

By Parseval's theorem, the quadratic cost function in the ARMA model estimation can be formulated in the frequency domain

$$V(\theta) = \int_{-\omega_N}^{\omega_N} \left|\Gamma(e^{-j\omega T_m})\right|^2 \Phi_{\tilde{y}}(\omega)\,d\omega \tag{3.90}$$

$$= \int_{-\omega_N}^{\omega_N} \left|\Gamma(e^{-j\omega T_m})\right|^2 \left|H(e^{-j\omega T_m})\right|^2 ([\Phi_s](\omega) + \Phi_n(\omega))\,d\omega \tag{3.91}$$

where ω_N is the Nyquist frequency. Consider a simplified situation in which the filtered signal $H(q^{-1})\,s(t)$ and the filtered noise $H(q^{-1})\,n(t)$ can be perfectly separated about ω_s and $n(t)$ can be expressed as a filtered white noise (Equation 2.7), the cost function can then be split into two parts:

$$\begin{aligned} V(\theta) = &\int_{-\omega_s}^{\omega_s} \left|\Gamma(e^{-j\omega T_m})\right|^2 \left|H(e^{-j\omega T_m})\right|^2 [\Phi_s](\omega)\,d\omega \\ &+ \int_{\omega_s<|\omega|<\omega_N} \left|\Gamma(e^{-j\omega T_m})\right|^2 \left|H(e^{-j\omega T_m})\,M(e^{-j\omega T_m})\right|^2 \sigma_e^2\,d\omega \end{aligned} \tag{3.92}$$

To whiten the innovation sequence, $\Gamma^{-1}(e^{-j\omega T_m})$ will approximate $H(e^{-j\omega T_m})$ at frequencies below ω_s and $H(e^{-j\omega T_m})\,M(e^{-j\omega T_m})$ at higher frequencies. With an appropriate choice of noise filter, $H(q^{-1})\,s(t) \ll H(q^{-1})\,M(q^{-1})\,e(t)$. Coupling with the fact that ω_s should be less than a tenth of ω_N (Guideline 3.2), the second term in Equation 3.92 will certainly play a predominant role in the optimization process. Nonetheless, the signal suppression capability of $H(q^{-1})$ within its stop band ($\omega < \omega_s$) will inevitably be 'neutralized' to certain degrees by the whitening filter $\Gamma(q^{-1})$. In cases when the measurement signal is significantly nonstationary (as in Example 3.7), this counteracting effects will be absolutely disastrous.

It is interesting to revisit Example 3.7 and examine the effects of the whitening filters. Frequency responses of $H(q^{-1})$ (prior to estimation) and $\Gamma(q^{-1})\,H(q^{-1})$ (after estimation)

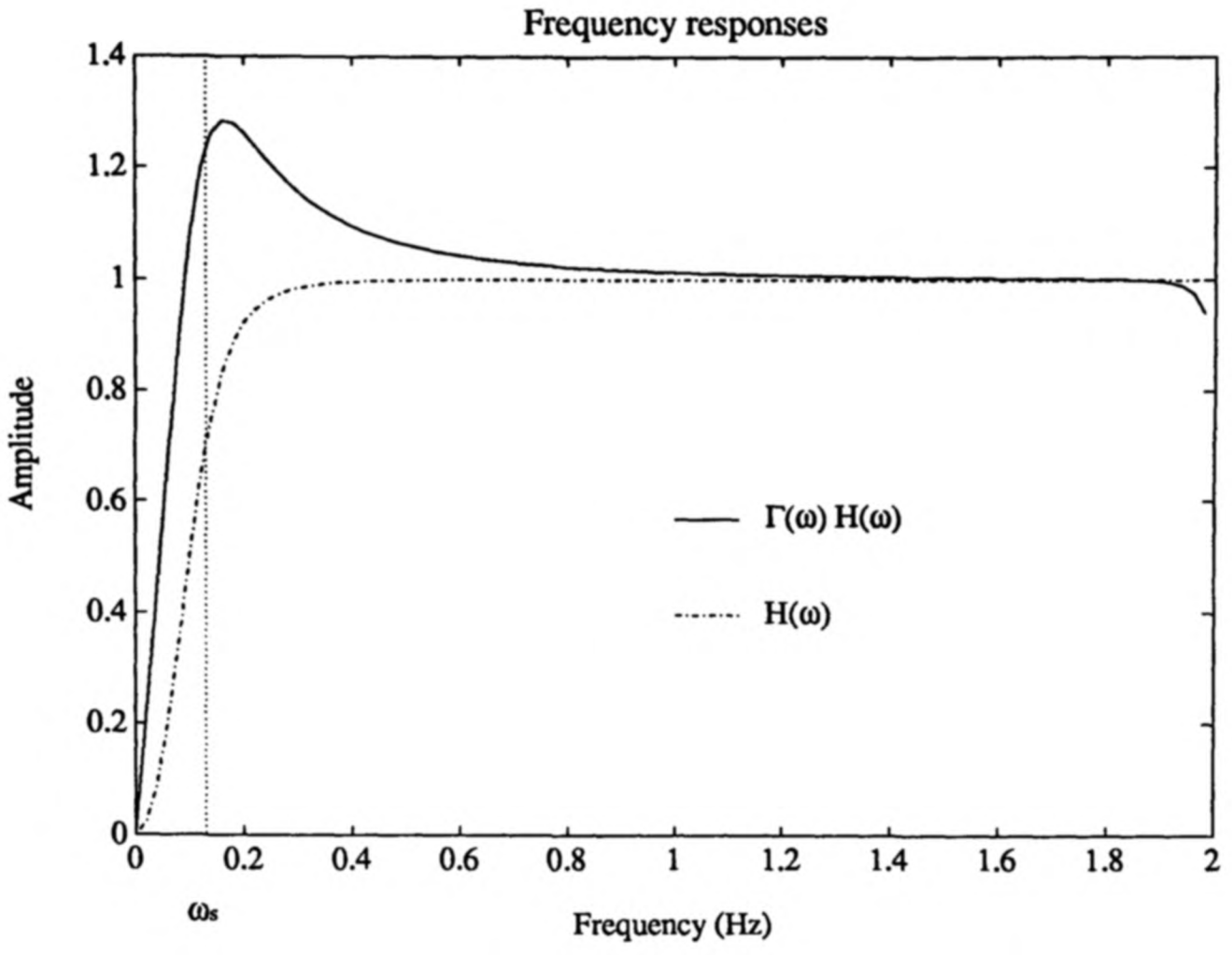

Figure 3.23: Frequency responses of $H(q^{-1})$ and $\Gamma(q^{-1})\,H(q^{-1})$ (Example 3.7)

are compared in Figure 3.23. It is obvious that the signal suppression actions ($\omega < \omega_s$) has been significantly[28] compensated by the whitening filter.

One appealing scenario is to impose frequency-dependent weightings on the optimization of the cost function. This can be achieved with the use of *prefilters* in input-output model estimation. This technique has attracted a lot of interest in system identification [Ljung, 1989; Wahlberg and Ljung, 1986; Ljung, 1987, Chapter 13] and adaptive control [Gunnarsson, 1988; Robinson and Clarke, 1991]. Mohtadi [1988] provides an in-depth explanation on the role of prefiltering and highlights the compromise between the matching of the input transfer function and that of the noise transfer function. Unfortunately, this approach is inappropriate for time-series estimation because of the lack of leverage between the known input and the random noise. Simple prefiltering of $\tilde{y}(t)$ is unproductive in providing frequency-dependent weightings, bearing in mind that $H(q^{-1})$ can already be considered as a prefilter by itself. All these call for a novel strategy to improve the estimation of the whitening filter $\Gamma(q^{-1})$.

[28]The frequency response of $\Gamma(q^{-1})\,H(q^{-1})$ will not be completely flat because the RML algorithm prevents $\Gamma(q^{-1})$ from exactly cancelling the differentiators in $H(q^{-1})$.

3.11.2 Injection of dither in sensor signal modelling

There are three basic problems in sensor ARMA model estimation:

- Nonstationarity of the measurement signal within the signal bandwidth ω_s;
- Unavailability of a 'worst-case' of sensor output during the learning stage;
- Counteraction of signal suppression within the stop band of $H(q^{-1})$ by the estimated whitening filter.

The key objective is to design a whitening filter $\Gamma(q^{-1})$ such that the innovation sequence is a zero-mean white noise process and is independent of the nonstationary measurement signal. It is proposed that all the three problems can be solved by deliberately injecting a bandlimited stochastic signal, called *dither*, into the estimation process.

Dithering, or addition of random signals, has been a well known technique in signal discretization (as briefly discussed in Section 3.6.3) [Blesser and Locanthi, 1987; de Lotto and Paglia, 1986; Vanderkooy and Lipshitz, 1987]. It has also found wide applications in nonlinear system control and analysis. Dither has been used to eliminate limit cycle behaviour in quantizers [Franklin and Powell, 1980, Section 7.5] and to minimize the influence of small amplitude nonlinearities (e.g. backlash) in closed loop control systems [Shinners, 1978, Section 8.10]. In addition, a small dither signal can also aid an identification process by exciting the required modes of the system [Brogan, 1991, Section 1.3]. For sensor signal modelling, the dither applied is specific in three ways:

Guideline 3.5 *The dither utilized in local sensor validation should satisfy the following properties:*

- *It should be a stationary zero-mean stochastic process with a rational spectral density function;*
- *It should be bandlimited within the signal bandwidth* ω_s*;*
- *It should be of considerable intensity, at least comparable with the measurement noise* $n(t)$ *and much larger than the 'worst' filtered signal* $H(q^{-1})\,s(t)$.

In contrast, dither in nonlinear systems is often selected to be outside the closed loop system bandwidth and typically has a meagre amplitude.

Consider the noise-dominant component being perturbed by a dither $d(t)$,

$$\tilde{y}_p(t) = \tilde{y}(t) + d(t) \tag{3.93}$$

where $d(t)$ is represented by an independent white noise $e_d(t)$ bandlimited by a filter $D(q^{-1})$ within the signal bandwidth ω_s

$$d(t) = D(q^{-1})\, e_d(t) \qquad \left|D(e^{-j\omega T_m})\right| \simeq 0 \quad \text{for } \omega > \omega_s \tag{3.94}$$

Since $d(t)$ is a stationary signal with a rational spectral density function, the perturbed noise-dominant component $\tilde{y}_p(t)$ can also be modelled by an ARMA process

$$A(q^{-1})\, \tilde{y}_p(t) = C(q^{-1})\, e(t) \tag{3.95}$$

The RML identification algorithm (Sections 3.9) and the validation tests (Section 3.10) are still applicable without any modification. Furthermore, based on Guideline 3.5, the quadratic estimation cost can now be expressed in the frequency domain as

$$\begin{aligned} V(\theta) \;=\; & \int_{-\omega_s}^{\omega_s} \left|\Gamma(e^{-j\omega T_m})\right|^2 \left(\left|H(e^{-j\omega T_m})\right|^2 [\Phi_s](\omega) + \Phi_d(\omega)\right) d\omega \\ & + \int_{\omega_s<|w|<\omega_N} \left|\Gamma(e^{-j\omega T_m})\right|^2 \left|H(e^{-j\omega T_m})\, M(e^{-j\omega T_m})\right|^2 \Phi_e(\omega)\, d\omega \qquad (3.96) \\ \simeq \; & \int_{-\omega_s}^{\omega_s} \left|\Gamma(e^{-j\omega T_m})\right|^2 \left|D(e^{-j\omega T_m})\right|^2 \Phi_{e_d}(\omega)\, d\omega \\ & + \int_{\omega_s<|w|<\omega_N} \left|\Gamma(e^{-j\omega T_m})\right|^2 \left|H(e^{-j\omega T_m})\, M(e^{-j\omega T_m})\right|^2 \Phi_e(\omega)\, d\omega \qquad (3.97) \end{aligned}$$

A few important issues can be deduced:

- Unlike $\tilde{y}(t)$, the perturbed noise-dominant component $\tilde{y}_p(t)$ is quasi-stationary over the entire observable bandwidth due to the dominance of the stationary dither within ω_s;

- Within the signal bandwidth ω_s, the response of the whitening filter $\Gamma(q^{-1})$ is dictated by the spectrum of the injected dither and is independent of the measurement signal and the noise filter. Hence, $\Gamma(q^{-1})$ is not compelled to be inversely related to $H(q^{-1})$;

- The response of $\Gamma(q^{-1})$ above ω_s is determined basically by the spectrum of the measurement noise ($\left|H(e^{-j\omega T_m})\right| \simeq 1, \omega > \omega_s$). Note that the injected dither is bandlimited and plays no part at frequencies above ω_s. This implies that the addition of dither will not affect the detectability of the sensor failures of interest;

- The magnitude of the dither regulates the response of $\Gamma(q^{-1})$ below ω_s and in turn provides an independent 'tuning knob' to enhance or reduce the effective suppression of the measurement signal in the final innovation sequence. Moreover, the absence of a 'worst case' during the learning stage will no longer be a problem;

Referring to Equation 3.96, as long as the dither $d(t)$ is comparable with the measurement noise $n(t)$, the resultant whitening filter $\Gamma(q^{-1})$ will not counteract the efforts of $H(q^{-1})$ in suppressing the bandlimited $s(t)$. Furthermore, by boosting $d(t)$ well above the measurement noise level, additional filtering within ω_s can be achieved.

Some guidelines are provided below for a successful implementation of dithering in sensor signal modelling:

Guideline 3.6 *If the measurement signal is significantly nonstationary, a dither,*

$$d(t) = D(q^{-1})\, e_d(t)$$

satisfying the properties laid down in Guideline 3.5, should be combined with the noise-dominant component $\tilde{y}(t)$ before being fitted by an ARMA model.

1. *$D(q^{-1})$ should be a relatively high order lowpass filter (e.g. Butterworth or Chebyshev) with cut-off frequency at the measurement signal bandwidth ω_s;*

2. *$e_d(t)$ should be a stationary zero-mean white noise with a variance exceeding that of the measurement noise σ_n^2. If a more exciting input is expected in the tracking stage and extra filtering of the measurement signal is called for, $\sigma_{e_d}^2$ should be increased accordingly. Considering the two input signal categories in Section 3.3.5,*
   - *White noise input* $\quad \sigma_{e_d}^2 = \mathcal{G}_o^2\, (\sigma_e^2)_m$
   - *Step input* $\quad \sigma_{e_d}^2 = \mathcal{G}_o^2\, (\Delta v)_m^2$

3. *With the presence of dither in the perturbed noise-dominant component $\tilde{y}_p(t)$, the selection of ARMA model orders (as discussed in Section 3.9.4) should be adjusted: $na = nc \simeq n_D + n_M$, where n_D is the order of $D(q^{-1})$ and n_M is used to model the noise spectrum at high frequencies.*

Example 3.8

This example sets out to explore the effectiveness of dither injection in sensor signal modelling. The same sensor output, with identical decomposition filters, as in Example 3.7

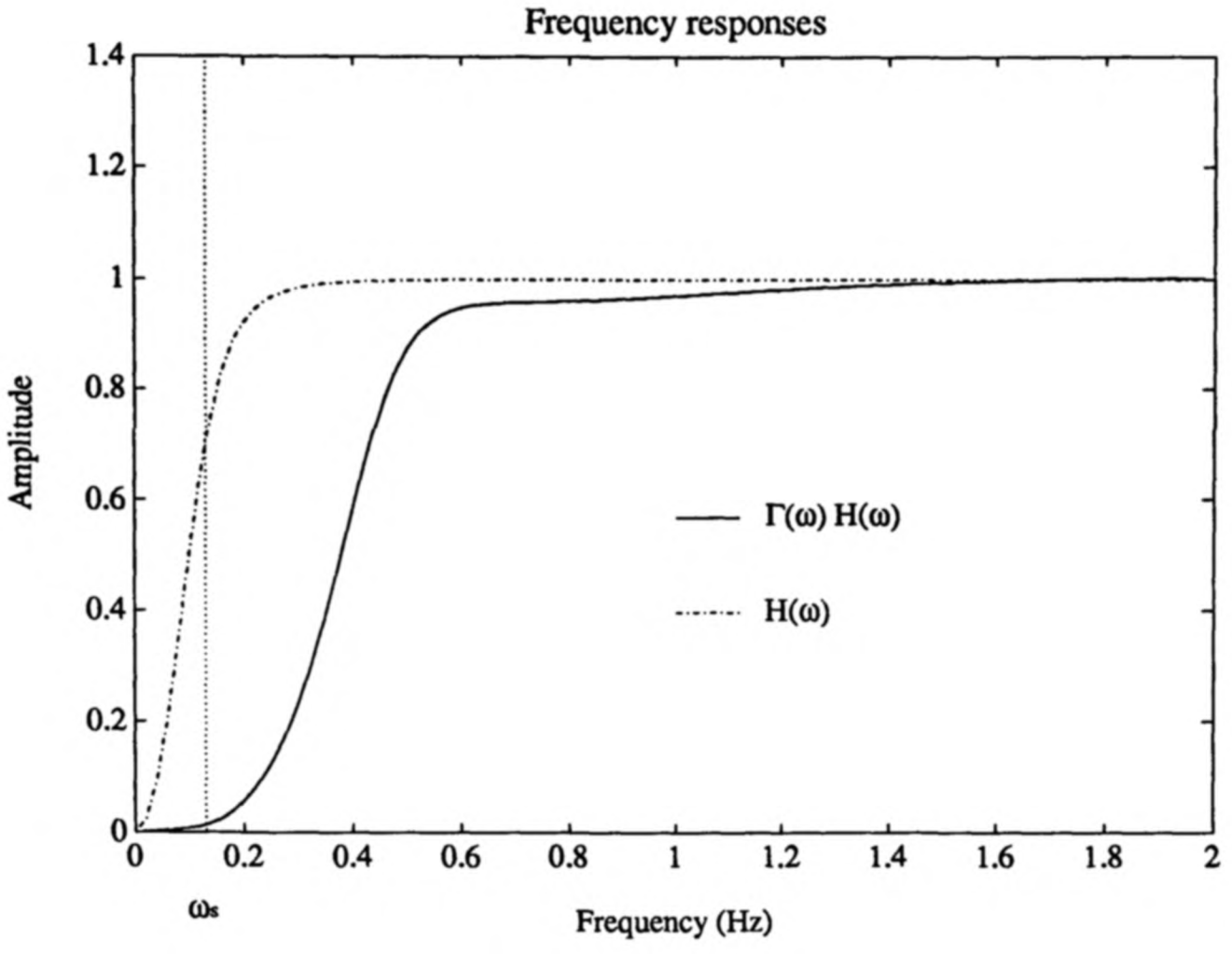

Figure 3.24: Frequency responses of $H(q^{-1})$ and $\Gamma(q^{-1})\,H(q^{-1})$ (dither injected)

is re-examined. Since a maximum step change of 0.3 unit is expected in the tracking stage, a dither is initiated with $D(q^{-1})$ selected as a 3rd order Chebyshev lowpass filter (cut-off at 0.13 Hz) and $\sigma^2_{e_d}$ fixed at 0.09 $(= \mathcal{G}_o^2\ (\Delta v)^2_m)$.

A third order ARMA model is fitted to the perturbed noise-dominant component $\tilde{y}_p(t)$ and the final estimates (by RML) are given by

$$\begin{aligned} \hat{A}(q^{-1}) &= 1 - 2.59q^{-1} + 2.25q^{-2} - 0.65q^{-3} \\ \hat{C}(q^{-1}) &= 1 - 1.53q^{-1} + 0.97q^{-2} - 0.18q^{-3} \end{aligned}$$

The frequency responses of the original noise filter $H(q^{-1})$ and its cascade with the whitening filter $\Gamma(q^{-1})\,H(q^{-1})$ are shown in Figure 3.24. Rather than opposing the signal suppression (Figure 3.23), it is clear that, with the addition of dither, the whitening filter imposes an even more severe filtering action within the measurement signal bandwidth. The sensor output $y(t)$, the signal-dominant component $\bar{y}(t)$, the perturbed noise-dominant component $\tilde{y}_p(t)$ and the innovation sequence $\epsilon(t)$ during the learning as well as the tracking stages are displayed in Figure 3.25. In contrast to Example 3.7, no evidence of leaked signature of $s(t)$ has been observed in the innovation.

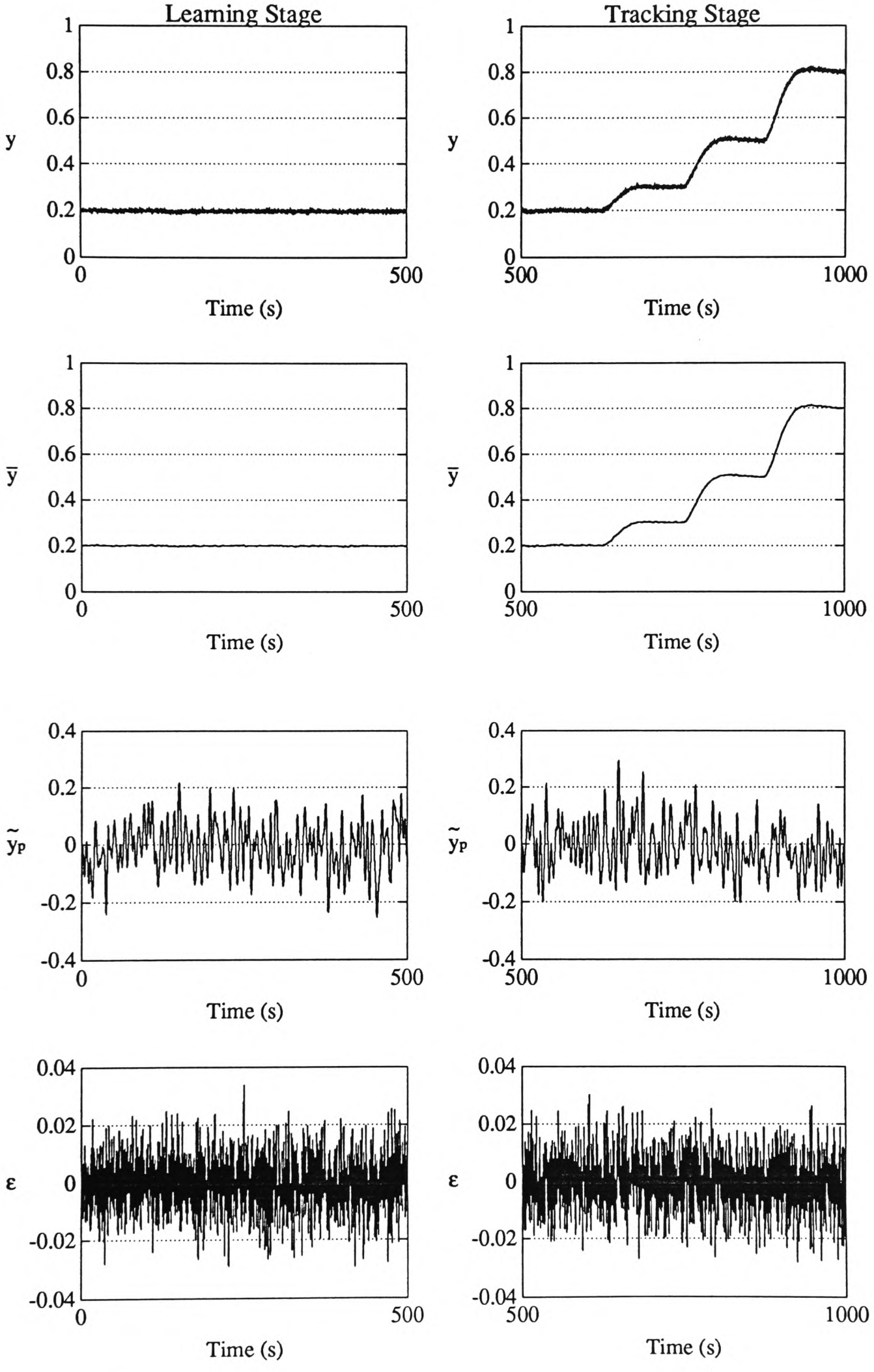

Figure 3.25: Decomposed signals and innovation sequence of a nonstationary sensor output with the injection of dither

3.12 Reference statistical and spectral properties

After adopting a sensible signal decomposition strategy (possibly with the assistance of dither injection) and obtaining a validated sensor ARMA model, the closing episode in the learning stage is to acquire some characteristic properties of the sensor signal that are needed in the tracking stage. Their utilities are multi-fold and they serve as:

- initialization quantities in signal processing algorithms;
- reference standards in failure detection;
- comparative benchmarks for failure identification.

Some reference statistical and spectral properties essential for the subsequent tracking stage are:

- Innovation mean $(\bar{\epsilon})_{\text{ref}}$;
- Innovation variance $(\sigma_\epsilon^2)_{\text{ref}}$;
- Innovation spectrum $(\Phi_\epsilon(\omega))_{\text{ref}}$.

Both $(\bar{\epsilon})_{\text{ref}}$ and $(\sigma_\epsilon^2)_{\text{ref}}$ are directly available from the zero-mean test in model validation (Equations 3.83 and 3.84) and $(\Phi_\epsilon(\omega))_{\text{ref}}$ can be evaluated by taking a Fourier Transform of the sample autocorrelation coefficient $\hat{R}_{\epsilon\,\epsilon}(\tau)$ accessible from the whiteness test (Equation 3.86).

3.13 Conclusions

The commissioning stage and the learning stage in the local sensor validation scheme and various problems encountered therein have been considered in detail in this chapter. These first two stages are inter-related and tightly interwoven. Together, they set up the necessary configurations and pave the way for the ensuing detection and diagnosis of sensor failures.

In the commissioning stage, a set of assumptions on the measurement signals, the measurement noise and the conditions of other equipments have been laid down to facilitate the analysis of a number of issues and a brief summary of the results of such investigation is as follows:

- A list of pertinent information, on both the sensor and the process, useful to local sensor validation is recommended.

- The measurement signal bandwidth has been formally defined in Equation 3.3. It is dependent on the process gain, the process bandwidth, the rate of roll-off at high frequencies, the 'worst' input spectrum and the strength of the measurement noise. Methods for extracting these relevant information have been discussed and for two typical input signals, namely steps and white noise, the signal bandwidth can be approximated based on Guideline 3.1.

- Comparing with typical control applications, a much faster sampling rate is required in a local sensor validation scheme. It is suggested that the Nyquist frequency should be at least ten times the measurement signal bandwidth (Guideline 3.2).

- The role of decimating filter in signal acquisition and interface has been explored. Not only does it provide a proper tool for signal downsampling, it can also alleviate the demanding requirement of anti-aliasing filter design by exchanging analog filtering for digital filtering. Furthermore, it has been found that the resolution of the discretized signal can be increased by augmenting the initial sampling rate and then applying the decimating filter to downsample the signal. It has been shown in Property 3.1 that under favourable conditions, every four-fold increase in the initial sampling rate will effectively increase the signal resolution by an extra bit.

- Various classical approaches in optimal filtering have been considered for the partition of the sensor output into the two components: measurement signal and measurement noise. None of the approaches is suitable and adequate for the local sensor validation scheme. Studies on optimal Wiener filtering reveal a number of basic properties (Guideline 3.3) on which the design of non-optimal decomposition filters could be based. The selection of corner frequencies and orders of the pair of decomposition filters is explained in Guideline 3.4.

A stochastic time-series model is selected during the learning stage to represent the 'healthy' sensor signal characteristics. An ARMA process is demonstrated to be superior to the more widely used AR approach in modelling the noise-dominant component. Based on a 'failure-free' observation, the unknown model parameters are identified by the RML algorithm. Practical choice of various 'tuning-knobs' in the identification algorithm is

also examined. Prior to its acceptance as a code of normal behaviour, the sensor ARMA model has to be validated by performing statistical tests on the mean and the whiteness of the innovation sequence. Finally, statistical and spectral properties of the sensor signals are acquired as reference standards and benchmarks for the ensuing failure detection and identification.

Sensor ARMA modelling can alternatively be considered as a design of a whitening filter and hence it tends to revive the measurement signals suppressed by the noise filter. In particular, when the signal is significantly nonstationary, this counteracting action can become unacceptable. The novel application of a low frequency bandlimited stochastic signal, called 'dithering' (Guideline 3.5), is proposed and its effects on the design of the whitening filter (or the sensor ARMA model) are evaluated. The injection of dither has several advantages:

- ensuring stationarity of the noise-dominant component within the measurement signal bandwidth,
- simulating a 'worst-case' of sensor output during the learning stage,
- providing a leverage to tune the desired response of the whitening filter.

Even in situations where the measurement signals are not particularly nonstationary, dither injection can still benefit signal decomposition and enhance model identification. Practical issues on the implementation of dither injection is covered in Guideline 3.6.

The work done in the commissioning stage and the learning stage has laid down solid groundwork on which the subsequent tracking stage could be built. The development of this final stage will be discussed in Chapter 4.

Chapter 4

The Tracking Stage

4.1 Introduction

During the commissioning and the learning stage, appropriate strategies to 'decompose' (Section 3.7) and to 'whiten' (Sections 3.9 and 3.11) the sensor outputs are formulated. The resulting signals available to the tracking stage consist of the raw sensor output $y(t)$, the signal-dominant component $\bar{y}(t)$, the noise-dominant component $\tilde{y}(t)$ and its whitened counterpart, the innovation, $\epsilon(t)$. A prime objective in the tracking stage is to extract and capture essential characteristics of these four signals which will reflect any anomalies in the sensor. In principle, it is not possible to distinguish sensor malfunctions from legitimate sensor output changes within the measurement signal bandwidth ω_s without further prior assumptions (Section 2.7). Except for hardover failures (which are specified directly in terms of the raw sensor outputs) and drift failures (whose failure signatures are often minute, if at all present, in $\tilde{y}(t)$ and $\epsilon(t)$ (Section 3.7.3)), the validation scheme should focus on signal behaviour outside ω_s.

The tracking stage is divided into the ordinary and the alert phase. In the ordinary phase, simple and proficient signal processing techniques are employed to extract and to monitor sensor signal characteristics. A primarily innovation-based approach is to be adopted and failure alarm indicators are provided to signify any abnormality in the sensor output. The development of various efficient processing tools, namely mean, variance, rate of change and measure of bias, and the formulation of alarm indicators will be discussed in detail in this chapter.

The alert phase is initiated whenever an alarm is triggered during the ordinary phase. A 'rule-based' system, supported by additional signal processing algorithms, is proposed to diagnose the sensor failure based on the reference properties acquired in the learning

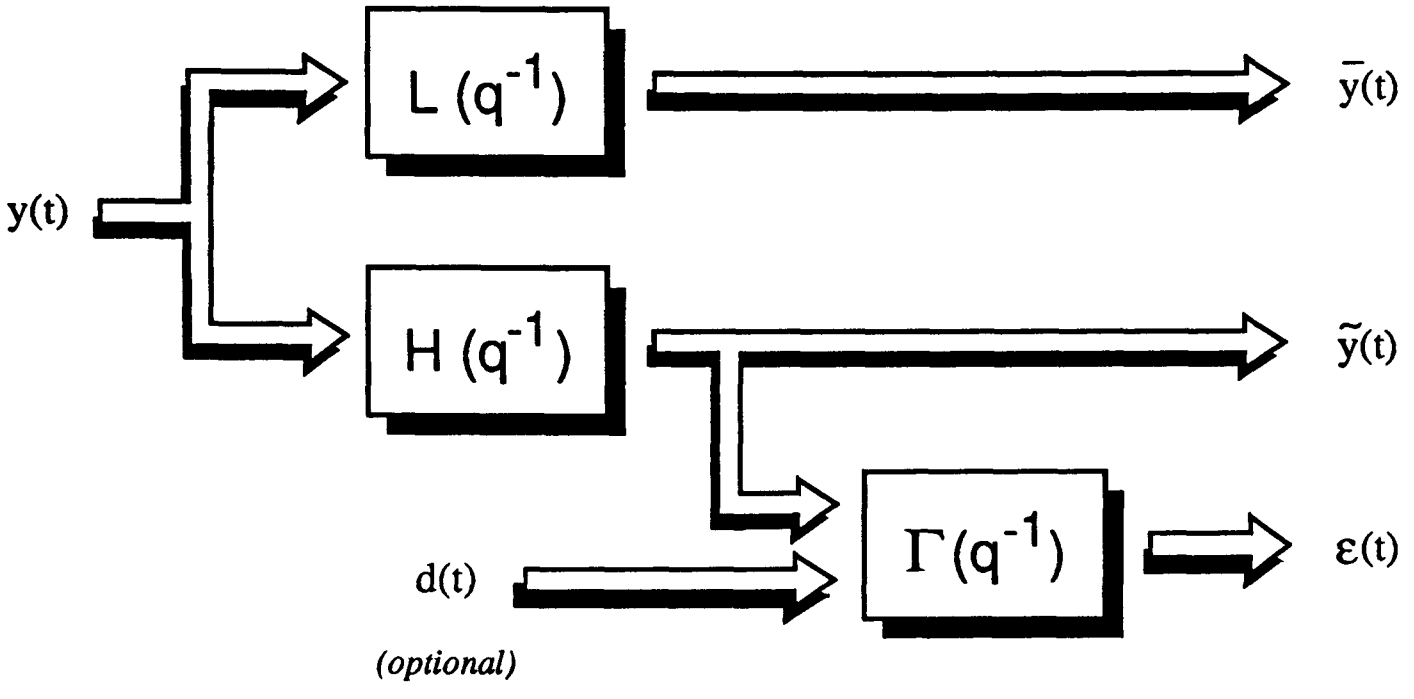

Figure 4.1: Innovation generation and signal decomposition of the sensor output

4.2 Innovation-based failure detection

Sensor validation in the tracking stage is primarily based on the *innovations* of the ARMA model on $\tilde{y}(t)$ (Section 3.8). The final estimate of the model, $\hat{A}(q^{-1})$ and $\hat{C}(q^{-1})$, are used to design a *whitening filter* $\Gamma(q^{-1})$ (Section 3.11.1) to generate the innovation sequence

$$\epsilon(t) = \frac{\hat{A}(q^{-1})}{\hat{C}(q^{-1})}\tilde{y}(t) \tag{4.1}$$

$$= \Gamma(q^{-1})\,\tilde{y}(t) \tag{4.2}$$

Figure 4.1 illustrates the signal decomposition and the innovation generation procedures during the tracking stage.

Apart from playing a critical role in model validation (Section 3.10), innovations also find wide applications in system identification [Aasnaes and Kailath, 1973] and control [Milito *et al.*, 1973]. Innovation-based approach is also one of the mainstreams in conventional failure detection and identification. Two key and original papers are Kailath [1970] and Mehra and Peschon [1971]. Other references include Bellingham and Lees [1977a], Emami-Naeini *et al.* [1988], Halme and Selkäinaho [1984], Usoro *et al.* [1985] and Yoshimura *et al.* [1979].

In local sensor validation, an innovation-oriented technique has an overwhelming advantage over an approach based simply on the noise-dominant component $\tilde{y}(t)$. For a 'healthy' sensor, despite $\tilde{y}(t)$ being 'coloured' by the measurement noise and the decomposition filter, the innovation sequence $\epsilon(t)$ should still be a zero-mean white noise process. These well defined statistics enable established statistical tests to be directly applicable and simplify the implementation of the subsequent detection algorithms.

Example 4.1

This example examines the innovation signal characteristics for various typical sensor failure modes[1] as discussed in Section 2.4.2. The legitimate sensor output in an open loop environment is simulated as

$$y_l(t) = G(q^{-1})\, u(t) + n(t)$$

where $G(q^{-1})$ is a 2nd order Butterworth lowpass filter with a system bandwidth ω_B of 0.01 Hz while the input signal $u(t)$ is a random noise with mean 0.5 and variance 2.5×10^{-3}. The measurement noise is taken to be zero-mean Gaussian white noise with variance 2.5×10^{-5}. From Equation 3.26, the measurement signal bandwidth ω_s is estimated to be 0.047 Hz. A total of 3000 s of data are sampled at 1 Hz.

Failures are introduced into the sensor output at time t_f equals to 2500 s. For additive failures (bias, spike, erratic, cyclic and drift),

$$y(t) = y_l(t) + f(t)$$

and for non-additive failures (stuck and nonlinear),

$$y(t) = h_f\,(y_l(t))$$

With reference to Equations 2.12 to 2.16 in Section 2.5.1 and Equations 2.18 and 2.19 in Section 2.5.2, the various failures simulated in this example are summarized as follows:

[1] Hardover failures are left out in this example since their detection is based directly on the sensor output $y(t)$.

Failure mode	*Failure parameters*	*Equation*
Bias	$\Theta(q^{-1}) = 1,\ \vartheta_1 = 0.05$	(2.12)
Spike	$\Theta(q^{-1}) = 1,\ \vartheta_1 = -0.05$	(2.13)
Erratic	$\Theta(q^{-1}) = 1,\ \vartheta_1 = 7 \times 10^{-3}$	(2.14)
Cyclic	$\vartheta_1 = 0.01,\ \vartheta_2 = 0.1,\ \vartheta_3 = 0$	(2.15)
Drift	$\vartheta_1 = -0.0004$	(2.16)
Stuck	$y_{\text{stuck}} = y(t)\|_{t=2499\,\text{s}}$	(2.18)
Nonlinear (saturation)	$\underline{y}_{\text{sat}} = 0.49,\ \bar{y}_{\text{sat}} = 0.51$	(2.19)

A pair of 2nd order lowpass and highpass Butterworth filters with corner frequencies at ω_s are chosen to be the signal and the noise filters respectively. In addition, Gaussian distributed dither is injected ($D(q^{-1})$ is a 3rd order Chebyshev lowpass filter cutting off at ω_s and $\sigma_{e_d}^2$ is 2.5×10^{-3}) to enhance the effectiveness of signal suppression. During the learning stage (first 2000 s), a third order ARMA model ($na = nc = 3$) is identified by RML and validated for adequacy. The final estimates of the two polynomials are:

$$\begin{aligned} \hat{A}(q^{-1}) &= 1 - 0.78q^{-1} - 0.94q^{-2} + 0.83q^{-3} \\ \hat{C}(q^{-1}) &= 1 - 0.14q^{-1} - 0.65q^{-2} + 0.49q^{-3} \end{aligned}$$

The innovation sequences are then generated by Equation 4.1 in the tracking stage (2001 s to 3000 s). Both the sensor outputs and the innovations for different sensor failures are displayed in Figures 4.2 and 4.3. Except for the drift failure[2] (Figure 4.3(c)), all other failures exhibit recognizable signatures in the innovations. Bias (Figure 4.2(b)) and spike (Figure 4.2(c)) failures manifest themselves as abrupt jumps in $\epsilon(t)$ whilst stuck[3] (Figure 4.2(d)), erratic (Figure 4.3(a)), cyclic (Figure 4.3(b)) and saturation (Figure 4.3(d)) failures alter the excitation of the innovation. These signal patterns will be closely monitored by the validation scheme in the tracking stage.

[2]Refer to Section 3.7.3 for an explanation.

[3]The small variations in $\epsilon(t)$ when the sensor becomes stuck are due to the injected dither.

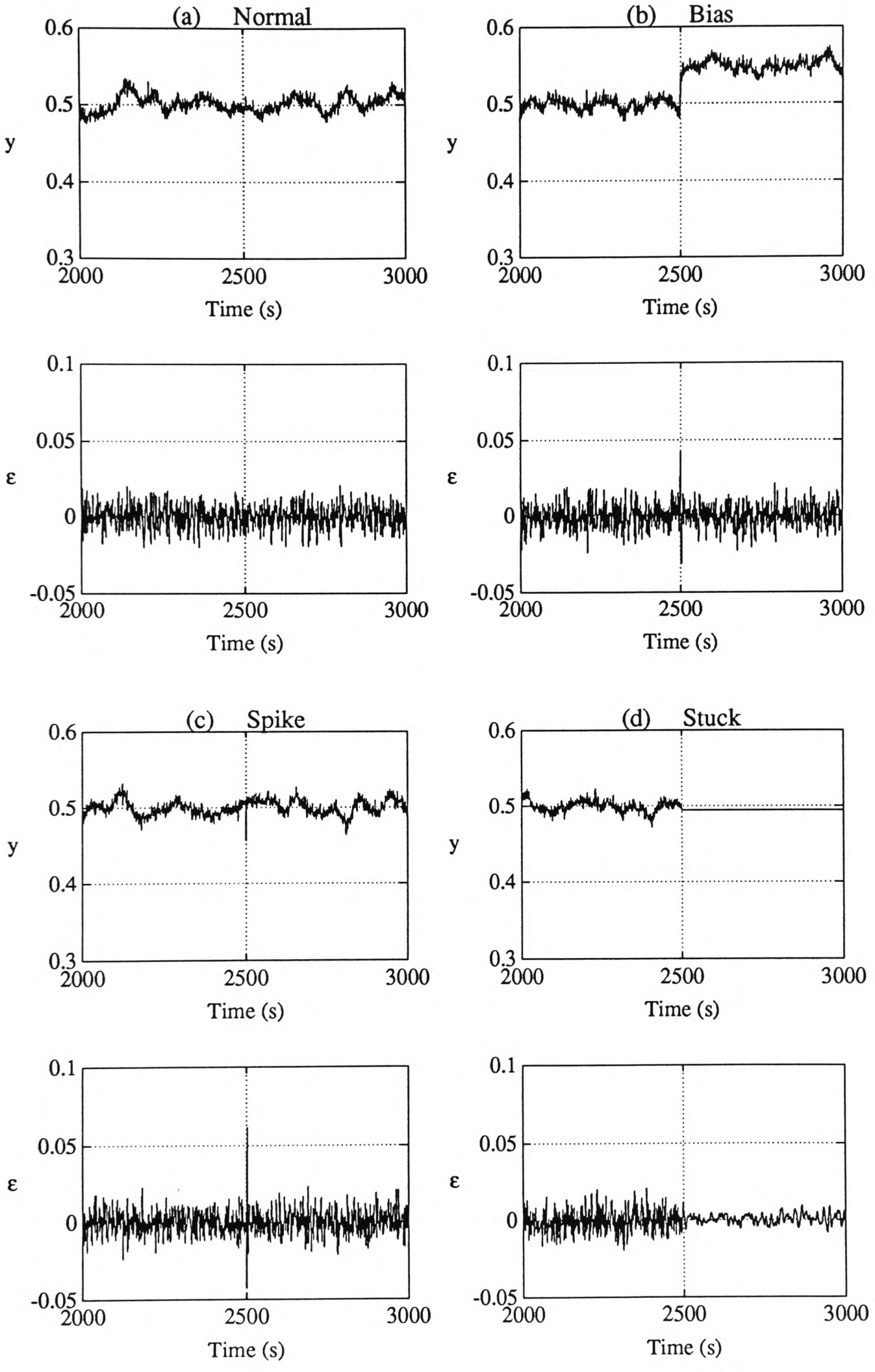

Figure 4.2: Sensor outputs and innovation sequences for various failure modes (normal, bias, spike and stuck)

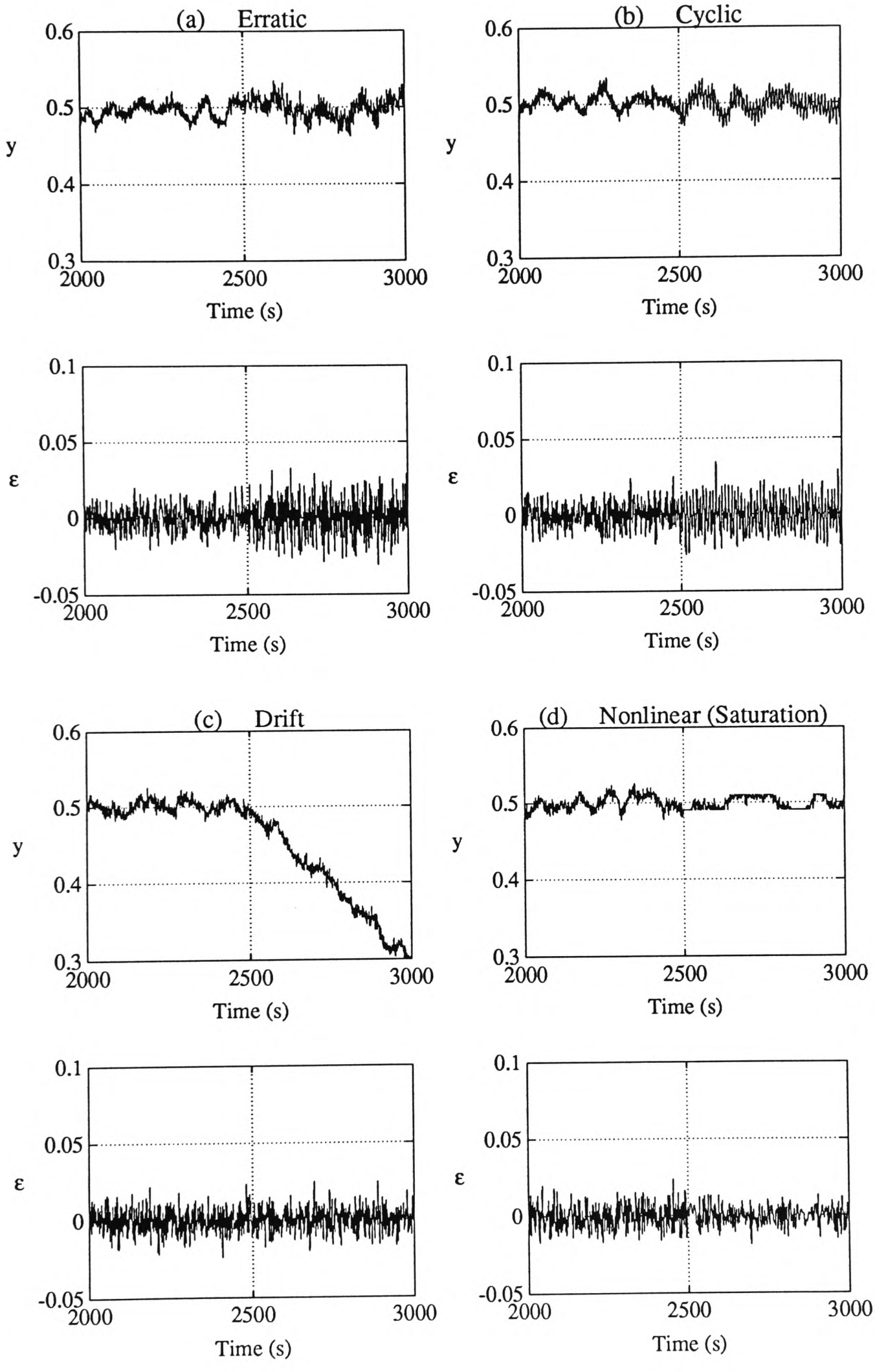

Figure 4.3: Sensor outputs and innovation sequences for various failure modes (erratic, cyclic, drift and nonlinear)

4.3 Signal processing in sensor validation

Signal characteristics of the sensor output $y(t)$, the signal-dominant component $\bar{y}(t)$ and the innovation $\epsilon(t)$ are extracted by signal processing techniques during the tracking stage. Current 'integrated' or 'smart' sensors have restricted computational capabilities (Section 2.8), simple and efficient algorithms are therefore much preferred in order to attain expeditious detection.

It is suggested in Sections 2.4.2 and 4.2 that an excessive rate of change of $y(t)$, a persistent drifting action in $\bar{y}(t)$, an abrupt jump in $\epsilon(t)$ and a significant alteration in the excitation of $\epsilon(t)$ are all evidences of sensor failures. Quantities that are continuously being monitored include:

- Mean
- Variance
- Rate of change
- Measure of bias

Appropriate algorithms to estimate these variables in a recursive manner will be derived and the selection of various 'tuning-knobs' will be discussed. Although specifically designed for the sensor validation scheme, the following algorithms can be utilized in any general applications.

4.3.1 Recursive mean computation

The aggregate sample mean of a discrete signal $x(t)$ up to time t is given by (c.f. Equation 3.83)

$$\bar{x}(t) = \frac{1}{t} \sum_{k=1}^{t} x(k) \tag{4.3}$$

It is clearly an inefficient way of mean estimation as it requires an indefinitely growing buffer to store all the values of $x(t)$. An equivalent recursive version can be written as

$$\bar{x}(t) = \left(1 - \frac{1}{t}\right) \bar{x}(t-1) + \frac{1}{t} x(t) \tag{4.4}$$

The current sample mean is then given by a weighted sum of the previous mean and the current value $x(t)$. A serious drawback of this approach is that the weighting $1/t$ will tend

to zero over time and the estimator will become insensitive to any new information. The adaptivity can be maintained by fixing the weightings of the estimator at predetermined levels. This results in an efficient mean estimator which can be implemented recursively as

$$\hat{\bar{x}}(t) = (1-\alpha)\,\hat{\bar{x}}(t-1) + \alpha\, x(t) \tag{4.5}$$

where $0 < \alpha \leq 1$. The performance of this mean estimator will be analyzed below in both the time domain (Property 4.1) and the frequency domain (Property 4.2).

Property 4.1 *The mean estimator presented in Equation 4.5 is asymptotically unbiased with an effective window length of* $(2/\alpha) - 1$.

The computation of the sample mean $\hat{\bar{x}}(t)$ can be expressed explicitly as a sum of the current and the past values of the signal, $\{x(1),\ x(2),\ \ldots,\ x(t)\}$, with exponentially decaying weightings (recalling that $0 < \alpha \leq 1$)

$$\hat{\bar{x}}(t) = (1-\alpha)^t\,\hat{\bar{x}}(0) + \alpha \sum_{k=0}^{t-1} (1-\alpha)^k\, x(t-k) \tag{4.6}$$

Assuming $x(t)$ to be a stationary and ergodic random variable with population mean μ_x and population variance σ_x^2. Taking the expectation over both sides of Equation 4.6,

$$\begin{aligned} E\left[\hat{\bar{x}}(t)\right] &= (1-\alpha)^t\,\hat{\bar{x}}(0) + \alpha\,\mu_x \sum_{k=0}^{t-1} (1-\alpha)^k \\ &= (1-\alpha)^t\,\hat{\bar{x}}(0) + \mu_x \left(1 - (1-\alpha)^t\right) \end{aligned} \tag{4.7}$$

As $t \to \infty$,

$$E\left[\hat{\bar{x}}(t)\right] = \mu_x \tag{4.8}$$

Hence, Equation 4.5 is an asymptotically unbiased estimator of the mean. If $x(t)$ is further assumed to be uncorrelated, the variance of the mean estimate will be

$$\begin{aligned} \mathrm{var}\left(\hat{\bar{x}}(t)\right) &= \alpha^2\,\sigma_x^2 \sum_{k=0}^{t-1} (1-\alpha)^{2k} \\ &= \frac{\alpha}{2-\alpha}\,\sigma_x^2 \left(1 - (1-\alpha)^{2t}\right) \end{aligned} \tag{4.9}$$

Again, as $t \to \infty$,

$$\mathrm{var}\left(\hat{\bar{x}}(t)\right) = \frac{\alpha}{2-\alpha}\,\sigma_x^2 \tag{4.10}$$

It is well known that the variance of a moving-average mean with a fixed window size n (i.e. constant weights of $1/n$) is given by σ_x^2/n [Mulholland and Jones, 1983, Section 14.4].

It therefore follows that the effective window length of the adopted mean estimator should be

$$m = \frac{2}{\alpha} - 1 \tag{4.11}$$

and

$$\alpha = \frac{2}{m+1} \tag{4.12}$$

Property 4.2 *To a first approximation, the mean estimator in Equation 4.5 is equivalent to a first order lowpass filter with unity gain and a cut-off frequency at* $\alpha\, f_m/(1-\alpha)\ rads^{-1}$, *where* f_m *is the sampling frequency in Hz.*

From Equation 4.5, the mean estimator can be rewritten in a transfer function formulation

$$\hat{\bar{x}}(t) = \frac{\alpha}{1-(1-\alpha)\,q^{-1}}\, x(t) \tag{4.13}$$

It is obvious that the transfer function has a steady state gain of one, which agrees with the unbiased property of the estimator (Property 4.1). Consider a first order unity-gain lowpass filter with cut-off frequency at $\omega_c\,\mathrm{rad\,s^{-1}}$. An approximate transformation of the filter transfer function from the continuous to the discrete time domain ($s \mapsto (1-q^{-1})\, f_m$) will yield

$$\frac{\omega_c}{s+\omega_c} \mapsto \frac{\dfrac{\omega_c}{\omega_c+f_m}}{1-\left(1-\dfrac{\omega_c}{\omega_c+f_m}\right) q^{-1}} \tag{4.14}$$

Comparing Equations 4.13 and 4.14, the mean estimator can be regarded as a first order lowpass filter where

$$\alpha = \frac{\omega_c}{\omega_c+f_m} \tag{4.15}$$

and equivalently, the cut-off frequency of the filter is found to be

$$\omega_c = \frac{\alpha\, f_m}{1-\alpha} \tag{4.16}$$

Finally, issues on the initialization and on the selection of α are discussed in Guideline 4.1

Guideline 4.1

1. **Initialization of the mean estimator**

   The only initial information required by the mean estimator is $\hat{\bar{x}}(0)$, *which should be used to incorporate any prior knowledge on the mean level if available. Otherwise, a sensible choice is to set* $\hat{\bar{x}}(0)$ *to be equal to the first sample* $x(1)$ *(i.e.* $\hat{\bar{x}}(1) = x(1)$*).*

2. **Choice of α**

The selection of α is based either on the effective window length m (Property 4.1), which is directly related to the response time to a genuine change of mean, or on the bandwidth of the estimator (Property 4.2), which should be smaller than the bandwidth of the signal of interest.

For instance, the recursive mean estimation of the innovation sequence during the tracking stage can be initialized with $\hat{\bar{\epsilon}}(0) = (\bar{\epsilon})_{\text{ref}}$ (Section 3.12), while α should be less than $\frac{\omega_s}{\omega_s + f_m}$ in computing the mean of the sensor output.

4.3.2 Spike-insensitive variance estimation

The variance provides an authentic and a reliable indication of the excitation of a signal. It serves as a forefront watchdog for a large variety of sensor failures (e.g. stuck, erratic, cyclic and saturation). Although variance is a critical parameter in numerous application areas, issues concerning its estimation are rarely touched upon. By far the most popular recursive approach is the use of a sliding window (or a moving-average procedure) in which the sample variance is computed on-line from a collection of the current value and a certain amount of the past values. This is definitely inefficient both in terms of storage and computational requirements. In this section, an efficient recursive variance estimator is first developed for general purposes and is subsequently 'updated' to incorporate robustness against spikes and outliers.

An exponential variance filter

An unbiased sample variance of a discrete signal $x(t)$ up to time t is given by [Mulholland and Jones, 1983, Section 14.4]

$$\sigma_x^2(t) = \frac{1}{t-1} \sum_{k=1}^{t} (x(k) - \bar{x}(t))^2 \tag{4.17}$$

$$= \frac{t}{t-1} \left(\overline{x^2}(t) - (\bar{x}(t))^2 \right) \tag{4.18}$$

where $\bar{x}(t)$ is the sample mean defined in Equation 4.3 and $\overline{x^2}(t)$ is the sample mean square of the signal defined similarly as

$$\overline{x^2}(t) = \frac{1}{t} \sum_{k=1}^{t} (x(k))^2 \tag{4.19}$$

Following the same lines of arguments in Section 4.3.1, an efficient on-line variance estimator can be derived as a scaled difference between the mean square estimate and the square of the mean estimate,

$$\hat{\sigma}_x^2(t) = \frac{2-\alpha}{2(1-\alpha)} \left(\widehat{\overline{x^2}}(t) - \left(\hat{\bar{x}}(t) \right)^2 \right) \tag{4.20}$$

where the sample mean estimate $\hat{\bar{x}}(t)$ is computed from Equation 4.5 and the sample mean square estimate $\widehat{\overline{x^2}}(t)$ is implemented likewise as the output of an exponential filter

$$\widehat{\overline{x^2}}(t) = (1-\alpha)\, \widehat{\overline{x^2}}(t-1) + \alpha\, (x(t))^2 \tag{4.21}$$

The leading scaling factor in Equation 4.20 is introduced to guarantee that the estimator is unbiased.

Property 4.3 *The recursive algorithm defined in Equation 4.20 is an asymptotically unbiased estimator of variance with an effective window length of* $(2/\alpha)-1$ *and a bandwidth of* $\alpha\, f_m/(1-\alpha)\ rads^{-1}$, *where* f_m *is the sampling frequency in Hz.*

Assuming $x(t)$ to be a stationary and ergodic stochastic process with population mean μ_x, population mean square μ_{x^2} and population variance σ_x^2. Following a similar procedure to that in Property 4.1, it is straightforward to show that the mean square estimator (Equation 4.21) is asymptotically unbiased, i.e. as $t \to \infty$,

$$E\left[\widehat{\overline{x^2}}(t)\right] = \mu_{x^2} \tag{4.22}$$

Taking the expectation over both sides of Equation 4.20 and letting $t \to \infty$,

$$E\left[\hat{\sigma}_x^2(t)\right] = \frac{2-\alpha}{2(1-\alpha)} \left(\mu_{x^2} - \left(\text{var}\left(\hat{\bar{x}}(t) \right) + \left(E\left[\hat{\bar{x}}(t) \right] \right)^2 \right) \right) \tag{4.23}$$

Substituting Equations 4.8 and 4.10 into Equation 4.23,

$$\begin{aligned} E\left[\hat{\sigma}_x^2(t)\right] &= \frac{2-\alpha}{2(1-\alpha)} \left(\left(\mu_{x^2} - (\mu_x)^2 \right) - \frac{\alpha}{2-\alpha} \sigma_x^2 \right) \\ &= \sigma_x^2 \end{aligned} \tag{4.24}$$

Therefore, Equation 4.20 is an asymptotically unbiased estimator of variance. The effective window length and the bandwidth of the estimators has been derived in Properties 4.1 and 4.2 respectively. It is interesting to express the scaling factor in Equation 4.20 in terms of the effective window length m (Equation 4.11)

$$\frac{2-\alpha}{2(1-\alpha)} = \frac{m}{m-1} \tag{4.25}$$

which agrees with the theoretical scaling adopted in Equation 4.18.

Guideline 4.2

1. **Initialization of the exponential variance estimator**

   The initial condition for the mean estimator, $\hat{\bar{x}}(0)$*, has already been recommended in Guideline 4.1. The initial value for the mean square estimate can be formulated as*

$$\widehat{\overline{x^2}}(0) = \left(\hat{\bar{x}}(0)\right)^2 + \hat{\sigma}_x^2(0) \tag{4.26}$$

   where $\hat{\sigma}_x^2(0) \geq 0$*. If prior knowledge about the variance of the signal is available,* $\hat{\sigma}_x^2(0)$ *should be selected accordingly. Otherwise,* $\hat{\sigma}_x^2(0)$ *can be set to 0.*

2. **Choice of** α

   Refer to Guideline 4.1 for a discussion of the selection of α*.*

For example, in estimating the variance of the innovation sequence during the tracking stage, $\hat{\bar{\epsilon}}(0)$ can be set to $(\bar{\epsilon})_{\text{ref}}$ and $\hat{\sigma}_\epsilon^2(0)$ to $(\sigma_\epsilon^2)_{\text{ref}}$.

Example 4.2

This example evaluates the tracking performance and the outlier sensitivity of the variance estimator defined in Equation 4.20.

A white noise $x_1(t)$ with time-varying variances is simulated at 1 Hz for a duration of 5000 s. The variances at different time intervals are specified as follows:

Time (s)	*Variance*
0 – 1000	1
1001 – 2000	1.5
2001 – 3000	0.5
3001 – 4000	2
4001 – 5000	1

Equation 4.20 is employed to estimate the variance recursively ($\alpha = 0.01$, $\hat{\bar{x}}_1(0) = x_1(1)$ and $\hat{\sigma}_{x_1}^2(0) = 1$) and the results (Figure 4.4) are very encouraging. Not only is the estimator able to track the increases and decreases in variances, but it also returns unbiased estimates at the various time intervals.

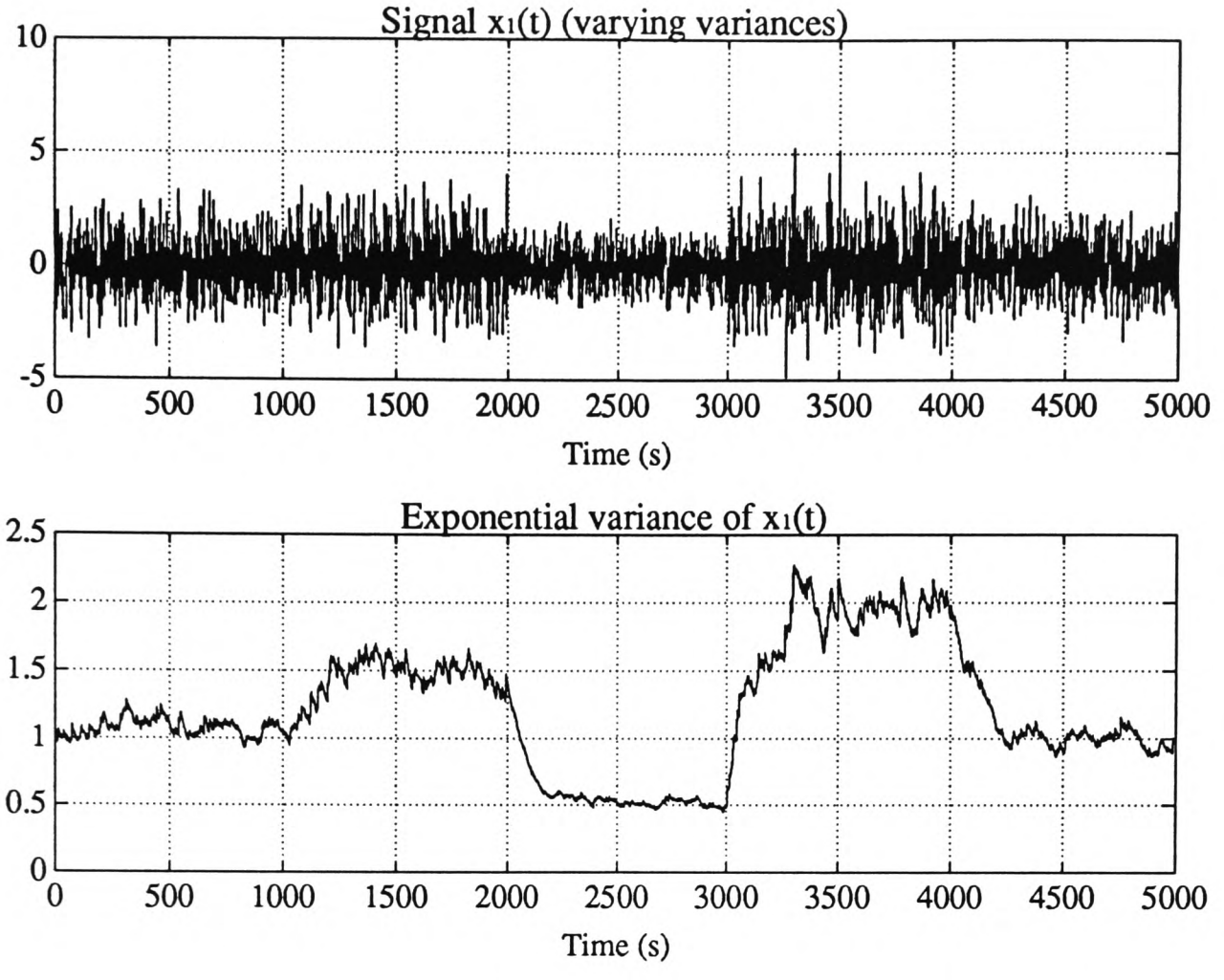

Figure 4.4: Exponentially filtered variance

In another trial, an outlier and a lowpass filtered spike are introduced at 2500 s and 3500 s respectively ($x_2(t)$). The recursive estimates of the variance are displayed in Figure 4.5. Both the outlier and, in particular, the filtered spike generate misleading estimates of the variance. Local sensor validation demands a reliable measure of the excitation of innovation and the on-line estimates of the innovation variance should therefore be insensitive to the 'spikes' produced by a bias or a spike sensor failure. The rest of this section will address this problem in more details and an improved estimator with a combination of logical and exponential filters will be developed.

A spike-insensitive variance filter

The study of outlier-insensitive estimation has received a lot of attention in the field of *robust identification* [Huber, 1981; Sprent, 1989, Chapter 9]. Various techniques have evolved and representative examples include robust L_p estimators [McMichael, 1990], median filters [Juhola *et al.*, 1991], nonlinear 'fractal' filters [Strahle, 1988], and logical filters [Pehrson, 1968; Clarke, 1983]. Among all these, logical filtering is the most efficient to be computed and the easiest to be implemented.

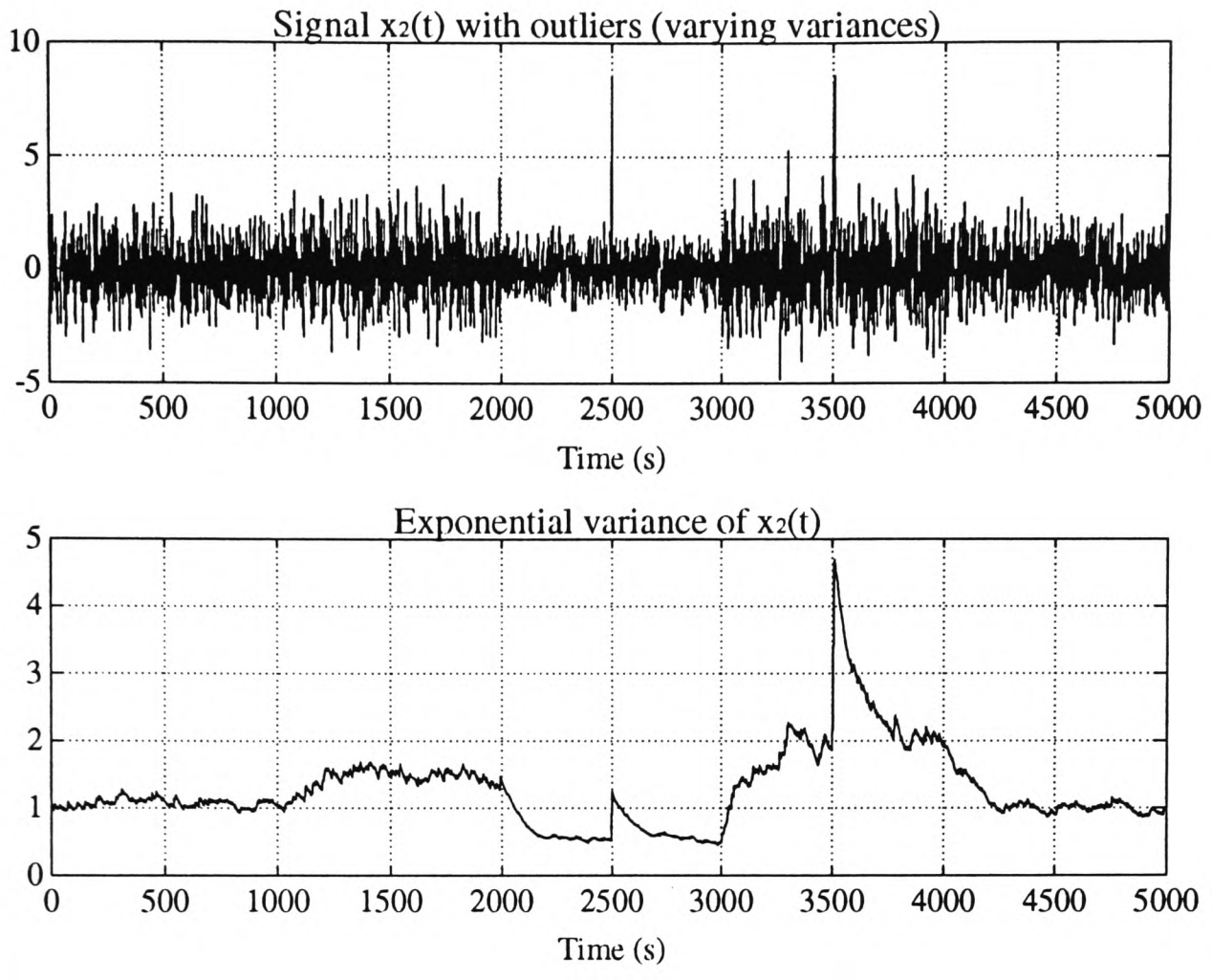

Figure 4.5: Exponentially filtered variance (with outliers)

In local sensor validation, the variance of the innovation sequence is one of the fundamental signal parameters to be monitored. It has been demonstrated in Example 4.2 that an outlier or a filtered spike (signatures of a bias or a spike failure in $\epsilon(t)$) will seriously upset an exponential variance estimator. An improved alternative is required and should satisfy the following two specifications:

- The estimator should be able to track changes in variance and should return an on-line unbiased estimate;
- The estimator should be robust against outliers and filtered spikes.

One immediate complication is the dilemma between the demand of insensitivity towards filtered spikes and the requirement of trackability of variance increases. Features of the signal during the initial stage of a variance increase actually look very similar to the presence of spikes.

To gain some insights, an exponential variance estimator preceded by an independent logical spike filter put forward in Clarke [1983] is first studied. The logical filter has a 'dynamic' window which allows small variations through but clips excessive deviations.

The gap of the window is expanded (doubled each time) or contracted (halved each time) according to the excitation of the signal in order that the filter can track step changes. Consider $x(t)$ and $x_f(t)$ to be the raw signal and the output from the logical filter respectively. $W(t)$ is the window gap at time t which is bounded by a lower limit of W_m. The procedures carried out within a single iteration are summarized as follows:

A cascade of a logical filter and an exponential variance estimator (4.27)

1. Evaluate the deviation
$$\delta_x(t) = x(t) - x_f(t-1)$$

2. If $|\delta_x(t)| \leq W(t)$ (i.e. deviation within window gap), the signal will be passed straight on and the window gap will be reduced,
$$\begin{aligned} x_f(t) &= x(t) \\ W(t+1) &= \max\left(\frac{1}{2}W(t), W_m\right) \end{aligned}$$

3. If $|\delta_x(t)| > W(t)$ (i.e. deviation exceeding the window gap), the signal will be clipped and the window gap will be expanded,
$$\begin{aligned} x_f(t) &= x_f(t-1) + W(t)\,\mathrm{sign}\,(\delta_x(t)) \\ W(t+1) &= 2\,W(t) \end{aligned}$$
where sign $(\delta_x(t))$ is the sign of the deviation.

4. Estimate the variance of $x(t)$ by computing on-line the variance of $x_f(t)$, $\hat{\sigma}^2_{x_f}(t)$, using the exponential filter algorithm given in Equation 4.20.

The initial conditions required are $x_f(0)$, $\hat{\bar{x}}_f(0)$ and $\hat{\sigma}^2_{x_f}(0)$ (e.g. $x_f(0) = \hat{\bar{x}}_f(0) = x(1)$, $\hat{\sigma}^2_{x_f}(0) = 0$), and at the outset, the window gap is set to the minimum value $W(1) = W_m$. This approach is proficient in minimizing the effects of single outliers but fails to suppress filtered spikes. Furthermore, the choice of W_m is ad hoc and the logical spike filter is not designed to handle variations in variances.

A full integration of a more sophisticated logical filter and the unbiased exponential variance estimator is proposed. Two 'dynamic', rather than one, thresholds are employed: a lower *warning* threshold $W_\ell(t)$ and an upper *failing* threshold $W_u(t)$. Both are initialized by their respective lower limits, $(W_\ell)_m$ and $(W_u)_m$ (where $(W_\ell)_m < (W_u)_m$), and

are increased or decreased by a fixed step of $\Delta W = ((W_u)_m - (W_\ell)_m)/2$. In addition, information on both the current and the previous sign of excessive deviation, $s_{\bar{\delta}_x}(t)$ and $s_{\bar{\delta}_x}(t-1)$, are utilized in the update of the thresholds. The two thresholds introduce three operating states in the variance estimator: *normal*, *warning* and *failed*. The estimator will be declared 'normal' if no unexpected deviation has occurred. On the other hand, the estimator will be flagged 'failed' if a significant outlier is observed and all estimation processes will then be suspended. The intermediate 'warning' state indicates that a suspicious, but not definite, spike is present but if the deviations consecutively exceed the warning threshold, the estimator will automatically signify a 'failed' state. The steps taken in each iteration are laid down as follows:

An integrated logical and exponential variance estimator (4.28)

1. Compute the 'normalized' deviation

$$\bar{\delta}_x(t) = \frac{x(t) - \hat{\bar{x}}(t-1)}{\hat{\sigma}_x(t-1)}$$

2. If the warning indicator (or the failed indicator) is on and the current deviation is of opposite sign to the previous excessive deviation, both the warning and the failed indicators will be reset.

3. If $\bar{\delta}_x(t) \leq W_\ell(t)$ (small variations),

   - If the failed indicator is on, the estimation will be frozen (i.e. $\hat{\bar{x}}(t) = \hat{\bar{x}}(t-1)$, $\widehat{\overline{x^2}}(t) = \widehat{\overline{x^2}}(t-1)$ and $\hat{\sigma}_x^2(t) = \hat{\sigma}_x^2(t-1)$). Note that Step 2 implies that the current deviation is still of the same sign as the previous excessive deviation and the sign of excessive deviation will be kept on a hold: $s_{\bar{\delta}_x}(t) = s_{\bar{\delta}_x}(t-1)$.
   - If the failed indicator is off,
     - the mean, the mean square and the variance estimate ($\hat{\bar{x}}(t)$, $\widehat{\overline{x^2}}(t)$ and $\hat{\sigma}_x^2(t)$) will be updated by the exponential algorithms given in Equations 4.5, 4.21 and 4.20;
     - the warning indicator will be turned off and $s_{\bar{\delta}_x}(t)$ will be set to 0.
   - Both the warning and the failing thresholds will be decreased

$$\begin{aligned} W_\ell(t+1) &= \max\left(W_\ell(t) - \Delta W, (W_\ell)_m\right) \\ W_u(t+1) &= \max\left(W_u(t) - \Delta W, (W_u)_m\right) \end{aligned}$$

4. If $\bar{\delta}_x(t) > W_\ell(t)$ (warning threshold exceeded),

   - The current sign of excessive deviation will be updated

     $$s_{\bar{\delta}_x}(t) = \text{sign}(\bar{\delta}_x(t))$$

   - If $\bar{\delta}_x(t) \leq W_u(t)$ and the warning indicator is off (i.e. the very first warning encountered),

     - the mean, the mean square and the variance will be updated with the exponential filters (Equation 4.5, 4.21 and 4.20);
     - the warning indicator will be flagged and the failing threshold will be decreased,

       $$W_u(t+1) = \max\left(W_u(t) - \Delta W, (W_u)_m\right)$$

   - If $\bar{\delta}_x(t) > W_u(t)$ or warning indicator has already been on, (i.e. a significant outlier or a double warning),

     - if $\bar{\delta}_x(t) > W_u(t)$ (a significant outlier) and $s_{\bar{\delta}_x}(t)\, s_{\bar{\delta}_x}(t-1) = -1$ (different signs of excessive deviations), the failing threshold will be increased;

       $$W_u(t+1) = W_u(t) + \Delta W$$

     - if $\bar{\delta}_x(t) \leq W_u(t)$ (a double warning), the failing threshold will be decreased;

       $$W_u(t+1) = \max\left(W_u(t) - \Delta W, (W_u)_m\right)$$

     - the estimation of mean, mean square and variance will be disabled;
     - both the warning and failing indicators will be turned on.

   - If $s_{\bar{\delta}_x}(t)\, s_{\bar{\delta}_x}(t-1) = -1$ (different signs of excessive deviations), the warning threshold will be increased;

     $$W_\ell(t+1) = W_\ell(t) + \Delta W$$

   - The relative magnitudes of the two thresholds will be verified

     $$W_u(t+1) = \max\left(W_\ell(t+1), W_u(t+1)\right)$$

At its normality, the spike-insensitive variance estimator is unbiased and efficient because of the underlying exponential filter algorithm. Once the estimator is declared 'failed', it

will not be reset until the deviation $\bar{\delta}_x(t)$ becomes opposite in sign to the detected outlier and the estimator remains temporarily disabled. This allows the estimator not only to be robust against simple outliers, but also to be insensitive to filtered spikes as well. One drawback is its inability to track large step changes which, fortunately, are extremely rare in the innovation sequence[4]. By normalizing the deviations and permitting the thresholds to expand and to contract, the tracking property of the variance estimator is preserved and the effects of spikes are continually minimized.

Guideline 4.3

1. **Initialization of the spike-insensitive variance estimator**

   A number of variables have to be initialized for the spike-insensitive variance filter. The selection of $\hat{\bar{x}}(0)$ *and* $\widehat{\overline{x^2}}(0)$ *has been recommended in Guidelines 4.1 and 4.2 respectively. The choice of the initial variance is more critical (c.f. Guideline 4.2) and it is in general safer to overestimate* $\hat{\sigma}_x^2(0)$*. If* $\hat{\sigma}_x^2(0)$ *is too small, the estimator will be continuously flagged 'failed' and completely suspended from scratch. If there is a good reason to believe that the signal is zero-mean (e.g. the innovation sequence), a sensible option is to set* $\hat{\sigma}_x^2(0)$ *to* $(x(1))^2$*.*

   Moreover, both the warning and the failed indicators should initially be off and the sign of excessive deviation, $s_{\bar{\delta}_x}(0)$*, should be set to 0. Finally, the warning and the failing thresholds should start from their respective lower limits, i.e.* $W_\ell(t) = (W_\ell)_m$ *and* $W_u(t) = (W_u)_m$*.*

2. **Choice of** α**,** $(W_\ell)_m$ **and** $(W_u)_m$

   The choice of α *has been discussed in Guideline 4.1. Since* $\bar{\delta}_x(t)$ *is normalized by the on-line estimates of the standard deviation, the two thresholds can be chosen with reference to the significance levels provided that the distribution of the signal is known. Even with an unknown distribution, a reasonable pair of thresholds (e.g. somewhere between 2 and 4) will suffice for the application. In fact, the estimator is capable of adapting the thresholds to cater for the particular distribution. If the signal* $x(t)$ *is Gaussian,* $(W_\ell)_m$ *can be elected to be 2.58 (1% significance level) and* $(W_u)_m$ *to be 3.89 (0.01% significance level).*

---

[4]The presence of differentiators in the noise filter $H(q^{-1})$ (Guideline 3.3) removes any direct bias in $\tilde{y}(t)$ as well as in $\epsilon(t)$. The step changes in $\epsilon(t)$ introduced by the drifting actions in the sensor output $y(t)$ are usually insignificant.

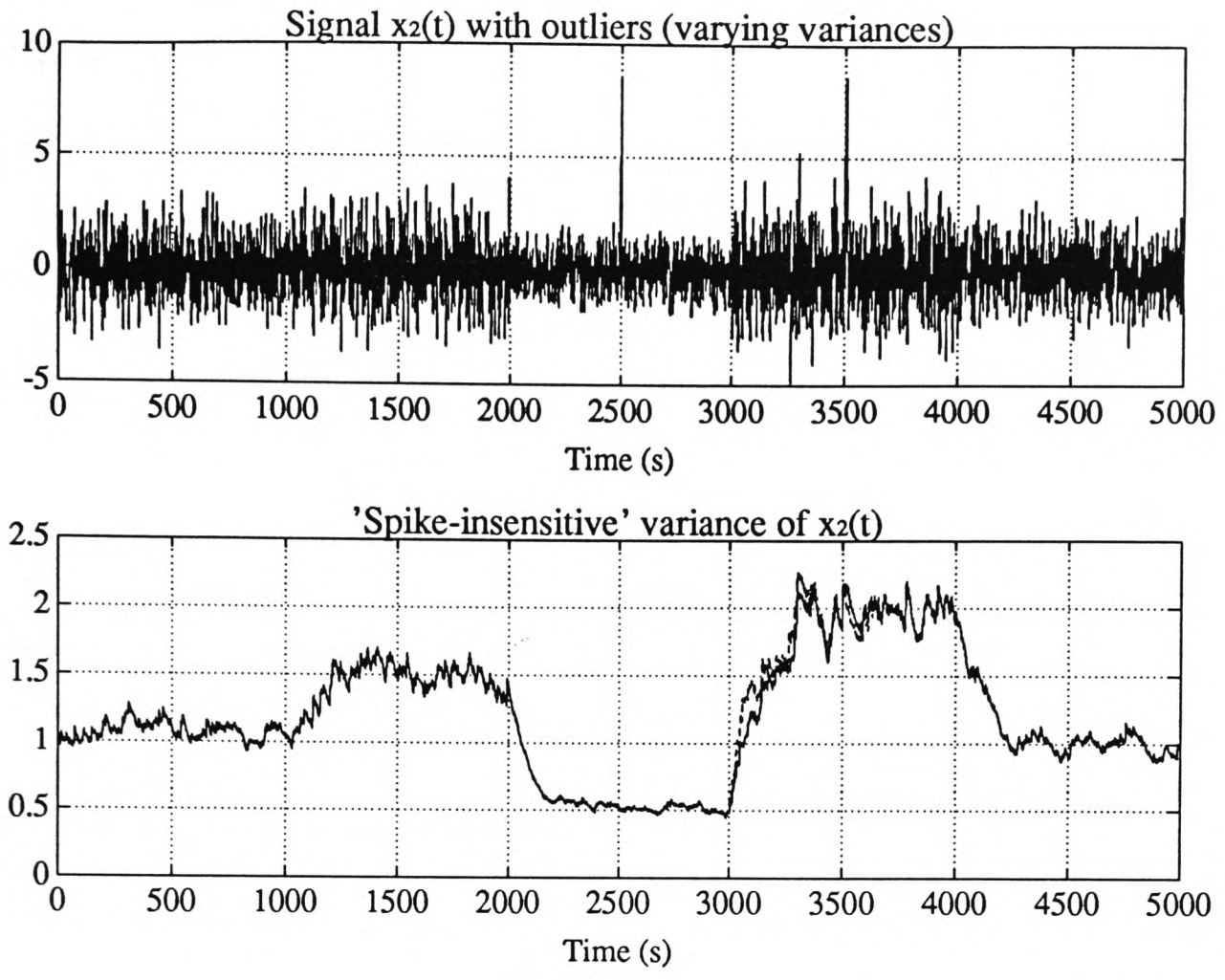

Figure 4.6: 'Spike-insensitive' variance with outliers (dashed: exponentially filtered variance without outliers)

Example 4.3

The spike-insensitive variance filter (Algorithm 4.28) is applied to estimate the variance of the signal $x_2(t)$ in Example 4.2. The various settings of the estimator are: $\alpha = 0.01$, $(W_\ell) = 2.58$, $(W_u) = 3.89$, $\hat{\bar{x}}_2(0) = x_2(1)$ and $\hat{\sigma}^2_{x_2}(0) = 1$. The variance estimates are compared with the exponential filter output for $x_1(t)$ (i.e. without spikes) in Figure 4.6. Its robustness against both the simple outlier at 2500 s and the filtered spike at 3500 s are excellent and it also provides unbiased estimates at various time intervals. Furthermore, the response time of the spike-insensitive variance estimator to a decrease or a modest increase in variance compares favourably with that of the exponential filter. Only when the increase is significant (4 times at 3000 s) can one observe a marginally slower response because the spike-insensitive algorithm has inevitably mistaken the initial increase in variance as unwanted spikes.

4.3.3 Efficient filtered rate of change algorithm

The evaluation of the rates of change of signals is crucial in local sensor validation. An excessive rate of change of the sensor output indicates a hardover failure and in the case of a drift failure, there will be a persistent bias in the rates of change of both $y(t)$ and $\bar{y}(t)$.

Direct computation of the rate of change or the derivative of a signal $x(t)$ usually gives rise to a noisy output. In many cases, it is the smoothed or filtered version that is of more practical value. The difference between adjacent samples is approximately proportional to the rate of change of the signal. A 'smoothed' adaptation can be obtained by taking the difference between two sample means over two windows of different lengths [Gertler and Chang, 1986]. Unfortunately, Gertler and Chang's formula is improperly scaled. It is modified and an efficient algorithm for an on-line estimate of the filtered rate of change $\hat{\dot{x}}(t)$ is proposed:

$$\hat{\dot{x}}(t) = \frac{\alpha_1 \alpha_2 f_m}{\alpha_1 - \alpha_2} \left(\hat{\bar{x}}_1(t) - \hat{\bar{x}}_2(t) \right) \tag{4.29}$$

where f_m is the sampling frequency in Hz and $\hat{\bar{x}}_1(t)$ and $\hat{\bar{x}}_2(t)$ are recursive averages over two different window lengths given by (c.f. Equation 4.5)

$$\hat{\bar{x}}_i(t) = (1 - \alpha_i)\, \hat{\bar{x}}_i(t-1) + \alpha_i\, x(t) \qquad i = 1 \text{ and } 2 \tag{4.30}$$

and $0 < \alpha_2 < \alpha_1 \leq 1$.

Property 4.4 *To a first approximation, the rate of change $\hat{\dot{x}}(t)$ given by Equation 4.29 represents the derivative of $x(t)$ filtered by a cascade of two first order unity-gain lowpass filters with cut-off frequencies ω_{c_1} and ω_{c_2} $(\omega_{c_2} < \omega_{c_1})$ where*

$$\omega_{c_1} = \frac{\alpha_1 f_m}{1 - \alpha_1} \tag{4.31}$$

$$\omega_{c_2} = \frac{\alpha_2 f_m}{1 - \alpha_2} \tag{4.32}$$

Substituting Equation 4.13 into Equation 4.29, the filtered rate of change can be rewritten as

$$\begin{aligned} \hat{\dot{x}}(t) &= \frac{\alpha_1 \alpha_2 f_m}{\alpha_1 - \alpha_2} \left(\frac{\alpha_1}{1 - (1 - \alpha_1) q^{-1}} - \frac{\alpha_2}{1 - (1 - \alpha_2) q^{-1}} \right) x(t) \\ &= \frac{\alpha_1}{1 - (1 - \alpha_1) q^{-1}} \frac{\alpha_2}{1 - (1 - \alpha_2) q^{-1}} \left(1 - q^{-1}\right) f_m \end{aligned} \tag{4.33}$$

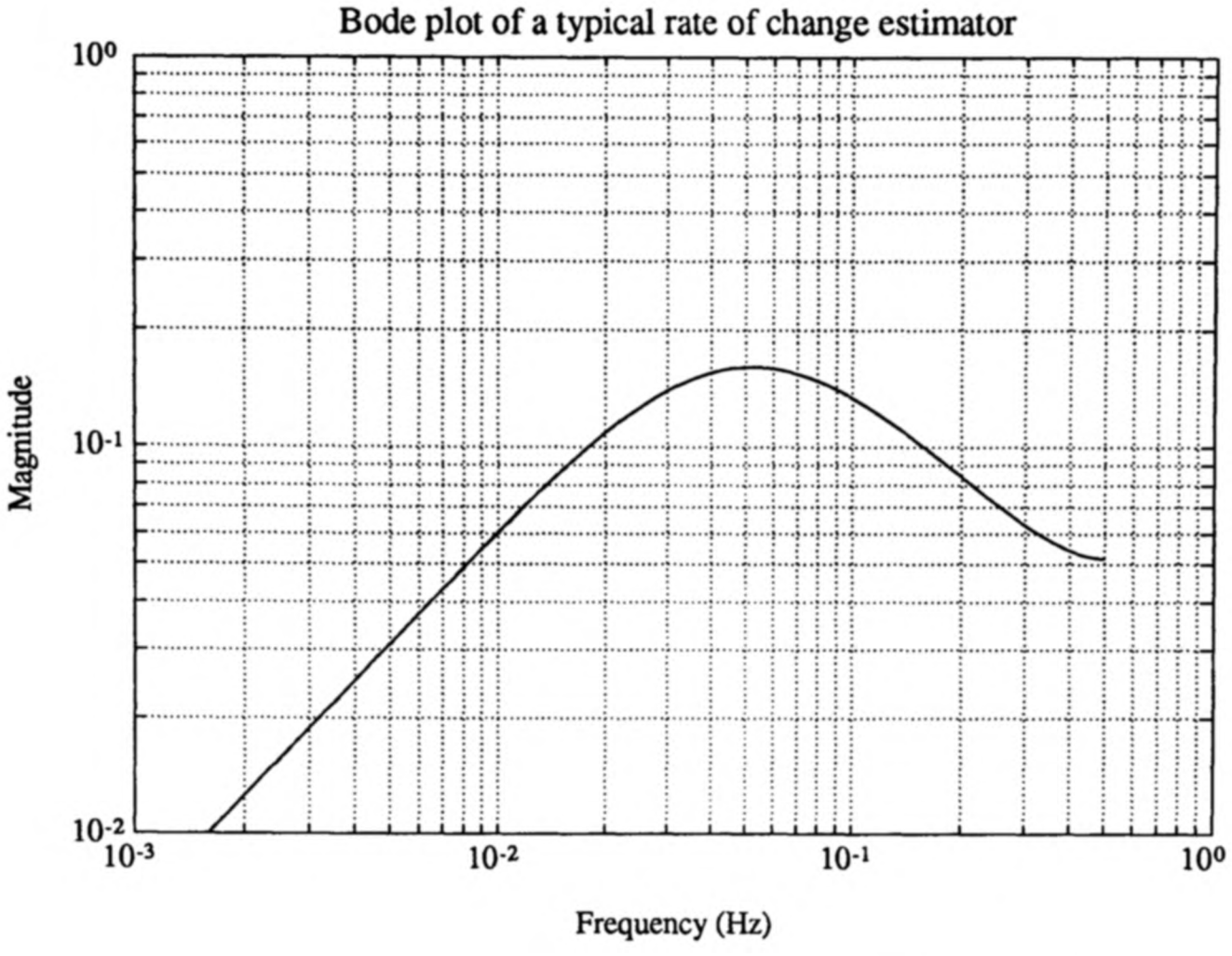

Figure 4.7: Frequency response of a typical rate of change estimator

Applying the first order approximate transformation of $s \mapsto (1-q^{-1})\, f_m$ as in Property 4.2, the transfer function of the rate of change estimation (Equation 4.29) in the continuous time domain becomes

$$\frac{\omega_{c_1}}{s+\omega_{c_1}} \frac{\omega_{c_2}}{s+\omega_{c_2}} s$$

which is the derivative, represented by s in Laplace Transform, filtered by a cascade of two 1st order unity-gain lowpass filters. From Property 4.2 and Equation 4.16, the cut-off frequencies ω_{c_1} and ω_{c_2} are given by Equations 4.31 and 4.32 respectively. Since $0 < \alpha_2 < \alpha_1 \leq 1$, it follows immediately that $\omega_{c_2} < \omega_{c_1}$. A bode plot of a typical rate of change estimator ($\alpha_1 = 0.32$, $\alpha_2 = 0.24$ and $f_m = 1$ Hz) is sketched in Figure 4.7. The frequency response agrees favourably with the predicted cut-off frequencies of $\omega_{c_1} = 0.075$ Hz and $\omega_{c_2} = 0.05$ Hz.

Guideline 4.4

1. **Initialization of the filtered rate of change**

   All that are required to set off the rate of change estimator are the initial conditions of the sample means, $\hat{\bar{x}}_1(0)$ and $\hat{\bar{x}}_2(0)$. The choice of the two variables has already been discussed in Guideline 4.1.

2. **Choice of α_1 and α_2**

   α_1 and α_2 can be determined indirectly by first selecting the cut-off frequencies ω_{c_1} and ω_{c_2}, which depend heavily on the signal and the noise bandwidths. The ultimate decision is a compromise between noise suppression and bias minimization in the estimates of rate of change. Once the cut-off frequencies are chosen, α_1 and α_2 can be found by Equation 4.15.

Example 4.4

Two separate tests on the effectiveness of the rate of change estimator (Equation 4.29) are conducted. The first involves the rate of change of drifts and a step change, while the other studies the derivative of a noisy sine wave and, in particular, the choice of α_1 and α_2. Both synthetic data are sampled at 1 Hz and the duration is 500 s.

1. A signal, $x(t)$, initially at -0.25 unit, has a step change of 0.25 unit at 100 s. A positive drift of 0.01 unit/s occurs between 200 and 300 s and a 'mirror image' of -0.01 unit/s drift takes place between 300 and 400 s. In addition, a small amount of white noise (variance 10^{-4}) is added.

   The filtered rate of change $\hat{\dot{x}}(t)$ is estimated by Equation 4.29 ($\alpha_1 = 0.4$, $\alpha_2 = 0.3$ and $\hat{\dot{x}}_1(0) = \hat{\dot{x}}_2(0) = x(1)$) and the results are depicted in Figure 4.8. It is interesting to find that the rate of change estimator is, as expected, unbiased (derivatives of both drifts are estimated accurately at ± 0.01 unit/s) and the modest step change at 200 s is capable of introducing a substantial spike in $\hat{\dot{x}}(t)$.

2. A sine wave at 0.01 Hz is simulated:

$$x(t) = \sin(0.02\,\pi\,t)$$

   and its theoretical derivative is given by

$$\dot{x}(t) = 0.02\,\pi\,\cos(0.02\,\pi\,t)$$

   The sinusoid is corrupted by a high frequency random noise which has been highpass filtered about 0.1 Hz. With reference to Figure 4.7, ω_{c_2} is chosen to be 0.31 rad s^{-1} (0.05 Hz), which is well above the signal bandwidth, and ω_{c_1} is fixed at 0.47 rad s^{-1} (0.075 Hz), in order to suppress the noise above 0.1 Hz. Based on Equation 4.15, $\alpha_1 = 0.32$ and $\alpha_2 = 0.24$. The initial values $\hat{\dot{x}}_1(0)$ and $\hat{\dot{x}}_2(0)$ are once more assigned

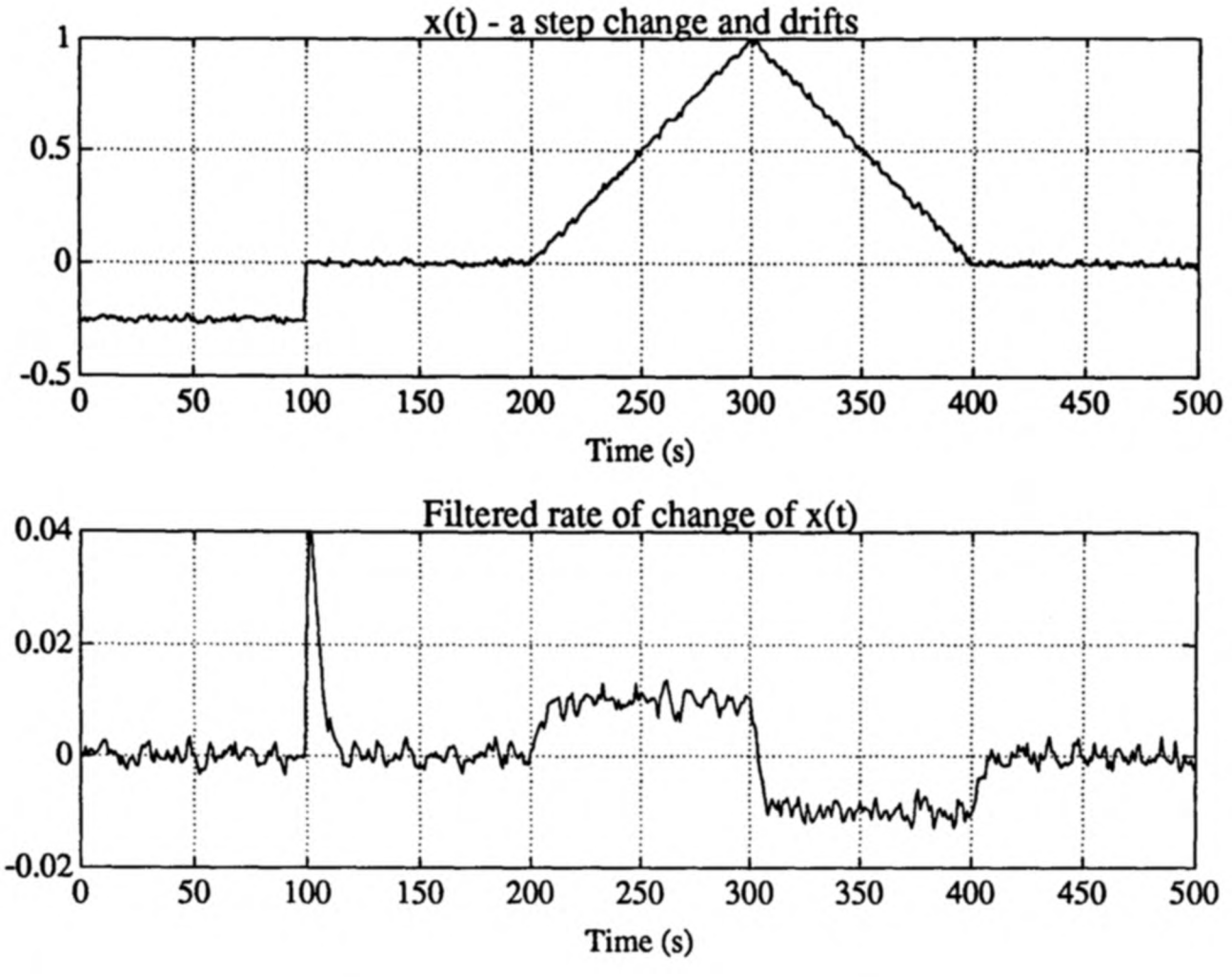

Figure 4.8: Filtered rate of change of drifts

to $x(1)$. The estimate $\hat{\dot{x}}(t)/(0.02\,\pi)$ (Figure 4.9) has a unit amplitude and a nearly $\pi/2$ phase lead over $x(t)$. This reconfirms the unbiased property of the estimator and the minor phase discrepancy from the ideal $\pi/2$ phase difference is attributed to the phase lags introduced by the lowpass filters.

4.3.4 On-line measure of bias

It has been mentioned in the beginning of Section 4.3.3 that a drift failure will impose either a persistently positive or a persistently negative bias in the rates of change of both the sensor output $y(t)$ and the signal-dominant component $\bar{y}(t)$. Since drifting actions are often fairly slow, the biases caused by drift failures are generally modest. On the other hand, a legitimate step response in the sensor output, a bias failure or a spike failure will all introduce a considerable, but temporary, bias in the rates of change (Example 4.4). As in the estimation of variance in Section 4.3.2, a 'spike-insensitive' algorithm is most beneficial to avoid unnecessary transient effects in the on-line measure of bias.

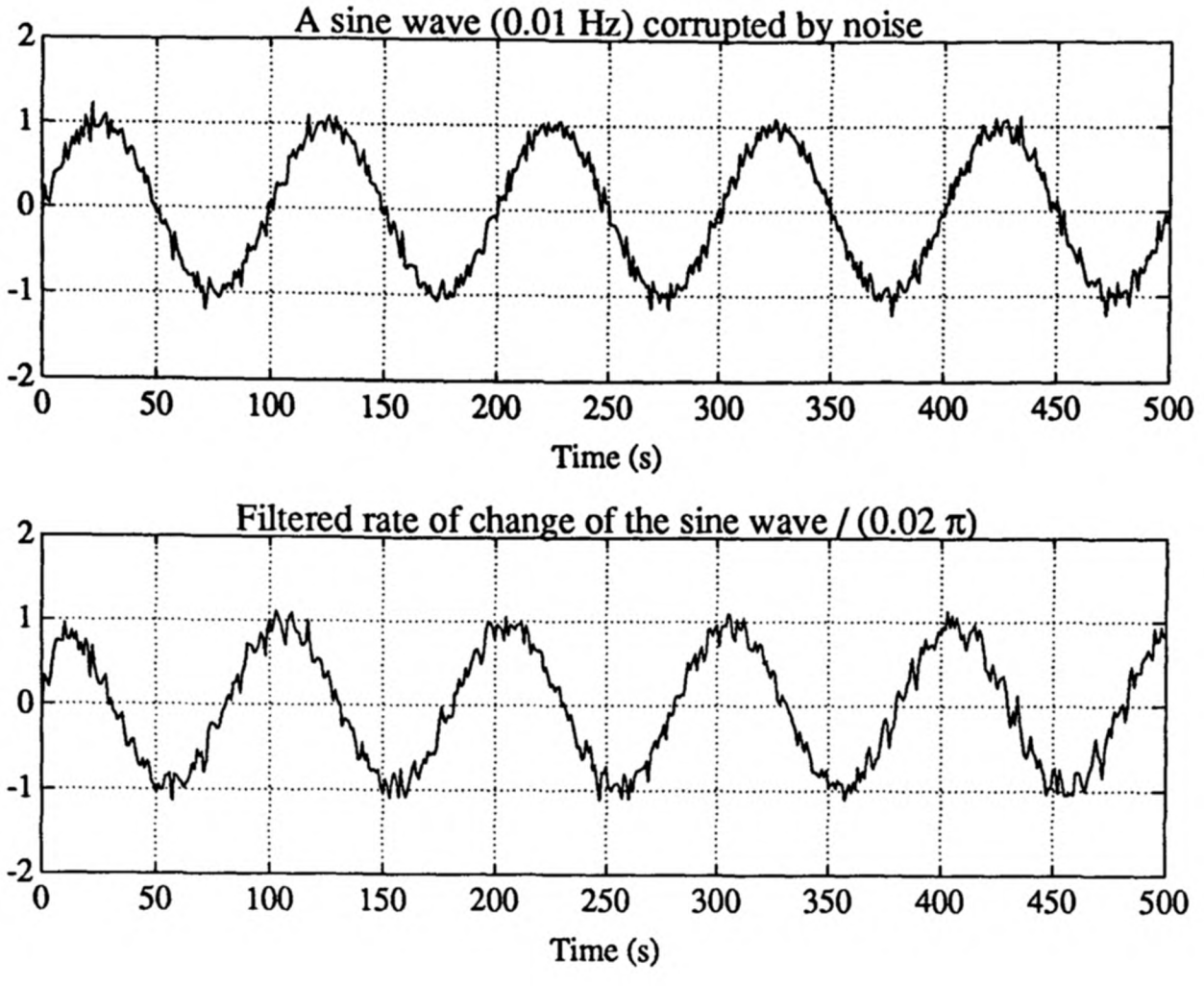

Figure 4.9: Filtered rate of change of a sinusoid

Consider a random variable $x(t)$, and take only its sign into account

$$x_s(t) = \text{sign}(x(t)) \tag{4.34}$$

where the signum operator is defined as

$$\text{sign}(x) = \begin{cases} -1, & x < -\delta_o \\ 0, & -\delta_o \leq x \leq \delta_o \\ 1, & x > \delta_o \end{cases} \tag{4.35}$$

and δ_o is a small constant to cater for the finite numerical precision. A stochastic variable $\varrho_x(t)$ is then defined as the recursive sample mean (Equation 4.5) of $x_s(t)$

$$\varrho_x(t) = (1-\gamma)\,\varrho_x(t-1) + \gamma\, x_s(t) \tag{4.36}$$

and $0 < \gamma \leq 1$. The on-line measure of bias is suggested to be a scaled variant of $\varrho_x(t)$ given by

$$b_x(t) = \sqrt{\frac{2-\gamma}{\gamma}}\,\varrho_x(t) \tag{4.37}$$

The signum operation (Equation 4.34) robustifies the algorithm against spikes and outliers and drives the on-line measure $b_x(t)$ to focus on the persistence, rather than the size, of bias.

Property 4.5 *The on-line measure of bias $b_x(t)$ defined in Equation 4.37 will be a standardized normal variate if the signal $x(t)$ is zero-mean and follows a symmetric distribution.*

Provided that $x(t)$ is zero-mean and has equal probabilities of being positive and negative (e.g. a symmetric distribution), i.e.

$$\begin{aligned} \Pr(x(t) > 0) &= \Pr(x(t) < 0) \\ \Pr(x(t) = 0) &\simeq 0 \end{aligned} \tag{4.38}$$

$x_s(t)$ will have a symmetric two-point distribution with mass 0.5 each at $+1$ and -1 (i.e. $x_s(t)$ has a zero mean and a unity variance). From Equation 4.11, the effective window length of the sample mean estimator in Equation 4.36 is determined by γ

$$m_\varrho = \frac{2}{\gamma} - 1 \tag{4.39}$$

By the *Central Limit Theorem*, if γ is sufficiently small (i.e. large m_ϱ), $\varrho_x(t)$ will follow approximately a Gaussian distribution with mean 0 and variance $\gamma/(2-\gamma)$, irrespective of the original distribution[5] of the signal $x(t)$. It is then straightforward that the on-line measure of bias $b_x(t)$ given in Equation 4.37 will satisfy a Gaussian distribution with zero mean and unity variance.

Guideline 4.5

1. **Initialization of the measure of bias**
   Since $x_s(t)$ is assumed to be a zero-mean process, it is reasonable to initialize the mean estimator in Equation 4.36 with $\varrho_x(0) = 0$.

2. **Choice of γ**
   The choice of γ, which controls the effective window length and the bandwidth of the estimator of $\varrho_x(t)$, is similar to that of α detailed in Guideline 4.1.

Example 4.5

The first test in Example 4.4 (step change and drifts) is revisited. For clarity, only the initial 300 s is examined. An on-line measure of bias of $\hat{\dot{x}}(t)$ is computed ($\gamma = 0.02$,

[5] As long as Equation 4.38 is satisfied.

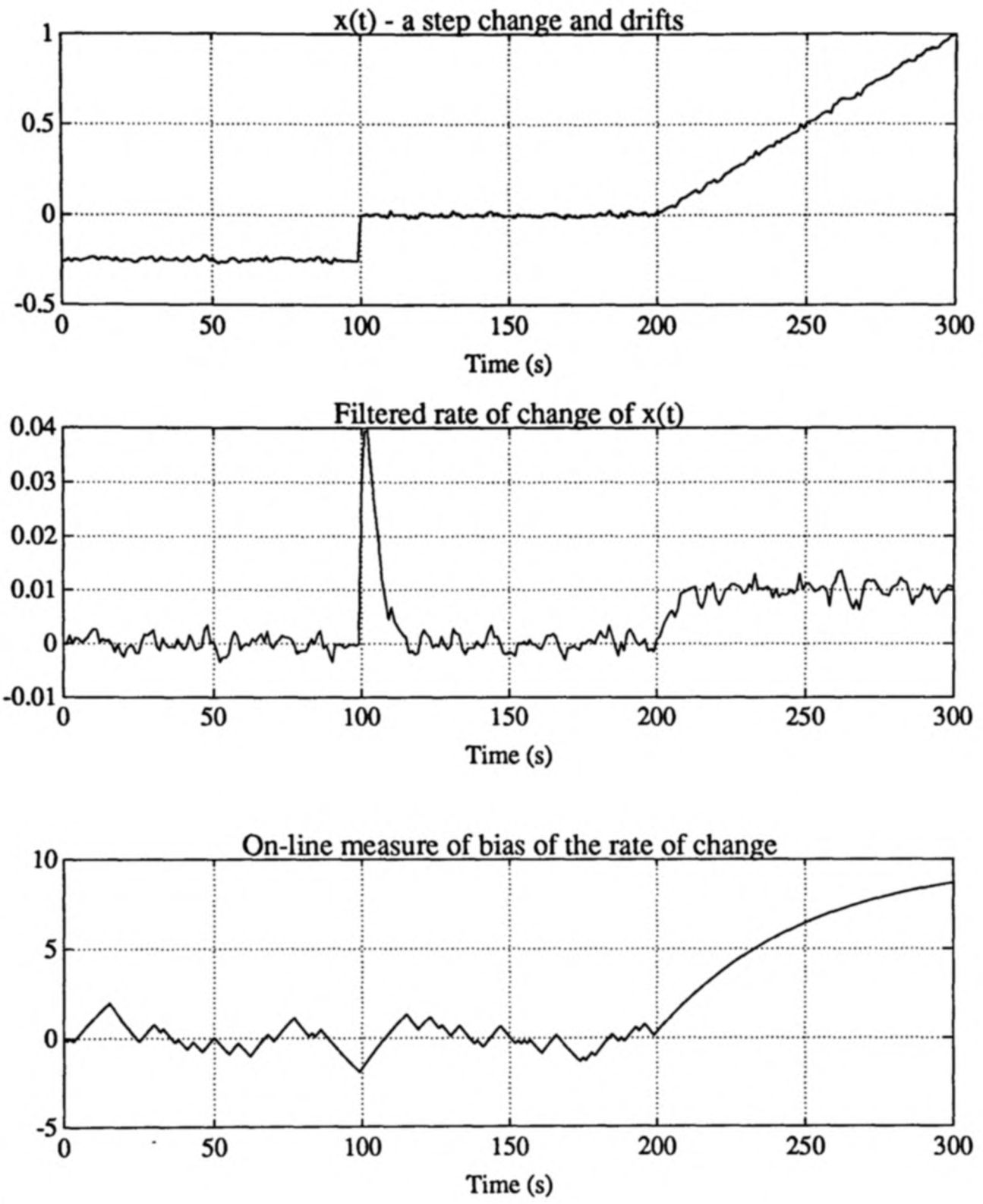

Figure 4.10: On-line bias of filtered rate of change in drifting actions

$\delta_o = 10^{-14}$ and $\varrho_{\hat{\dot{x}}}(0) = 0$) and is plotted in Figure 4.10. Both $x(t)$ and $\hat{\dot{x}}(t)$ are reproduced for comparison. It is evident that $b_{\hat{\dot{x}}}(t)$ is insensitive to the considerable, but temporary, deviation in $\hat{\dot{x}}(t)$ caused by the step change (at 100 s). On the other hand, the persistent drift is continuously winding $b_{\hat{\dot{x}}}(t)$ up since its inception at 200 s. The on-line measure of bias $b_{\hat{\dot{x}}}(t)$ approaches $\sqrt{(2/\gamma) - 1}$ $(= 9.95)$ asymptotically.

4.4 Failure alarm indicators (Ordinary phase)

The fundamental task in the tracking stage is to monitor the condition of the sensor and to detect any anomalies in its output signals. Appropriate signal processing tools to efficiently extract pertinent sensor characteristics have been developed in Section 4.3. During the first phase (named the *ordinary phase*) in the tracking stage, a number of key sensor signal parameters are estimated recursively: the mean of the innovation $\hat{\bar{\epsilon}}(t)$, the variance of the innovation, $\hat{\sigma}_\epsilon^2(t)$, the rate of change of the sensor output $\hat{\dot{y}}(t)$, the derivative of the signal-dominant component $\hat{\bar{\dot{y}}}(t)$ and the measure of its bias $b_{\bar{\dot{y}}}(t)$. Based on these signal patterns, a set of primary *failure alarm indicators* is computed:

- the limit indicator $I_l(t)$;
- the jump indicator $I_j(t)$;
- the noise indicator $I_n(t)$;
- the drift indicator $I_d(t)$.

The test statistics for the various indicators will be defined and the selection of the thresholds and other relevant parameters will be discussed.

4.4.1 Limit indicator

The limit indicator merely entails checking whether the sensor output $y(t)$ or its filtered rate of change $\hat{\dot{y}}(t)$ has violated some prescribed bounds, i.e. whether a hardover failure has occurred. The derivative $\hat{\dot{y}}(t)$ is estimated on-line by Equation 4.29. The threshold values y_{min}, y_{max} and $\dot{y}_{max}$ are determined based on the prior knowledge acquired in the commissioning stage (Section 3.2). The limit indicator has three possible states:

$$I_l(t) = \begin{cases} -1 & \text{if} \quad y(t) < y_{min} \\ 0 & \text{if} \quad y_{min} \leq y(t) \leq y_{max} \quad \text{AND} \quad \left|\hat{\dot{y}}(t)\right| \leq \dot{y}_{max} \\ 1 & \text{if} \quad y(t) > y_{max} \quad\quad\; \text{OR} \quad \left|\hat{\dot{y}}(t)\right| > \dot{y}_{max} \end{cases} \tag{4.40}$$

Guideline 4.6 *The thresholds of the limit indicator depend both on the sensor specification and the operating environment and each imposes its own permissible ranges on outputs and rates of change. For sensor validation, the larger y_{min}, the smaller y_{max} and the smaller $\dot{y}_{max}$ should be selected.*

In the case of a platinum resistance thermometer with a range of -50 to 50°C measuring the temperature of a water bath at atmospheric pressure, y_{min} should be set to 0°C and y_{max} to 50°C.

4.4.2 Jump indicator

The jump indicator detects excessive displacement in the innovation sequence which may be a result of a bias or a spike failure. The size of the displacement is measured by the *jump variable* $\xi(t)$, which is defined as the deviation of the innovation $\epsilon(t)$ from the current estimate of its sample mean $\hat{\bar{\epsilon}}(t)$ (by Equation 4.5) normalized by the estimate of its sample standard deviation $\hat{\sigma}_\epsilon(t)$ (by Algorithm 4.28), i.e.

$$\xi(t) = \frac{\epsilon(t) - \hat{\bar{\epsilon}}(t)}{\hat{\sigma}_\epsilon(t)} \tag{4.41}$$

The jump indicator will be highlighted if $|\xi(t)|$ exceeds a specified threshold ξ_o:

$$I_j(t) = \begin{cases} -1 & \text{if} \quad \xi(t) < -\xi_o \\ 0 & \text{if} \quad -\xi_o \leq \xi(t) \leq \xi_o \\ 1 & \text{if} \quad \xi(t) > \xi_o \end{cases} \tag{4.42}$$

As mentioned in Section 2.3, multiple random noise sources exist in most industrial processes. By the Central Limit Theorem, the aggregate measurement noise will follow an approximate Gaussian distribution. Basically, the innovation sequence can be considered as a linear combination of the measurement noise and the injected dither. Hence, if the dither is designed to be Gaussian, $\epsilon(t)$ will also approach a normal distribution. The jump variable $\xi(t)$ will then become a standardized normal variate.

Guideline 4.7 *The choice of ξ_o depends on the expected distribution of the innovation sequence and is a compromise between the probability of false alarms and that of missed alarms. If $\epsilon(t)$ is normally distributed, ξ_o can be set to 3.89 which will correspond to a false alarm rate of 0.01%.*

An upper bound on ξ_o can be imposed based on the *Chebyshev's inequality* [Bendat and Piersol, 1986, Section 3.1.5]. For any arbitrary distribution of $\epsilon(t)$,

$$\Pr\left(|I_j(t)| \geq \xi_o\right) \leq \frac{1}{\xi_o^2} \tag{4.43}$$

Hence, for a prescribed false alarm rate of $\mu\%$,

$$\xi_o \leq \sqrt{\frac{100}{\mu}} \tag{4.44}$$

For $\mu = 0.01\%$, $\xi_o \leq 100$.

4.4.3 Noise indicator

The noise indicator monitors the innovation variance and identifies changes in the excitation of $\epsilon(t)$. Stuck failure, erratic failure and cyclic failure will all introduce persistent alteration in the innovation variance. It is also believed that a saturation failure will reduce the effective excitation as well.

A powerful test for comparing the equality of the population variances from two independent samples is the *variance-ratio test* [Mulholland and Jones, 1983, Chapter 12]. Similar sensor failure detection algorithms are employed in the adaptive filtering scheme in Halme and Selkäinaho [1984] and in the intelligent fault tolerant control system in Selkäinaho and Halme [1987]. Suppose $\hat{\sigma}_\epsilon^2(t)$ is the innovation variance estimated recursively by the spike-insensitive filter (Algorithm 4.28) during the tracking stage and $(\sigma_\epsilon^2)_{\text{ref}}$ is the reference innovation variance (Section 3.12) computed in the learning stage (typically when the sensor ARMA model is being validated). Under normal conditions (Assumption 3.3), the innovation variance should remain constant. Therefore, the null hypothesis to be tested is $\hat{\sigma}_\epsilon^2(t) = (\sigma_\epsilon^2)_{\text{ref}}$ and the alternative hypothesis is $\hat{\sigma}_\epsilon^2(t) \neq (\sigma_\epsilon^2)_{\text{ref}}$. This is a *two-tailed significance test* and the null hypothesis will be accepted if the *variance-ratio*

$$F(t) = \frac{\hat{\sigma}_\epsilon^2(t)}{(\sigma_\epsilon^2)_{\text{ref}}} \tag{4.45}$$

satisfies the following condition

$$\underline{F}_o \leq F(t) \leq \overline{F}_o \tag{4.46}$$

where $\underline{F}_o$ and $\overline{F}_o$ are the lower and the upper thresholds respectively. The noise indicator is set according to the value of $F(t)$:

$$I_n(t) = \begin{cases} -1 & \text{if} \quad F(t) < \underline{F}_o \\ 0 & \text{if} \quad \underline{F}_o \leq F(t) \leq \overline{F}_o \\ 1 & \text{if} \quad F(t) > \overline{F}_o \end{cases} \tag{4.47}$$

Guideline 4.8 *Similar to the choice of ξ_o discussed in Guideline 4.7, the two thresholds $\underline{F}_o$ and $\overline{F}_o$ can be selected based on a prescribed level of significance if the distribution of the innovation is available. In particular, if $\epsilon(t)$ is Gaussian, the variance-ratio will follow the F-distribution [Mulholland and Jones, 1983, Chapter 12]. At μ% significance level, the thresholds should be chosen as*

$$\underline{F}_o = \frac{1}{F_{\mu/2\%}(\nu_2, \nu_1)} \tag{4.48}$$

$$\overline{F}_o = F_{\mu/2\%}(\nu_1, \nu_2) \tag{4.49}$$

where ν_1 and ν_2 are the degrees of freedom for the test statistics. ν_1 and ν_2 are directly related to the effective window length of the variance estimator (Property 4.3) and the number of samples, N, used in the estimation of the reference variance (Equation 3.84). If α is the parameter in the variance filter (Equation 4.20), the two can be specified as

$$\nu_1 = \frac{2}{\alpha} - 2 \tag{4.50}$$

$$\nu_2 = N - 1 \tag{4.51}$$

Values of F-distribution statistics, $F_{\mu\%}(\nu_1, \nu_2)$, are tabulated for various combinations of ν_1, ν_2, and μ.

For a typical application where the innovation sequence is assumed to be Gaussian, let $N = 2000$ and $\alpha = 0.01$. At 0.1% level of significance, the thresholds are given by

$$\underline{F}_o = \frac{1}{F_{0.05\%}(1999, 198)} = 0.69$$

$$\overline{F}_o = F_{0.05\%}(198, 1999) = 1.39$$

4.4.4 Drift indicator

The drift indicator involves a statistical test on whether there is a *persistent* drifting action in the sensor output. One fundamental complication is to distinguish the initial transients of a legitimate step or setpoint change from an actual sensor drift failure. Step responses are commonplaces in sensor outputs, particularly in closed loop environments, and they behave initially like drifts for an appreciable period corresponding to the rise time of the process. Based on the knowledge acquired in the commissioning stage, a new design variable τ_d is introduced (Guideline 4.9) which specifies the minimum duration of drifting required prior to the declaration of a drift failure.

As explained in Section 4.2, an innovation-based detection on drift failures is ineffective and most likely to be futile. An alternative approach which directly monitors the derivatives of the sensor signal is adopted. A drift failure will manifest itself as a persistent bias in the rate of change of either the sensor output or the signal-dominant component. To minimize the undesirable effects of the measurement noise, the filtered rate of change of $\bar{y}(t)$ is preferred. In short, the statistical test can be divided into three consecutive steps:

- The filtered rate of change of $\bar{y}(t)$ ($\hat{\dot{\bar{y}}}(t)$) is computed from Equation 4.29. Recommended values of α_1 and α_2 for this particular application will be given in Guideline 4.9.
- An on-line measure of bias of $\hat{\dot{\bar{y}}}(t)$ ($b_{\dot{\bar{y}}}(t)$) is estimated (Equation 4.37). It is robust against abrupt spikes appearing in $\hat{\dot{\bar{y}}}(t)$ and is independent of the magnitudes of the estimated derivatives.
- A *drift counter* $\eta(t)$ is introduced which represents a 'normalized' duration of significant drifting actions.

A sensor will be diagnosed to have a drift failure only if the bias of the derivative of the measurement signal is both *significant* and *persistent*. An auxiliary indicator, known as the ***bias indicator***, registers the significance of the drifting behaviour and will be flagged if $\left|b_{\dot{\bar{y}}}(t)\right|$ exceeds the selected threshold b_o:

$$I_b(t) = \begin{cases} -1 & \text{if} \quad b_{\dot{\bar{y}}}(t) < -b_o \\ 0 & \text{if} \quad -b_o \leq b_{\dot{\bar{y}}}(t) \leq b_o \\ 1 & \text{if} \quad b_{\dot{\bar{y}}}(t) > b_o \end{cases} \tag{4.52}$$

The persistence of significant drifting is measured by the drift counter $\eta(t)$. The counter $\eta(t)$ is stepped up or down depending on the current status of $I_b(t)$. The update procedure for $\eta(t)$ is presented as follows:

Update of the drift counter $\eta(t)$ (4.53)

1. If the bias indicator is not significant (i.e. $I_b(t) = 0$), the counter will be stepped down in the appropriate direction

$$\eta'(t) = \eta'(t-1) - \text{sign}\left(\eta(t-1)\right)$$

and any excessive reduction in the counter will be clipped

$$\eta'(t) = \begin{cases} \max(\eta'(t), 0) & \text{if} \quad \text{sign}(\eta'(t-1)) > 0 \quad \text{(positive drifting)} \\ \min(\eta'(t), 0) & \text{if} \quad \text{sign}(\eta'(t-1)) < 0 \quad \text{(negative drifting)} \end{cases}$$

2. If the bias indicator is significant (i.e. $|I_b(t)| = 1$), the counter will be stepped up accordingly. If the significant bias is in opposite direction to the drifting action, the counter will first be reset to zero:

$$\eta'(t) = \begin{cases} I_b(t) & \text{if} \quad \text{sign}(\eta'(t-1)\, I_b(t)) = -1 \\ \eta'(t-1) + I_b(t) & \text{otherwise} \end{cases}$$

3. The drift counter is then normalized by the minimum drift time τ_d

$$\eta(t) = \frac{\eta'(t)}{\tau_d\, f_m}$$

and f_m is the sampling frequency in Hz.

Finally, the drift indicator will be set off if $|\eta(t)|$ creeps over the unity limit:

$$I_d(t) = \begin{cases} -1 & \text{if} \quad \eta(t) < -1 \\ 0 & \text{if} \quad -1 \leq \eta(t) \leq 1 \\ 1 & \text{if} \quad \eta(t) > 1 \end{cases} \tag{4.54}$$

Recommendations on the initial conditions and various design variables will be given in Guideline 4.9.

Guideline 4.9

1. **Initialization**

   The initial conditions for the filtered rate of change $\hat{\dot{\bar{y}}}(t)$ *and the on-line measure of bias* $b_{\dot{\bar{y}}}(t)$ *have been detailed in Guidelines 4.4 and 4.5 respectively. In computing the drift indicator, the only additional initial variable required is the counter* $\eta'(0)$*, which should be set to 0.*

2. **Choice of α_1 and α_2**

   Given a criterion on the slowest detectable drift Δ_{min}*, the signal variance* σ_s^2 *and the*

measurement signal bandwidth ω_s (in $rads^{-1}$), a reasonable pair of cut-off frequencies of the derivative filter is given by:

$$\omega_{c_2} = \min\left(\omega_o, \frac{\omega_s}{2}\right) \tag{4.55}$$

$$\omega_{c_1} = 2\omega_{c_2} \tag{4.56}$$

where

$$\omega_o = \left(\frac{1}{12}\omega_s\left(\frac{\Delta_{min}}{\sigma_s}\right)^2\right)^{\frac{1}{3}} \tag{4.57}$$

α_1 and α_2 can then be obtained via Equation 4.15.

3. **Choice of γ and b_o**

In normal situations (i.e. absence of any significant drifts), it is plausible to assume that the filtered rate of change $\hat{\dot{y}}(t)$ will have a symmetric distribution. It then follows from Property 4.5 that the on-line measure of bias $b_{\hat{\dot{y}}}(t)$ will satisfy a standardized normal distribution. At 0.1% significance level, b_o should be set to 3.29. The choice of γ has been discussed in Guideline 4.5.

4. **Choice of τ_d**

To the validation scheme, the initial drifting period during a step change consists of three components: the rise time of the process T_r, the effective window length of the derivative filter $m_{\hat{\dot{y}}}$ and that of the bias estimator m_ϱ. In computing the drift indicator, a safety factor of two is suggested and the minimum drifting duration for a significant failure, τ_d, is elected to be

$$\tau_d = 2\left(T_r + \frac{m_\varrho}{f_m} + \frac{m_{\hat{\dot{y}}}}{f_m}\right) \tag{4.58}$$

and the rise time[6] is estimated by

$$T_r = \frac{4}{\omega_B} \tag{4.59}$$

where the process bandwidth ω_B is in $rads^{-1}$. Finally, the effective window lengths are given by

$$m_\varrho = \frac{2}{\gamma} - 1 \tag{4.60}$$

$$m_{\hat{\dot{y}}} = \frac{2}{\alpha_2} - 1 \tag{4.61}$$

[6]The estimation laid down in Equation 4.59 corresponds to the time required for a step response to reach within 2% of the destined level in a first order system.

Drift failures are often gradual and their rates of change are usually fairly small. In order to keep the validation scheme sensitive to sluggish drifts, it is imperative to ensure their failure signatures to be sufficiently above the background signal level in the derivative domain. This can be achieved by tuning the two design parameters α_1 and α_2 in the rate of change estimator (Equation 4.29). For simplicity, the signal-dominant component $\bar{y}(t)$ is assumed to be a stochastic signal with variance σ_s^2 and is perfectly bandlimited and 'white' within the measurement signal bandwidth ω_s. Furthermore, the derivative filter is assumed to have a perfect cut-off at ω_{c_1} and the frequency pair, ω_{c_1} and ω_{c_2}, is taken to be $2\omega_o$ and ω_o respectively, where $2\omega_o \leq \omega_s$. The variance of $\dot{\bar{y}}$ can then be estimated to be

$$\begin{aligned} \sigma_{\dot{\bar{y}}}^2 &\simeq \left(\int_{-\omega_o}^{\omega_o} \omega^2 \, d\omega + 2\omega_o^3 \right) \frac{\sigma_s^2}{2\omega_s} \\ &= \frac{4\,\omega_o^3\,\sigma_s^2}{3\,\omega_s} \end{aligned} \tag{4.62}$$

To guarantee the detectability of the slowest drift, Δ_{min} is chosen to be three times the standard deviation of the background signal derivative level, i.e. $\Delta_{min} = 3\,\sigma_{\dot{\bar{y}}}$. After rearranging the equations, ω_o is given by Equation 4.57 and the two cut-off frequencies of the derivative filter are selected based on Equations 4.55 and 4.56.

Example 4.6

A sensor signal is simulated by injecting a random noise (mean 0.5 and variance 2.5×10^{-4}) through a 2nd order Chebyshev lowpass filter with a bandwidth of 0.01 Hz. A step change of 0.1 unit is activated at 500 s and a slow drift of -2×10^{-4} unit/s is initiated at 1500 s. The output is constantly corrupted by a stationary white noise with variance 2.5×10^{-5}. Sampling frequency is selected to be 1 Hz and the data spans 2000 s.

From Equation 3.27, the measurement signal bandwidth ω_s is estimated to be 0.089 Hz, i.e. $0.56\,\mathrm{rad\,s^{-1}}$ ($\mathcal{R}_s = 400$, $\omega_B = 0.063\,\mathrm{rad\,s^{-1}}$). Let the minimum detectable drift Δ_{min} be 2×10^{-4} unit/s, the signal variance σ_s^2 be 5×10^{-6} and γ be 0.05. It then follows from Guideline 4.9 that $\alpha_1 = 0.13$, $\alpha_2 = 0.067$ and $\tau_d = 264$ s.

A 2nd order Butterworth lowpass filter (cut-off at ω_s) is employed to generate the signal-dominant component $\bar{y}(t)$. The filtered rate of change $\hat{\dot{\bar{y}}}(t)$, its measure of bias $b_{\dot{\bar{y}}}(t)$ and the drift counter $\eta(t)$ are computed and the results are illustrated in Figure 4.11. It is evident that with the appropriate choice of α_1 and α_2, the signatures of the minimum

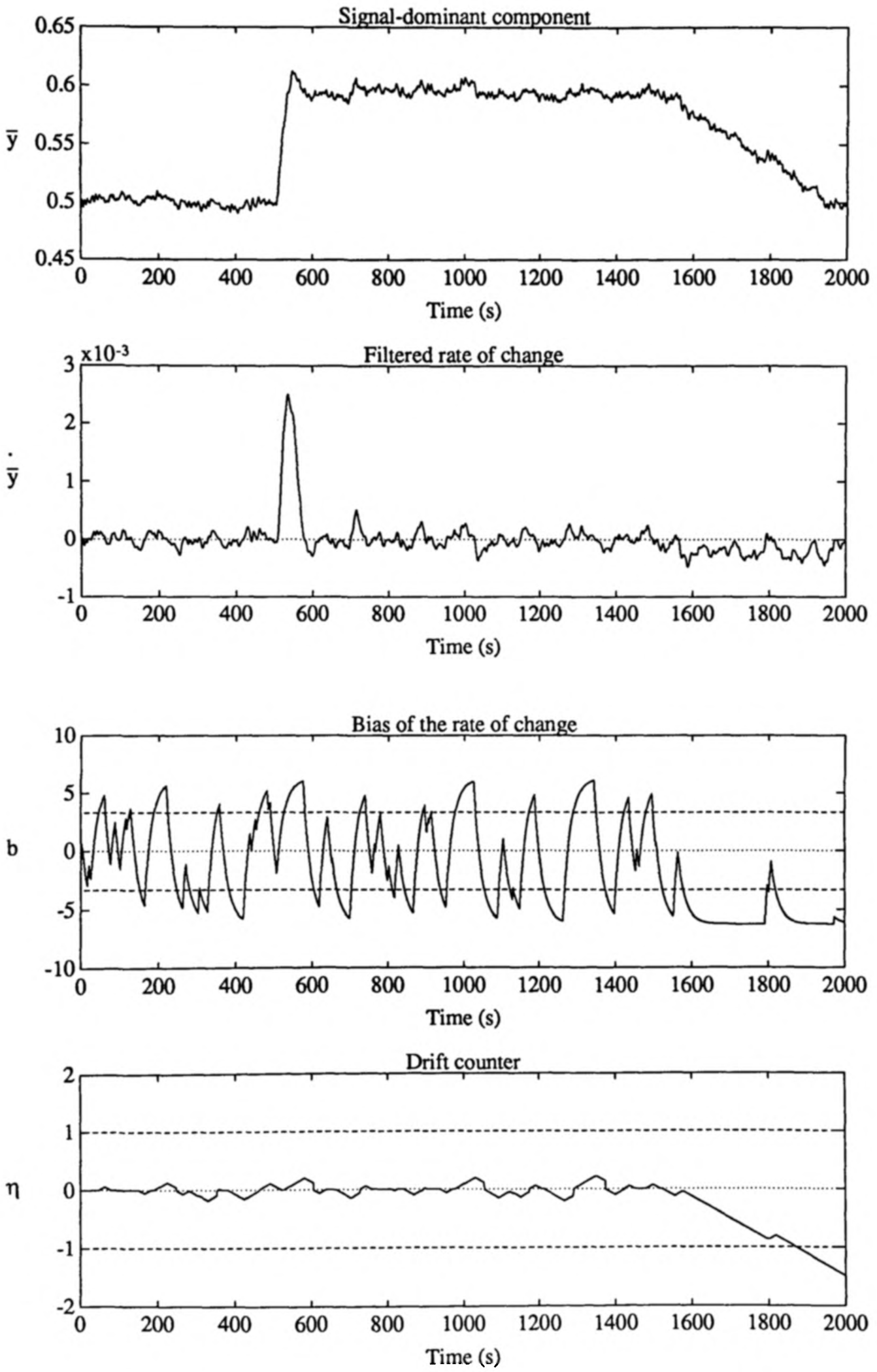

Figure 4.11: Detection of a drift failure in the presence of a legitimate step change

drift failure become just noticeable as a persistent bias in the derivative $\hat{\dot{\bar{y}}}(t)$. Although the step change introduces a massive 'kick' in $\hat{\dot{\bar{y}}}(t)$, its comparatively short-lived nature is insufficient to flag the alarm. As expected, the sensor output has to drift for at least a period of τ_d before the drift indicator is triggered at 1871 s.

4.4.5 A simulated example

Example 4.7

This example illustrates the effectiveness of the signal processing tools presented in Section 4.3 and demonstrates the ability of the four failure alarm indicators, laid down in this section, in detecting various typical sensor failures.

The series of data sets in Example 4.1 with a comprehensive collection of sensor failure modes are examined. The signal decomposition (with dither injection) strategies in the commissioning stage and the sensor modelling procedures in the learning stage are duplicated and the identical results can be directly applied in this example. A number of the critical information is recapitulated below:

$$\begin{aligned} f_m &= 1\,\text{Hz} \\ \omega_B &= 0.01\,\text{Hz} \quad (0.063\,\text{rads}^{-1}) \\ \omega_s &= 0.047\,\text{Hz} \quad (0.30\,\text{rads}^{-1}) \end{aligned}$$

During the tracking stage, the innovation sequence is generated (as in Example 4.1) and simple signal processing techniques are utilized to extract relevant information. The variables that are being monitored and the design parameters of the associated processing tools are summarized as follows:

Variable		*Design parameters*	*Equation*
Mean	$\hat{\bar{\epsilon}}(t)$	$\alpha = 0.01$	(4.5)
Variance	$\hat{\sigma}^2_\epsilon(t)$	$\alpha = 0.01$, $(W_\ell)_m = 2.58$, $(W_u)_m = 3.89$	(4.28)
Rate of change	$\hat{\dot{y}}(t)$	$\alpha_1 = 0.22$, $\alpha_2 = 0.13$	(4.29)
Rate of change	$\hat{\dot{\bar{y}}}(t)$	$\alpha_1 = 0.053$, $\alpha_2 = 0.027$, $\Delta_{min} = 0.03\sigma_s$	(4.29)
Measure of bias	$b_{\dot{\bar{y}}}(t)$	$\gamma = 0.05$, $\delta_o = 8 \times 10^{-5}$	(4.37)

The failure alarm indicators are then computed and the prescribed thresholds are given by

Alarm	*Thresholds*	*Equation*
Limit indicator $I_l(t)$	$y_{min} = 0$, $y_{max} = 1$, $\dot{y}_{max} = 0.5$	(4.40)
Jump indicator $I_j(t)$	$\xi_o = 3.89$	(4.42)
Noise indicator $I_n(t)$	$\underline{F}_o = 0.69$, $\overline{F}_o = 1.39$	(4.47)
Drift indicator $I_d(t)$	$b_o = 3.29$, $\tau_d = 350$ s	(4.54)

The sensor output $y(t)$, the jump variables $\xi(t)$, the variance-ratios $F(t)$, the drift counter $\eta(t)$, and the four failure alarm indicators for the eight data sets are displayed in Figures 4.12 to 4.19. The alarm indicators are shown to be capable of detecting the appropriate sensor failures both accurately and expeditiously. A summary of the validation results during the ordinary phase is tabulated as follows:

Mode	*Initial alarm*
Normal	No alarm triggered
Bias	$I_j(t) = 1$ at 2500 s
Spike	$I_j(t) = -1$ at 2500 s
Stuck	$I_n(t) = -1$ at 2529 s
Erratic	$I_n(t) = 1$ at 2542 s
Cyclic	$I_n(t) = 1$ at 2515 s
Drift	$I_d(t) = -1$ at 2848 s
Saturation	$I_n(t) = -1$ at 2663 s

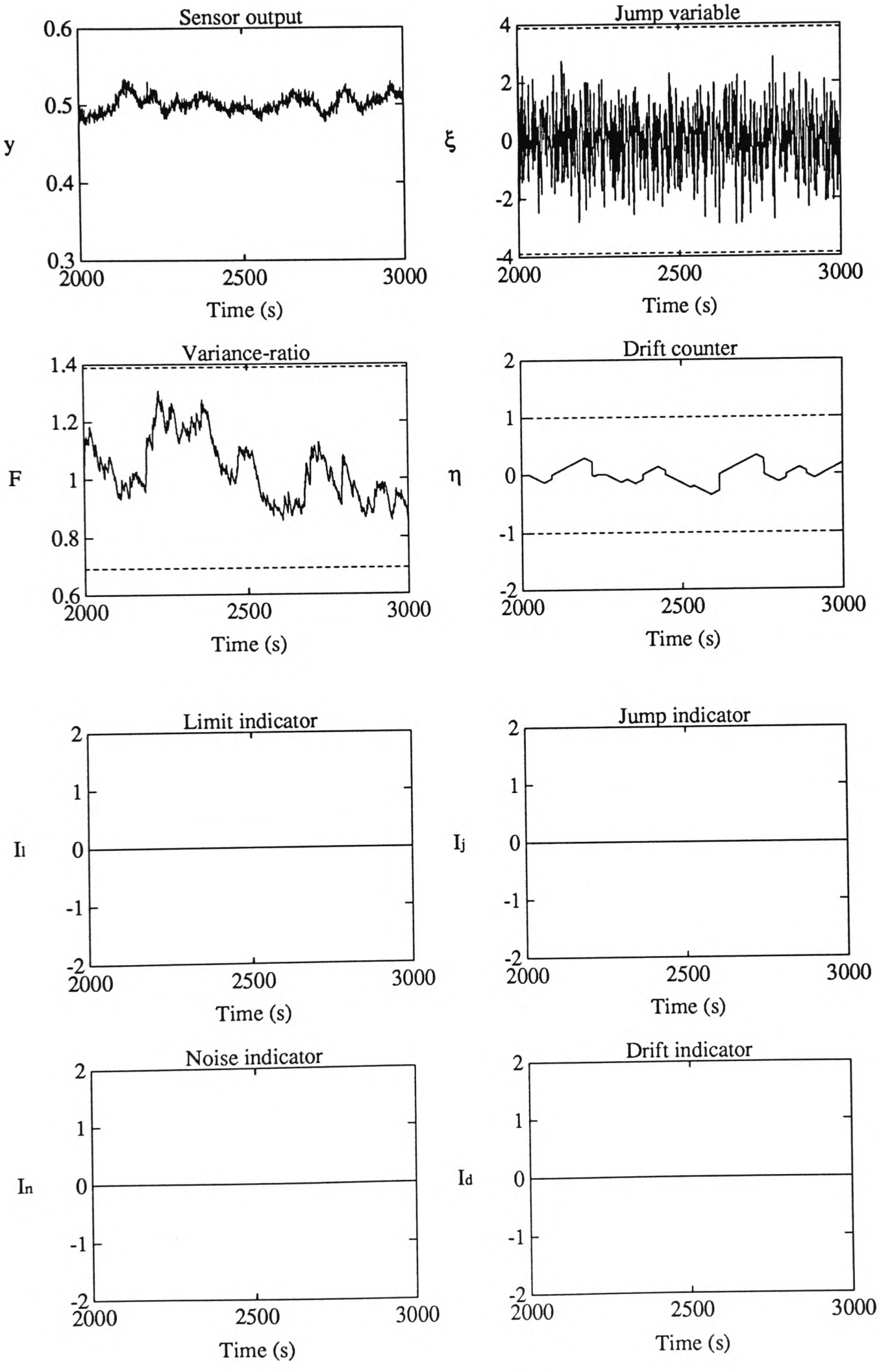

Figure 4.12: Alarm indicators of a normal sensor

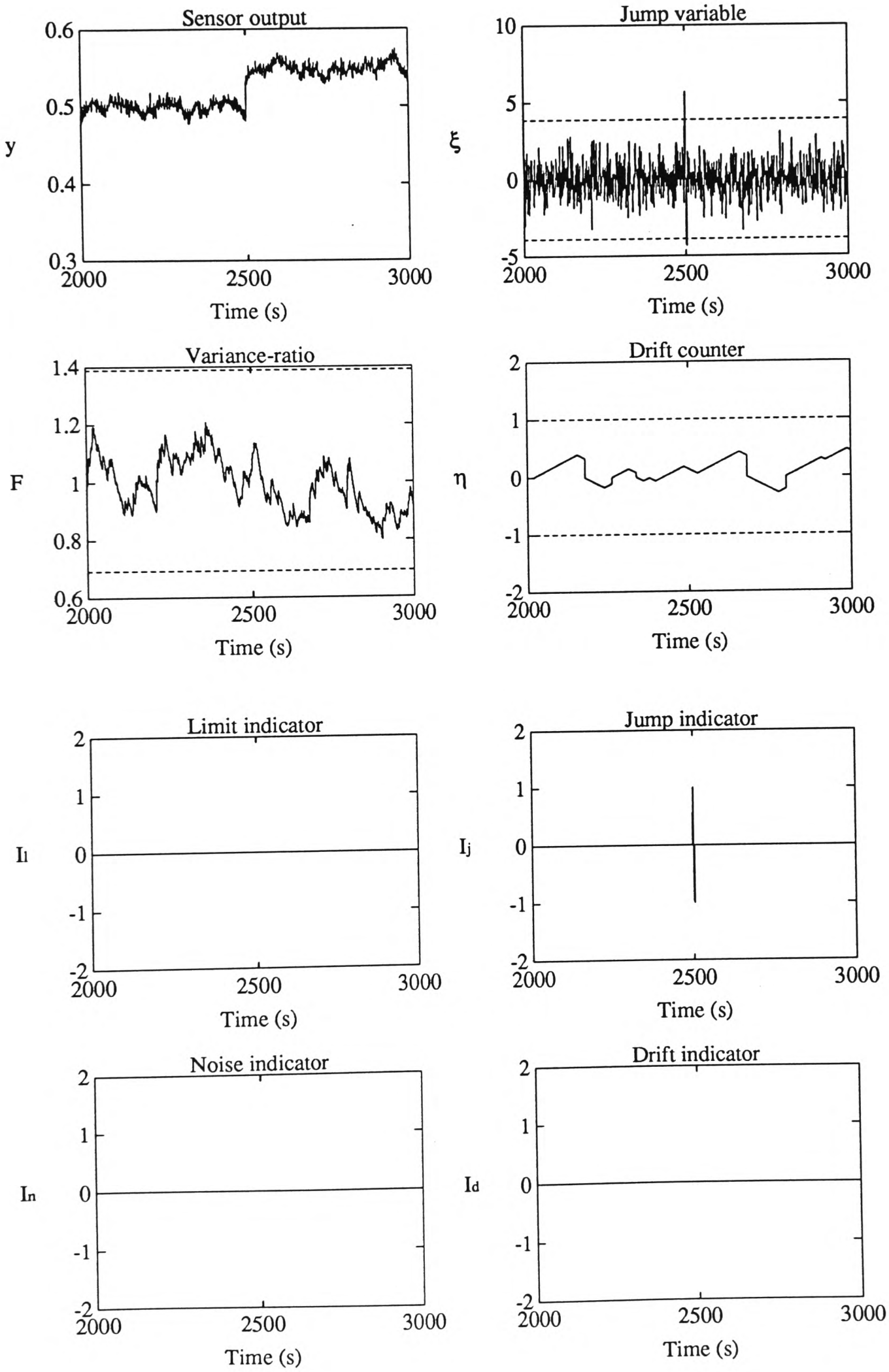

Figure 4.13: Alarm indicators of a bias failure

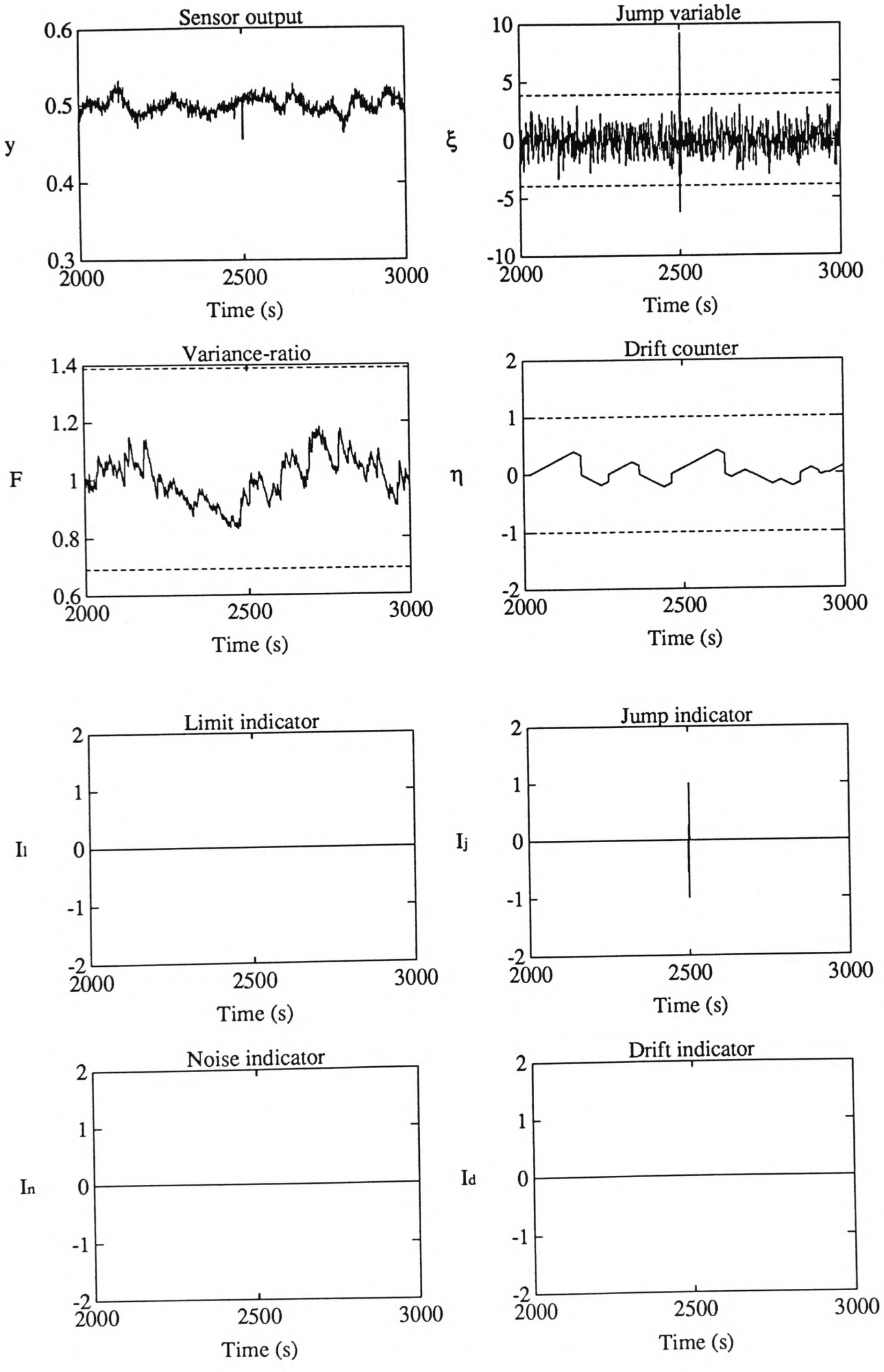

Figure 4.14: Alarm indicators of a spike failure

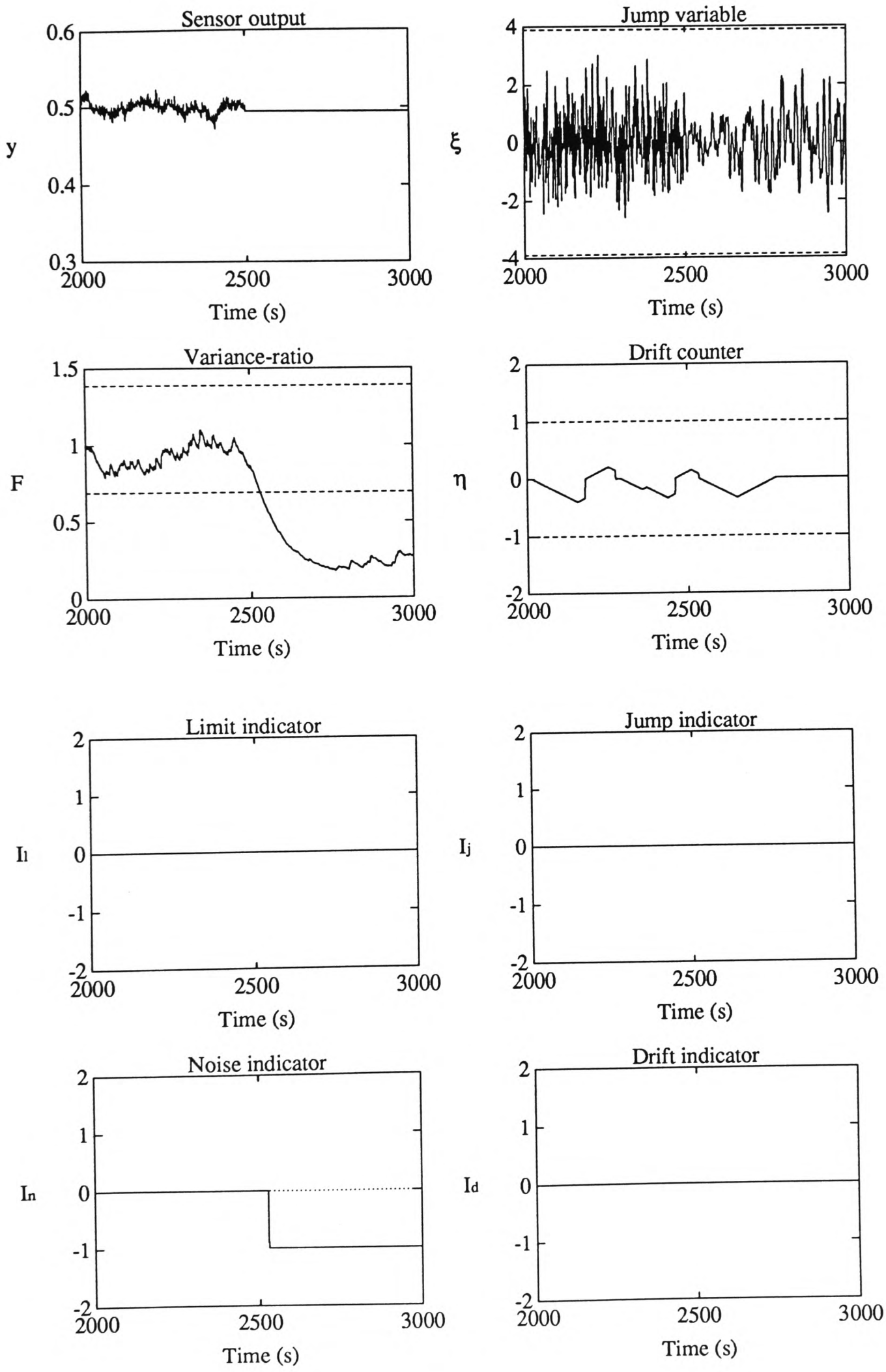

Figure 4.15: Alarm indicators of a stuck failure

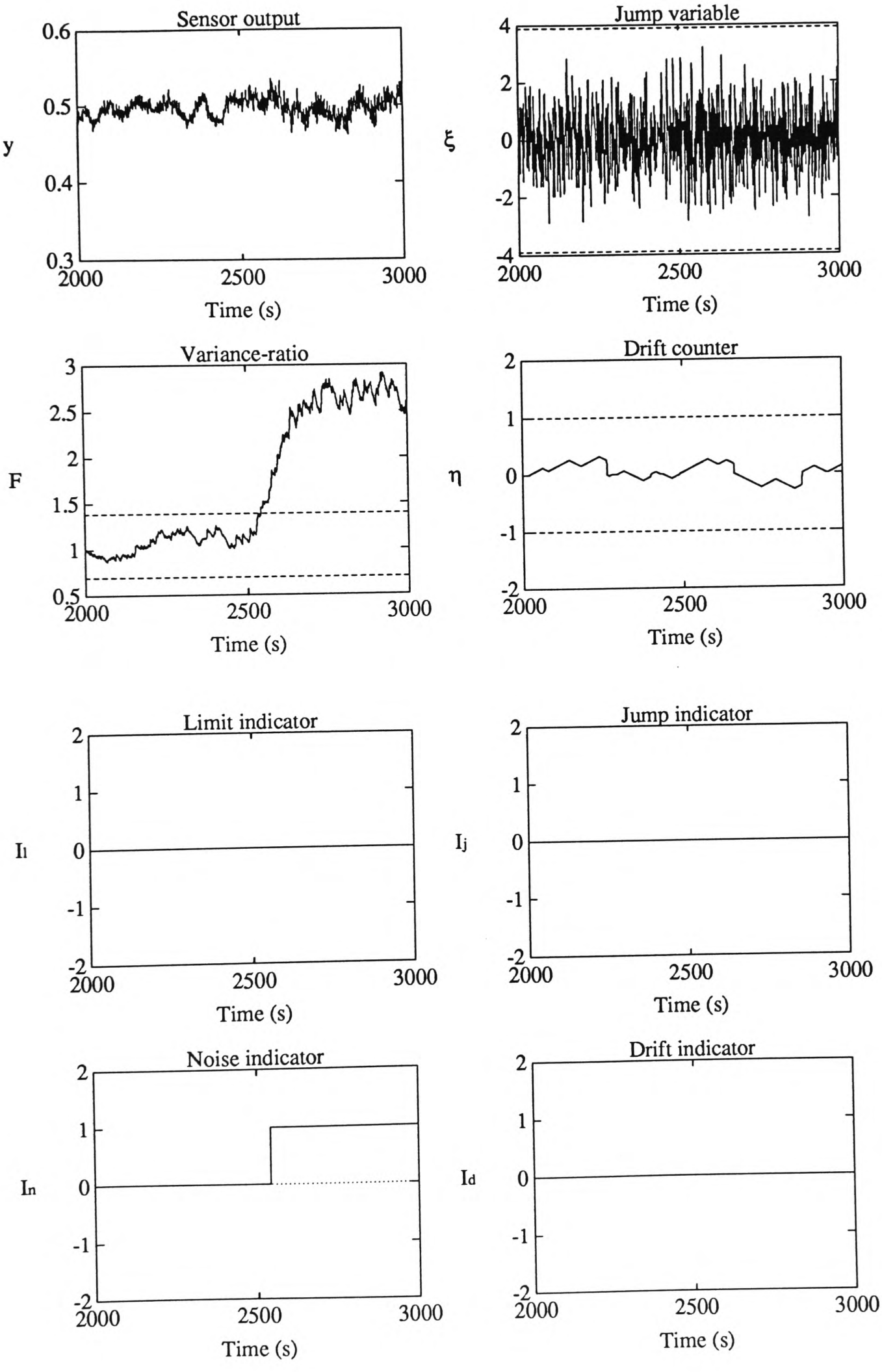

Figure 4.16: Alarm indicators of an erratic failure

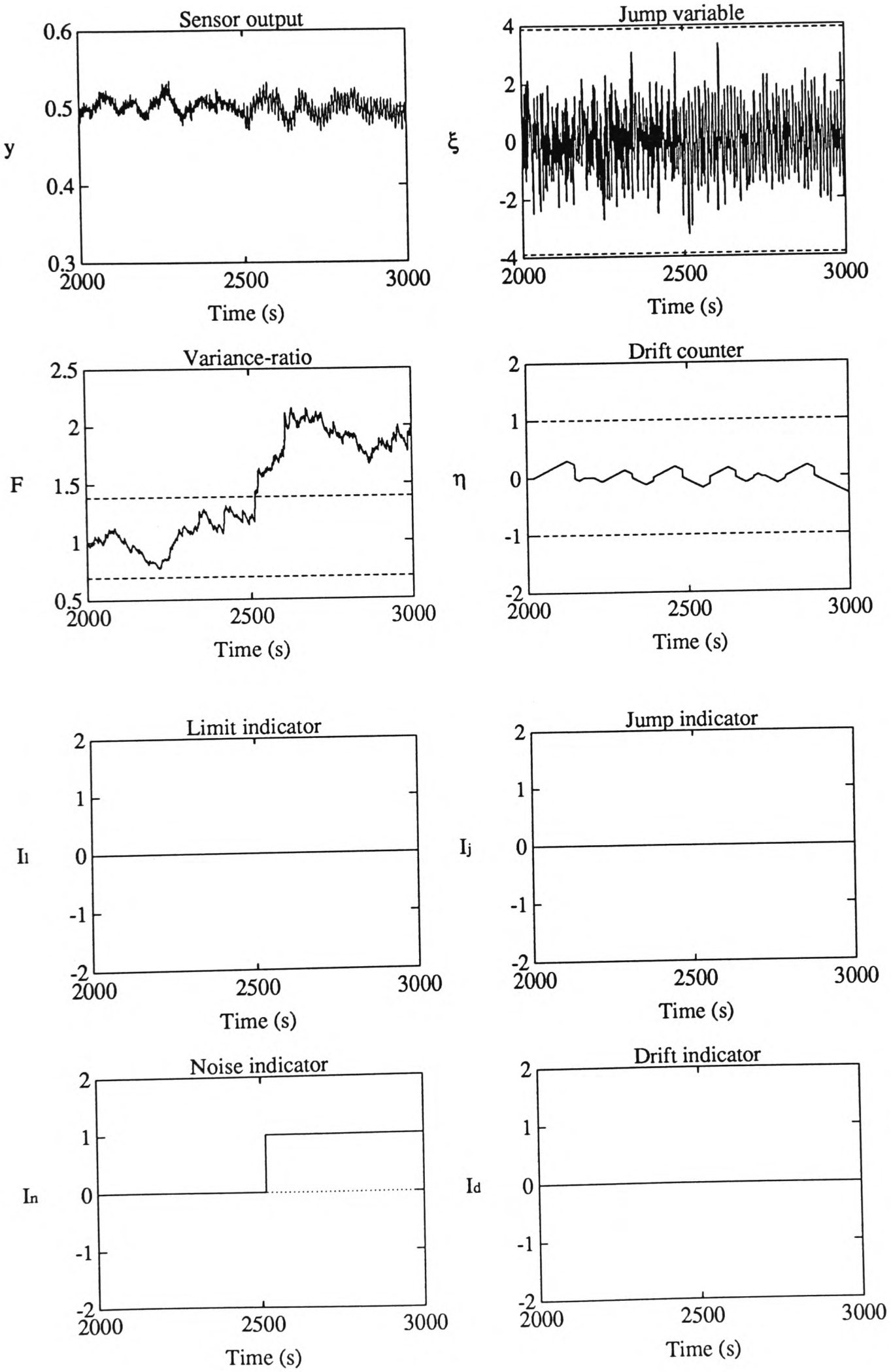

Figure 4.17: Alarm indicators of a cyclic failure

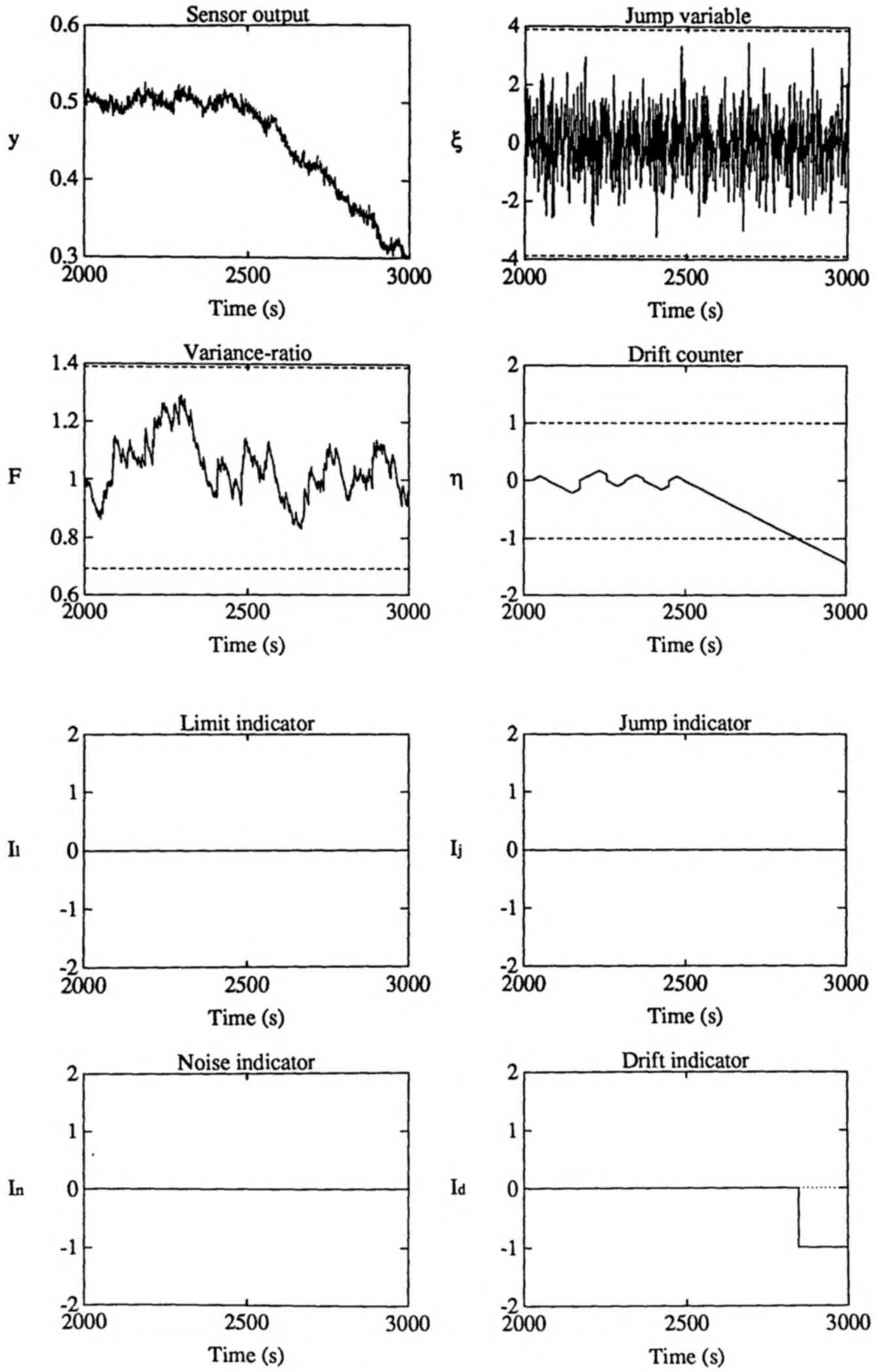

Figure 4.18: Alarm indicators of a drift failure

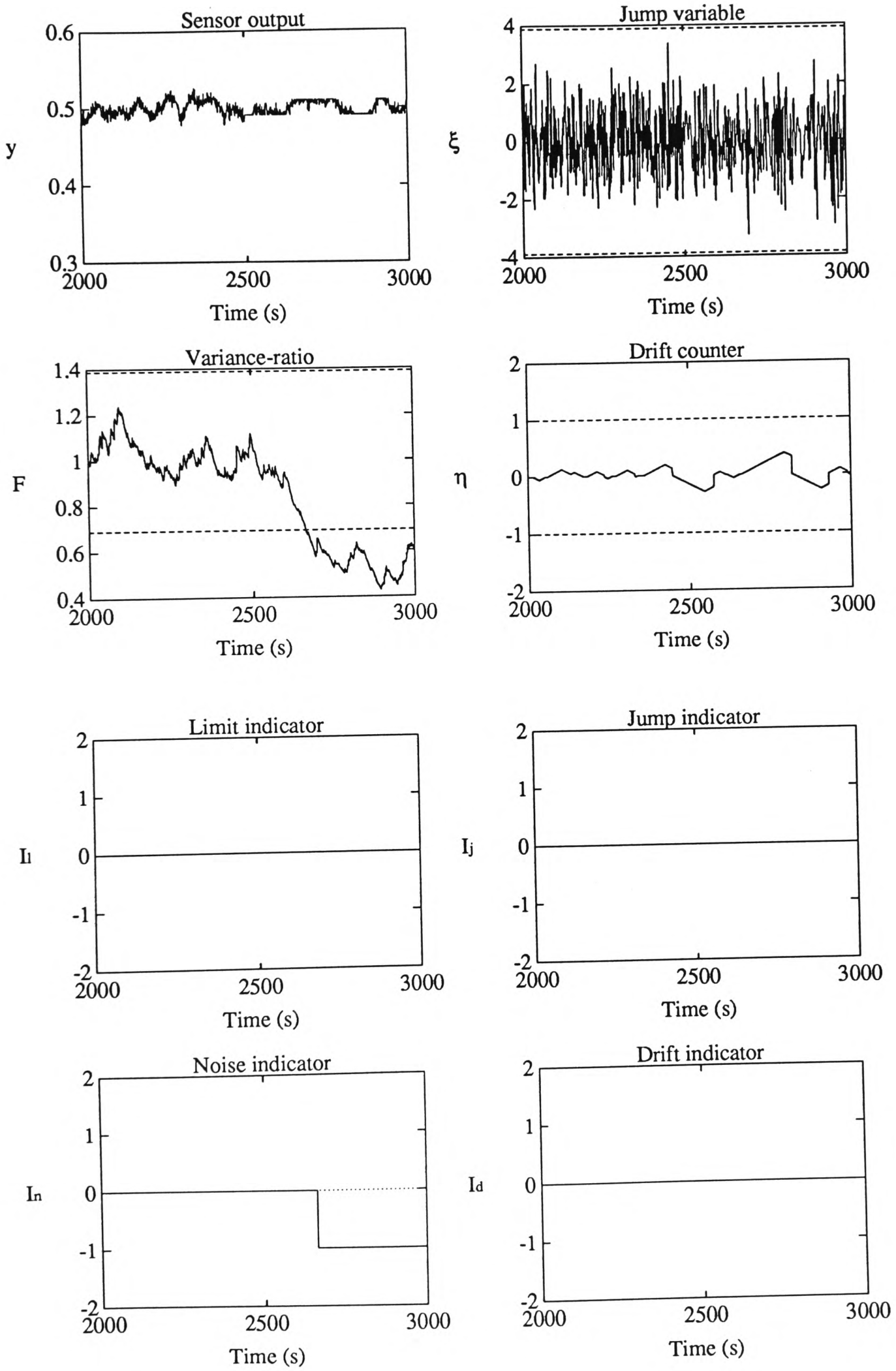

Figure 4.19: Alarm indicators of a saturation failure

4.5 Failure mode indicator (Alert phase)

If any of the failure alarm indicators is triggered in the ordinary phase, the validation scheme will switch automatically into the *alert phase*. Each of the failure alarm indicator carries some information about the particular type of detected abnormalities and the main objective during the alert phase is to uniquely identify the sensor failure mode (*failure identification*) and to predict the severity of the failure (*failure estimation*).

Failure diagnosis in the local sensor validation scheme is accomplished with a simple 'rule-based' system. A batch of data (including the raw sensor output $y(t)$ and/or the innovation sequence $\epsilon(t)$) is collected after the initialization of a failure alarm indicator to establish a representative database of post-failure signal characteristics. Depending on the alarm activated in the ordinary phase, various additional signal processing and statistical tests on the data set may be required to determine the states of the *failure mode indicator* and to estimate the size of the failure. The adopted diagnostic rules and procedures are laid down below and the basic logics for failure identification are summarized in Table 4.1 (page 156)[7]:

- **No failure alarm indicator is activated**

  The default value of the failure mode indicator is 'NORMAL' which indicates that the sensor is functioning properly. The failure mode will remain at 'NORMAL' until a failure alarm indicator is triggered and the corresponding failure mode is identified.

- **The limit indicator is activated**

  This signifies that the sensor has totally broken down. It is likely that other alarm indicators, especially the jump indicator, may be triggered at the same instance. But in all circumstances, the limit indicator will take precedence and the failure mode indicator is immediately set to 'HARDOVER_HIGH' if $I_l = 1$ and 'HARDOVER_LOW' if $I_l = -1$.

- **The jump indicator is activated**

  The abrupt deviation detected in the innovation sequence is due either to a bias or to a spike failure. One way to distinguish between the two is to compare the mean

[7]Except for the limit indicator, if more than one of the failure alarm indicators are triggered, all the relevant diagnostic procedures will be carried out either in parallel or in a sequence depending on the severity of the potential failure mode.

levels of the sensor output prior and subsequent to the trigger-off of the alarm. The sample mean of the 'failed' sensor output $\{y_f(1), y_f(2), \ldots, y_f(N_{y_f})\}$ is

$$\hat{\bar{y}}_f = \frac{1}{N_{y_f}} \sum_{k=1}^{N_{y_f}} y_f(k) \tag{4.63}$$

and an unbiased estimate of its sample variance is given by

$$\hat{\sigma}^2_{y_f} = \frac{1}{N_{y_f} - 1} \sum_{k=1}^{N_{y_f}} \left(y_f(k) - \hat{\bar{y}}_f \right)^2 \tag{4.64}$$

The mean of the sensor output before the inception of failure has already been tracked on-line as $\hat{\bar{y}}_2(t)$ and is inherent in the computation of the sensor output derivative[8] during the ordinary phase (c.f. Equation 4.29). Assuming that the measurement signal is relatively stationary within the N_{y_f} samples, the mean levels should remain constant in case of a spike failure, i.e. the null hypothesis is $\hat{\bar{y}}_2(t_f - 1) = \hat{\bar{y}}_f$ (where t_f is the alarm trigger time). For a bias failure, the alternative hypothesis will either be $\hat{\bar{y}}_2(t_f - 1) < \hat{\bar{y}}_f$ if $I_j = 1$ or $\hat{\bar{y}}_2(t_f - 1) > \hat{\bar{y}}_f$ if $I_j = -1$. A test statistic Λ is formulated as

$$\Lambda = \frac{\hat{\bar{y}}_f - \hat{\bar{y}}_2(t_f - 1)}{\hat{\sigma}_{y_f} \sqrt{\frac{1}{N_{y_f}} + \frac{1}{m_2}}} \tag{4.65}$$

where m_2 is the effective window length of the recursive mean estimator (Equation 4.30)

$$m_2 = \frac{2}{\alpha_2} - 1 \tag{4.66}$$

If $|\Lambda| \leq \Lambda_o$, the failure is identified as a spike and the failure mode indicator is flagged as 'SPIKE_POS' if $I_j = 1$ and 'SPIKE_NEG' if $I_j = -1$. Otherwise, the failure mode indicator is set to 'BIAS_POS' if $I_j = 1$ and 'BIAS_NEG' if $I_j = -1$.

For sufficiently large[9] m_2 and N_{y_f}, Λ defined in Equation 4.65 should follow a standardized normal distribution [Mulholland and Jones, 1983, Section 9.6]. The statistical test should be *one-tailed* and at 1% significance level, the threshold Λ_o is 2.33.

In failure estimation, the size of the spike is estimated to be

$$\vartheta_{\text{spike}} = y(t_f) - \hat{\bar{y}}_2(t_f - 1) \tag{4.67}$$

---

[8] $\hat{\bar{y}}_2(t)$ is preferred to $\hat{\bar{y}}_1(t)$ because of its longer effective window length.

[9] For small m_2 or N_{y_f}, Λ will follow a Student's t distribution [Mulholland and Jones, 1983, Section 9.7].

while that of the bias is taken to be

$$\vartheta_{\text{bias}} = \hat{\bar{y}}_f - \hat{\bar{y}}_2(t_f - 1) \tag{4.68}$$

- **The noise indicator is activated (variance too small)**

  If the noise indicator I_n is set to -1, indicating a decrease in variance, one possible explanation will be that the sensor is stuck. This is verified by inspecting the sample variance of the 'failed' sensor output $\hat{\sigma}^2_{y_f}$ (Equation 4.64). If $\hat{\sigma}^2_{y_f} < \delta_f$ (δ_f is a small positive constant to account for the finite numerical precision), the failure mode indicator will be classified as 'STUCK'. If not, it is set to 'ERRATIC_LOW'[9] and the failure size is taken to be the variance shrinkage factor

$$\vartheta_{\text{erratic}} = \frac{\hat{\sigma}^2_{\epsilon_f}}{(\sigma^2_\epsilon)_{\text{ref}}} \tag{4.69}$$

  where the sample innovation variance $\hat{\sigma}^2_{\epsilon_f}$ is computed in a similar way to Equations 4.63 and 4.64 from a data set of 'failed' innovation $\{\epsilon_f(1), \epsilon_f(2), \ldots, \epsilon_f(N_{\epsilon_f})\}$ and $(\sigma^2_\epsilon)_{\text{ref}}$ is the reference innovation variance acquired during the learning stage.

- **The noise indicator is activated (variance too large)**

  If the noise indicator is set to 1, the sensor is suffering from either an erratic or a cyclic failure. The basis of their differentiation lies on the spectral characteristics of the 'failed' signals (either the sensor output or the innovation). In cyclic failures, the spectrum of a set of 'failed' data should have a prominent peak and the signal power should localize around the cycling frequency. On the other hand, erratic signals should have their power more evenly distributed over the frequency range, though the signature is not necessarily white. Since the innovation sequence has better defined spectral properties at normality (a relatively flat spectrum), an innovation-based spectral diagnosis is employed.

  A spectral difference $\Delta\Phi_\epsilon(\omega)$ with respect to the reference innovation spectrum obtained in the learning stage (Section 3.12) is defined as

$$\Delta\Phi_\epsilon(\omega) = \Phi_{\epsilon_f}(\omega) - (\Phi_\epsilon(\omega))_{\text{ref}} \tag{4.70}$$

[9]Nonlinear failures such as saturation and dead-band will decrease the effective excitation of the innovation and is currently identified as 'ERRATIC_LOW'.

where $\Phi_{\epsilon_f}(\omega)$ is the spectrum computed from a collection of 'failed' innovation $\{\epsilon_f(1), \epsilon_f(2), \ldots, \epsilon_f(N_{\epsilon_f})\}$ and evaluated at a set of discrete frequency points given by

$$\Omega = \{\omega_1, \omega_2, \ldots, \omega_{n_\epsilon}\} \tag{4.71}$$

Automatic classification of cyclic and erratic failures is by no means straightforward. A technique similar to the *influence analysis* in statistics [Cook and Weisberg, 1982, Chapters 3, 4, 5] is adopted in which the perturbation of a property due to the deletion of a group of data is studied. The frequency $\omega_{k_{\max}}$ that maximizes $\Delta\Phi_{\epsilon_f}(\omega)$ is first determined. A new frequency supporting set Ω' is then formed by removing a narrow frequency band around $\omega_{k_{\max}}$

$$\Omega' = \{\omega_1, \ldots, \omega_{k_{\max}-\delta k}, \omega_{k_{\max}+\delta k}, \ldots, \omega_{n_\epsilon}\} \qquad \delta k \geq 1 \tag{4.72}$$

$\Delta\omega = \omega_{k_{\max}+\delta k} - \omega_{k_{\max}-\delta k}$ represents the maximum bandwidth of the corrupting signal to be classified as a cyclic failure. A statistical measure φ is defined to be

$$\varphi = \frac{\sum_{\omega\in\Omega'} \Delta\Phi_\epsilon(\omega)}{\sum_{\omega\in\Omega} \Delta\Phi_\epsilon(\omega)} \tag{4.73}$$

By Parseval's Theorem, the statistics φ approximates the contribution at frequencies outside the narrow bandwidth towards the increase in the innovation variance. A small φ indicates that the variance increase is clustering within a narrow frequency band and strongly suggests a cyclic failure. The failure mode indicator is declared as 'CYCLIC' if $\varphi < \varphi_o$ and as 'ERRATIC_HIGH' otherwise. The design variable φ_o should depend on the prescribed bandwidth $\Delta\omega$ and is selected by

$$\varphi_o = 1 - k_\varphi \left(\frac{2\delta k - 1}{n_\epsilon}\right) \tag{4.74}$$

where k_φ is a positive integer larger than 1.

In cyclic failures, it is often the perturbation frequency that is of most interest. The size of failure is determined as

$$\vartheta_{\text{cyclic}} = \omega_{k_{\max}} \tag{4.75}$$

Similar to the case of 'ERRATIC_LOW', the size of the erratic failure is taken to be

$$\vartheta_{\text{erratic}} = \frac{\hat{\sigma}^2_{\epsilon_f}}{(\sigma^2_\epsilon)_{\text{ref}}} \tag{4.76}$$

where $\hat{\sigma}^2_{\epsilon_f}$ is the sample variance of the 'failed' innovation data.

- **The drift indicator is activated**

  This aberration is a direct result of a drift failure and the failure mode indicator is labelled as 'DRIFT_POS' if $I_d = 1$ and as 'DRIFT_NEG' if $I_d = -1$. The actual time of the onset of the drift failure can be predicted to be τ_d before the trigger-off of the failure alarm indicator. Given a set of 'failed' sensor output $\{y_f(1), y_f(2), \ldots, y_f(N_{y_f})\}$, the slope of the drift (assumed to be linear) can be estimated by a linear regression analysis [Press *et al.*, 1987, Section 14.2]:

$$\vartheta_{\text{drift}} = \frac{6\, f_m \sum_{k=1}^{N_{y_f}} \left(2k - N_{y_f} - 1\right) y_f(k)}{N_{y_f}\left(N_{y_f}^2 - 1\right)} \tag{4.77}$$

  where f_m is the sampling frequency in Hz.

Unique identification of various nonlinear failures is not covered in the proposed scheme. For specific nonlinear failures such as saturation and dead-band, the effective excitation of the sensor output and that of the innovation sequence will be reduced and the noise indicator will be triggered ($I_n = -1$). Except when the output is being clipped for the entire period during the alert phase (which will be identified as a stuck failure), the failure mode indicator will be classified as 'ERRATIC_LOW'. Additional evidence relating to a saturation or a dead-band failure can be acquired by examining the histogram of the output signal or by conducting a calibration test on the sensor.

In the alert phase, prior knowledge on the absence of some particular failure modes will both simplify and enhance the diagnostic procedures by pruning the fault tree. For example, if the sensor is operating in a type-2 closed loop environment, bias or drift failure patterns will not appear in the sensor output (Property 2.1). Whenever the jump indicator is activated, the failure mode indicator can immediately be set to 'SPIKE_POS' or 'SPIKE_NEG' according to the sign of the excessive deviation. No further processing or statistical tests are then required.

Example 4.8

Following on from Example 4.7, a detailed diagnosis of the various aberrations detected in the ordinary phase is performed. The design variables and the thresholds utilized in the alert phase are given below:

$$N_{y_f} = 200$$

Failure alarm indicator	*Additional tests in alert phase*		*Failure mode indicator*
All alarm indicators OFF	*none*		NORMAL
Limit indicator ON	$I_l = 1$		HARDOVER_HIGH
	$I_l = -1$		HARDOVER_LOW
Jump indicator ON	$\|\Lambda\| \leq \Lambda_o$ (Equation 4.65)	$I_j = 1$	SPIKE_POS
		$I_j = -1$	SPIKE_NEG
	$\|\Lambda\| > \Lambda_o$ (Equation 4.65)	$I_j = 1$	BIAS_POS
		$I_j = -1$	BIAS_NEG
Noise indicator ON	$I_n = -1$ (Equation 4.64)	$\hat{\sigma}^2_{y_f} < \delta_f$	STUCK
		$\hat{\sigma}^2_{y_f} \geq \delta_f$	ERRATIC_LOW
	$I_n = 1$ (Equation 4.73)	$\varphi \geq \varphi_o$	ERRATIC_HIGH
		$\varphi < \varphi_o$	CYCLIC
Drift indicator ON	$I_d = 1$		DRIFT_POS
	$I_d = -1$		DRIFT_NEG

Table 4.1: Summary of failure mode indicators

$$
\begin{aligned}
N_{\epsilon_f} &= 256 \\
\Lambda_o &= 2.33 \\
\delta_f &= 10^{-15} \\
\varphi_o &= 0.53
\end{aligned}
\qquad
\begin{cases}
n_\epsilon &= 128 \\
\delta k &= 2 \\
k_\varphi &= 20
\end{cases}
$$

The eight cases are studied individually and the final results from the local sensor validation scheme is summarized in Table 4.2. Reference on original failure simulation parameters can be found in Example 4.1.

1. *A simulated normal mode* (no alarm triggered)

   The failure mode indicator remains at the default value of 'NORMAL'.

2. *A simulated bias failure* ($I_j = 1$ at 2500 s)

   The sample mean and the sample variance of the 'failed' sensor output are estimated to be 0.55 and 5.16×10^{-5} respectively. The sample mean prior to the failure is 0.50 ($m_2 = 14$). The test statistics is then computed from Equation 4.65: $\Lambda = 30.04$. Since $I_j = 1$ and $\Lambda > \Lambda_o = 2.33$, the failure mode indicator is set to 'BIAS_POS' and the size of the jump is estimated to be 0.060 (Equation 4.68).

3. *A simulated spike failure* ($I_j = -1$ at 2500 s)

   In this case, the test statistics Λ (Equation 4.65) is evaluated to be -0.11 ($\hat{\bar{y}}_f = 0.51$, $\hat{\sigma}^2_{y_f} = 6.40 \times 10^{-5}$, $\hat{\bar{y}}_2(t_f - 1) = 0.51$ and $m_2 = 14$). Since $I_j = -1$ and $|\Lambda| < \Lambda_o = 2.33$, the failure mode indicator is flagged as 'SPIKE_NEG' and the estimate of the size of the spike is -0.054 (Equation 4.67).

4. *A simulated stuck failure* ($I_n = -1$ at 2529 s)

   The sample variance of the 'failed' sensor output is 9.00×10^{-31} (Equation 4.64) which is much less than the threshold δ_f ($= 10^{-15}$). The failure mode indicator is declared as 'STUCK'.

5. *A simulated erratic failure* ($I_n = 1$ at 2542 s)

   The spectral difference $\Delta\Phi_\epsilon(\omega)$ is computed at 128 frequency points (Figure 4.20(a)). $\omega_{k_{\max}}$ is estimated to be 0.32 Hz and δk is taken to be 2 (i.e. $\Delta\omega = 0.016$ Hz). From Equation 4.73, $\varphi = 0.85$ which is larger than the predetermined threshold of φ_o ($= 0.53$). The failure mode indicator is set to 'ERRATIC_HIGH' and the variance expansion factor is determined to be 2.80 (Equation 4.76).

6. *A simulated cyclic failure* ($I_n = 1$ at 2515 s)

   Similar to the above erratic failure, the spectral difference is evaluated at 128 frequency samples and is plotted in Figure 4.20(b). The suspected cycling frequency $\omega_{k_{\max}}$ is found to be 0.10 Hz and the narrow bandwidth $\Delta\omega$ is set to 0.016 Hz. The test statistics is computed from Equation 4.73: $\varphi = 0.24 < \varphi_o = 0.53$. The failure is hence classified as 'CYCLIC' and the perturbation frequency is estimated to be 0.10 Hz ($= \omega_{k_{\max}}$).

7. *A simulated drift failure* ($I_d = -1$ at 2848 s)

   The failure mode indicator is identified as 'DRIFT_NEG'. The predicted failure time

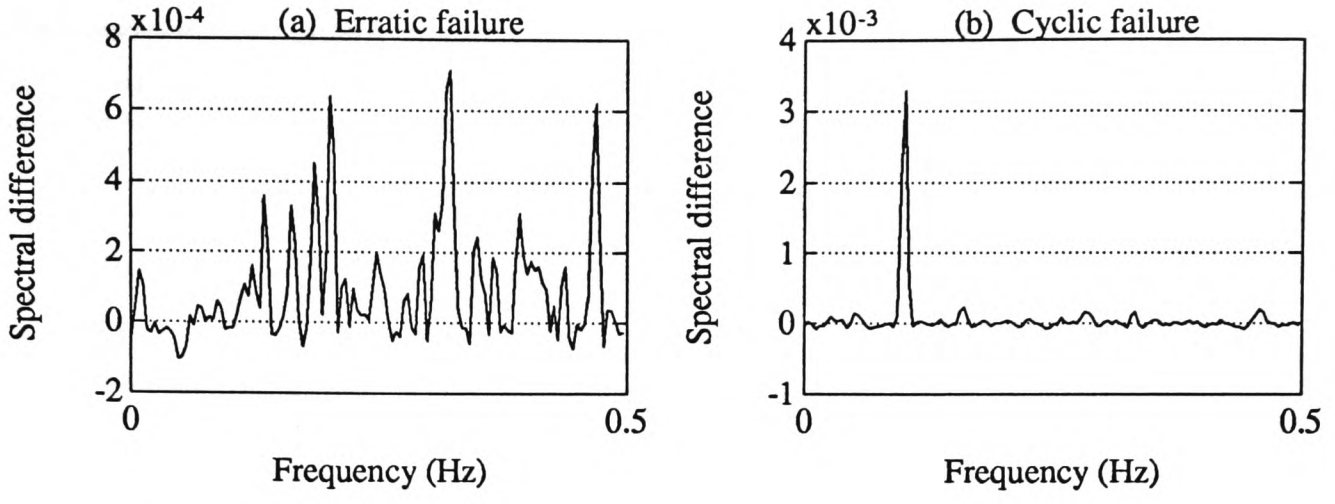

Figure 4.20: Spectral differences $\Delta\Phi_\epsilon(\omega)$ of an erratic and a cyclic failure

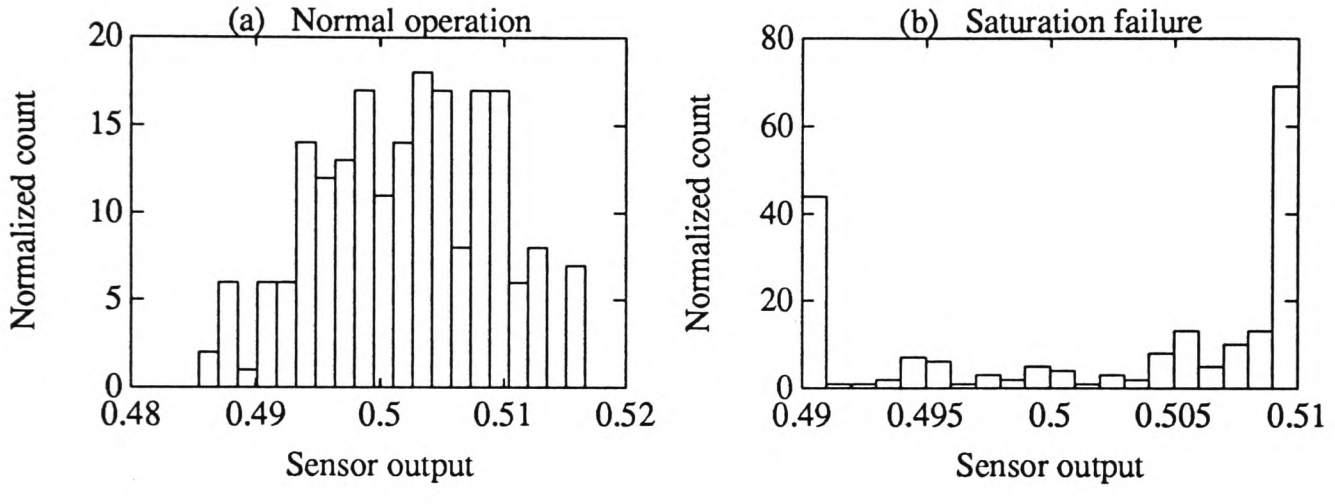

Figure 4.21: Histograms of the sensor outputs at normality and in a saturation failure

is corrected to 2498 s ($\tau_d = 350$ s)[10]. By linear regression (Equation 4.77), the slope of the drift is estimated to be -0.00041 unit/s.

8. *A simulated saturation failure* ($I_n = -1$ at 2663 s)
   Since the computed sample variance of the 'failed' sensor output $\hat{\sigma}^2_{\epsilon_f}$ ($= 6.49 \times 10^{-5}$) exceeds the minimum threshold δ_f, the failure mode indicator is labelled as 'ERRATIC_LOW'. The variance shrinkage factor is computed to be 0.49 (Equation 4.69). In addition, normalized histograms of the sensor outputs during the learning stage and after the trigger-off of the alarm are displayed in Figure 4.21. The clustering at the two extremes in Figure 4.21(b) is an evidence of a saturation failure.

---

[10]The predicted time of failure is before the actual onset of the drift failure at 2500 s due to the presence of some earlier legitimate negative drifting actions.

Mode (simulated)	*Failure mode indicator*	*Time of failure*	*Size of failure*
Normal	NORMAL	N/A	N/A
Bias	BIAS_POS	2500 s	0.060 unit
Spike	SPIKE_NEG	2500 s	−0.054 unit
Stuck	STUCK	2529 s	N/A
Erratic	ERRATIC_HIGH	2542 s	2.80
Cyclic	CYCLIC	2515 s	0.10 Hz
Drift	DRIFT_NEG	2498 s	−0.00041 unit/s
Saturation	ERRATIC_LOW	2663 s	0.49

Table 4.2: Failure diagnosis results of Example 4.8

4.6 Conclusions

The detection and the diagnosis of typical sensor failures in the tracking stage has been extensively studied in this chapter. An efficient and flexible detection scheme has been developed. In the initial ordinary phase, minimal signal processing is utilized to focus on a small subset of signal characteristics and this is sufficient to register the occurrence of any of the eight failure modes proposed in Section 2.4.2. This simple approach minimizes the computational demand at a local sensor level and warrants an expeditious failure detection. A group of failure alarm indicators have been designed to classify the aberrations observed in the ordinary phase. It is only after an alarm has been triggered that the alert phase will be initiated and a detailed diagnosis on the sensor failure will be carried out. Additional processing may be required to uniquely identify the particular failure mode and this increase in computational load can be compensated by reallocation of the available resources.

The local sensor validation scheme is primarily innovation-based. The well-defined statistics of the innovation sequence for a healthy sensor (zero-mean and uncorrelated) both simplify and enhance the subsequent failure detection procedures. Except for hardover and drift failures, all the other six typical sensor failures exhibit identifiable signatures in the innovation. Bias and spike failures generate abrupt deviations and stuck, erratic, cyclic and saturation failures modify the excitation. As for hardover and drift failures,

the crude sensor outputs (or their derivatives) will exceed some prescribed thresholds in the occurrence of the former, and the latter introduce persistent biases in the derivatives of the signal-dominant components.

A number of proficient signal processing algorithms have been implemented to track the following properties on-line:

- **Mean** (Equation 4.5)
  An efficient unbiased estimator of the sample mean is presented. It is made up of a growing sliding-window with exponentially decaying weightings (Property 4.1) and can be considered approximately as a first-order lowpass filter with unity gain (Property 4.2).

- **Variance** (Algorithm 4.28)
  An exponential variance filter, which is a direct extension of the mean estimator, is first derived. It is asymptotically unbiased (Property 4.3) but is sensitive to spikes and outliers. A robust solution combining nonlinear logical and linear exponential filtering is then proposed. The integrated approach will preserve the desirable tracking ability of the exponential estimator and, in addition, the embedded logical filtering will minimize the effects of filtered spikes and outliers.

- **Rate of change** (Equation 4.29)
  The derivative of a signal is estimated by the difference between the outputs of two mean estimators with different effective window lengths. The resulting algorithm has attractive noise suppression properties and resembles an ideal differentiator cascaded by two first order lowpass filters (Property 4.4).

- **On-line measure of bias** (Equation 4.37)
  A measure of the bias of a signal has been developed. The inherent signum operation robustifies the algorithm against spikes and outliers and places more emphasis on the persistence rather than the magnitudes of the bias. Moreover, as long as the original signal distribution is symmetrical, the adopted measure of bias will approach a standardized normal variate (Property 4.5).

The choice of the initial conditions and the 'tuning-knobs' for the mean, the variance, the rate of change and the measure of bias estimator are recommended in Guidelines 4.1, 4.3, 4.4 and 4.5 respectively. Despite being developed and analyzed with the local sensor

validation scheme in mind, the signal processing tools are directly applicable to a wide variety of problems.

In the ordinary phase, the following five variables are computed recursively with the above-mentioned techniques: the innovation mean, the innovation variance, the rate of change of the sensor output, the derivative of the signal-dominant component as well as its on-line measure of bias. These are employed to formulate four different alarm indicators:

- The **limit indicator** simply tracks the occurrence of a hardover failure, in which either the raw output or its derivative exceeds the physical constraints imposed by the sensor and the operating environment.

- The **jump indicator** detects excessive deviations of the innovation sequence from its mean level, which are attributed to either a bias or a spike failure.

- The **noise indicator** follows the excitation of the innovation sequence by comparing the on-line estimates of the innovation variance with the reference variance obtained during the learning stage. Any unanticipated departure from the nominal noise level can be a symptom of a stuck, an erratic, a cyclic or a saturation failure.

- The **drift indicator** is dedicated to monitor the presence of continuous drifting actions. A drift counter is designed to register the significance and the persistence of the drifts. By specifying a minimum drifting duration, the drift indicator is capable of distinguishing legitimate step responses from a genuine drift failure.

The selection of the thresholds for the four failure alarm indicators and the design of various parameters in the construction of the drift indicator are detailed in Guidelines 4.6 to 4.9. In cases when the innovation sequence can be considered to be normally distributed (when the measurement noise and the injected dither are both Gaussian) and given the desired significance levels, 'optimal' thresholds can be evaluated for the jump and the noise indicator.

During the alert phase, a simple 'rule-based' system is adopted to diagnose the anomalies detected in the preceding ordinary phase. A number of rules and their associated actions are laid down in Section 4.5 and are summarized in Table 4.1. Depending on the status of the failure alarm indicators, additional signal processing (viz. mean and variance computation, spectral analysis and linear regression) and statistical tests are applied to

a collection of 'failed' data to uniquely identify the sensor failure. The diagnosed classification is then returned in the failure mode indicator. Furthermore, the severity of the failure is estimated and the result is provided in a failure size parameter.

The development of the theoretical background and various principal techniques on the local sensor validation scheme have been completed. Aspects of its applications on experimental thermocouple data and its implementation as a user-friendly software package will be explored in Chapter 5.

Chapter 5

Implementation and Application of the Local Sensor Validation Scheme

5.1 Introduction

The integrity and the practicality of the proposed local sensor validation scheme have to be examined by extensive experimentations with synthetic, and more importantly, real sensor data. With an abundance of design parameters, processing algorithms and statistical testings required, the embodiment of the commissioning, the learning and the tracking stage in a single integrated package is called for. Although the validation scheme is generically sensor and process independent, it is by no means the objective here to verify its applicability to a large variety of sensors. Thermocouple, one of the most popular instruments in industry, is selected to be the representative. Notwithstanding the inherent nonlinearity, the thermocouple experiments probe into the fundamentals and the effectiveness of the validation scheme and offer a set of exemplary operating procedures from initial commissioning to ultimate failure diagnosis. Moreover, the utility of the validation scheme can be further broadened by developing strategies to cope with the relaxation of underlying assumptions or the imposition of additional constraints.

5.2 LOSVAL — a local sensor validation package

The proposed local sensor validation scheme comprises of three distinct stages, namely the commissioning, the learning and the tracking stage. Each stage has to achieve a number of individual targets. In order to unify the initialization, the decomposition, the modelling, the detection and the diagnostic procedures, all the algorithms and techniques discussed

in Chapters 2, 3 and 4 have been implemented in a single *integrated* environment. It is by no means the intention here to realize the validation scheme directly into merchandise with priority on execution speed and elaborated front-end interfaces. Rather, the prime objective is to provide a *flexible* and *user-friendly* tool for prototyping novel ideas and analyzing both synthetic and real sensor data. The resultant package is coined LOSVAL — LOcal Sensor VALidation.

LOSVAL is developed in MATLAB†, a popular engineering package for numerical linear algebra and matrix computation. MATLAB is selected as the platform because of its versatility and other attractive properties:

- It provides an efficient and high-performance programming environment with excellent numerical stability properties;
- It has a large collection of routines for data analysis, filter designs, model identification and signal processing;
- It offers a comprehensive range of machine-independent graphical functions;
- It supports most computers used in industry: such as IBM compatibles, Sun Workstations, VAX, Macintosh and HP Workstations;
- It is capable of importing and exporting a wide variety of data formats;
- It allows C and Fortran routines to be called to access special hardware like the data acquisition board.

The LOSVAL package has been extensively tested on Sun-3, Sun-4/SPARC as well as PC's 286 and 386 machines. More detailed specifications for LOSVAL, including computational workload, are set out in Appendix A.

5.2.1 Primary features of the package

LOSVAL is designed to be widely adaptable and self-contained. Its major characteristics are as follows:

†MATLAB is a trademark of The MathWorks, Inc.

- **User-friendly**

  The package is entirely menu-driven and is arranged in a hierarchical structure. Display of its working status and any pertinent information are constantly updated. Default or suggested values are provided in all input prompts[1]. Initialization of various parameters can easily be customized[2] and particular settings can be stored and later recovered for similar applications.

- **Flexible**

  Apart from a few required sequences[3], the package can be steered through in any preferred order. At strategic locations, options are provided to enter the interactive MATLAB command mode. This offers complete freedom to access and manipulate internal variables and to carry out additional processing and prototyping. Data input structure is also highly flexible. Sensor data can either be simulated internally, retrieved from recorded log files, or acquired in real-time.

- **Portable**

  The package is not tied down to a particular hardware configuration. All routines[4] are implemented in plain text files which are fully portable to any machines supported by MATLAB.

- **Extensible**

  LOSVAL can easily be extended to cater for specific acquisition boards and to accommodate for additional sensor signal processing and alarm testings. Furthermore, the collection of MATLAB routines (e.g. for model identification, signal processing and statistical testings) can be adopted for other applications.

- **Real-time capability**

  Since MATLAB is an interpretive, not a compiled, language, its merit is not in computational speed or real-time processing. Within its limitations, basic real-time

---

[1] In an input prompt, the default value is shown in square brackets and can be selected by simply entering a dash ('-').

[2] By editing the default settings in `default.m` and the configuration file `conf_lsv.m`.

[3] The learning stage must take place before the ordinary phase in the tracking stage which in turn must be prior to the failure diagnosis in the alert phase.

[4] Except for the `a2d` routine for reading data from the signal acquisition board (Appendix A.3).

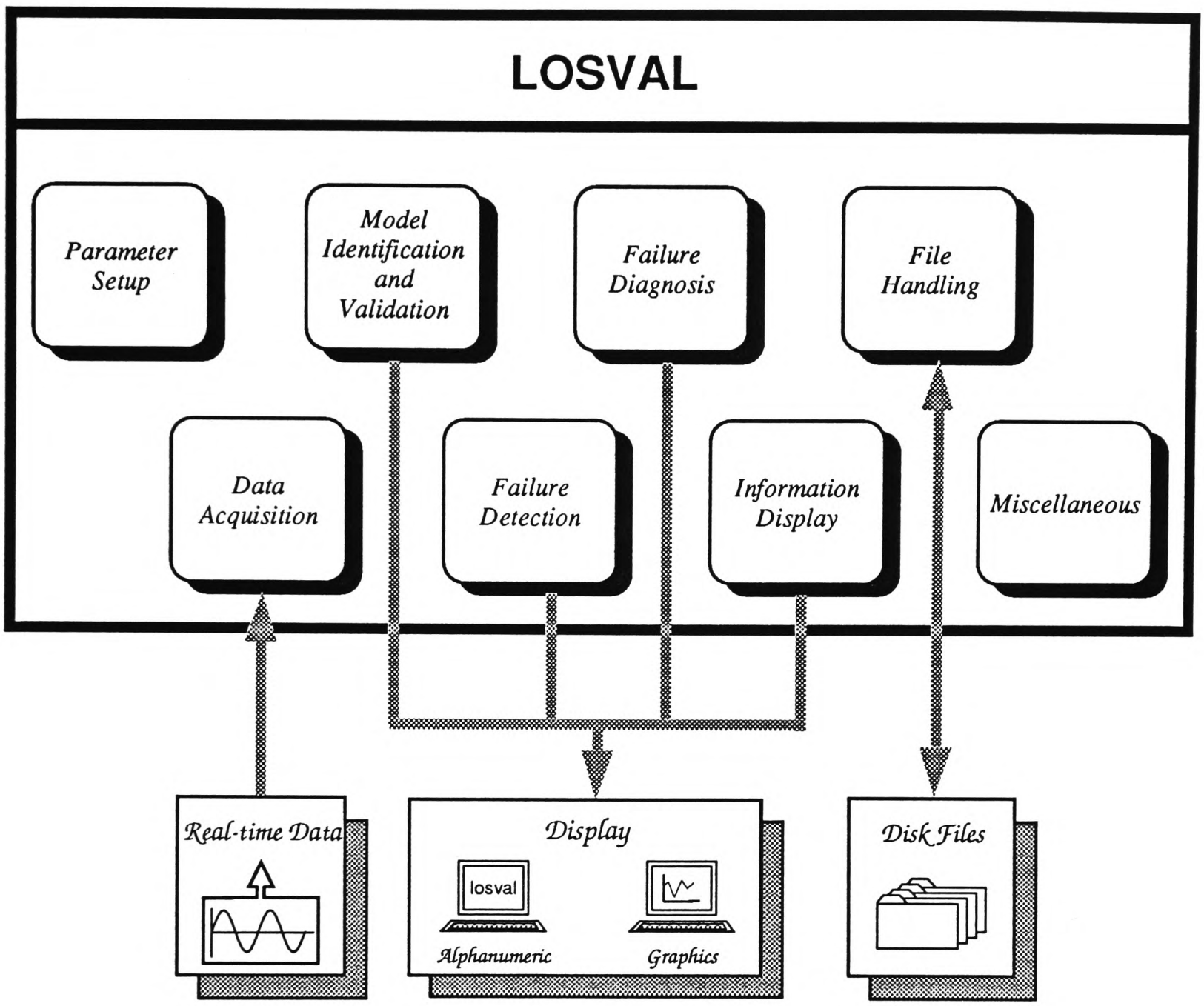

Figure 5.1: Schematic diagram of the local sensor validation package

capabilities have been installed by pulling the system clock via a MATLAB built-in function. Communication with an external signal acquisition board has been established by linking a C routine into the MATLAB environment.

LOSVAL is not merely a sensor signal validation program but a fully integrated environment consisting of a comprehensive range of supportive facilities for modifying the settings, generating or acquiring sensor data and presenting relevant information and results. A schematic diagram of the package is depicted in Figure 5.1. In brief, the package can be divided into eight key operating modules:

- **Parameter setup (the commissioning stage)**

  Key variables required in LOSVAL can be modified in the setup menu. This cov-

ers the determination of sampling period, the regulation of data generation, the design of decomposition filters and dither injection procedure, the detailed specification of various parameters in the learning and the tracking stage, and the control of on-line graphical display and audio alarm. Default values of all variables are provided and, in addition, guidelines for the measurement signal bandwidth estimation (Guideline 3.1) and the tuning of the drift indicator (Guideline 4.9) have been implemented.

- **Data acquisition**

  The sensor data can be generated in three different ways:

  - *Real-time acquisition*

    With an appropriate combination of signal acquisition board and interfacing routine, the real-time mode can be enabled[5] by toggling a single flag in the configuration file (Appendix A.3). Currently, LOSVAL supports a Metrabyte DASH–16 acquisition board [Metrabyte, 1986] residing in a PC-286 machine. The analog input signal can be calibrated into engineering units and an optional decimating filter (Section 3.6) can be employed to increase the effective signal resolution and to alleviate the demands on the anti-aliasing filter.

  - *Internal simulation*

    Data can be simulated to mimic a sensor in an open loop or a closed loop environment (Section 2.2). In open loop, the sensor output is given by

$$y(t) = \underbrace{\frac{Q(q^{-1})}{P(q^{-1})}u(t)}_{signal} + \underbrace{\frac{C(q^{-1})}{A(q^{-1})}e(t)}_{noise} + \underbrace{f_o(t)}_{failure} \tag{5.1}$$

    The signal and the noise transfer function ($P(q^{-1})$, $Q(q^{-1})$, $A(q^{-1})$ and $C(q^{-1})$) can either be designed as classical lowpass filters or directly specified. $e(t)$ is a zero-mean Gaussian white noise with user-specified variance while $u(t)$ can be a white noise or a sequence of steps. In closed loop, $u(t)$ is constrained by the control algorithm

$$u(t) = \frac{S(q^{-1})}{R(q^{-1})}(r(t) - y(t)) \tag{5.2}$$

    Again, the reference signal $r(t)$ can be a random or a pulse sequence. The control strategy can either be defined in a PID framework or detailed explicitly.

[5]The real-time acquisition mode is disabled by default.

Moreover, all the eight sensor failure modes described in Section 2.4.2 can be incorporated in $f_o(t)$.

- *Retrieval of log files*

  Recorded files of sensor data can be loaded into the package (see 'file handling' below). This allows data to be logged by other systems and interesting data sets to be reprocessed under a variety of test conditions.

- **Model identification and validation (the learning stage)**

  LOSVAL is designed to cope with both AR and ARMA time-series modelling of the noise-dominant component $\tilde{y}(t)$ or the perturbed noise-dominant component $\tilde{y}_p(t)$ (Section 3.8). Besides the RML and the ELS identification methods (Sections 3.9 and 3.11.2), off-line optimization approaches[6] are also included. Furthermore, the learning stage can be operated either off-line (for computational speed) or recursively (for continuous update of information). In recursive mode, if on-line graphical display is enabled, the sensor output $y(t)$, the decomposed signals $\bar{y}(t)$ and $\tilde{y}(t)$, and the innovation sequence $\epsilon(t)$ will be plotted; otherwise, the sensor output will be updated in the alphanumeric screen. On completion of the identification procedure, the estimated sensor model will be validated by testing the innovation sequence for zero-mean and whiteness (Section 3.10) and reference statistical and spectral properties of the sensor output (Section 3.12) will be computed.

- **Failure detection (the normal phase)**

  All the efficient processing techniques proposed in Section 4.3: mean, variance, rate of change and measure of bias, have been implemented in the package. During the normal phase, the sensor signal characteristics are continually monitored and the four failure alarm indicators (Section 4.4) are evaluated. Similar to the learning stage, the normal phase can either be in an off-line or a recursive mode. On-line graphical display includes the rate of change of the sensor output $\hat{\dot{y}}(t)$, the jump variable $\xi(t)$, the variance ratio $F(t)$, and the drift counter $\eta(t)$; and both the current sensor output and failure alarm status are shown in the alphanumeric screen. In the event that any alarm is flagged, an audio alarm, if enabled, will be activated.

- **Failure diagnosis (the alert phase)**

  LOSVAL provides a post-mortem diagnosis of sensor failures. Basing on the rules

[6]Modified from the MATLAB System Identification Toolbox.

and logics summarized in Section 4.5 and Table 4.1, the sensor failure mode can be identified and both the size and occurrence time of the failure can be estimated.

- **Information display**

  Up-to-date information on the setup and the results can be easily accessed through the hierarchical menu in either text or graphical format. This includes a list on the current setup, a summary on the failure alarms and diagnosis, displays of various filters (e.g. simulation functions and decomposition filters) and the estimated sensor model, a record of model validation outcomes, as well as graphical plots of signals, spectra, filter frequency responses and detailed results from the learning and the tracking stage.

- **File handling**

  The package is capable of handling input and output files in standard MATLAB format. Other data structures (e.g. ASCII data and binary stream) can be interfaced via the translation utility provided in MATLAB. All or a specified subset of internal variables can be exported for storage. This permits knowledge 'learned' from representative sensor data and standard templates of test conditions to be shared.

- **Miscellaneous**

  Other supplementary functions include regular 'garbage collection' to reclaim memory storage and facility to invoke the interactive MATLAB command mode.

5.2.2 A brief tour of the package

LOSVAL is a versatile and powerful tool for local sensor validation. To discuss each and every utility and to document exhaustively all operations in the package is superfluous and monotonous. Instead, it will be more enlightening to examine the procedures of running LOSVAL on a particular example. The validation of a simulated erratic sensor failure, as described in Examples 4.1, 4.7 and 4.8, is used here as an illustration:

1. LOSVAL can be initiated by issuing the command `losval`[7] within the MATLAB environment[8]. The main menu of LOSVAL will appear as in Figure 5.2. All option numbers hereafter are by reference to those in the main menu.

[7]Assuming that the package is properly installed.

[8]Beware that all variables in the current MATLAB session will be cleared.

```
*********************************************
*  LOSVAL - Local Sensor Validation Package  *
*********************************************
   Oxford University Engineering Laboratory
   (c)  S. K. Yung, 1990-1992 (Version 1.0)

(1)     Display current settings
(2)     Modify current setup
(3)     Real-time data acquisition (not installed)
(4)     Simulation
(5)     Run ''Learning Stage''
(6)     Run ''Tracking Stage''
(7)     Run ''Alert Phase''
(8)     Failure alarms summary report
(9)     Graphical display
(10)    Filter and polynomial display
(11)    Save and restore data files
(12)    Reset default settings
(13)    Interactive keyboard commands
(14)    Garbage collection (free memory)

(0)     Quit


Select an option (0 - 14) [1] :
```

Figure 5.2: Main menu of LOSVAL

```
                        *************************
                        * Current Setup Display *
                        *************************
   Sampling period :     1 sec          Total number of samples :    3001
                           [Signal generation]
Generation mode :  Simulation  (Open-loop)
Bandwidth -  System :   0.01 Hz   Noise :     .5 Hz      S/N ratio :     100
Failure   -   Mode  :  Erratic    From : Sample   2501   To : Sample    3001
              [Signal decomposition - ''dither'' on ( 0.05)]
L(q^-1)  -   Type :   Butterworth     Order :    2      Cut-off :  0.04731 Hz
H(q^-1)  -   Type :   Butterworth     Order :    2      Cut-off :  0.04731 Hz
D(q^-1)  -   Type :    Chebyshev      Order :    3      Cut-off :  0.04731 Hz
                        [Learning stage : off-line]
Number of samples :   2000
Model estimation  -    RML    (Off-line)       NA :    3      NC :  3
Validation plot   -    101 samples       Reference spectrum  -    256 samples
                        [Tracking stage : off-line]
Number of samples :   1001          M1 :    8  M2 :   14  Delta :  8e-05 /s
Signal processing -  Alpha :  0.01  N1 :   37  N2 :   72  Gamma :  0.05
Limits -  Output :      0 to     1    Rate :    .5 /sec   Drift :   350 sec
Significant levels -    Jump :  0.01%      Noise :    .1%      Drift :   .1%
                             [Graphical output]
Graphical output :  Disabled            Audio alarm :   Enabled
                  [Type <Return> to return to main menu]
```

Figure 5.3: A list of current settings in LOSVAL

2. On initiation, a set of default values have been imported. The simulation and validation conditions can be modified, if necessary, to meet those described in Examples 4.1, 4.7 and 4.8. This can be achieved by selecting option 2 and following the 'setup modification' sub-menu step-by-step.

3. The modifications can be verified by entering option 1 and a list of current settings will be displayed (Figure 5.3). Return to Step 2 if further adjustment is required.

4. Prior to the actual sensor validation, the data can be inspected visually by first rehearsing a simulation run (option 4)[9]. The graphical utilities (option 9) can then be invoked to display the simulated sensor signal, the decomposed signals, their power spectra and the frequency responses of various filters. Although this step is not compulsory, it may provide beneficial insights and clues to fine-tune the estimate of the measurement signal bandwidth and the parameters needed in the learning and the tracking stage.

5. When the setup is ready, enter option 5 to trigger off the learning stage. Modify the sensor model structure and estimator initialization (Step 2) and repeat this step until the model validation tests are satisfactory. The estimated ARMA model (together with its zeros and poles) can be displayed by choosing 10 and then the 'Model estimation results' option. An example of the layout is illustrated in Figure 5.4.

6. The normal phase in the tracking stage can be activated by selecting option 6. This should be followed by the failure diagnosis in the alert phase (option 7). A summary of the failure alarms and diagnosis (option 8) is reproduced in Figure 5.5.

7. Option 9 and option 10 can be utilized throughout to present the validation results in graphical and text formats respectively.

8. The simulated sensor data and the validation results can be saved by choosing option 11.

9. Finally, the package can be terminated by selecting 0 and then confirmed by entering y.

---

[9]For real-time applications, a test set of sensor data can be obtained by first selecting an appropriate acquisition duration (Step 2) and then activating option 3.

```
                    ********************
                    * Model estimation *
                    ********************

                                  -1
                           -     C(q  )
                           y (t) = ------ e(t)
                            p          -1
                                      A(q  )

   -1                    -1              -2              -3
A(q  )  =  1 - 0.77632 q   - 0.944434 q   + 0.82911 q

   -1                    -1              -2              -3
C(q  )  =  1 - 0.142789 q   - 0.653326 q   + 0.487132 q

              [Type <Return> for roots of polynomials]
```

Figure 5.4: Display of estimated sensor model in LOSVAL

```
                  ********************************
                  * Failure Alarm Summary Report *
                  ********************************

Noise indicator (+) has gone on from     2542 sec  (sample  2543)

                     ****************************
                     * Failure Diagnosis Report *
                     ****************************

                  Failure mode indicator  :  ERRATIC_HIGH
                  Estimated failure time  :      2542 sec
                  Estimated failure size  :    2.8032

                      [Type <Return> to continue]
```

Figure 5.5: Failure alarm summary report in LOSVAL

5.3 The thermocouple experiment

A bench-top experiment has been designed and set up to demonstrate the feasibility and practicality of the proposed local sensor validation scheme. Thermocouple, as one of the most widely used sensors in industries[10], has been selected for this experiment.

While thermocouples are relatively trouble free, improper installation or prolonged exposure to critical temperature limits can introduce drifting and erratic output behaviour and ultimately leads to a complete breakdown [Smith, 1988]. Early and expeditious detection of any anomaly is most beneficial; and in some cases, crucial. Anyakora and Lees [1973] attempted to identify thermocouple degradation by monitoring solely the output signal power. This is indeed inadequate and is incapable of dealing with gradual drifts or abrupt biases. A centralized model-based approach on thermocouple failure detection in an air conditioning unit was described in Usoro *et al.* [1985].

5.3.1 Experimental setup

A schematic diagram of the experimental setup is shown in Figure 5.6. A type K Chromel/Alumel ungrounded thermocouple is immersed in an insulated bath of water, 0.21 m $\times$ 0.32 m in cross-section. The water temperature is regulated by a 1.2 kW heating element under on/off (bang-bang) control. Three reference temperature levels are preset at 59°C, 60°C and 61°C and can be adjusted manually. Since the feedback signal is measured by an independent temperature sensor, the thermocouple to be validated is essentially in open loop. In addition, the stirrer incorporated in the heater ensures a homogeneous distribution of water temperature.

The thermocouple is connected directly to a Labfacility 897H two-wire transmitter which provides automatic cold junction compensation. The transmitter, powered by a 30 V d.c. supply, has an operating range from 0°C to 200°C and a response time of 300 ms and it amplifies the thermocouple signal from a few millivolts to the standard 4 – 20 mA output. Although the thermocouple output is not explicitly linearized, the tight operating range (59°C – 61°C) warrants a reasonably linear relationship between the thermocouple temperature and the transmitter output[11].

---

[10]Thermocouple has a 50% share in the temperature measurement market [Doebelin, 1983]

[11]Refer to Figure B.3 in Appendix B.3.

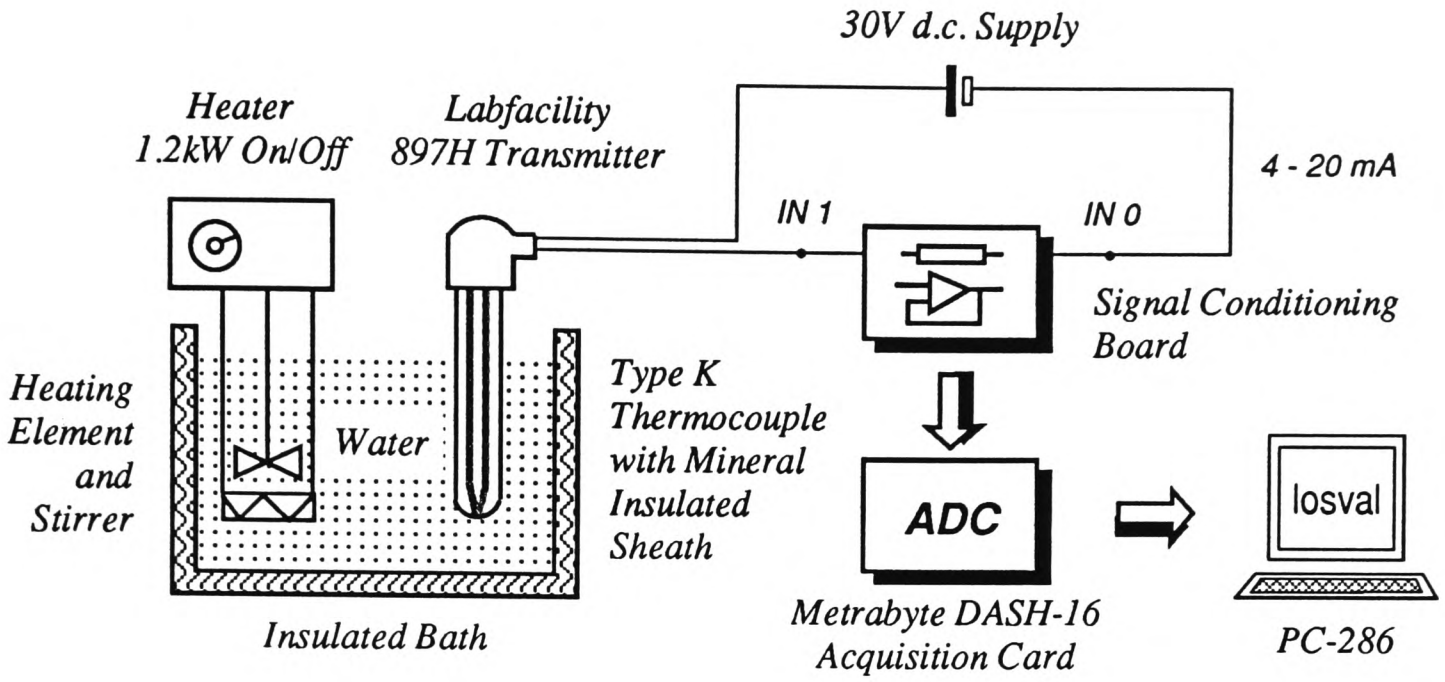

Figure 5.6: Schematic diagram of the thermocouple experiment

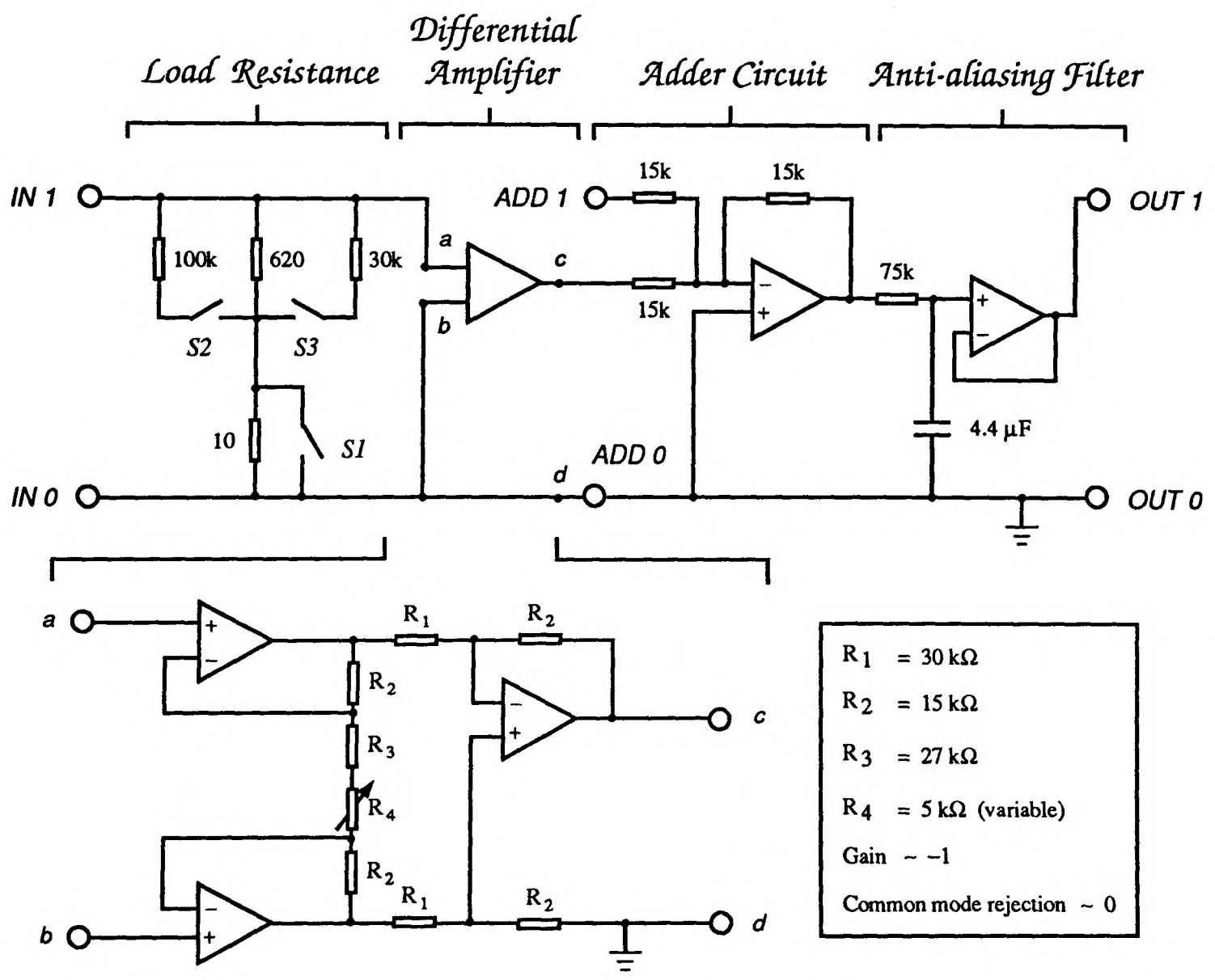

Figure 5.7: Signal conditioning board in the thermocouple experiment

Before being discretized, the output in current is first transformed into a voltage signal by a self-designed signal conditioning board (Figure 5.7), which can be divided into four main stages:

- an initial load resistance network across which the output voltage is tapped — the nominal shunt resistance is 620 Ω and switches to alter the nominal value (0.6% decrease, 2% decrease or 1.6% increase) are provided to imitate bias or spike failures:

Shunt Resistance		*Switches*		
		S1	*S2*	*S3*
Nominal	620 Ω	Closed	Open	Open
0.6% decrease	616 Ω	Closed	Closed	Open
2% decrease	607 Ω	Closed	Open	Closed
1.6% increase	630 Ω	Open	Open	Open

- a classical unity-gain instrumentation (or differential) amplifier [Horowitz and Hill, 1980, Section 7.09] to reject any common mode voltage;
- an adder circuit in which optional interference (e.g. wide band noise) can be injected to simulate erratic failures;
- a first order anti-aliasing filter with cut-off at 0.48 Hz.

Finally, the thermocouple signal is digitized by a 12-bit Metrabyte DASH–16 acquisition board in a PC-286 machine via the LOSVAL package (Section 5.2.1).

For supplementary information on the dynamics and the closed loop behaviour of the process, a mathematical model of the experiment is derived in Appendix B.

5.3.2 Commissioning stage

After all the apparatus and the peripheral acquisition hardware have been assembled and tested, the local sensor validation scheme has to be properly initialized and commissioned. Four key issues have been identified and are discussed separately below: the estimation of the measurement signal bandwidth, the selection of sampling frequency, the installation of the decimating filter, and finally the design of the decomposition filters and dither injection procedures.

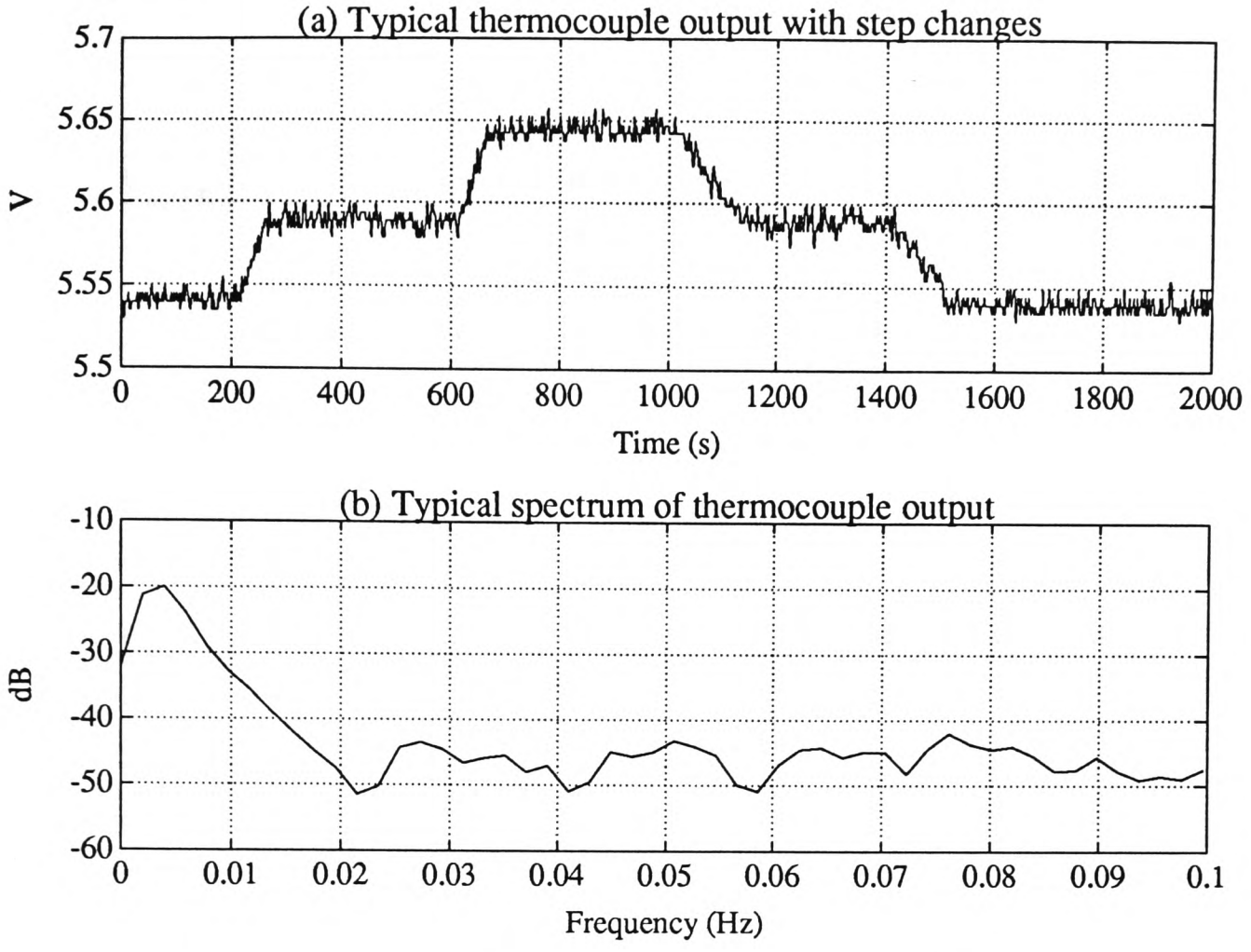

Figure 5.8: Typical thermocouple output (with step changes) and its spectrum

Measurement signal bandwidth

Due to the bang-bang control of the heating element, the response of the thermocouple output is generally nonlinear and depends heavily on the operating conditions. Throughout the experiment, the normal operating range of the thermocouple temperature is constrained within 59°C and 61°C with a maximum step change of 1°C. The primitive heater prohibits elaborated tests with complicated setpoint sequences to be carried out. In estimating the measurement signal bandwidth, one way to circumvent this limitation is to collect representative spectra of the sensor signals and identify the 'break-off' points from the measurement noises at high frequencies (Section 3.3.8). A typical record of thermocouple output, with a series of step changes between 59°C and 61°C, is acquired. The sensor signal and its corresponding spectrum (first 0.1 Hz) are shown in Figure 5.8. It is evident that the signal is confined to a low frequency band and the measurement signal bandwidth ω_s is estimated to be 0.025 Hz. This agrees well with the predicted value of 0.022 Hz in Appendix B.4 based on a mathematical model of the experimental setup.

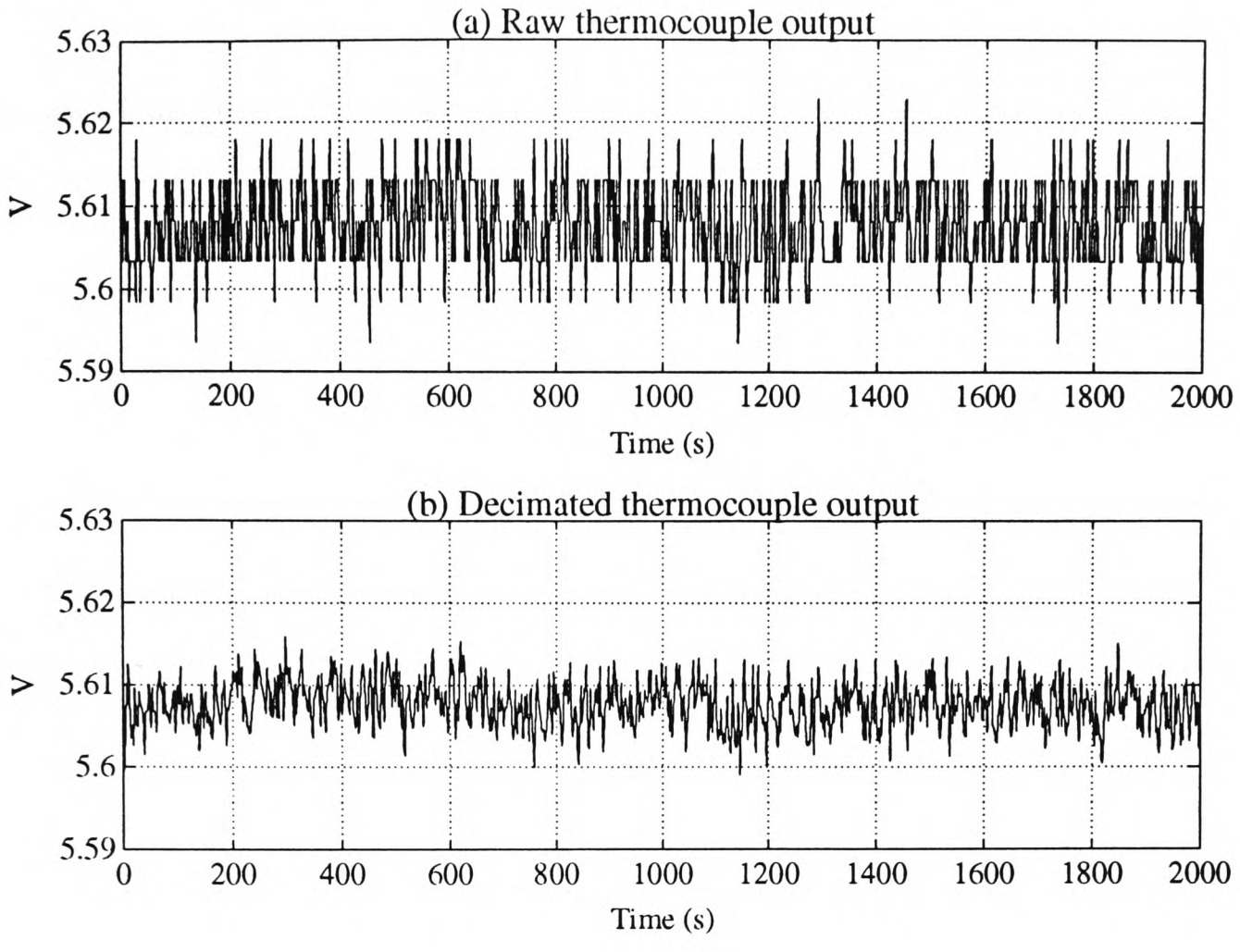

Figure 5.9: Raw and decimated thermocouple output

Sampling frequency

Following Guideline 3.2 which suggests that the Nyquist frequency should be at least 10 times the measurement signal bandwidth ω_s, the sampling rate f_m is chosen to be 0.5 Hz. As commented in Section 3.5, this is about 10 times faster than the recommended sampling frequency for conventional digital control of temperature [Åström and Wittenmark, 1984, Section 8.3].

Decimating filter

A log of the thermocouple output at constant temperature, sampled at 0.5 Hz, is depicted in Figure 5.9(a). Not only has the signal been aliased (anti-aliasing filter cuts off at 0.48 Hz), but it has also been found that the measurement noise occupies 3 bits (out of a 12-bit ADC) which results in a coarsely discretized response. Since the measurement noise plays a leading role in the local sensor validation scheme, this jagged behaviour due to quantization is unacceptable and degrades the overall performance. One solution is to rescale the thermocouple voltage output (Section 3.6.3) to fit the limited operating range imposed in this experiment. However, many applications require a much wider operat-

ing range and this option is intentionally ruled out. Without committing the validation scheme to restricted operating conditions, a decimating filter is employed to increase the resolution of the digitization process (Section 3.6.3). Subject to the availability of computing power, the thermocouple output is initially sampled at 2 Hz and then downsampled by a factor of 4 with a 14th order FIR decimating filter. This effectively provides an extra bit of resolution (Property 3.1) and the requirement on the anti-aliasing filter is relieved. The decimated thermocouple output, covering the same acquisition period as the raw signal in Figure 5.9(a), is shown in Figure 5.9(b). The reduction in the quantization noise and the smoothing of the digitized signal will enhance the subsequent modelling and validation process.

Decomposition filters and dither injection

The decimated thermocouple output has to be decomposed into the signal-dominant component $\bar{y}(t)$ and the noise-dominant component $\tilde{y}(t)$. Following Guideline 3.4, the pair of decomposition filters are designed as 2nd order Butterworth lowpass and highpass filters respectively[12] with cut-off frequencies at the signal bandwidth of 0.025 Hz. The signal filter $L(q^{-1})$ is given by

$$L(q^{-1}) = \frac{0.020(1+q^{-1})^2}{1-1.56q^{-1}+0.64q^{-2}} \tag{5.3}$$

and the noise filter $H(q^{-1})$ by

$$H(q^{-1}) = \frac{0.80(1-q^{-1})^2}{1-1.56q^{-1}+0.64q^{-2}} \tag{5.4}$$

To cater for the nonstationary setpoint changes, dither is injected to the noise-dominant component. Basing on Guideline 3.6, the dither filter $D(q^{-1})$ is designed to be a 3rd order Chebyshev lowpass filter cutting off at 0.025 Hz

$$D(q^{-1}) = \frac{0.0023+0.0069q^{-1}+0.0069q^{-2}+0.0023q^{-3}}{1-2.54q^{-1}+2.24q^{-2}-0.68q^{-3}} \tag{5.5}$$

and the associated generating white noise $e_d(t)$ is Gaussian with a variance of 3.03×10^{-3} $(= \mathcal{G}_o^2(\Delta v)_m^2)$[13].

The decimation, decomposition and dithering procedures are applied to the thermocouple data with step changes as shown in Figure 5.8(a). The decimated output, the

[12]Note that the thermocouple is in open loop and drift failure is a possibility.

[13]$\mathcal{G}_o$ and $(\Delta v)_m$ for the thermocouple experiment are given in Appendix B.4.

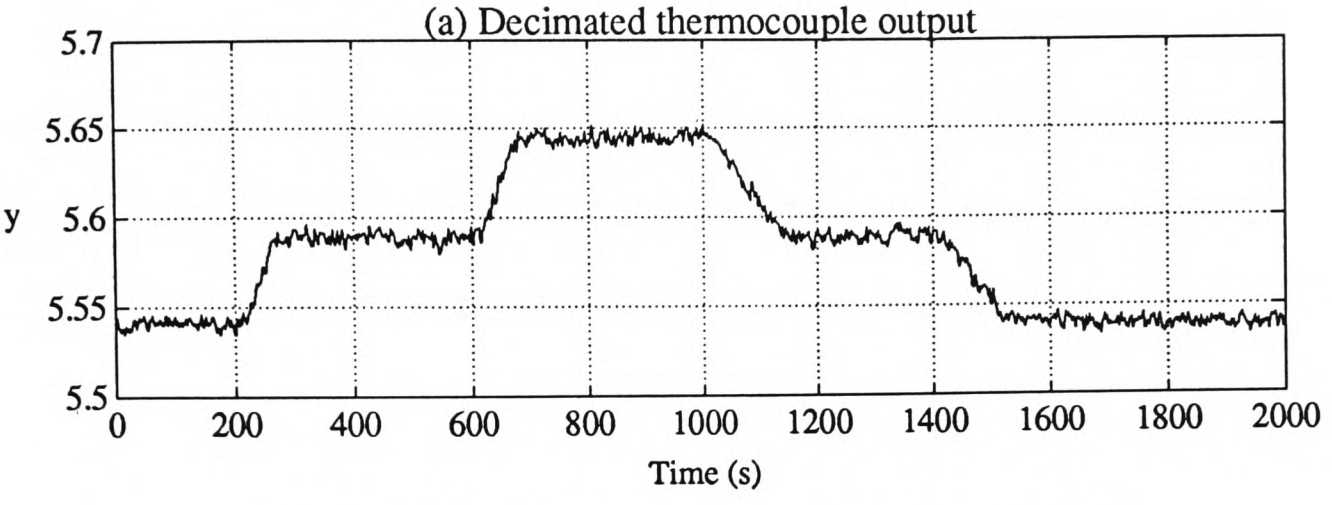

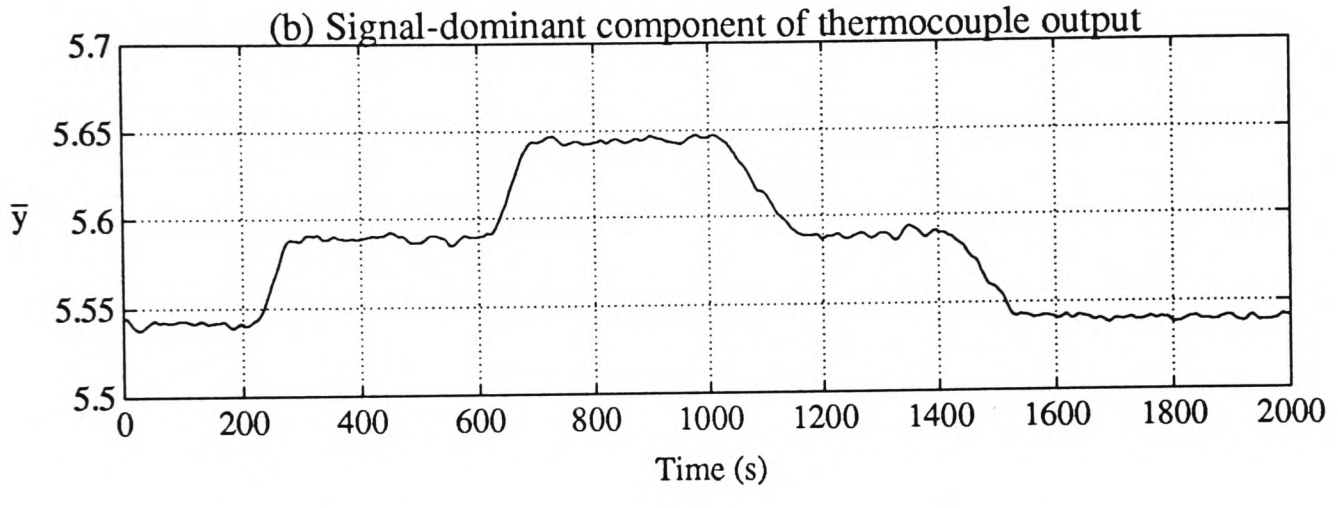

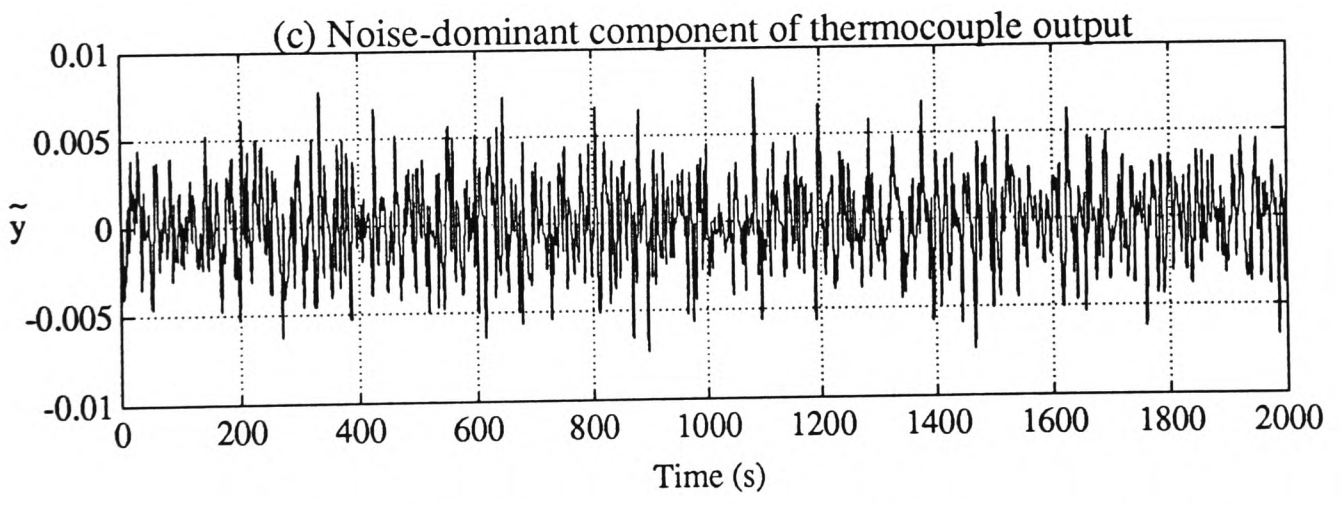

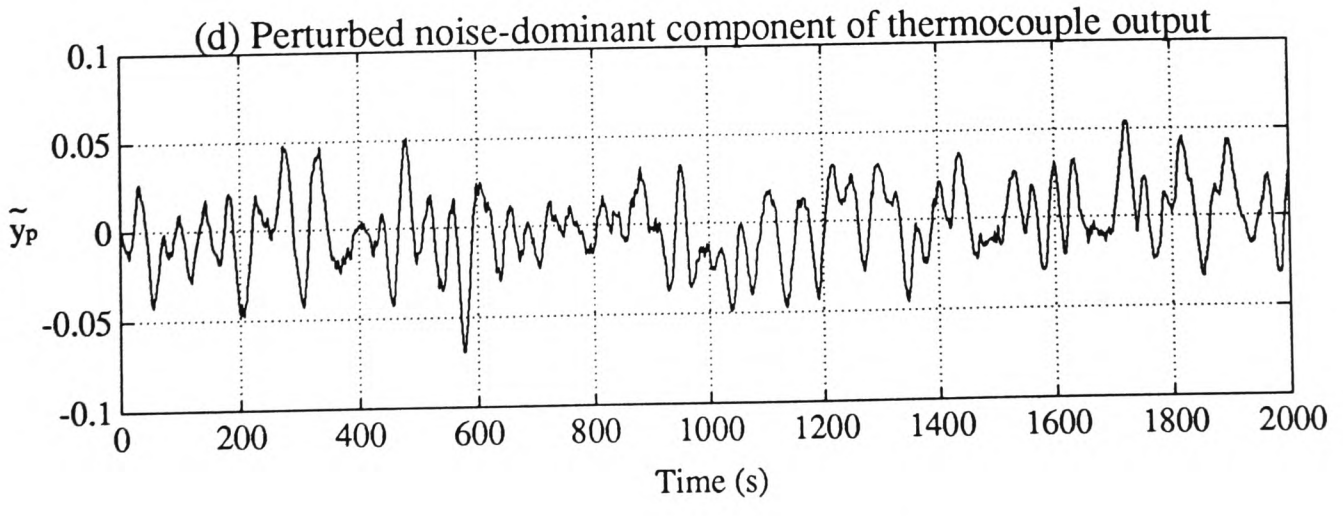

Figure 5.10: Signal decimation, signal decomposition and dither injection in the thermocouple experiment

decomposed signals and the perturbed noise-dominant component are displayed in Figure 5.10. No nonstationary features due to various setpoint changes are observed in either $\tilde{y}(t)$ or $\tilde{y}_p(t)$.

5.3.3 Learning stage

A failure-free record of thermocouple output, as depicted in Figure 5.9(b), is used to construct a baseline model during the learning stage. The data are decimated and decomposed as discussed in Section 5.3.2. A 3rd order ARMA model ($na = nc = 3$) is fitted to the perturbed noise-dominant component $\tilde{y}_p(t)$ and the unknown model parameters are identified by the Recursive Maximum Likelihood method (Section 3.9.2). The parameters $\hat{\theta}(0)$, $\phi(0)$ and $\psi(0)$ are all initialized to zero vectors and the covariance matrix P(0) to $10^5 I$. The online estimates of the autoregressive and the moving-average polynomials are shown in Figures 5.11(a) and (b) respectively. After 1000 samples (i.e. 2000 s), both polynomials converge and the final estimates are given by

$$\hat{A}(q^{-1}) = 1 - 1.10q^{-1} - 0.41q^{-2} + 0.58q^{-3} \tag{5.6}$$

$$\hat{C}(q^{-1}) = 1 + 0.20q^{-1} - 0.25q^{-2} + 0.16q^{-3} \tag{5.7}$$

Innovation sequence is then generated by Equation 3.82 (Figure 5.11(c)) and the validity of the estimated ARMA model is confirmed upon passing both the zero-mean and the whiteness test (Figure 5.11(d)) of the innovation.

These verified estimation results, together with a set of properties of the innovation ($(\bar{\epsilon})_{\text{ref}} = -8.86 \times 10^{-5}$, $(\sigma_\epsilon^2)_{\text{ref}} = 1.41 \times 10^{-5}$ and $(\Phi_\epsilon(\omega))_{\text{ref}}$ as displayed in Figure 5.12), will be employed as reference in the ensuing tracking stage.

5.3.4 Tracking stage

Thermocouple failures

With a single thermocouple available, one practical challenge is to design appropriate failures for the sensor system. Not only must the failures be representative and realistic, but they should also be non-destructive and repeatable. A series of tests have been carried out which involve a variety of failures introduced either at the signal conditioning board or as a consequence of improper installation. The thermocouple outputs are depicted in Figure 5.13 and the tests are described below and are summarized in Table 5.1:

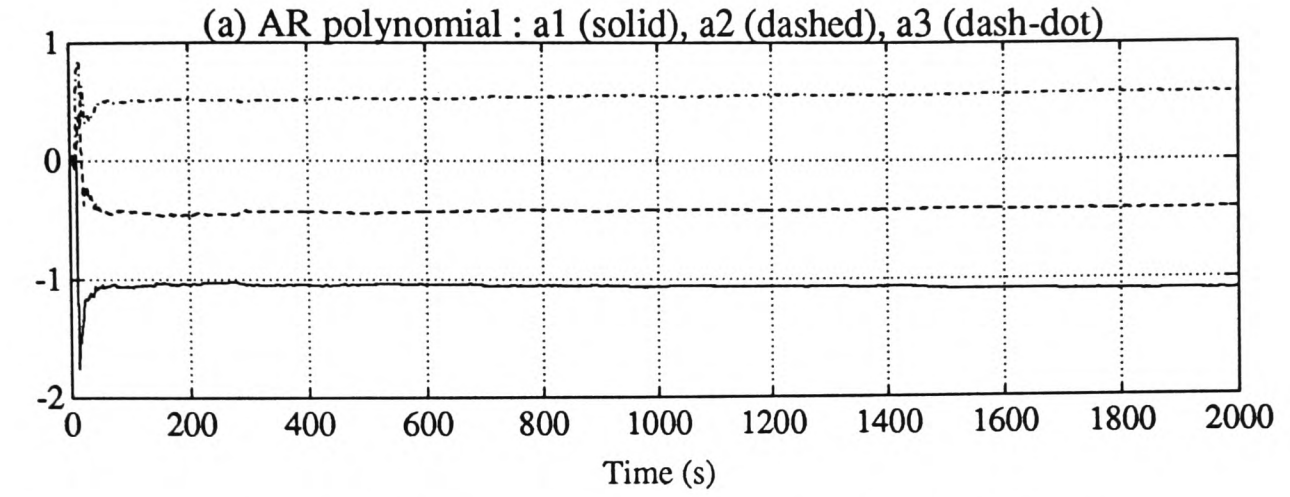

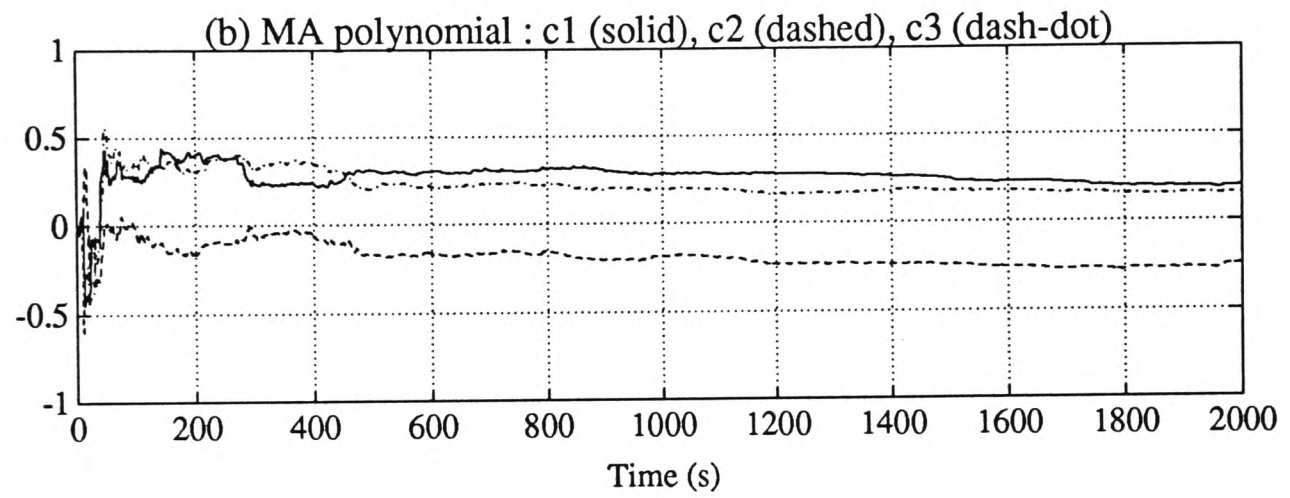

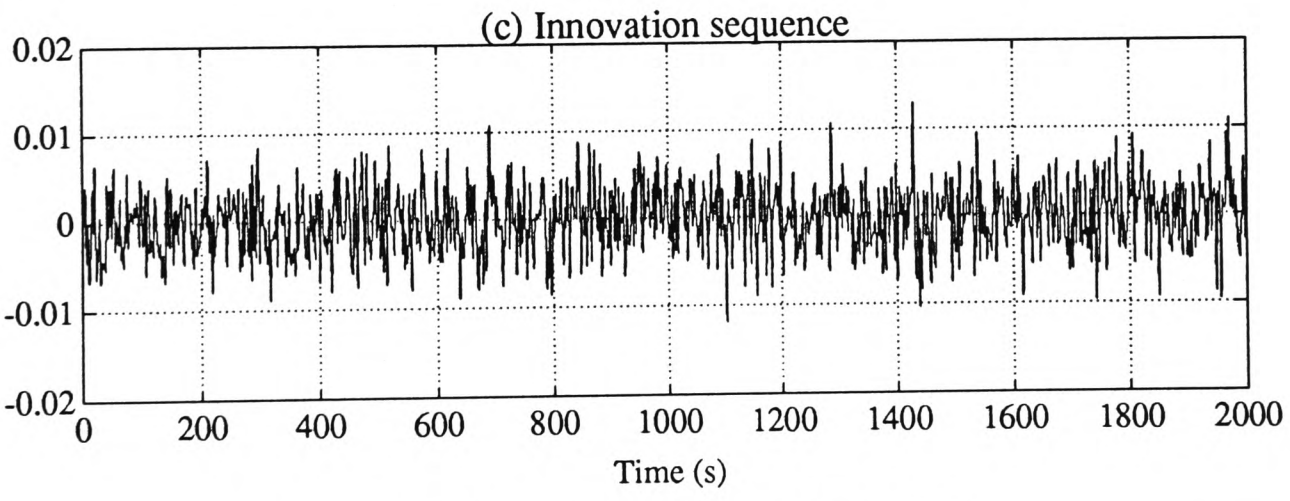

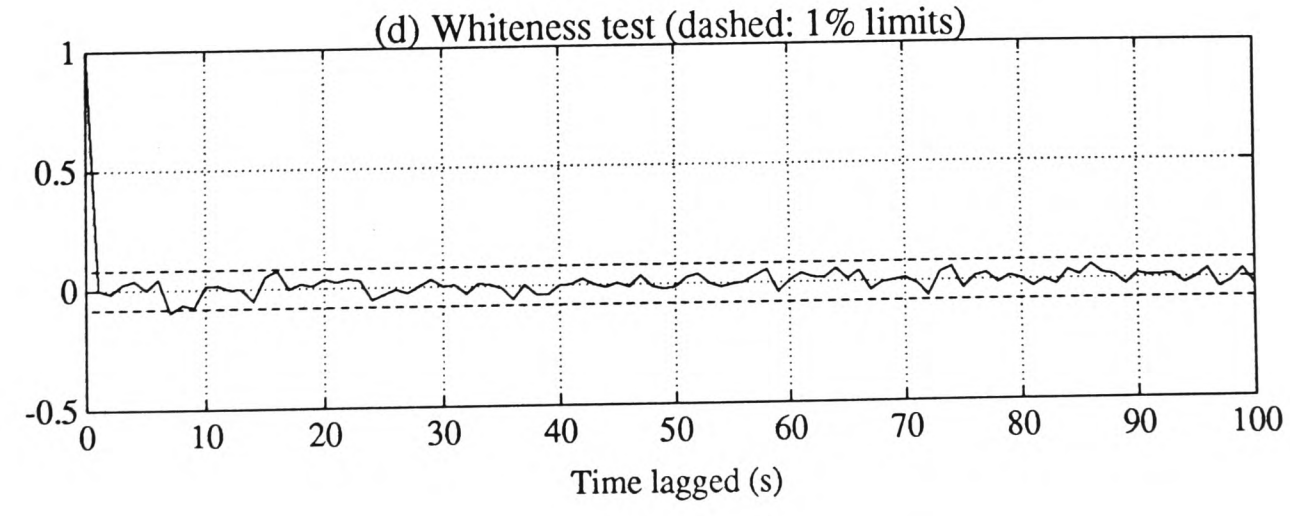

Figure 5.11: Model estimation and validation results for the thermocouple experiment

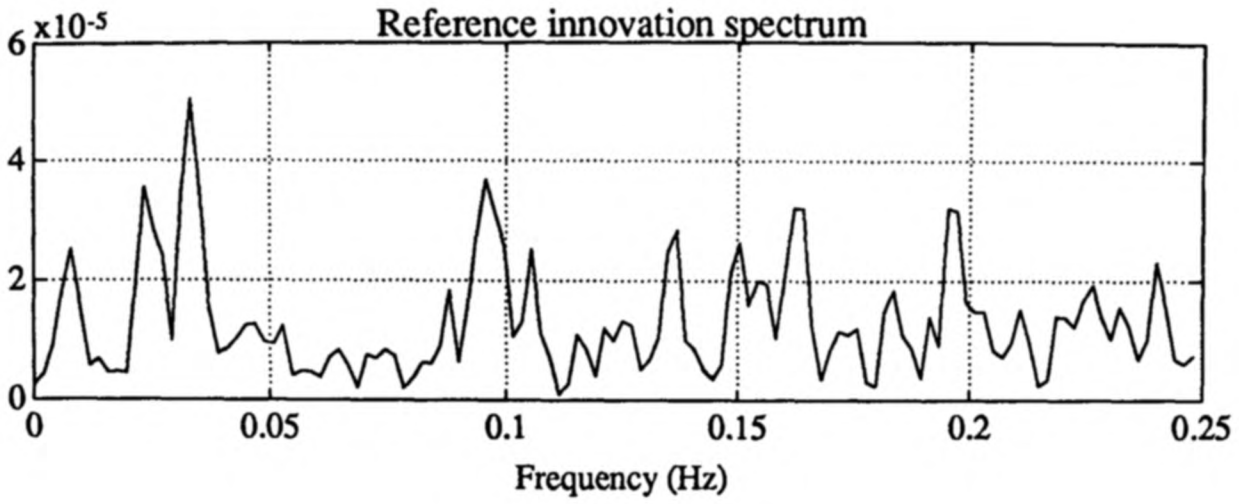

Figure 5.12: Reference innovation spectrum for the thermocouple experiment

- *Normal operation*

  Two failure-free records have been acquired: one being kept at a constant temperature of 60°C (code: `thermo_normal`; Figure 5.13(a)) while the other includes legitimate step changes between 60°C and 61°C (code: `thermo_step`; Figure 5.13(b)).

- *Hardover failure*

  Two types of catastrophic breakdown have been included. A total power failure in the sensor system cuts the output to 0 V (code: `thermo_power`). On the other hand, a blown out operational amplifier in the adder circuit (Figure 5.7) pulls the output to a maximum of 10 V (code: `thermo_opam`; Figure 5.13(c)).

- *Bias failure*

  Abrupt steps have been initiated by altering the shunt resistance network in the signal conditioning board (Figure 5.7): opening switch S1 increases the output by 1.6% (code: `thermo_posjump`; Figure 5.13(d)) whereas closing switch S2 decreases the output by 0.6% (code: `thermo_negjump`; Figure 5.13(e)).

- *Spike failure*

  A negative surge has been introduced by momentarily closing switch S3 in Figure 5.7, imitating a loose connection in the system or a misfire in the data acquisition procedure (code: `thermo_surge`; Figure 5.13(f)).

- *Erratic failure*

  Wide-band interfering signal from an analog noise generator has been injected through the adder circuit in the signal conditioning board to mimic unforeseen external interference or sensor degradation (code: `thermo_noise`; Figure 5.13(g)).

Test code	*Failure mode*	*Summary*
`thermo_normal`	Normal	Failure-free at 60°C
`thermo_step`	Normal	Legitimate setpoint changes between 60°C and 61°C
`thermo_power`	Hardover	Power cut in the sensor — pull-low
`thermo_opam`	Hardover	Defective operational amplifier — pull-high
`thermo_posjump`	Bias	An abrupt increase in the thermocouple output
`thermo_negjump`	Bias	An abrupt decrease in the thermocouple output
`thermo_surge`	Spike	Transient drop in the thermocouple output
`thermo_noise`	Erratic	Additional wide-band measurement noise
`thermo_drift`	Drift	Steady decrease in output due to improper installation

Table 5.1: Summary of various thermocouple tests

- *Drift failure*

  The thermocouple has been intentionally positioned such that only about 3 mm of its protective sheath is immersed in water. As the water slowly evaporates and the surface level lowers, the tip of the thermocouple is brought into the temperature transition zone and the thermocouple output starts to drift downwards (code: `thermo_drift`; Figure 5.13(h)).

All tests cover a duration of 4000 s. Failures are introduced at about 3000 s while the tracking stage is initiated at 2000 s.

Parameter setup

A record of the parameters and the thresholds associated with the tracking stage is listed below:

- *Ordinary phase*

  The design parameters for various signal processing techniques carried out during the ordinary phase are given by

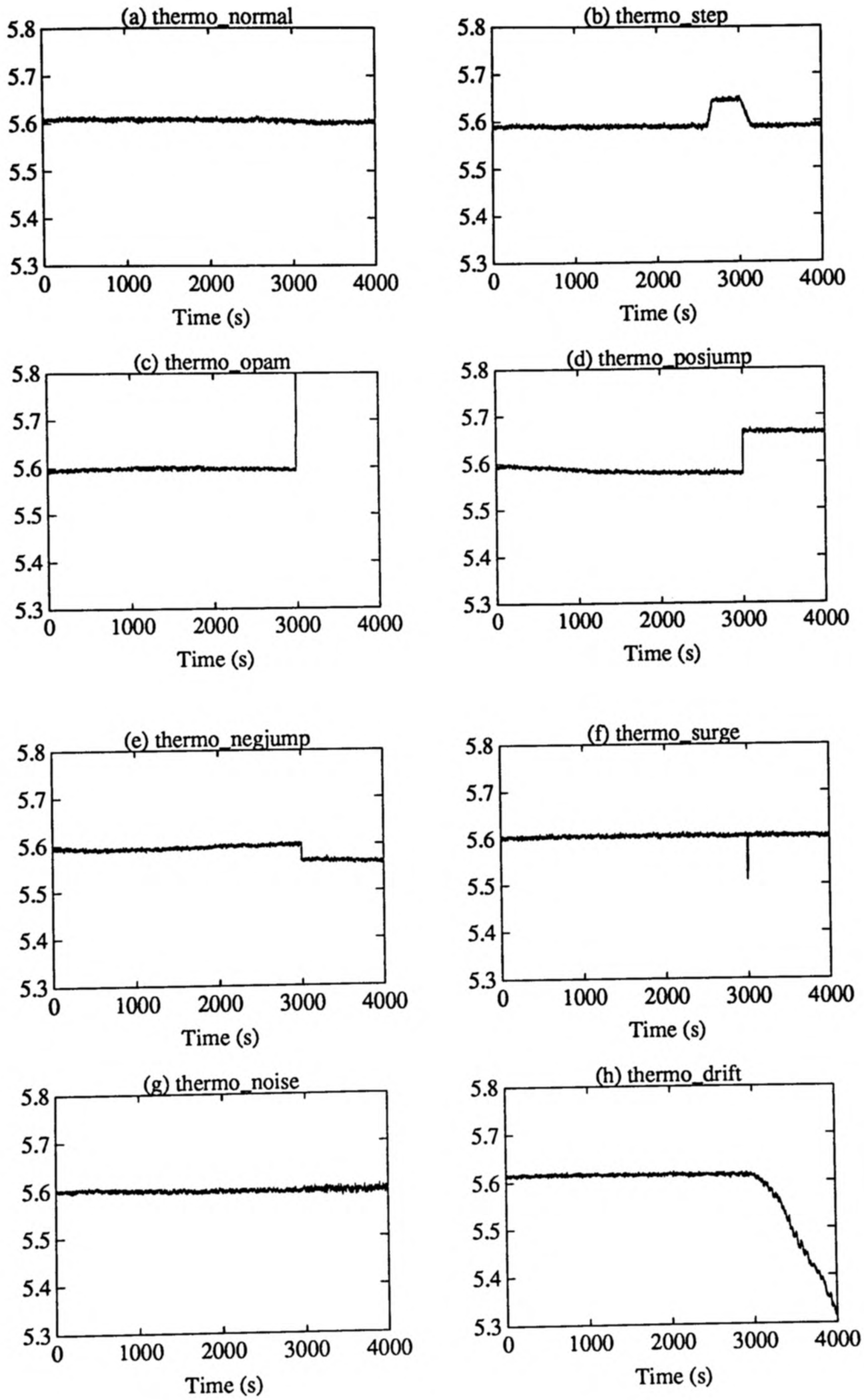

Figure 5.13: A series of thermocouple tests with various failure modes

Variable	*Design parameters*	*Equation*
Mean $\hat{\bar{\epsilon}}(t)$	$\alpha = 0.01$	(4.5)
Variance $\hat{\sigma}_\epsilon^2(t)$	$\alpha = 0.01$, $(W_\ell)_m = 2.58$, $(W_u)_m = 3.89$	(4.28)
Rate of change $\hat{\dot{y}}(t)$	$\alpha_1 = 0.25$, $\alpha_2 = 0.13$	(4.29)
Rate of change $\hat{\bar{\dot{y}}}(t)$	$\alpha_1 = 0.17$, $\alpha_2 = 0.091$, $\Delta_{min} = 0.1\sigma_s$	(4.29)
Measure of bias $b_{\hat{\bar{\dot{y}}}}(t)$	$\gamma = 0.05$, $\delta_o = 8 \times 10^{-5}$	(4.37)

The mean and the variance parameter α correspond to a window of 99.5 s (199 samples) and the measure of bias spans a window of 19.5 s (39 samples). The cut-off frequencies of the $\hat{\dot{y}}(t)$ estimator are selected to be $\omega_{c_2} = \omega_s/2 = 0.078\,\text{rad}\,\text{s}^{-1}$ (0.0125 Hz) and $\omega_{c_1} = \omega_s = 0.16\,\text{rad}\,\text{s}^{-1}$ (0.025 Hz) and those of the $\hat{\bar{\dot{y}}}(t)$ estimator are given by Equations 4.55 to 4.57, i.e. $\omega_{c_2} = \omega_o = 0.05\,\text{rad}\,\text{s}^{-1}$ and $\omega_{c_1} = 2\omega_{c_2} = 0.1\,\text{rad}\,\text{s}^{-1}$.

The prescribed thresholds for the failure alarm indicators are summarized as follows:

Alarm	*Thresholds*	*Equation*
Limit indicator $I_l(t)$	$y_{min} = 5\,\text{V}$, $y_{max} = 6\,\text{V}$, $\dot{y}_{max} = 0.5\,\text{Vs}^{-1}$	(4.40)
Jump indicator $I_j(t)$	$\xi_o = 3.89$	(4.42)
Noise indicator $I_n(t)$	$\underline{F}_o = 0.69$, $\overline{F}_o = 1.39$	(4.47)
Drift indicator $I_d(t)$	$b_o = 3.29$, $\tau_d = 440\,\text{s}$	(4.54)

y_{min} and y_{max} represent temperatures at around 49°C and 67°C respectively and τ_d has been evaluated based on Equation 4.58, in which the rise time T_r is estimated to be 100 s (Figure 5.8(a)), $m_\rho/f_m = 78\,\text{s}$ and $m_{\hat{\bar{\dot{y}}}}/f_m = 42\,\text{s}$.

- *Alert phase*

  During the alert phase, failure diagnosis is carried out with reference to the following settings:

Failure modes	*Parameters or thresholds*
General	$N_{y_f} = 200$, $N_{\epsilon_f} = 256$
BIAS/SPIKE	$\Lambda_o = 2.33$
STUCK/ERRATIC_LOW	$\delta_f = 10^{-15}$
ERRATIC_HIGH/CYCLIC	$\varphi_o = 0.53$ ($n_\epsilon = 128$, $\delta k = 2$, $k_\varphi = 20$)

Fault detection and diagnosis

The data from the nine thermocouple tests are individually monitored and validated by the LOSVAL package. The sensor output $y(t)$, the jump variable $\xi(t)$, the variance-ratio $F(t)$, the drift counter $\eta(t)$, and the four failure alarm indicators during the ordinary phase are displayed in Figures 5.14 to 5.22. In addition, the final diagnostic results are summarized in Table 5.2.

- `thermo_normal` (Figure 5.14)

  No alarm has been triggered throughout this test and the failure mode indicator remains at the default value of 'NORMAL'.

- `thermo_step` (Figure 5.15)

  Although the legitimate step changes at around 2600 s and 3000 s introduce temporary drifts in the thermocouple output, the effects are not sufficiently persistent to initiate any alarm and the failure mode indicator stays at 'NORMAL'.

- `thermo_power` (Figure 5.16)

  The sudden power failure brings the thermocouple output to 0 V, well below the lower threshold y_{min} at 5 V. The limit indicator I_l, which is set to -1 at 3002 s, takes precedence over all other alarms and the thermocouple is immediately identified as 'HARDOVER_LOW'.

- `thermo_opam` (Figure 5.17)

  The malfunction of the operational amplifier results in a pull-high output and the limit indicator I_l is set to 1 at 3002 s. Without further processing, the failure mode indicator is declared as 'HARDOVER_HIGH'.

- `thermo_posjump` (Figure 5.18)

  The jump indicator is triggered ($I_j = 1$) at 3002 s due to an abrupt increase in

the shunt resistance. The sample mean and the sample variance of the 'failed' thermocouple output are estimated to be 5.67 V and 6.72×10^{-6} V^2 while the output sample mean prior to failure is 5.58 V ($m_2 = 14$). Based on Equation 4.65, the test statistics $\Lambda = 124.18 > \Lambda_o (= 2.33)$. The failure mode indicator is flagged as 'BIAS_POS' and the size of the jump is estimated (Equation 4.68) to be 0.089 V.

- `thermo_negjump` (Figure 5.19)
  Following on the activation of the jump indicator ($I_j = -1$) at 3002 s, the test statistics Λ is evaluated by Equation 4.65 to be -49.60 ($\hat{\bar{y}}_f = 5.57$ V, $\hat{\sigma}^2_{y_f} = 6.12 \times 10^{-6}$ V^2, $\hat{\bar{y}}_2(t_f - 1) = 5.60$ V and $m_2 = 14$). Since $|\Lambda| > \Lambda_o$, the failure mode indicator is set to 'BIAS_NEG' and the bias is found (Equation 4.68) to be -0.034 V.

- `thermo_surge` (Figure 5.20)
  Similar to the negative bias, $I_j = -1$ at 3004 s. However, Λ from Equation 4.65 is -0.41 ($\hat{\bar{y}}_f = 5.60$ V, $\hat{\sigma}^2_{y_f} = 6.80 \times 10^{-6}$ V^2, $\hat{\bar{y}}_2(t_f - 1) = 5.60$ V and $m_2 = 14$) and $|\Lambda| < \Lambda_o = 2.33$. The failure is therefore classified as 'SPIKE_NEG' and the estimate of the size of the spike is -0.091 V.

- `thermo_noise` (Figure 5.21)
  The unanticipated increase in signal variance is detected at 3046 s when the noise indicator I_n is set to 1. To discriminate between an erratic and a cyclic failure, the spectral difference $\Delta\Phi_\epsilon(\omega)$ with respect to the reference innovation spectrum is computed at 128 frequency points and is displayed in Figure 5.23. The suspected cycling frequency $\omega_{k_{max}}$ is found to be 0.24 Hz and, from Equation 4.73, the test statistics $\varphi = 0.84$ which is larger than the prescribed threshold of φ_o ($= 0.53$). The failure mode indicator is hence identified as 'ERRATIC_HIGH' and the variance expansion factor is determined (Equation 4.76) to be 2.97.

- `thermo_drift` (Figure 5.22)
  Since the drift indicator I_d is turned on to -1 at 3476 s, the failure mode indicator is labelled as 'DRIFT_NEG'. The predicted failure time is corrected to 3036 s ($\tau_d = 440$ s) and by linear regression (Equation 4.77), the slope of the drift is estimated to be -0.00029 Vs^{-1}.

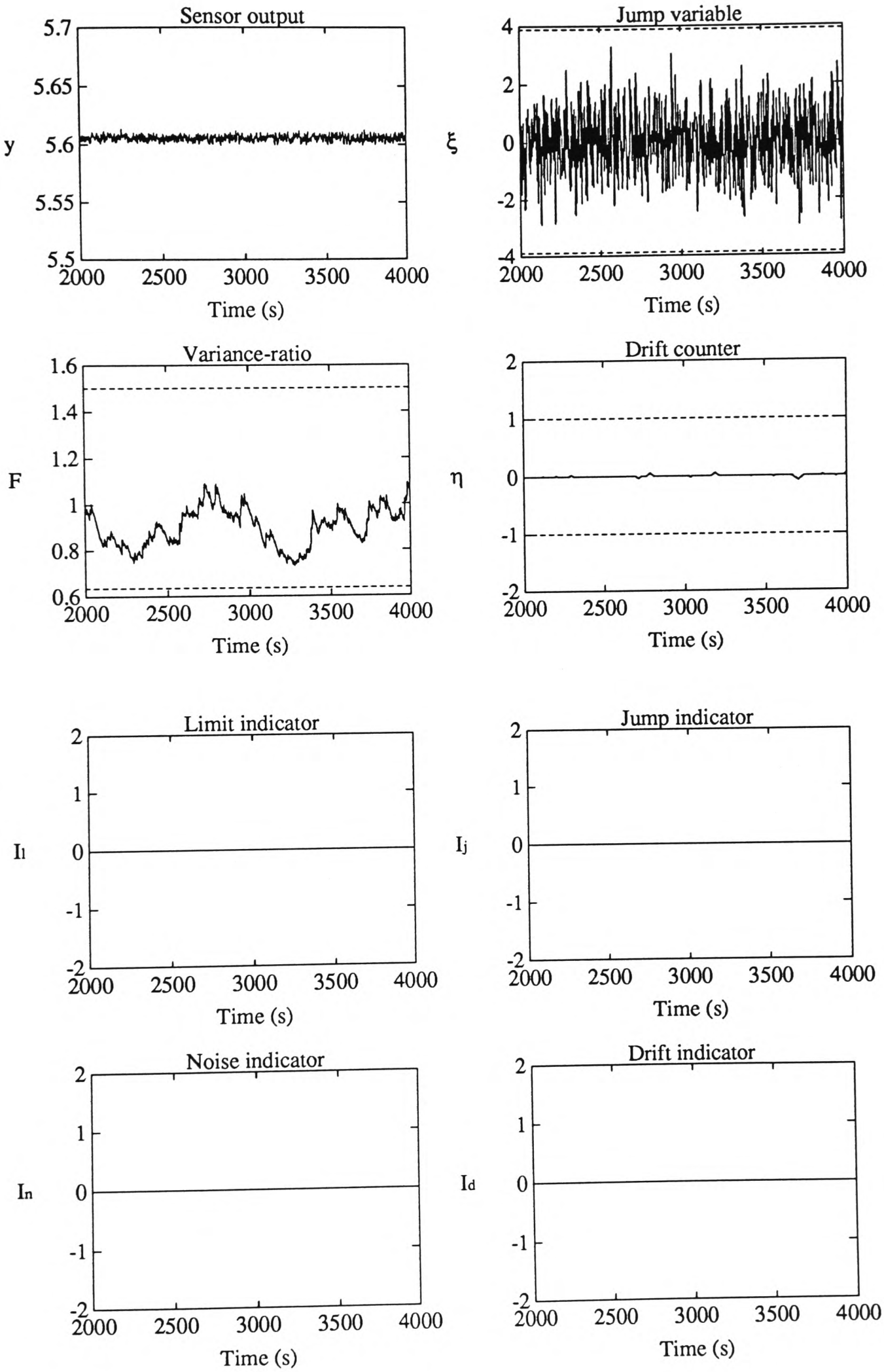

Figure 5.14: Alarm indicators in `thermo_normal`

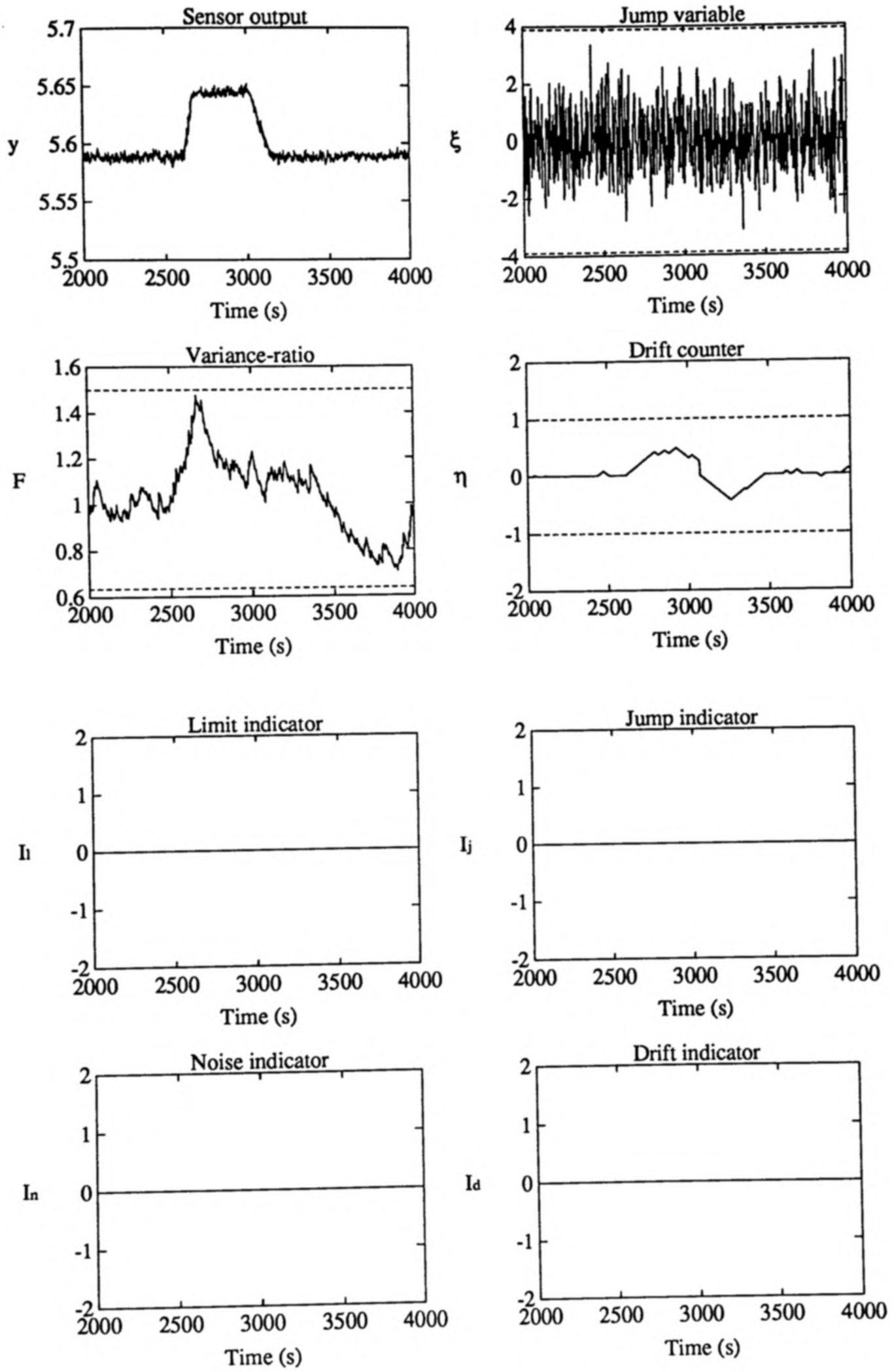

Figure 5.15: Alarm indicators in `thermo_step`

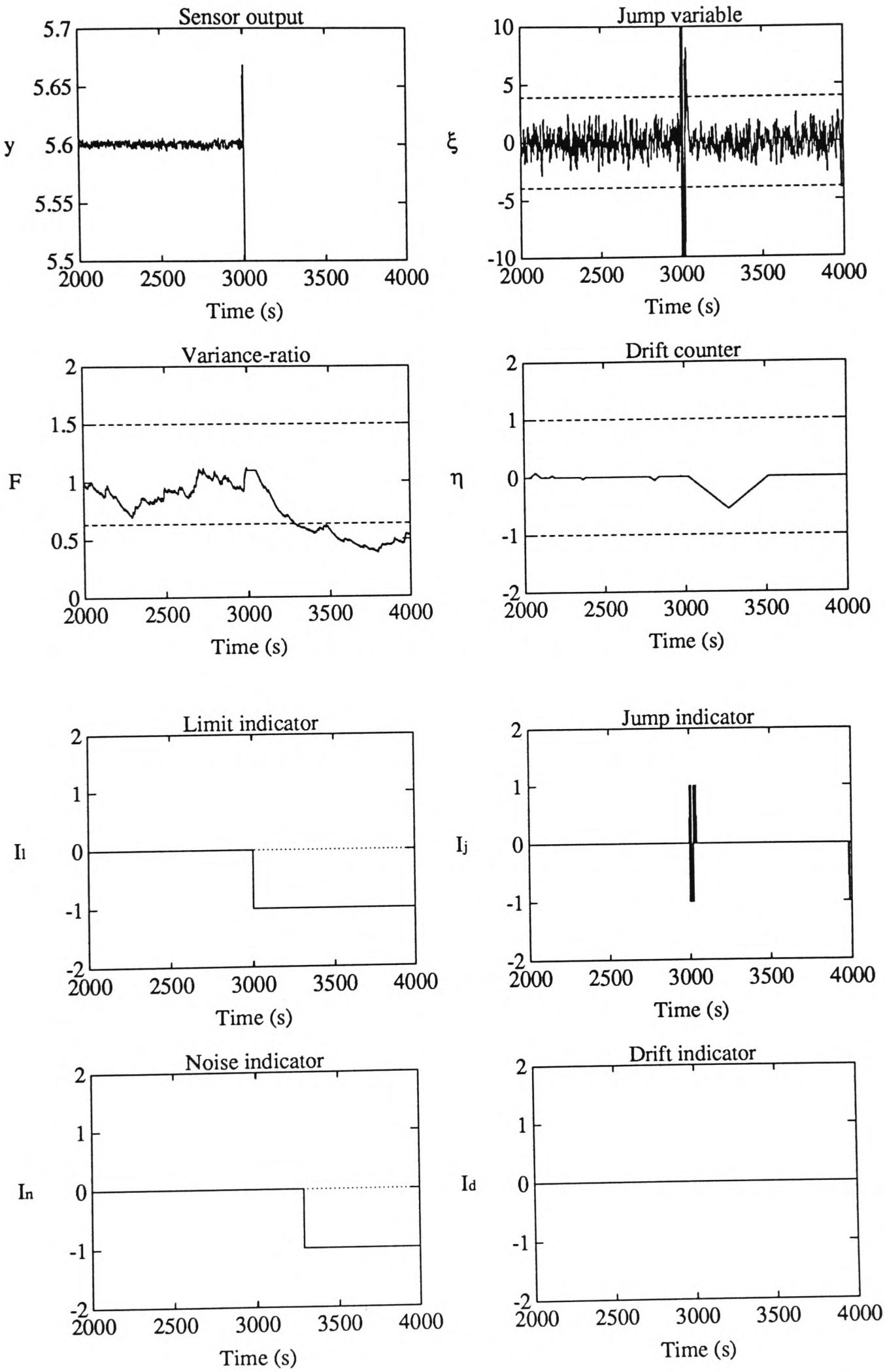

Figure 5.16: Alarm indicators in `thermo_power`

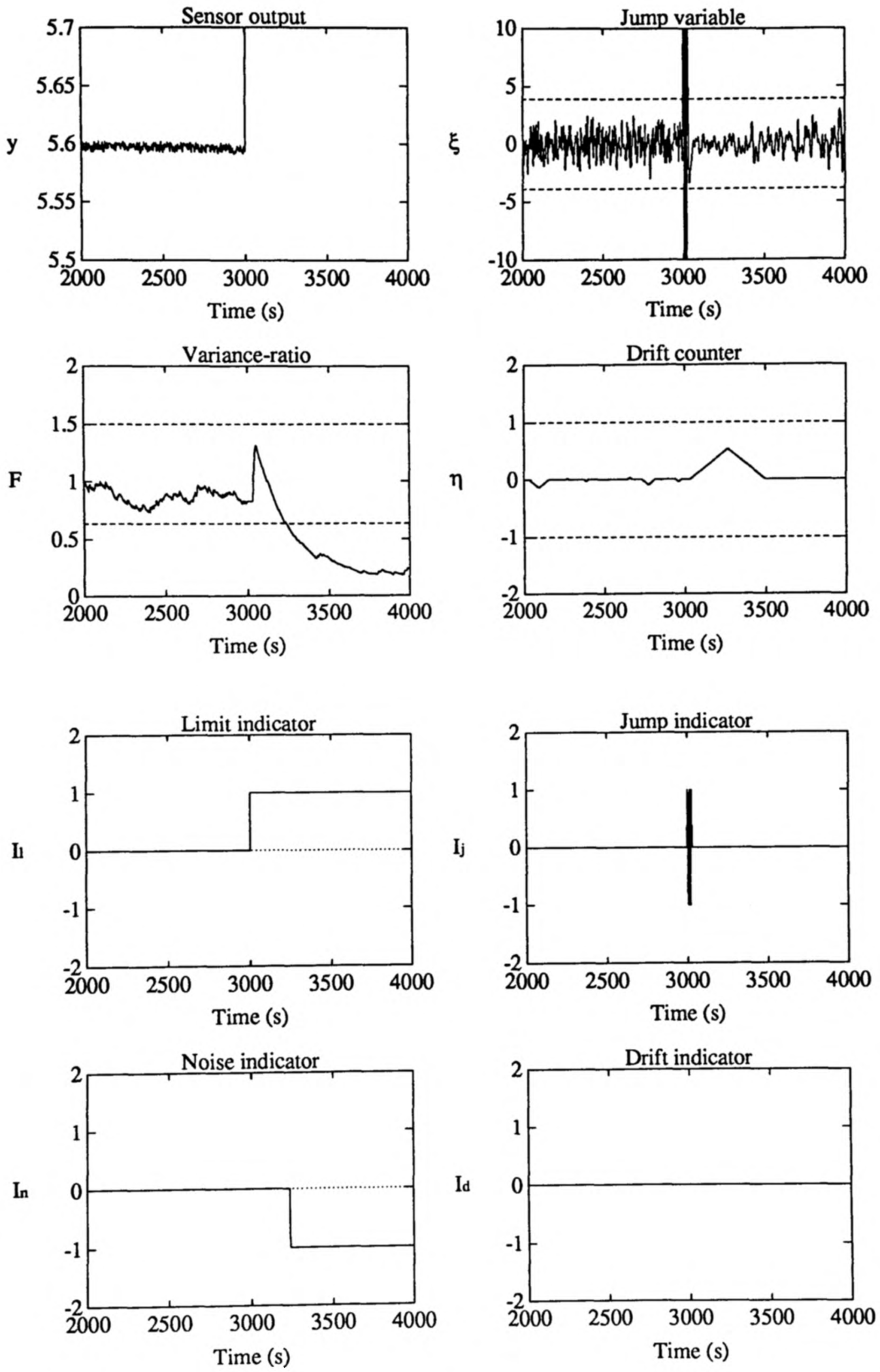

Figure 5.17: Alarm indicators in `thermo_opam`

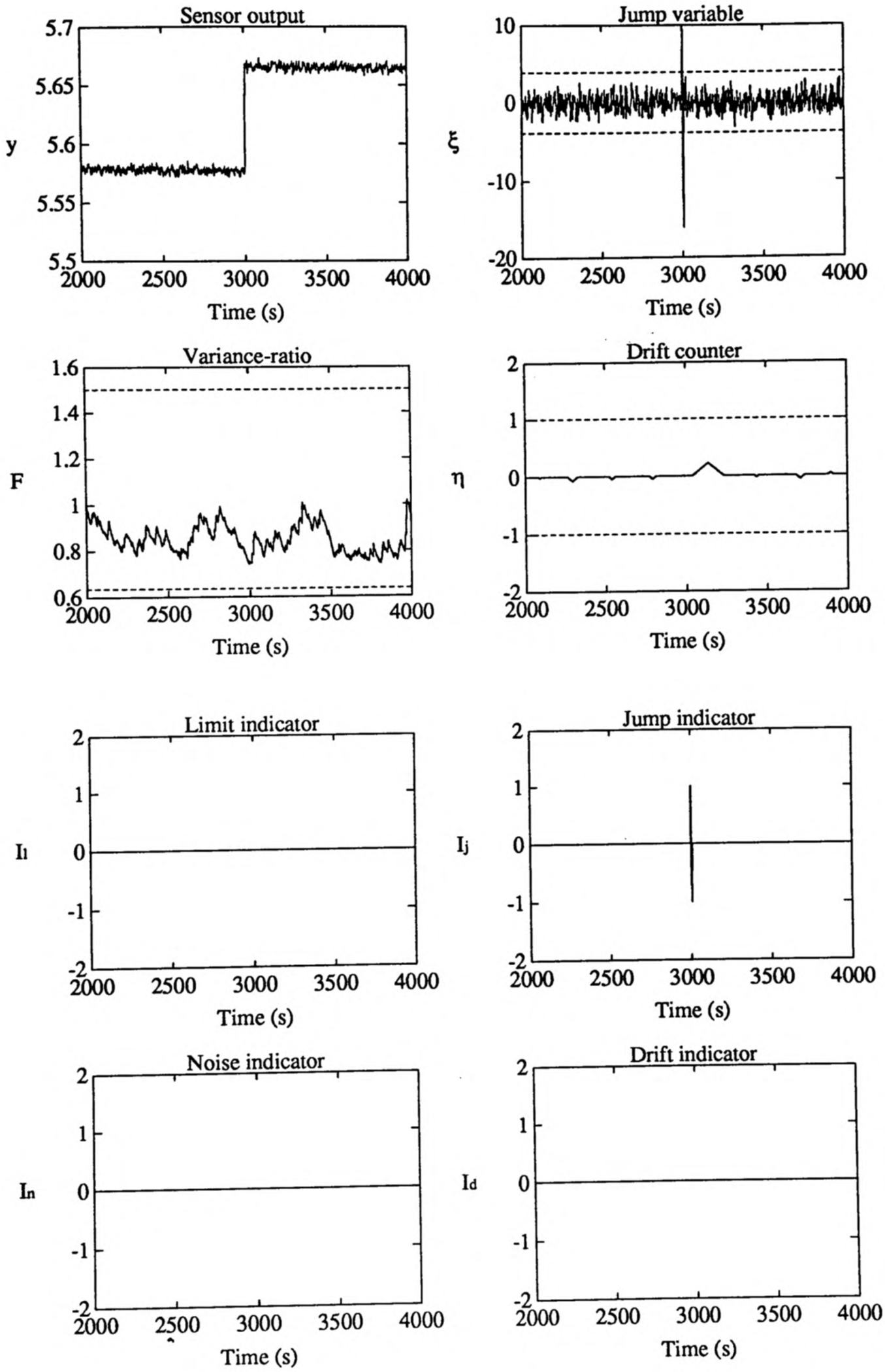

Figure 5.18: Alarm indicators in `thermo_posjump`

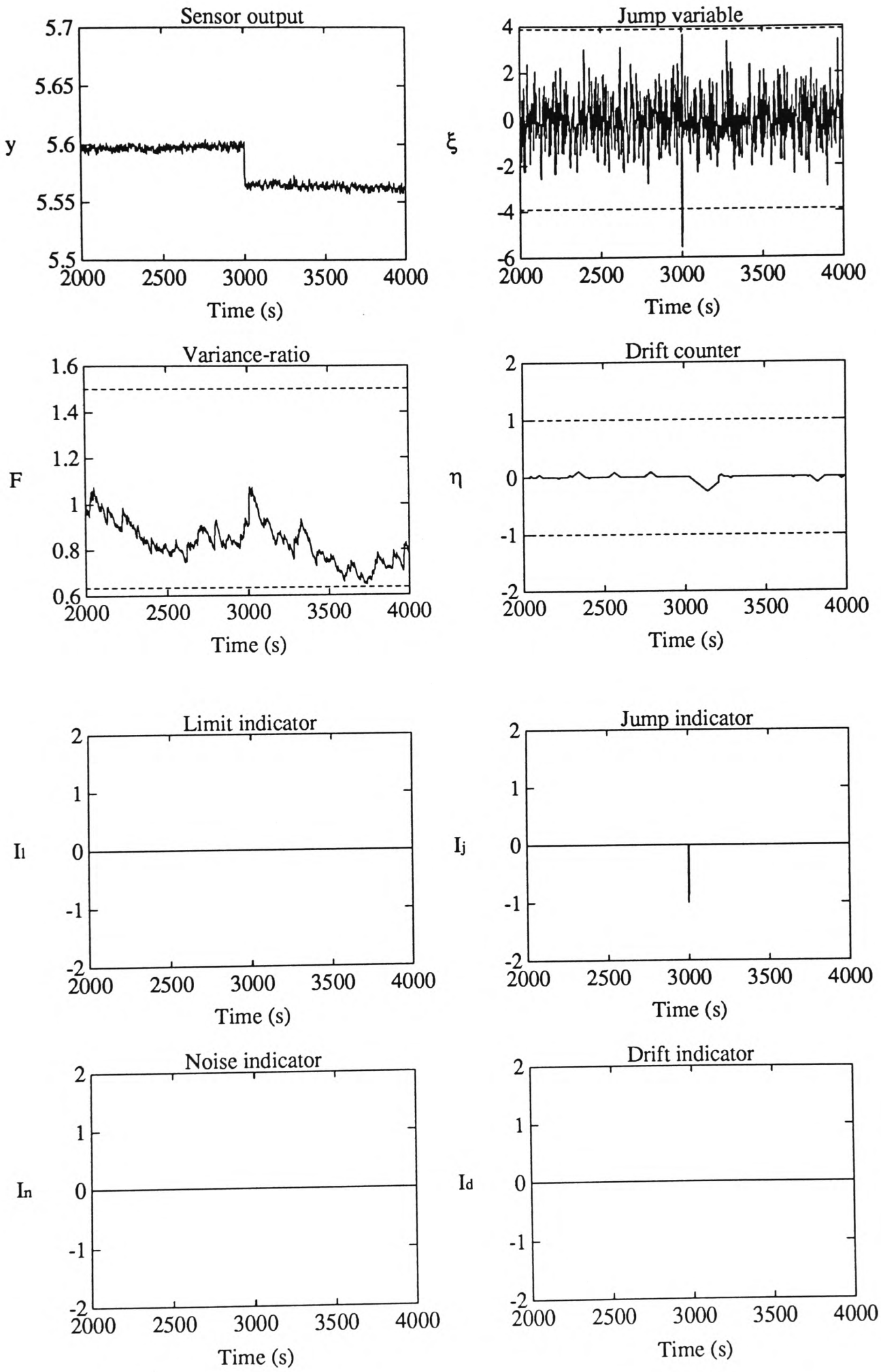

Figure 5.19: Alarm indicators in `thermo_negjump`

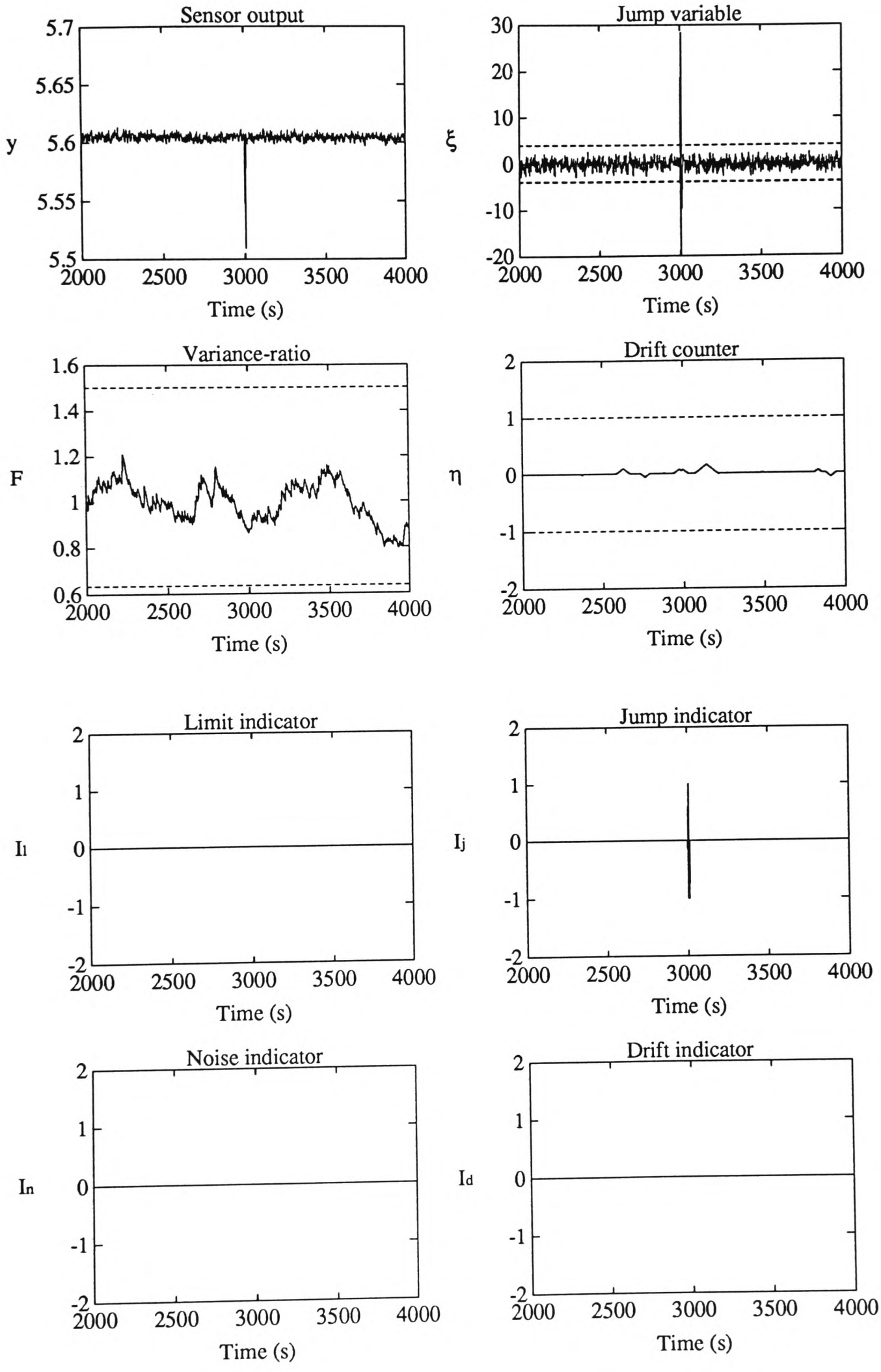

Figure 5.20: Alarm indicators in `thermo_surge`

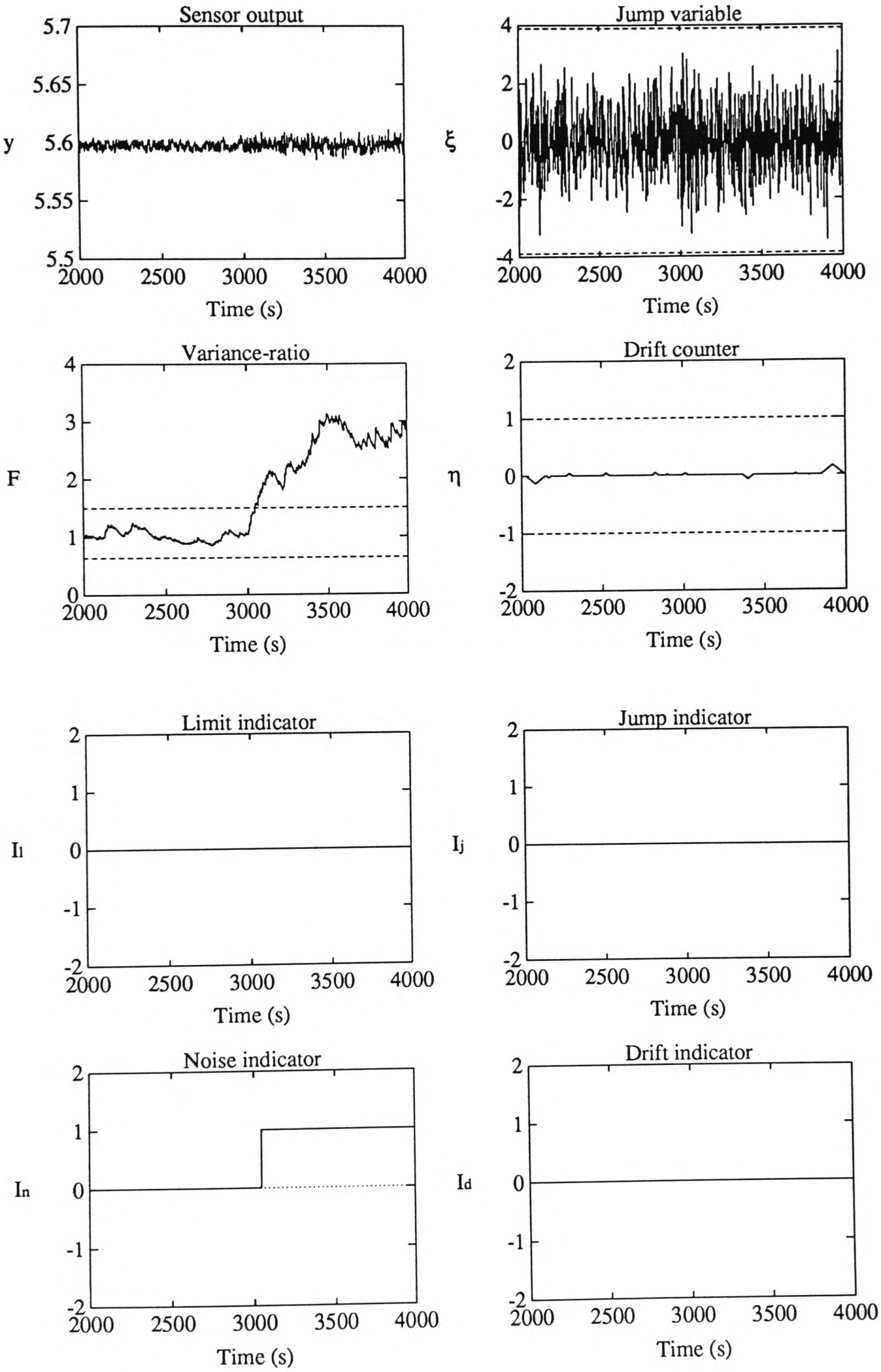

Figure 5.21: Alarm indicators in `thermo_noise`

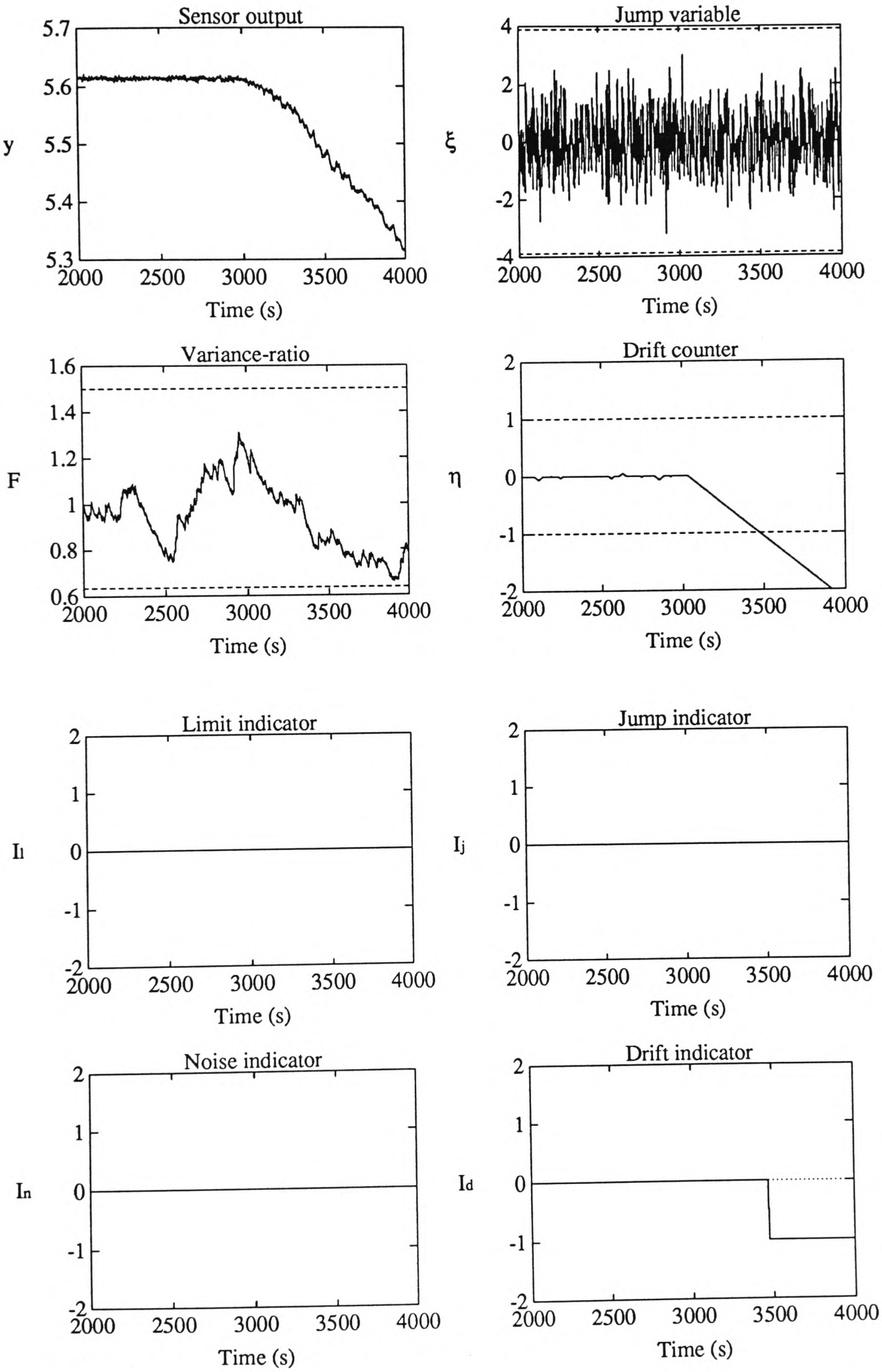

Figure 5.22: Alarm indicators in `thermo_drift`

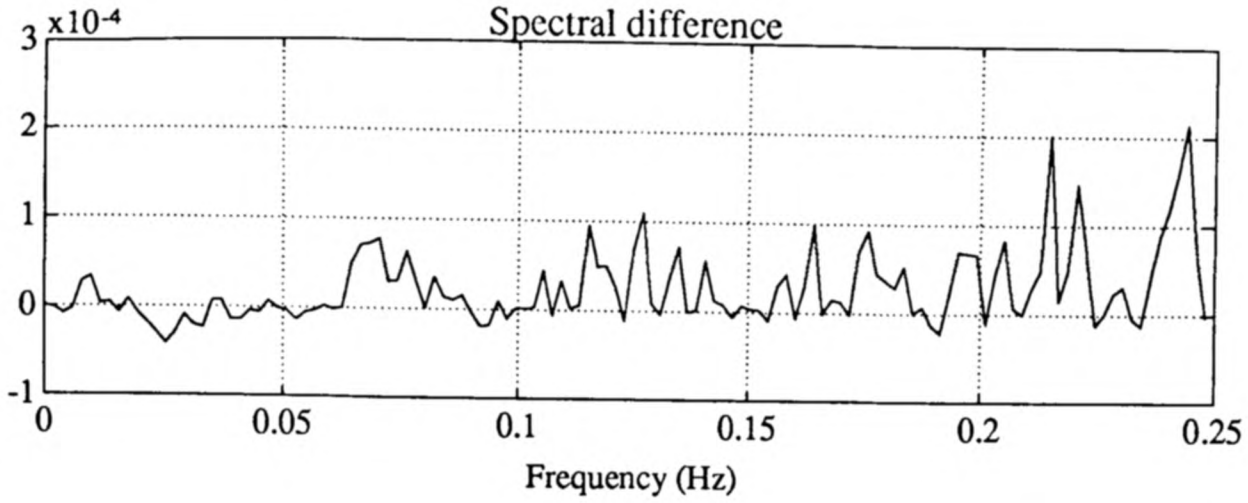

Figure 5.23: Spectral difference $\Delta\Phi_\epsilon(\omega)$ in `thermo_noise`

Code	*Failure mode indicator*	*Time of failure*	*Size of failure*
`thermo_normal`	NORMAL	N/A	N/A
`thermo_step`	NORMAL	N/A	N/A
`thermo_power`	HARDOVER_LOW	3002 s	N/A
`thermo_opam`	HARDOVER_HIGH	3002 s	N/A
`thermo_posjump`	BIAS_POS	3002 s	0.089 V
`thermo_negjump`	BIAS_NEG	3002 s	−0.034 V
`thermo_surge`	SPIKE_NEG	3004 s	−0.091 V
`thermo_noise`	ERRATIC_HIGH	3046 s	2.97
`thermo_drift`	DRIFT_NEG	3036 s	$-0.00029\ \mathrm{Vs}^{-1}$

Table 5.2: Local sensor validation results of the thermocouple tests

5.3.5 Summary

This section details a step-by-step procedure on the application of the local sensor validation scheme to a popular industrial sensor — the thermocouple. Although the failure signal patterns are by no means exhaustive due to practical constraints, the validation scheme has successfully diagnosed the nine experimental conditions and all sensor failures have been detected expeditiously. With portability and process independence as two of the prime design criteria, the validation scheme is capable of handling a wide variety of sensors and process environments by following a similar approach.

5.4 Extensions to the local sensor validation scheme

The proposed local sensor validation scheme is highly versatile and flexible, subject only to a minimal set of assumptions laid down in Sections 3.2, 3.3.1, 3.3.7, 3.8 and 3.8.1. Under circumstances when some assumptions have to be relaxed, the validation scheme can easily be adapted to accommodate a broader spectrum of operating environments. The modification required is often nominal as illustrated in the following two studies, in which:

- the variance of the measurement noise is nonstationary (violation of Assumption 3.2),
- the measurement signal is bandpass rather than lowpass (violation of Assumption 3.6).

5.4.1 Sensors subject to nonstationary measurement noise

Assumption 3.2 demands the measurement noise to be stationary and any significant change in the noise level is considered to be a sensor failure. In some situations, the excitation of the measurement noise may depend on the operating levels or may be a function of the ambient conditions and hence is time-varying. If the variation of the noise power is short term and is about a mean level, the sensitivity of the noise indicator can simply be reduced by altering the threshold levels $\underline{F}_o$ and $\overline{F}_o$ (Equation 4.46). On the other hand, if the noise variance is gradually drifting, the reference innovation variance $(\sigma_\epsilon^2)_{\mathbf{ref}}$ acquired in the learning stage will eventually be unrepresentative and outdated. The variance-ratio in the noise indicator (Equation 4.45) can be reformulated as

$$F(t) = \frac{\hat{\sigma}_\epsilon^2(t)}{\hat{\sigma'}_\epsilon^2(t)} \tag{5.8}$$

Similar to $\hat{\sigma}_\epsilon^2(t)$, the reference innovation variance in the denominator, $\hat{\sigma'}_\epsilon^2(t)$, is estimated recursively by the spike-insensitive filter (Algorithm 4.28) but with a longer effective window length. $\hat{\sigma'}_\epsilon^2(t)$ is able to track the gradual drift in the noise variance and can provide an up-to-date reference on the innovation excitation. A similar framework was adopted in the adaptive filtering scheme presented in Halme and Selkäinaho [1984].

Example 5.1

A sensor output in an open loop environment is simulated as in Example 4.1 except that the variance of the measurement noise increases linearly from 2.5×10^{-5} to 5×10^{-5} during the tracking stage between 2000 s and 4000 s (Figure 5.24(a)). No failure is introduced. Signal decomposition, dither injection and sensor modelling are identical to those in Example 4.1 and the innovation generated in the tracking stage is depicted in Figure 5.24(b). Based on the setups[14] laid down in Example 4.7, the on-line estimate $\hat{\sigma}_\epsilon^2(t)$ and the reference innovation variance $(\sigma_\epsilon^2)_{\text{ref}}$ are computed and shown in Figure 5.24(c). As expected, their ratio (Figure 5.24(d)) progressively creeps from 1 to 2. A false alarm is initiated and the sensor is diagnosed as 'ERRATIC_HIGH' at 2899 s. By simply substituting Equation 5.8 for Equation 4.45 while $\hat{\sigma'}_\epsilon^2(t)$ (Figure 5.24(e)) is estimated with an effective window length five times that of $\hat{\sigma}_\epsilon^2(t)$, the variance-ratio stays well within the threshold limits[15] (Figure 5.24(f)) and no alarm is flagged.

5.4.2 Sensor validation in bandpass processes

The basic structure of the local sensor validation scheme is built upon the assumption that the measurement noise covers a much wider bandwidth than the measurement signal (Assumption 3.3) and that the underlying process is confined to a low frequency band (Assumption 3.6). Most measurements encountered in industrial processes do fall into these categories. In a few cases such as vibration measurements, the measurand may be better described as bandpass and spans a frequency range between $(\omega_s)_l$ and $(\omega_s)_u$. A straightforward approach is to neglect the bandpass nature of the process and to consider it as lowpass with the measurement signal bandwidth ω_s set to the upper cut-off $(\omega_s)_u$. Nonetheless, any genuine sensor failure below the lower cut-off $(\omega_s)_l$ will be blindly ignored. In particular, if the measurement signal bandwidth is bandlimited at relatively high frequencies, a significant failure detection bandwidth will be wasted. An alternative strategy can be adopted to enhance the validation scheme:

- *Signal decomposition (Guidelines 3.3 and 3.4)*

  Instead of being a lowpass and a highpass filter, the decomposition filters $L(q^{-1})$

---

[14] $\alpha = 0.01$, $(W_\ell)_m = 2.58$, $(W_u)_m = 3.89$, $\underline{F}_o = 0.69$, $\overline{F}_o = 1.39$.

[15] The thresholds are: $\underline{F}_o = \dfrac{1}{F_{0.05\%}(498, 198)} = 0.67$ and $\underline{F}_o = F_{0.05\%}(198, 498) = 1.46$.

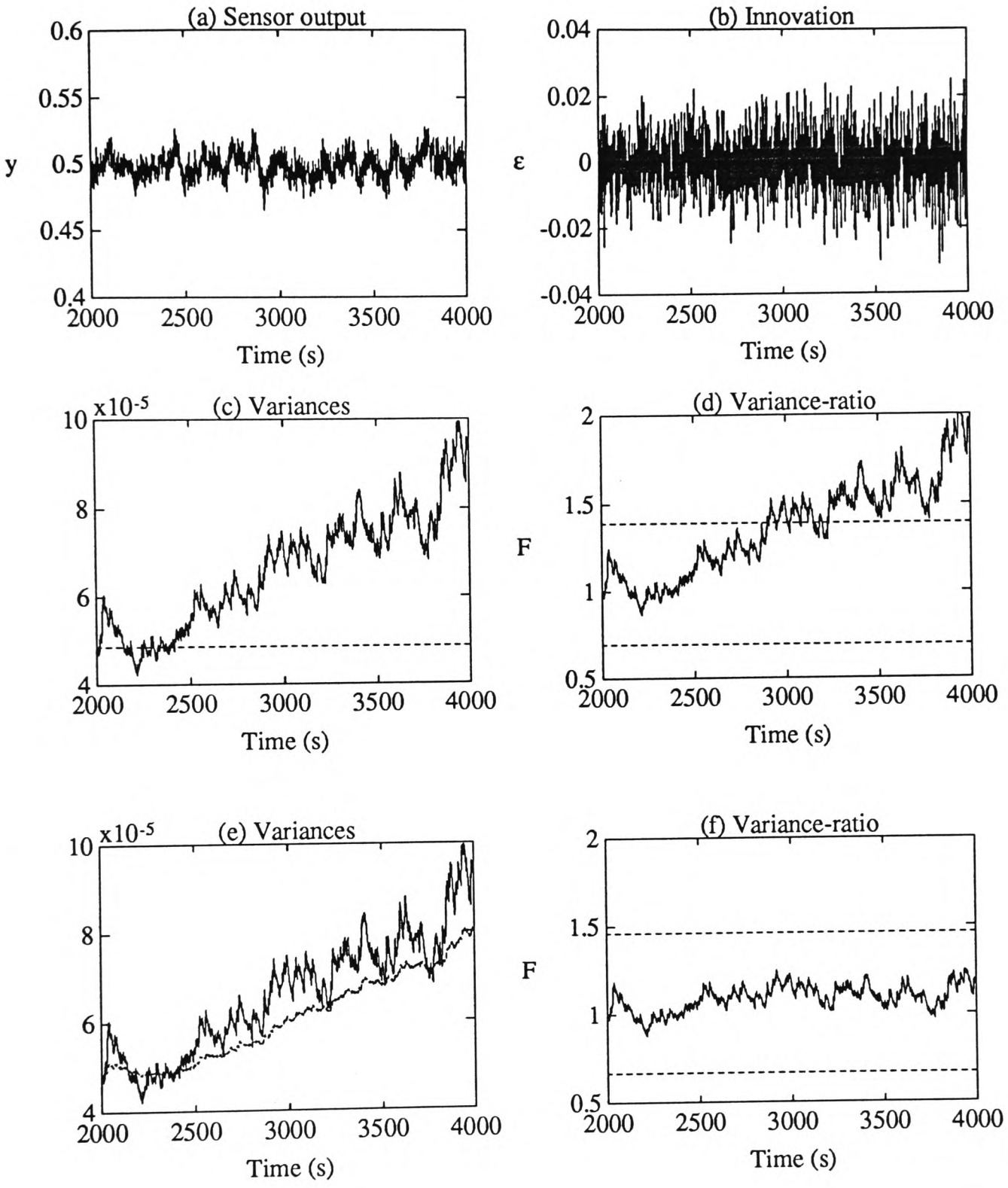

Figure 5.24: Sensor validation with nonstationary measurement noise: (a) Sensor output, (b) Innovation sequence, (c) Innovation variances — $\hat{\sigma}_\epsilon^2(t)$ (solid) and $(\sigma_\epsilon^2)_{\text{ref}}$ (dashed), (d) Variance-ratio (Equation 4.45), (e) Innovation variances — $\hat{\sigma}_\epsilon^2(t)$ (solid) and $\hat{\sigma'}_\epsilon^2(t)$ (dashed), (f) Variance-ratio (Equation 5.8)

and $H(q^{-1})$ should be designed as bandpass and bandstop filters respectively with cut-off frequencies at $(\omega_s)_l$ and $(\omega_s)_u$. Two immediate observations can be made:

- The noise-dominant component $\tilde{y}(t)$ is no longer guaranteed to be zero-mean $(H(1) \neq 0)$,
- Drift failures are not identifiable from the signal-dominant component $\bar{y}(t)$ but from $\tilde{y}(t)$.

For bandpass processes, the noise-dominant component $\tilde{y}(t)$ is further partitioned into two elements

$$\bar{\tilde{y}}(t) = L'(q^{-1})\,\tilde{y}(t) = L'(q^{-1})\,H(q^{-1})\,y(t) \tag{5.9}$$

$$\tilde{\tilde{y}}(t) = H'(q^{-1})\,\tilde{y}(t) = H'(q^{-1})\,H(q^{-1})\,y(t) \tag{5.10}$$

where $L'(q^{-1})$ and $H'(q^{-1})$ are a pair of lowpass and highpass filters with a low corner frequency ω_l $(< (\omega_s)_l)$. The key objective of the additional decomposition is to provide both a zero-mean time-series $\tilde{\tilde{y}}(t)$ for general sensor validation and a "smoothed" signal $\bar{\tilde{y}}(t)$ for the detection of drift failures. The standard validation techniques can then be applied by replacing $\bar{y}(t)$ by $\bar{\tilde{y}}(t)$ and $\tilde{y}(t)$ by $\tilde{\tilde{y}}(t)$.

- *Sensor signal modelling (Equation 3.62)*
  The baseline ARMA model is constructed on the high-frequency noise-dominant component $\tilde{\tilde{y}}(t)$ rather than the raw noise-dominant component $\tilde{y}(t)$

$$A(q^{-1})\,\tilde{\tilde{y}}(t) = C(q^{-1})\,e(t) \tag{5.11}$$

  All model estimation and validation procedures are still applicable.

- *Dither injection (Guidelines 3.5 and 3.6)*
  With reference to Guideline 3.6, the dither filter $D(q^{-1})$ should be designed as a high order bandpass filter with cut-off frequencies at $(\omega_s)_l$ and $(\omega_s)_u$ and dither is utilized to perturb the high-frequency noise-dominant component $\tilde{\tilde{y}}(t)$ (c.f. Equation 3.93)

$$\tilde{y}_p(t) = \tilde{\tilde{y}}(t) + d(t) \tag{5.12}$$

- *Failure alarm indicators (Section 4.4)*
  As discussed above, the drift indicator $I_d(t)$ is updated based on the derivative of the low-frequency noise-dominant component $\dot{\bar{\tilde{y}}}(t)$ and the innovation sequence, on

which the jump indicator $I_j(t)$ and the noise indicator $I_n(t)$ are based, is generated by

$$\epsilon(t) = \frac{\hat{A}(q^{-1})}{\hat{C}(q^{-1})}\tilde{\tilde{y}}(t) \tag{5.13}$$

Example 5.2

This example demonstrates that, with minimal modifications, the local sensor validation scheme can detect low frequency sensor failure in bandpass processes. The sensor output in an open loop environment is simulated as (Figures 5.25(a) and (b))

$$y(t) = G(q^{-1})\,u(t) + n(t) + f(t)$$

where $G(q^{-1})$ is a 4th order Butterworth bandpass filter with corner frequencies at 24.5 and 25.5 Hz while the input signal $u(t)$ is a zero-mean random noise with variance 2.5×10^{-3}. The output is corrupted by uncorrelated white noise $n(t)$ with variance 2.5×10^{-5} and a 10 Hz cyclic failure[16] is initiated from 25 s. The data are sampled at 100 Hz with a duration of 30 s (i.e. 3000 samples). Following a similar argument as in Equation 3.26, the lower and the upper measurement signal bandwidth are estimated to be $(\omega_s)_l = 22.64$ Hz and $(\omega_s)_u = 27.36$ Hz.

The signal ($L(q^{-1})$) and the noise ($H(q^{-1})$) filter are taken to be a pair of 4th order Butterworth bandpass and bandstop filters with cut-off frequencies at $(\omega_s)_l$ and $(\omega_s)_u$ (Figure 5.25(c)) and the additional decomposition filters $L'(q^{-1})$ and $H'(q^{-1})$ are designed as 2nd order Butterworth lowpass and highpass filters with corner frequencies at $\omega_l = 1$ Hz. To ensure stationarity and adequate filter suppression within the measurement signal bandwidth, dither is injected. $D(q^{-1})$ is a 6th order Chebyshev bandpass filter cutting off at $(\omega_s)_l$ and $(\omega_s)_u$ and $\sigma^2_{e_d}$ is 2.5×10^{-3}. During the learning stage (first 20 s), a fourth order ARMA model is fitted to the high-frequency noise-dominant component $\tilde{\tilde{y}}(t)$ and is validated for adequacy. The final estimates of the model are given by

$$\begin{aligned}
\hat{A}(q^{-1}) &= 1 - 0.0060q^{-1} + 1.76q^{-2} - 0.0099q^{-3} + 0.82q^{-4} \\
\hat{C}(q^{-1}) &= 1 - 0.0096q^{-1} + 1.13q^{-2} + 0.0064q^{-3} + 0.49q^{-4}
\end{aligned}$$

During the tracking stage, the innovation sequence is generated by Equation 5.13 (Figure 5.25(d)). The majority of the design parameters for the signal processing tools

[16]Refer to Equation 2.15 for a cyclic failure ($\vartheta_1 = 0.01$, $\vartheta_2 = 10$ and $\vartheta_3 = 0$).

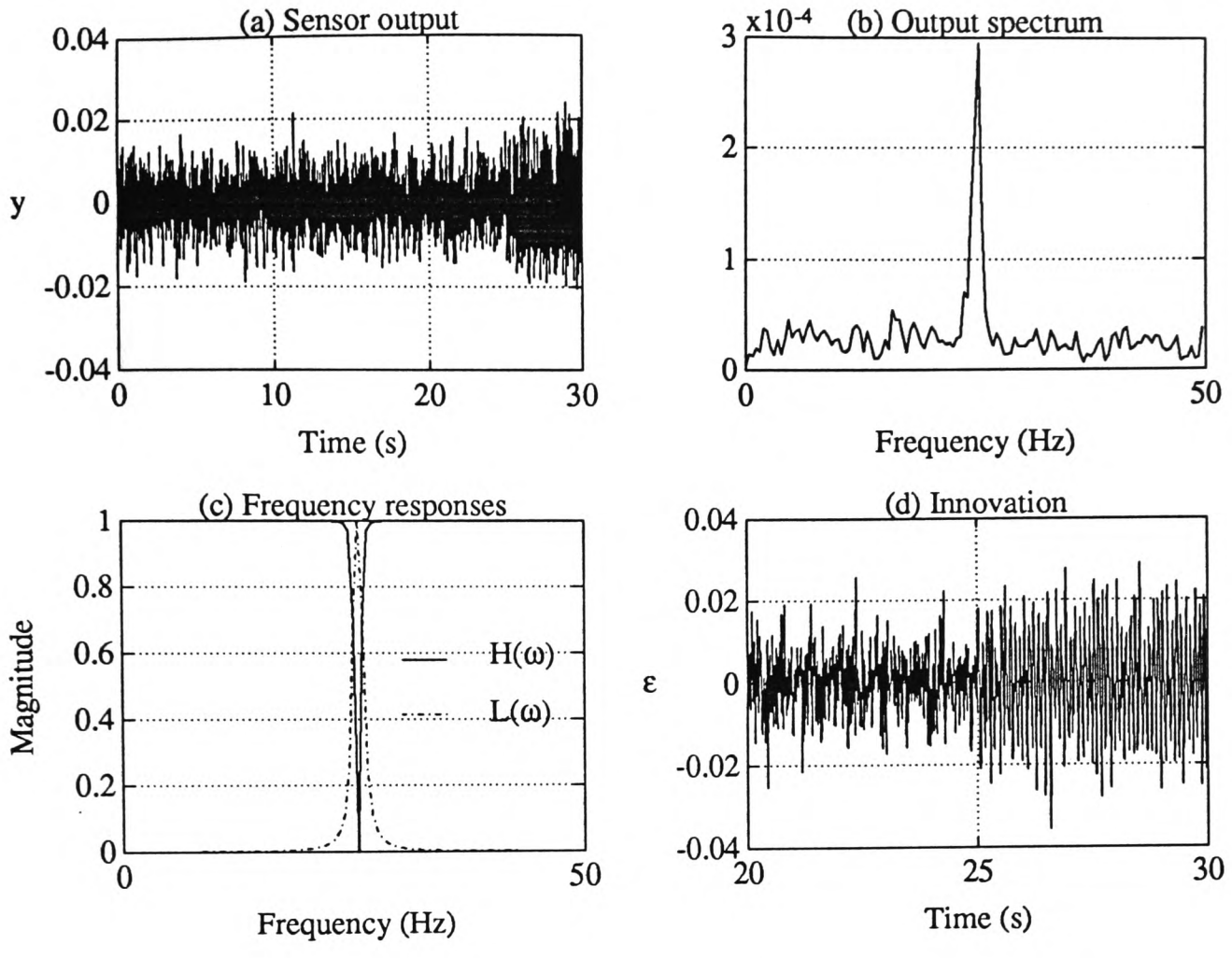

Figure 5.25: Bandpass process simulation

and the thresholds for various alarms are identical to those in Examples 4.7 and 4.8 except $\alpha_1 = 0.67$ and $\alpha_2 = 0.4$ for the output derivative, $\alpha_1 = 0.059$ and $\alpha_2 = 0.030$ for the derivative of the low-frequency noise-dominant component, $y_{min} = -1$, $y_{max} = 1$, $\dot{y}_{max} = 10$ and $\tau_d = 3$ s. The resulting failure alarm indicators are shown in Figure 5.26. The noise indicator $I_n(t)$ is triggered and the sensor output is diagnosed as 'CYCLIC' at 25.29 s with a cycling frequency at 10.16 Hz. The spectral difference $\Delta\Phi_\epsilon(\omega)$ is also depicted in Figure 5.27 in which the sinusoidal failure signature is clearly evident.

5.5 Conclusions

Armed with a sound theoretical foundation, this chapter sets out to explore various practical issues associated with the local sensor validation scheme:

- **Implementation**

  All the parameter designs, modelling techniques, signal processing algorithms and statistical tests of the local sensor validation scheme have been integrated into a single user-friendly environment. The resulting software package, named LOSVAL, is

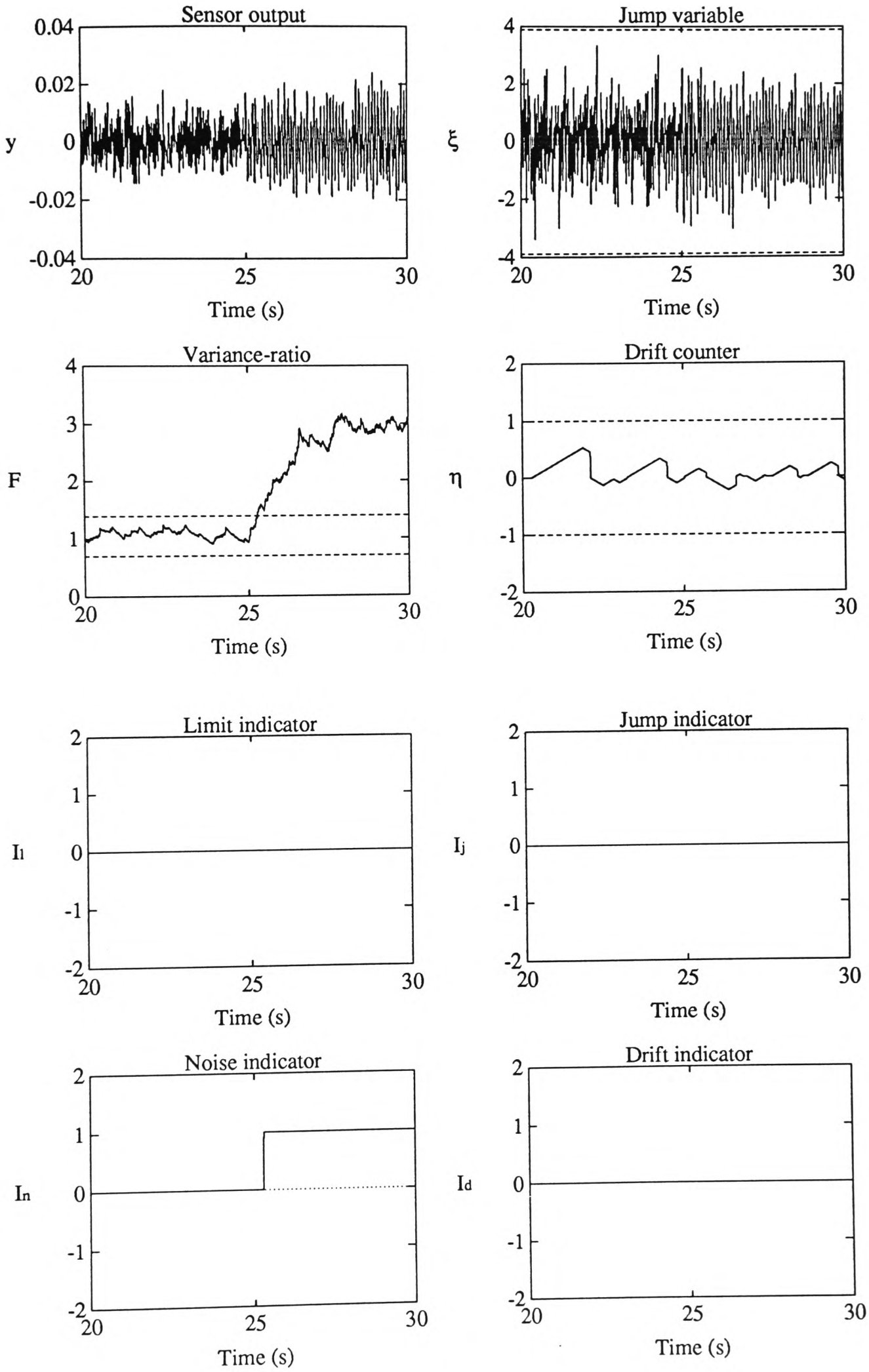

Figure 5.26: Alarm indicators in bandpass process simulation

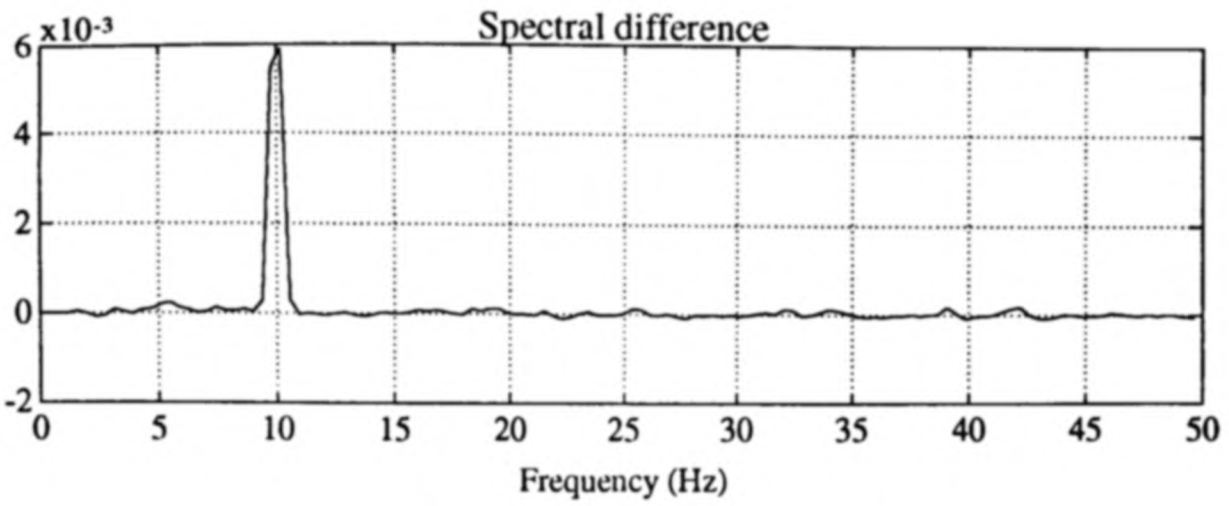

Figure 5.27: Spectral difference $\Delta\Phi_\epsilon(\omega)$ in bandpass process simulation

developed in MATLAB and can easily be ported to a variety of hardware platforms. A brief tour of the package is described, highlighting key features and utilities. LOSVAL provides a favourable tool to prototype novel ideas and to carry out extensive evaluation on both synthetic and real sensor data. As illustrated in Appendix A, the proposed sensor validation scheme requires only modest computational overhead and is therefore well tailored for implementation at the sensor end.

- **Operation**

  A bench-top thermocouple experiment has been set up as a testbed for the local sensor validation scheme. Within the practical constraints, a number of failure signal patterns are introduced and all are successfully detected and diagnosed. Every step through the commissioning, the learning and the tracking stage is documented in detail. This prescribes a model procedure on which applications on other sensors and operating environments can be based. Although not essential, a mathematical model of the thermocouple experiment is developed in Appendix B in an attempt to offer deeper background understanding and to verify some empirical findings.

- **Adaptation**

  With existing assumptions relaxed or additional constraints imposed, the validation scheme has been shown to be highly flexible in adapting to different operating conditions. Nonstationary measurement noise can be catered for by on-line tracking the reference innovation variance. An alternative, but similar, methodology for sensor signal decomposition and dither injection is put forward for bandpass measurement signals. This opens an opportunity for low frequency sensor failures beyond the measurement signal bandwidth to be detected.

Both the thermocouple experiments and the synthetic simulations substantiate the effectiveness and the efficiency of the local sensor validation scheme. Furthermore, they demonstrate that the proposed framework satisfies the characteristics of an ideal sensor validation scheme as laid down in Section 2.8: comprehensive, portable, simple, expeditious, reliable and process independent. Further experimental and field tests are most beneficial and evidence available strongly suggests that they are well worth pursuing.

Chapter 6

Conclusions and Future Research

6.1 Conclusions

Advanced alarm monitoring, adaptive control and process management systems depend heavily on the credibility of their sensor measurements. Incipient detection of sensor malfunction is of paramount importance in minimizing economic losses and in avoiding catastrophic failures. Conventional centralized failure detection techniques require precise mathematical models of the underlying process. Despite active research in the field of model uncertainty and robust detection [Chow and Willsky, 1984; Emami-Naeini *et al.*, 1988; Frank and Keller, 1980; Kosut and Walker, 1984; Wahlberg, 1990], the profound complexity of the algorithms and the demanding development costs prohibit their widespread popularity and confine their applications within safety critical systems such as the aerospace industry [Deckert *et al.*, 1977; Patton *et al.*, 1986] and the nuclear industry [El Madbouly and Frank, 1983; Kitamura and Türkcan, 1985; Ray *et al.*, 1983; Upadhyaya *et al.*, 1980]. The technological advance in smart sensors [Favennec, 1987; Howell and Hamilton, 1990] and digital Fieldbus [Jordan *et al.*, 1992; Wood, 1988] provides local sensor validation as a promising cost-effective alternative. The prime objective of this thesis is to design and evaluate a novel local sensor validation scheme, which is sufficiently simple to be implemented at the sensor level and is highly flexible to accommodate a wide variety of sensors and process conditions.

Origins of sensor failures are numerous [Lees, 1973, Table II]. With a scarcity of accessible information, it is more productive for the local validation scheme to classify sensor failures by their signal characteristics rather than by their original sources. Eight typical sensor failure modes, encompassing both 'hard' and 'soft' failures, are identified. Moreover, it is observed that measurement feedback can alter the failure signal patterns.

Their effects are studied with particular reference to the system type number and the closed loop bandwidth.

A hierarchical local sensor validation scheme is proposed which comprises three stages — the commissioning stage, the learning stage and the tracking stage. During the commissioning stage, issues relating to the acquisition, conditioning and decomposition of the sensor signal are resolved. Based on a period of failure-free observation, a simple time-series model of the decomposed sensor output is identified in the learning stage. Finally, a predominantly innovation-based method is adopted in the tracking stage to detect and diagnose any sensor aberration. Extensive guidelines are provided to facilitate the initializations of the parameters and the designs of the tuning knobs.

Measurement signal bandwidth is a vital piece of information to the validation scheme and its estimation is examined in detail. At a local level, sensor failures within the measurement signal bandwidth are fundamentally indistinguishable from legitimate changes in the measurand. Attention is therefore focused on signal characteristics beyond the bandwidth. This necessitates a relatively high sampling rate which may be incompatible with higher-level activities such as control and optimization. Decimating filter is introduced not only as a proper means of downsampling, but also as a relief to the analog anti-aliasing filter and as an enhancement in digital quantization. An expression is derived showing every four-fold increase in the initial sampling rate will effectively augment the signal resolution by an extra bit.

A pair of decomposition filters are utilized to partition the sensor outputs. The noise-dominant component is well modelled by a stochastic autoregressive moving-average process. The unknown coefficients are estimated by the Recursive Maximum Likelihood algorithm and the resulting model is validated by testing the innovations for both zero-mean and whiteness. Nonetheless, the model identification, which can be considered as a design of whitening filter, tends to counteract the signal suppression action of the decomposition filter. An innovative solution, termed dithering, is put forward. By deliberately perturbing the noise-dominant component with bandlimited random noise, stationarity is guaranteed and leakage of measurement signal is avoided.

A collection of efficient recursive signal processing algorithms is developed including mean, variance, rate of change and measure of bias. Variance and measure of bias are sensitive to both outliers and filtered spikes. Robustness is achieved through nonlinear and logical filtering. The processing techniques are employed to extract pertinent signal

properties on which statistical tests are carried out to monitor sensor anomalies. If any failure alarm indicator is triggered, a simple rule-based diagnosis will be initiated to identify the failure mode and to estimate the time and the size of failure.

The efficacy and practicality of the local sensor validation scheme are demonstrated by a bench-top thermocouple experiment. Although the process is inherently nonlinear and poses some challenging problems for conventional model-based detection, the proposed configuration is process-independent and only a representative measurement signal bandwidth is required. Various failure modes are introduced and all are successfully detected and diagnosed. Furthermore, with minimal modifications, the validation scheme can be adapted to handle nonstationary measurement noises and bandpass measurement signals. Both experimental and synthetic data analyses in this thesis are carried out in an integrated MATLAB package called LOSVAL, which provides a user-friendly environment for validating sensor signals and prototyping new algorithms.

Current commercial products on sensor failure detection only manage to cover the two extreme spectra of the market. On the lower end, straightforward alarm thresholding is becoming commonplace in modern data acquisition systems but fails to accommodate 'soft' sensor failures. On the other end, the considerable installation and maintenance cost of sophisticated centralized detection schemes restrain their applications to high-investment and safety-critical processes. The proposed local sensor validation scheme offers the market potential to bridge this enormous gap. It has the overwhelming advantage of being sensor and application independent and is therefore economical to be mass produced as 'off-the-shelf' units, either as embedded special purpose chips within smart sensors or as 'add-on' signal conditioning modules. It provides an efficient and cost-effective method to safeguard the integrity and credibility of measurement data.

6.2 Recommendations for future research

Compared with the centralized model-based techniques, the research in local sensor validation is still at its infancy. This thesis pioneers a feasibility study on local sensor validation and provides a unified framework for detecting typical classes of sensor failure signatures. Prior to being widely accepted in industry, extensive field tests on a broad range of sensors are of paramount importance. Other relevant areas of future research and their implications to the local sensor validation scheme are summarized as follows:

- An alternative philosophy to local sensor validation is to employ device-specific hardware tests on sensor internal signals for the monitoring of a set of anticipated physical failures (e.g. short and open circuit). With additional valuable information gained from the internal signals, this approach may be comparatively more precise than the device-independent validation scheme proposed in this thesis. However, such gain in precision would be at the expense of generality and flexibility. In fact, the two approaches are complementary with each other. An attempt to synthesize the validation results from the two different schemes in a consistent manner would be a fruitful exercise. An example of such an undertaking can be found in Kerr [1987], commenting on the utilization of built-in tests and the fusion of redundancy information in multisensor navigation.

- Hierarchical sensor validation demands an efficient and reliable communication interface to convey the diagnostic information (e.g. failure mode, time and size of failure) from a local to a central level. Conventional sensor interface technology is definitely inadequate and substantial research in this area is required. A prototype of a standard sensor interface is summarized in Henry and Clarke [1991].

- Once all the information are gathered at the central level, two inter-related questions would immediately arise: Is the information sufficient? How should the information be used? The latter concerns failure accommodation and is highly dependent on the redundancy structure of the underlying system and the severity of any failure detected. The integration of a local sensor validation scheme and an intelligent failure-tolerant control system [Martini *et al.*, 1987; Stengel, 1991] is well worth pursuing.

Last but not least, the potential of dithering (Section 3.11) has not yet been fully realized in this thesis. It has been demonstrated that dithering is capable of offering independent frequency weightings in time-series model estimation. Further research into its role in filter design and system identification will be most rewarding.

Appendix A

Specifications for LOSVAL

LOSVAL is an integrated environment for local sensor validation. Its salient characteristics and primary features have been covered in Section 5.2. The package is run under MATLAB with the support of the Signal Processing Toolbox, the System Identification Toolbox and the Control Systems Toolbox. It has been extensively tested on both Sun Workstations and IBM compatibles. Details of various configurations are depicted in Table A.1.

Machine	MATLAB *version*
Sun-4/SPARC	PRO-MATLAB 3.5e and 3.5i, MATLAB 4.0
Sun-3	PRO-MATLAB 3.27a and 3.5e
PC-386	386-MATLAB 3.5 and 3.5a
PC-286	PC-MATLAB 3.10

Table A.1: Environments in which LOSVAL has been tested

This appendix highlights the computational aspects of LOSVAL, both in terms of floating point operations (Appendix A.1) and a typical benchmark on processing time (Appendix A.2). Furthermore, issues on extending LOSVAL to cater for new signal acquisition boards (Appendix A.3) and new machine architectures (Appendix A.4) are addressed.

A.1 Algorithm complexity

A comprehensive itemized account of the computational workload of LOSVAL is presented in Table A.2. The unit 'FLOP' (floating point operation) is used to denote a combination of one floating point multiplication/division and one floating point addition/subtraction. The FLOP count is evaluated per iteration except for model validation. Integer operations

have been ignored and any additional requirements are highlighted in the 'comments' column.

A.2 Benchmark on computational time

The actual processing time required at various stages in LOSVAL is dictated by both the configurations of the hardware (e.g. computer host, available memory and any co-processor/accelerator installed) and the settings of the validation scheme (e.g. decomposition filter complexity and sensor model order). A particular benchmark on LOSVAL is provided to demonstrate the achievable performance. It is based on a Sun-4 SPARCstation IPC unit with 16 Mbyte of memory and running under PRO-MATLAB version 3.5e. A typical setup similar to Example 4.1 (except that the data is acquired in real-time) is employed as an illustration:

- The data are initially oversampled by a factor of 4 and then downsampled by a 14th order FIR decimating filter (i.e. $n_d = 14$).
- A pair of 2nd order lowpass and highpass Butterworth filters are chosen to be the signal and the noise filter respectively (i.e. $n_L = n_H = 2$).
- Dither is generated by a 3rd order Chebyshev lowpass filter (i.e. $n_D = 3$).
- The perturbed noise dominant component is modelled by a third order ARMA model (i.e. $na = nc = 3$) and is identified by RML.

Three different operating modes are considered:

Real-time data acquisition only involves sampling and calibrating the data and performing the necessary filtering for decimation.

ARMA model estimation encompasses data acquisition, signal decomposition, dither generation and recursive identification of the unknown parameters.

Alarm monitoring includes data acquisition, signal decomposition, dither generation, innovation construction, feature extraction by various signal processing techniques and finally failure alarm detection.

Operation	*FLOP*	*Comments*
Data acquisition		
Calibration	1	
Decimating filter	n_d	n_d is the order of the FIR decimating filter
Signal decomposition		
Signal filter	$2n_L$	n_L is the order of $L(q^{-1})$
Noise filter	$2n_H$	n_H is the order of $H(q^{-1})$
Dither generation	$2n_D$	n_D is the order of $D(q^{-1})$
Learning stage		na and nc are orders of $A(q^{-1})$ and $C(q^{-1})$
RML estimation[a]	$4l^2 + 5l + nc$	$l = na + nc$
Model validation		N is the number of innovation samples used
Zero-mean test	$2N + 3$	1 logical and 1 square-root operations
Whiteness test[b]	$\frac{1}{2}(N^2 + 3N)$	$N - 1$ logical and 1 square-root operations
Tracking stage		
Innovation generation	$na + nc$	
Feature extraction		
$\hat{\bar{\epsilon}}(t)$	2	
$\hat{\sigma}^2_{\epsilon}(t)$	9	6 logical and 1 square-root operations
$\hat{\bar{y}}(t)$	5	
$\hat{\bar{\bar{y}}}(t)$	5	
$b_{\hat{\bar{y}}}(t)$	3	1 logical comparison
Alarm indicators		
Limit	0	3 logical comparisons
Jump	1	1 logical and 1 square-root operations
Noise	1	1 logical comparison
Drift	1	4 logical comparisons

[a]Computational overheads for stability monitoring and polynomial projection are not included as these depend heavily on the locations of the roots of $\hat{C}(q^{-1}, t)$. Additional information on the workload of a spectral factorization algorithm is given in Vostrý [1975].

[b]Requires approximately $8N \log_2 N + N$ FLOP if a FFT approach is adopted via the Wiener-Khinchin Theorem [Bendat and Piersol, 1986].

Table A.2: FLOP counts in LOSVAL

Mode	*Processing time/iteration*
Real-time acquisition	0.087 s
ARMA modelling (learning stage)	0.242 s
Alarm monitoring (tracking stage)	0.141 s

Table A.3: LOSVAL's benchmark on Sun-4

The overheads of directly reading the sensor are assumed to be negligible and the average processing time per iteration in the three operating modes (with recursive alphanumeric displays) are summarized in Table A.3.

Table A.3 provides a yardstick on which the expected performance of LOSVAL in other machines can be based. To a first approximation, the computational time required in a variety of hardware platforms can be predicted by scaling the results in Table A.3 with a multiplicative factor derived from MATLAB's own comparative benchmarks (Table A.4). Furthermore, the processing time can be 'corrected' for other experimental conditions by incorporating the FLOP counts listed in Table A.2.

	Sun-4 SPARC	Sun-3	PC-286	PC-386[a]
Multiplicative factor	1	14	53	5.3

[a]With a 80387 co-processor.

Table A.4: Relative benchmark times (MATLAB bench command)

A.3 Real-time data acquisition

As described in Section 5.2.1, LOSVAL currently provides a utility to acquire data in real-time from a Metrabyte DASH–16 interfacing board [Metrabyte, 1986] residing in a PC-286 machine. The real-time mode can be enabled by editing the configuration file `conf_lsv.m` and toggling the flag `ACQ_INSTAL` to 1. LOSVAL can also be easily adapted to other data acquisition cards by modifying a single routine named `a2d`. In general, the routine `a2d` can be coded in C or Fortran and can be dynamically linked to MATLAB as a special MEX-file[1]. `a2d` should accept a single input parameter as the acquisition

[1]Consult the MATLAB manual for the required interfacing procedures.

channel number and subsequently should return the current sensor value. In addition, this arrangement provides great flexibility for LOSVAL to be interfaced with any signal generation module such as an independent simulator.

A.4 Implementation of LOSVAL to new hardware platforms

LOSVAL is specially designed to be as machine-independent as possible. On implementing LOSVAL to machines other than Sun Workstations and IBM compatibles, five hardware-related variables, `GRAPH`, `BUFFER`, `CRETURN`, `BELL` and `COMPUTER`, can be customized[2] according to the following rules:

	Yes	No
Are separate text and graphical windows available?	`GRAPH = 1`	`GRAPH = 0`
Is the text output buffered?	`BUFFER = 1`	`BUFFER = 0`
Does the routine `creturn` position cursor to the beginning of line?	`CRETURN = 1`	`CRETURN = 0`
Does the routine `bell` beep?	`BELL = 1`	`BELL = 0`
Is the MATLAB version earlier than 3.5?	`COMPUTER = 'PC'`	–

[2]By uncommenting the appropriate line in the configuration file `conf_lsv.m`.

Appendix B

A Mathematical Model of the Thermocouple Experiment

A mathematical model of the thermocouple experiment described in Section 5.3 will be derived in this appendix. The objective of the modelling exercise is to provide a deeper understanding of the process and should not be misconstrued as an essential procedure in the local sensor validation scheme. A schematic diagram outlining the heat flow in the apparatus together with a list of symbols are given in Figure B.1.

The mathematical model is derived based on the following assumptions:

1. The ambient temperature, θ_o, is assumed to be constant.

2. The water temperature, θ_w, is kept uniform within the bath by the stirrer.

3. The temperatures of the thermocouple and its sheath are identical.

4. Heat loss by the thermocouple and its sheath to the environment is negligible.

5. Heat loss due to evaporation is assumed to be proportional to the differential temperature, $\theta_w - \theta_o$, and its contribution is incorporated into the overall heat transfer coefficient U_{wo}. Other side effects such as the decrease in the mass of water and the reduction of immersed sheath area are assumed to be minimal.

6. The dynamics of the thermocouple temperature, θ_t, in response to the water temperature, θ_w, is much faster than that of θ_w itself.

7. The heat transfer coefficients, U_{wo} and U_{wt}, are independent of temperature.

An open loop transfer function between the heater output (q) and the thermocouple temperature (θ_t) will be developed (Appendix B.1). This is then followed by the inclusion of the nonlinear 'bang-bang' control of the heater which will result in two separate

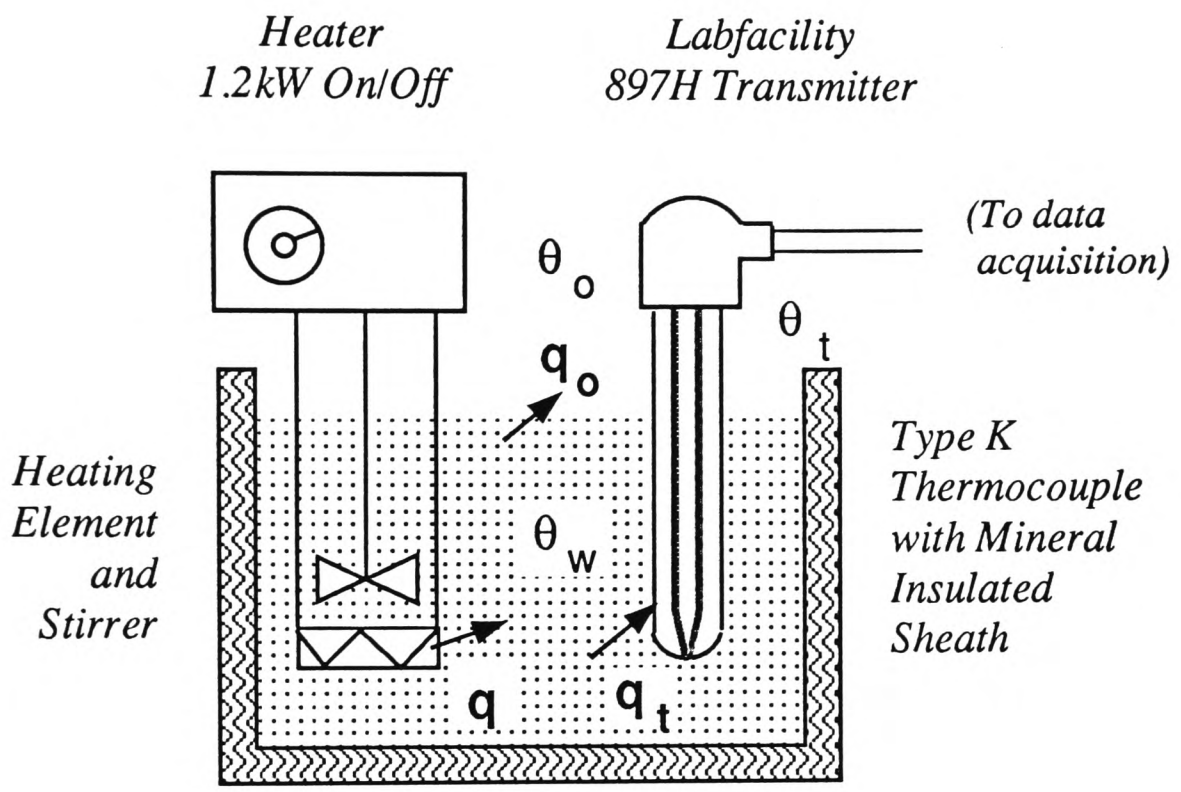

θ_w	Water temperature	q	Heat flow from heater
θ_o	Ambient temperature	q_o	Heat flow to the environment
θ_t	Thermocouple temperature	q_t	Heat flow to the thermocouple
m_w	Mass of water	m_s	Mass of the sheath
c_w	Specific heat of water	c_s	Specific heat of the sheath
U_{wo} [a]	Overall heat transfer coefficient between water and environment	U_{wt}	Overall heat transfer coefficient between water and thermocouple

[a]It includes heat loss through the water surface, the insulated walls as well as evaporation.

Figure B.1: Heat flow in the thermocouple experiment

step responses, one for the step-up and the other for the step-down (Appendix B.2). An experimental procedure to identify the dominant process bandwidth is proposed in Appendix B.3 and the measurement signal bandwidth is estimated in Appendix B.4 subject to the conditions laid down in Section 5.3.

B.1 An open loop model

Balancing the heat flow to and from the water in Figure B.1

$$q = m_w c_w \frac{d\theta_w}{dt} + q_o + q_t \tag{B.1}$$

$$m_w c_w \frac{d\theta_w}{dt} + U_{wo}(\theta_w - \theta_o) + U_{wt}(\theta_w - \theta_t) \tag{B.2}$$

Under assumption 6, the third term in Equation B.2 (q_t or $U_{wt}(\theta_w - \theta_t)$) would only contribute a transient effect to the response of θ_w. Hence, by the principle of averaging, the overall open loop model can be partitioned into two parts with distinct dynamics.

B.1.1 Model between the heater and the water temperature

By neglecting q_t and taking $\bar{\theta}_w$ $(= \theta_w - \theta_o)$ as the water temperature relative to the ambient, the slow or 'averaged' response of Equation B.2 can be written as

$$q = m_w c_w \frac{d\bar{\theta}_w}{dt} + U_{wo}\bar{\theta}_w \tag{B.3}$$

Taking the Laplace Transform, the transfer function between the heater and the water temperature is given by a first order model with time constant T_o,

$$\frac{\bar{\theta}_w(s)}{q(s)} = \frac{K_o}{1 + s T_o} \tag{B.4}$$

where

$$K_o = \frac{1}{U_{wo}} \tag{B.5}$$

$$T_o = \frac{m_w c_w}{U_{wo}} \tag{B.6}$$

B.1.2 Model between the water and the thermocouple temperature

The transient response of Equation B.2 can be obtained by balancing the heat flow to the thermocouple element

$$q_t = m_s c_s \frac{d\theta_t}{dt} = U_{wt}(\theta_w - \theta_t) \tag{B.7}$$

Once again, introducing $\bar{\theta}_t$ as the thermocouple temperature with respect to θ_o (i.e. $\bar{\theta}_t = \theta_t - \theta_o$)

$$m_s\, c_s \frac{d\bar{\theta}_t}{dt} + U_{wt}\, \bar{\theta}_t = U_{wt}\, \bar{\theta}_w \tag{B.8}$$

which, in the Laplace domain, can be represented as

$$\frac{\bar{\theta}_t(s)}{\bar{\theta}_w(s)} = \frac{1}{1 + s\, T_t} \tag{B.9}$$

where

$$T_t = \frac{m_s\, c_s}{U_{wt}} \tag{B.10}$$

B.1.3 Overall open loop model

The overall open loop model can be obtained by combining Equations B.4 and B.9

$$\bar{\theta}_t(s) = \frac{K_o}{(1 + s\, T_o)\,(1 + s\, T_t)}\, q(s) \tag{B.11}$$

Since $m_s \ll m_w$, $c_s \ll c_w$ and $U_{wt} \gg U_{wo}$, it can be deduced that $T_o \gg T_t$. To a first approximation, the open loop transfer function between the heater output and the thermocouple temperature can therefore be simplified to:

$$\bar{\theta}_t(s) \simeq \frac{K_o}{1 + s\, T_o}\, q(s) \tag{B.12}$$

B.2 A closed loop model

The mathematical model of the thermocouple experiment is completed by incorporating the 'bang-bang' control algorithm of the heater into the open loop configuration. The resulting closed loop system is illustrated in Figure B.2.

Suppose the system is initially operating at a steady state reference temperature of $\bar{\theta}_r^o$ and the heater output is 'chattering' at a mean level of q^o. The step response of the thermocouple temperature $\bar{\theta}_t$ *prior to* its settlement to the prescribed level can be examined in two separate cases:

- **Positive step change** $(\bar{\theta}_r > \bar{\theta}_r^o)$

  Since the error signal is positive $(e > 0)$, the heater is saturated at the maximum output of q^m or, equivalently, a positive step of $q^m - q^o$ is introduced.

$$\bar{\theta}_t(s) = \frac{K_o}{(1 + sT_o)(1 + s\, T_t)} \frac{q^m - q^o}{s} \tag{B.13}$$

$$\simeq \frac{K_o}{1 + s\, T_o} \frac{q^m - q^o}{s} \tag{B.14}$$

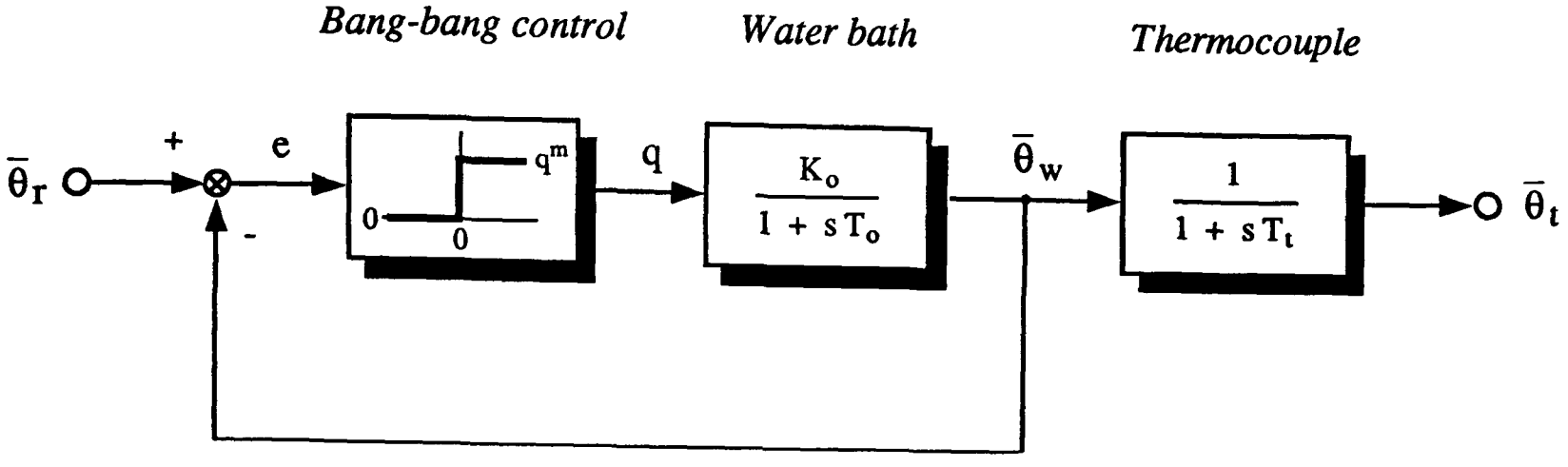

θ_r Reference temperature

$\bar{\theta}_r$ Reference temperature relative to ambient

θ_r^o Reference temperature at operating point

$\bar{\theta}_r^o$ Reference temperature at operating point relative to ambient

q^m Maximum heater output

q^o Mean heater output at operating point

e Error signal

Figure B.2: A closed loop model of the thermocouple experiment

In the time domain, the response of $\bar{\theta}_t$ is given by

$$\bar{\theta}_t(t) \simeq \bar{\theta}_r^o + (\bar{\theta}_t^m - \bar{\theta}_r^o)\left(1 - e^{-\frac{t}{T_o}}\right) \tag{B.15}$$

where $\bar{\theta}_t^m$ $(= K_o\, q^m)$ is the maximum attainable temperature relative to the ambient at full heater output and, by definition, $\bar{\theta}_r^o = K_o\, q^o$.

- **Negative step change** $(\bar{\theta}_r < \bar{\theta}_r^o)$

  With a negative error signal $(e < 0)$, the heater is off and the thermocouple temperature decays as if a negative step of q^o is initiated.

$$\bar{\theta}_t(s) = \frac{K_o}{(1 + sT_o)(1 + s\,T_t)} \frac{-q^o}{s} \tag{B.16}$$

$$\simeq \frac{K_o}{1 + s\,T_o} \frac{-q^o}{s} \tag{B.17}$$

Taking the inverse Laplace Transform, the negative step response becomes

$$\bar{\theta}_t(t) \simeq \bar{\theta}_r^o \, e^{-\frac{t}{T_o}} \tag{B.18}$$

It has to be reiterated that the trajectories given by Equations B.15 and B.18 are only applicable *before* θ_t reaches the reference temperature and both are independent of the sizes of the setpoint changes. Once θ_t arrives at the new setpoint, the heater will 'chatter' at a mean level of $\bar{\theta}_r / K_o$.

B.3 Estimation of the dominant process bandwidth

Due to the on/off control of the heater, the overall system is highly nonlinear and the responses depend heavily on the operating conditions. Nonetheless, the closed loop dynamic response can be characterized by a single time constant T_o which is related to the dominant process bandwidth ω_B by

$$\omega_B = \frac{1}{2\pi T_o} \qquad \text{(in Hz)} \tag{B.19}$$

In addition, the step responses (Equations B.15 and B.18) can be rewritten in terms of absolute temperatures as:

- **Positive step change**

$$\theta_t^m - \theta_t(t) = (\theta_t^m - \theta_r^o) \, e^{-\frac{t}{T_o}} \tag{B.20}$$

- **Negative step change**

$$\theta_t(t) - \theta_o = (\theta_r^o - \theta_o) \, e^{-\frac{t}{T_o}} \tag{B.21}$$

It then follows that after identifying the two gauging temperatures θ_t^m and θ_o, T_o can subsequently be estimated as the negative reciprocal of the slope of $\ln(\theta_t^m - \theta_t(t))$ versus t (for a positive step) or $\ln(\theta_t(t) - \theta_o)$ versus t (for a negative step).

Although the thermocouple output is not linearized in the experiment, the restricted temperature range of interest (20°C to 90 °C) assures a reasonable linearity between the measured temperature and the voltage output. The conjecture is verified in Figure B.3 by plotting some pre-amplified type K thermocouple data extracted from a standard calibration table [Labfacility, 1986]. This implies that the thermocouple voltage output can be used in place of the temperature variables in all the results derived so far.

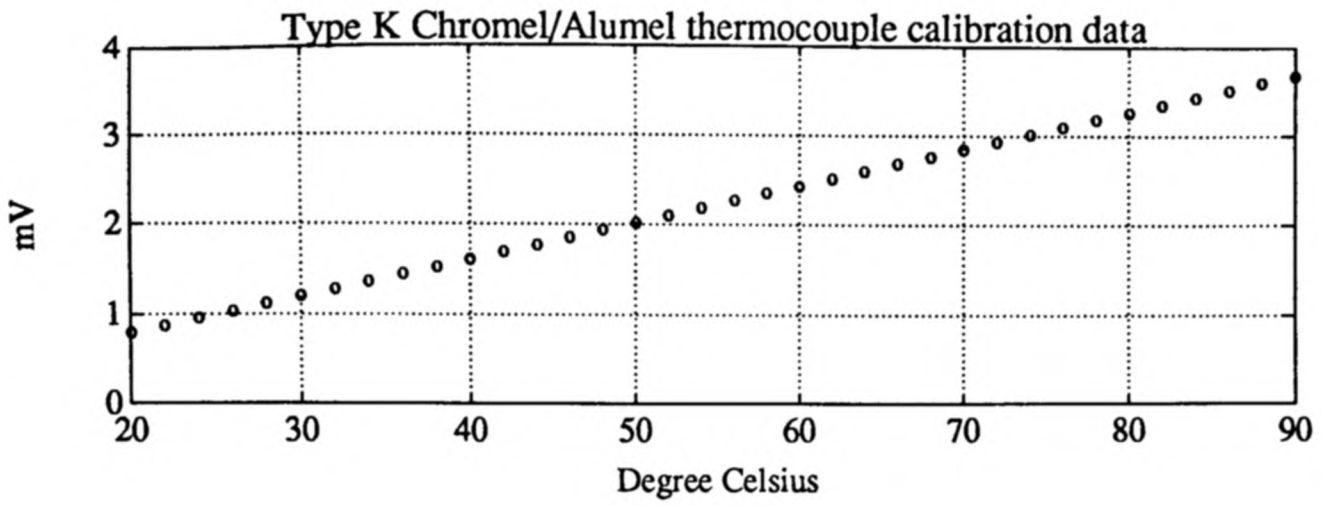

Figure B.3: Type K thermocouple calibration data

An experiment is carried out to estimate the dominant process bandwidth. By turning the heater fully on (reference temperature at 100°C), the maximum attainable temperature θ_t^m is found to be 7.1 V and by switching the heater off and allowing ample time for the water to cool, the ambient temperature θ_o is estimated to be 4.8 V. A transient step test is then conducted to estimate the time constant T_o. A positive step (59°C to 61°C) is initiated at 200 s and is followed by a negative one (61°C to 59°C) at 700 s (Figures B.4(a), (b) and (d)). Straight lines are fitted to $\ln(\theta_t^m - \theta_t(t))$ for 220 s $\leq t \leq$ 330 s (Figure B.4(c)) and $\ln(\theta_t(t) - \theta_o)$ for 740 s $\leq t \leq$ 950 s (Figure B.4(e)) by linear regression. The estimated slopes are $-5.56 \times 10^{-4}\,\mathrm{s}^{-1}$ and $-5.48 \times 10^{-4}\,\mathrm{s}^{-1}$ respectively which correspond to a mean time constant T_o of 1808 s. Substituting T_o into Equation B.19, the dominant process bandwidth ω_B of the thermocouple experiment is estimated to be 8.80×10^{-5} Hz.

B.4 Estimation of the measurement signal bandwidth

As described in Section 5.3, the operating range of the thermocouple experiment is kept between 59°C and 61°C with a maximum setpoint change $(\Delta v)_m$ of 1°C. The measurement signal bandwidth ω_s is given by Equation 3.3 in Guideline 3.1

$$\omega_s = \zeta\,\omega_B \tag{B.22}$$

where from Equation 3.27

$$\zeta = \left(\frac{5\,\mathcal{R}_s}{\omega_B^2}\right)^{\frac{1}{2(\ell+1)}} \tag{B.23}$$

and the signal-to-noise ratio is given by Equation 3.24

$$\mathcal{R}_s = \frac{\mathcal{G}_o^2\,(\Delta v)_m^2}{\sigma_n^2} \tag{B.24}$$

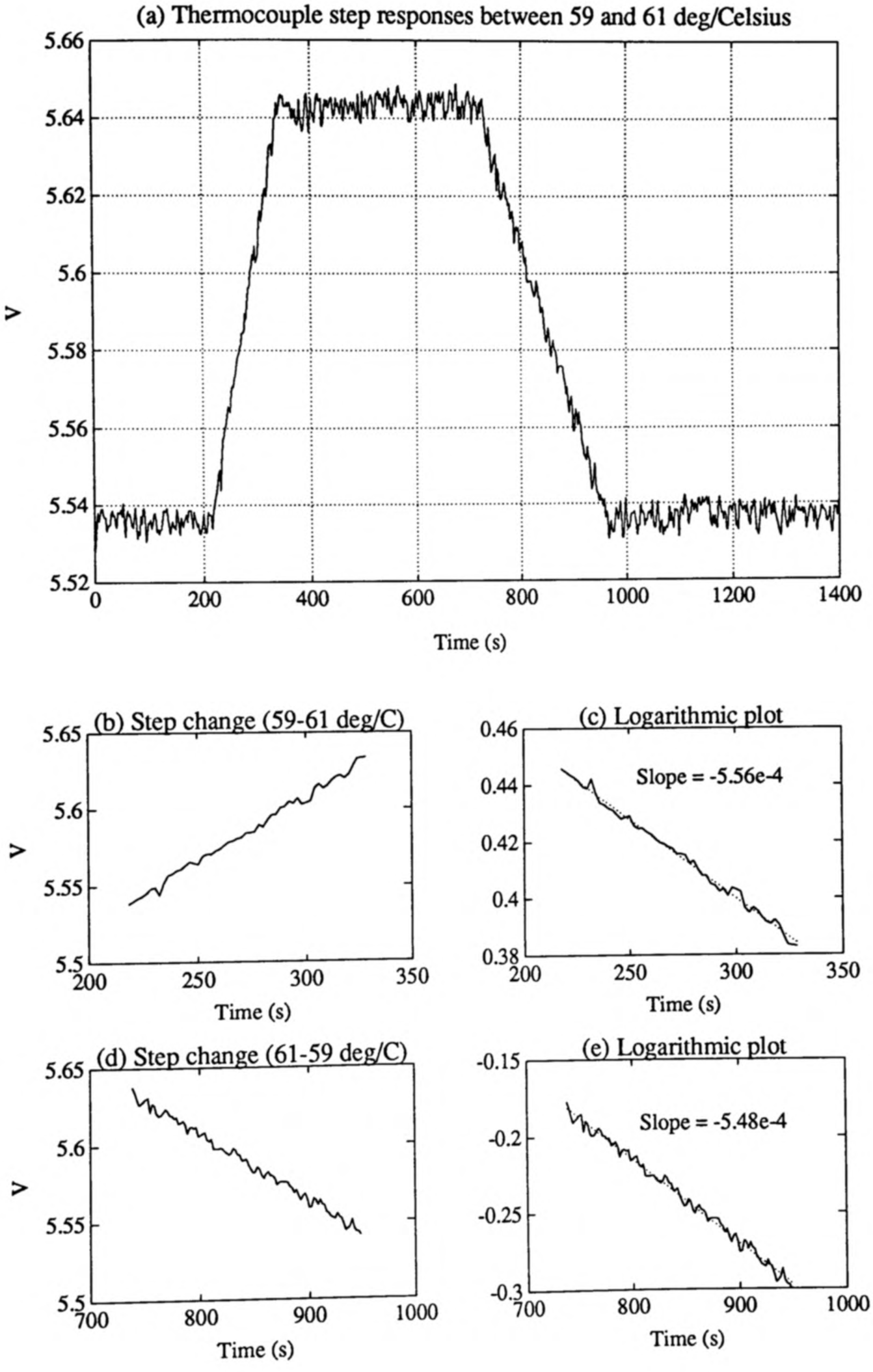

Figure B.4: Estimation of the time constant: (a) Thermocouple output, (b) Positive step change, (c) $\ln(\theta_t^m - \theta_t(t))$ vs t, (d) Negative step change, (e) $\ln(\theta_t(t) - \theta_o)$ vs t

From Figure B.4(a), the process gain $\mathcal{G}_o$ within the nominal operating range is taken to be $0.055\,\mathrm{VK}^{-1}$ and the noise variance σ_n^2 is approximated from the steady state regions to be $1.37 \times 10^{-5}\,\mathrm{V}^2$. Furthermore, the mathematical model (Equation B.12) suggests that $\ell = 1$ and the dominant process bandwidth ω_B is estimated to be $5.53 \times 10^{-4}\,\mathrm{rads}^{-1}$ (Appendix B.3). Integrating all the above information, the measurement signal bandwidth ω_s is estimated to be 0.022 Hz.

Appendix C

Nomenclature and Symbols

C.1 Abbreviations

ADC	Analog-to-digital converter
AF	Analog anti-aliasing filter
AR	Autoregressive
ARMA	Autoregressive and moving-average
DF	Digital filter
ELS	Extended Least Squares
FIR	Finite impulse response
IIR	Infinite impulse response
PID	Proportional-Integral-Derivative
Q	Quantizer
RML	Recursive Maximum Likelihood
S	Sampler
SRD	Sample rate decreaser

C.2 General nomenclature

$E[\cdot]$	Expectation operator
$\mathcal{F}\{\cdot\}$	Fourier Transform
$\mathcal{L}^{-1}\{\cdot\}$	Inverse Laplace Transform
$\Pr(\cdot)$	Probability operator
$Re[\cdot]$	Real part operator
$\text{sign}(\cdot)$	Signum operator
$\|\cdot\|_{\mathcal{D}}$	Projection into a subspace $\mathcal{D}$
$\hat{x}$	Estimate of x
$\dot{x}$	Derivative of x
$\hat{\dot{x}}$	Filtered rate of change of x
$\hat{\bar{\dot{x}}}$	Filtered rate of change of the sample mean of x
μ_x	Population mean of x
$\hat{\bar{x}}$	Sample mean of x
μ_{x^2}	Population mean square of x

$\widehat{\overline{x^2}}$	Sample mean square of x
σ_x	Standard deviation of x
σ_x^2, var(x)	Variance of x
$\hat{\sigma}_x^2$	Sample variance of x
$R_{xx}(\tau)$	Autocorrelation function of x
$\hat{R}_{xx}(\tau)$	Sample autocorrelation coefficient of x
$\hat{C}_{xx}(\tau)$	Sample autocovariance function of x
$\Phi_x(\omega)$	Spectrum of x
$\Phi_{xy}(\omega)$	Cross-spectrum between x and y
$X(s)$	Continuous-time transfer function of X
$X(q^{-1})$	Discrete-time transfer function of X
$X(j\omega)$	Continuous-time frequency response of X
$X(e^{-j\omega T_m})$	Discrete-time frequency response of X

C.3 Principal symbols

Γ	Whitening filter (Equation 3.88)
Δ	Quantization step (Equation 3.34)
	Difference operator ($\equiv 1 - q^{-1}$)
Δ_{min}	Slowest detectable drift (Guideline 4.9)
Θ	Failure signature filter (Equations 2.12 to 2.14)
Λ	Test statistics for bias and spike failure identification (Equation 4.65)
Λ_o	Threshold of Λ (Section 4.5)
$(\Phi_\epsilon(\omega))_{\text{ref}}$	Reference innovation spectrum (Section 3.12)
$\Delta\Phi_\epsilon(\omega)$	Spectral difference of innovation (Equation 4.70)
$[\Phi_s](\omega)$	Worst spectrum of measurement signal (Equation 3.2)
$[\Phi_v](\omega)$	Worst spectrum of generalized input (Section 3.3.5)
$[\Phi_v^e](\omega)$	Worst spectrum of white noise input (Equation 3.16)
$[\Phi_v^s](\omega)$	Worst spectrum of step input (Equation 3.18)
Ω	A set of discrete frequency points (Equation 4.71)
Ω'	A subset of discrete frequency points (Equation 4.72)
α	Parameter in recursive mean (Equation 4.5) and recursive variance (Equations 4.20 and 4.21) estimation
α_1, α_2	Parameters in rate of change estimation (Equation 4.29)
$\alpha(t)$	Heaviside step function (Section 2.5.1)
γ	Parameter in bias estimation (Equation 4.36)
δ_o	A small dead-band in the signum operator (Equation 4.35)
δ_f	Small threshold for stuck failure identification (Section 4.5)
$\delta(t)$	Dirac delta function (Section 2.5.1)
$\bar{\delta}(t)$	Unit impulse function (Section 3.7.3)

$\delta_x(t)$	Deviation of the signal $x(t)$ (Algorithm 4.27)
$\bar{\delta}_x(t)$	Normalized deviation of the signal $x(t)$ (Algorithm 4.28)
ϵ_Q	Quantization noise (Equation 3.6.3)
$\epsilon(t)$	Innovation sequence or a posteriori prediction error (Equation 3.76)
$\tilde{\epsilon}(t)$	A priori prediction error (Equation 3.72)
$\epsilon_f(t)$	'Failed' innovation sequence (Section 4.5)
$\hat{\bar{\epsilon}}_s$	Standardized innovation mean (Equation 3.85)
$(\bar{\epsilon})_{\text{ref}}$	Reference innovation mean (Section 3.12)
ζ	Multiplicative factor of measurement signal bandwidth (Equation 3.25)
$\eta(t)$	Drift counter (Algorithm 4.53)
$\eta'(t)$	Auxiliary drift counter (Algorithm 4.53)
$\theta(t)$	Parameter vector (Equation 3.68)
$\hat{\theta}$	Final estimate of the parameter vector (Equation 3.82)
ϑ, ϑ_1, ϑ_2, ϑ_3	Failure size parameters (Equations 2.12 to 2.16)
κ	System type number (Property 2.1)
$\lambda(t)$	Forgetting factor (Equations 3.73 and 3.74)
μ	Significance level (Equations 4.48 and 4.49)
ν_1, ν_2	Degrees of freedom in F-distribution (Equations 4.50 and 4.51)
ξ_o	Threshold of the jump variable (Equation 4.42)
$\xi(t)$	Jump variable (Equation 4.41)
$\varrho_x(t)$	Sample mean of the sign of $x(t)$ (Equation 4.36)
$(\sigma_e^2)_m$	Maximum expected variance of white noise input (Equation 3.16)
$(\sigma_\epsilon^2)_{\text{ref}}$	Reference innovation variance (Section 3.12)
$\hat{\sigma'}_\epsilon^2(t)$	Recursive reference innovation variance (Equation 5.8)
τ	Time lag in a correlation function
τ_d	Minimum drifting duration (Equation 4.58)
$v(t)$	Generalized input (Equation 2.3)
$(\Delta v)_m$	Maximum expected step change in input (Equation 3.18)
$\phi(t)$	Regressor vector (Equation 3.68)
φ	Test statistics for erratic and cyclic failure identification (Equation 4.73)
φ_o	Threshold of φ (Equation 4.74)
$\psi(t)$	Negative innovation gradient (Equations 3.73 and 3.74)
ω	Frequency
ω_B	Process bandwidth (Equation 3.10)
ω_H, ω_L	Corner frequencies of the noise and the signal filter (Section 3.7.3)
ω_N	Nyquist frequency (Equation 3.90)
ω_c	Cut-off frequency of the exponential mean filter (Equation 4.16)
ω_{c_1}, ω_{c_2}	Cut-off frequencies of the rate of change filter (Equations 4.31 and 4.32)
ω_h	High frequency reference point (Equation 3.22)
$\omega_{k_{\max}}$	Frequency at the maximum spectral difference (Section 4.5)
ω_l	Cut-off frequency of the filters for noise-dominant component (Section 5.4.2)
ω_m	Sampling frequency in rads^{-1} (Equation 3.33)

ω_o	Cut-off frequency of the derivative filter in the drift indicator (Equation 4.57)
ω_s	Measurement signal bandwidth (Equation 3.3)
$(\omega_s)_l$	Lower measurement signal bandwidth (Section 5.4.2)
$(\omega_s)_u$	Upper measurement signal bandwidth (Section 5.4.2)
$\Delta\omega$	Maximum bandwidth of a cyclic failure signal (Section 4.5)
A	Autoregressive polynomial (Equation 3.62)
$\hat{A}$	Final estimate of the autoregressive polynomial (Equation 3.88)
A_o	'True' autoregressive polynomial (Example 3.5)
C	Moving-average polynomial (Equation 3.62)
$\hat{C}$	Final estimate of the moving-average polynomial (Equation 3.88)
C_o	'True' moving-average polynomial (Section 3.9.3 and Example 3.5)
$\mathcal{C}$	Controller (Equation 2.22)
D	Dither filter (Equation 3.94)
F	Failure shaping function (Equation 2.25)
$\underline{F}_o, \overline{F}_o$	Lower and upper thresholds of the variance ratio (Equation 4.46)
$F(t)$	Variance ratio (Equation 4.45)
$\mathcal{G}$	Generalized process (Equation 2.3)
$\mathcal{G}_o$	Process gain (Equation 3.4)
G	Open loop process (Equation 2.4)
G_c	Closed loop process (Equations 2.5 and 2.24)
H	Noise filter (Equation 3.48)
H_w	Inverse Wiener filter (Equation 3.45)
$I_b(t)$	Bias indicator (Equation 4.52)
$I_d(t)$	Drift indicator (Equation 4.40)
$I_j(t)$	Jump indicator (Equation 4.42)
$I_l(t)$	Limit indicator (Equation 4.40)
$I_n(t)$	Noise indicator (Equation 4.47)
K	Gain factor
L	Signal filter (Equation 3.47)
L_w	Wiener filter (Equation 3.43)
$L(t)$	Estimator gain (Equation 3.74)
$\mathcal{M}$	Generalized noise model (Equation 2.6)
M	Noise model (Equation 2.7)
N	Noise shaping function (Equation 2.26)
	Oversampling rate for a decimating filter (Section 3.6.1)
	Number of samples in reference variance estimation (Equation 4.51)
N_{y_f}	Number of samples in the batch of 'failed' sensor output (Section 4.5)
N_{ϵ_f}	Number of samples in the batch of 'failed' innovation (Section 4.5)
$P(t)$	Covariance matrix of the estimator (Equation 3.73)
R	Input range of an ADC (Equation 3.34)
$\mathcal{R}_e$	Signal-to-noise ratio for white noise input (Equation 3.23)

$\mathcal{R}_s$	Signal-to-noise ratio for step input (Equation 3.23)
T_m	Sampling period (Guideline 3.3)
T_r	Rise time (Equation 4.59)
V	Estimation cost function (Equation 3.70)
$W(t)$	Window gap of the independent logical filter (Algorithm 4.27)
$W_\ell(t)$, $W_u(t)$	Lower warning threshold and upper failing threshold (Algorithm 4.28)
W_m, $(W_\ell)_m$, $(W_u)_m$	Lower limits of $W(t)$, $W_\ell(t)$ and $W_u(t)$ (Algorithms 4.27 and 4.28)
ΔW	Window update increment (Algorithm 4.28)
$a_1, a_2, \ldots, a_{na}$	Coefficients of the autoregressive polynomial (Equation 3.62)
b_o	Threshold of the bias indicator (Equation 4.52)
$b_x(t)$	On-line measure of bias of x (Equation 4.37)
$c_1, c_2, \ldots, c_{nc}$	Coefficients of the moving-average polynomial (Equation 3.62)
$d(t)$	Dither signal (Equation 3.94)
$e(t)$	White noise (Equation 2.6)
$\bar{e}(t)$	White noise with unit variance (Equation 2.14)
$e_d(t)$	White noise for dither generation (Equation 3.94)
f_m	Sampling frequency in Hz (Equation 3.33)
$f(t)$	Failure signal (Equation 2.11)
$f_o(t)$	Open loop failure signature (Equation 2.21)
$h_f(\cdot)$	Nonlinear failure function (Equation 2.17)
j	$\sqrt{-1}$
k	Number of bits of resolution of an ADC (Equation 3.34)
k_φ	Threshold factor of φ (Equation 4.74)
δk	Half maximum bandwidth points of a cyclic failure signal (Equation 4.74)
ℓ	Rate of roll-off at high frequencies or pole excess (Equation 3.12)
m	Effective window length of the recursive mean estimator (Equation 4.11)
m_2	The longer effective window of the derivative filter (Equation 4.66)
m_ϱ	Effective window length of the bias estimator (Equation 4.39)
$m_{\dot{\hat{y}}}$	Effective window length of the derivative filter (Equation 4.61)
n_D	Order of the dither filter (Guideline 3.6)
n_d	Order of decimating filter (Appendix A.1)
n_H, n_L	Orders of the noise and the signal filter (Section 3.7.3)
n_M	Complexity of the noise spectrum or order of the noise model (Section 3.9.4)
n_ϵ	Number of frequency points in Ω (Equation 4.71)
na, nc	Orders of the autoregressive and the moving-average polynomial (Equation 3.62)
nz, np	Number of zeros and poles in $\mathcal{G}$ (Equation 3.12)
$n(t)$	Measurement noise (Equation 2.1)
p_i	Poles of $\mathcal{G}$ (Equation 3.4)
q^{-1}	Shift operator

$r(t)$	Reference signal (Equation 2.4)
$s_{\bar{\delta}_x}(t)$	Sign of excessive deviation (Algorithm 4.28)
$s(t)$	Measurement signal (Equation 2.1)
t	Time
t'	Time from failure (Section 2.5.1)
t_f	Time of failure (Section 2.5.1)
$u(t)$	Extrageneous input to process G (Equation 2.4)
$x(t)$	An arbitrary signal (Section 4.3)
$x_f(t)$	Logical filtered signal (Algorithm 4.27)
$x_s(t)$	Sign of $x(t)$ (Equation 4.34)
y_o	Measurand (Section 2.2)
y_{min}, y_{max}	Minimum and maximum threshold of sensor output (Equation 4.40)
$\dot{y}_{max}$	Maximum threshold of the sensor output derivative (Equation 4.40)
y_{stuck}	Sensor output stuck level (Equation 2.18)
$\underline{y}_{\text{sat}}$, $\bar{y}_{\text{sat}}$	Lower and upper sensor output saturation limits (Equation 2.19)
$\underline{y}_{\text{db}}$, $\bar{y}_{\text{db}}$	Lower and upper sensor output dead-band limits (Equation 2.20)
$y(t)$	Sensor output (Equation 2.1)
$y_l(t)$	Legitimate sensor output (Equation 2.11)
$y_f(t)$	'Failed' sensor output (Section 4.5)
$\hat{\bar{y}}_1(t)$, $\hat{\bar{y}}_2(t)$	Sample means of sensor output in output derivative estimation (Equation 4.65)
$\bar{y}(t)$	Signal-dominant component (Equation 3.41)
$\tilde{y}(t)$	Noise-dominant component (Equation 3.41)
$\bar{\tilde{y}}(t)$	Low-frequency noise-dominant component (Equation 5.9)
$\tilde{\tilde{y}}(t)$	High-frequency noise-dominant component (Equation 5.10)
$\tilde{y}_p(t)$	Perturbed noise-dominant component (Equation 3.93)
z_i	Zeros of $\mathcal{G}$ (Equation 3.4)

Bibliography

[Aasnaes and Kailath, 1973] H. B. Aasnaes and T. Kailath. An innovations approach to least-squares estimation — part VII: Some applications of vector autoregressive-moving average methods. *IEEE Transactions on Automatic Control*, AC-18(6):601–607, December 1973.

[Agrawal and Shenoi, 1983] B. P. Agrawal and K. Shenoi. Design methodology for ΣΔM. *IEEE Transactions on Communications*, COM-31(3):360–369, March 1983.

[Andow, 1985] P. K. Andow. Fault diagnosis using intelligent knowledge based systems. *Chem. Eng. Res. Des.*, 63:368–372, 1985.

[Anyakora and Lees, 1972] S. N. Anyakora and F. P. Lees. Detection of instrument malfunction by the process operator. *Chemical Engineer*, (264):304–309, 1972.

[Anyakora and Lees, 1973] S. N. Anyakora and F. P. Lees. The detection of malfunction using a process control computer: Simple noise power techniques for instrument malfunction. In *IEE Conference on the Use of Digital Computers in Measurement*, pages 35–42, York, September 1973.

[Åström and Mayne, 1982] K. J. Åström and Q. Mayne. A new algorithm for recursive estimation of controlled ARMA processes. In *IFAC Identification and System Parameter Estimation*, pages 175–179, Washington, 1982.

[Åström and Wittenmark, 1984] K. J. Åström and B. Wittenmark. *Computer Controlled System: Theory and Design.* Prentice-Hall, New Jersey, 1984.

[Åström, 1969] K. J. Åström. On the choice of sampling rates in parametric identification of time series. *Information Sciences*, 1:273–278, 1969.

[Barney, 1985] G. C. Barney. *Intelligent Instrumentation: Microprocessor Applications in Measurement and Control.* Prentice-Hall, London, 1985.

[Basseville and Benveniste, 1983] M. Basseville and A. Benveniste. Design and comparative study of some sequential jump detection algorithms for digital signals. *IEEE Transactions on Acoustics, Speech, and Signal Processing*, ASSP-31(3):521–535, June 1983.

[Basseville and Benveniste, 1986] M. Basseville and A. Benveniste, editors. *Detection of Abrupt Changes in Signals and Dynamic Systems*, volume 77 of *Lecture Notes in Control and Information Sciences.* Springer-Verlag, Berlin, 1986.

[Basseville, 1988] M. Basseville. Detecting changes in signals and systems — a survey. *Automatica*, 24(3):309–326, 1988.

[Beard, 1971] R. V. Beard. Failure accommodation in linear systems through self-reorganization. Report No. MVT-71-1, Man Vechile Laboratory, Massachusetts, Cambridge, February 1971.

[Bellingham and Lees, 1977a] B. Bellingham and F. P. Lees. The detection of malfunction using a process control computer: A simple filtering technique for flow control loops. *Transactions of Institution of Chemical Engineers*, 55(1):1–16, 1977.

[Bellingham and Lees, 1977b] B. Bellingham and F. P. Lees. The detection of malfunction using a process control computer: A Kalman filtering technique for general control loops. *Transactions of Institution of Chemical Engineers*, 55(4):253–265, 1977.

[Bendat and Piersol, 1986] J. S. Bendat and A. G. Piersol. *Random Data: Analysis and Measurement Procedures.* John Wiley & Sons, New York, second edition, 1986.

[Bhattacharya, 1988] S. Bhattacharya. The intelligent instrument: Its role in factory automation. *IEE Review*, pages 203–206, May 1988.

[Bierman, 1977] G. J. Bierman. *Factorization Methods for Discrete System Estimation.* Academic Press, New York, 1977.

[Blesser and Locanthi, 1987] B. A. Blesser and B. N. Locanthi. The application of narrow-band dither operating at the Nyquist frequency in digital systems to provide improved signal-to-noise ratio over conventional dithering. *Journal of Audio Engineering Society*, 35(6):446–454, June 1987.

[Boozer and Daniel, 1972] D. D. Boozer and W. L. Daniel. On innovation testing of the Kalman filter. *IEEE Transactions on Automatic Control*, AC-17(1):158–160, February 1972.

[Box and Jenkins, 1976] G. Box and G. Jenkins. *Time Series Analysis: Forecasting and Control.* Holden-Day, San Francisco, 1976.

[Bradshaw, 1984] A. T. Bradshaw. Smart pressure transmitters. *Measurement and Control*, 17(9):353–357, October 1984.

[Bradshaw, 1989] A. T. Bradshaw. The smart approach to temperature. *Control and Instrumentation*, page 81, November 1989.

[Brignell and Dorey, 1983] J. E. Brignell and A. P. Dorey. Sensors for microprocessor-based applications. *Journal of Physics E: Scientific Instruments*, 16(10):952–958, October 1983.

[Brignell, 1986] J. E. Brignell. Sensors in distributed instrumentation systems. *Sensors and Actuators*, 10(3–4):249–261, 1986.

[Brignell, 1987] J. E. Brignell. Digital compensation of sensors. *Journal of Physics E: Scientific Instruments*, 20(9):1097–1102, September 1987.

[Brogan, 1991] W. L. Brogan. *Modern Control Theory.* Prentice-Hall, London, third edition, 1991.

[Candy and Temes, 1992] J. C. Candy and G. C. Temes, editors. *Oversampling Delta-Sigma Data Converters: Theory, Design, and Simulation.* IEEE Press, New York, 1992.

[Candy, 1986] J. V. Candy. *Signal Processing: The Model-Based Approach.* McGraw-Hill, New York, 1986.

[Candy, 1988] J. V. Candy. *Signal Processing: The Modern Approach.* McGraw-Hill, New York, 1988.

[Chandrasekaran and Punch III, 1988] B. Chandrasekaran and W. F. Punch III. Hierarchical classification: Its usefulness for diagnosis and sensor validation. *IEEE Journal on Selected Areas in Communications*, 6(5):884–891, June 1988.

[Chatfield, 1984] C. Chatfield. *The Analysis of Time Series — An Introduction.* Chapman and Hall, London, third edition, 1984.

[Chien and Adams, 1976] T. T. Chien and M. B. Adams. A sequential failure detection technique and its application. *IEEE Transactions on Automatic Control*, AC-21(5):750–757, October 1976.

[Chow and Willsky, 1984] E. Y. Chow and A. S. Willsky. Analytical redundancy and the design of robust failure detection systems. *IEEE Transactions on Automatic Control*, AC-29(7):603–614, 1984.

[Clark and Setzer, 1980] R. N. Clark and W. Setzer. Sensor fault detection in a system with random disturbances. *IEEE Transactions on Aerospace and Electronics Systems*, AES-16(4):468–473, 1980.

[Clark *et al.*, 1975] R. N. Clark, D. C. Fosth, and V. M. Walton. Detecting instrument malfunctions in control systems. *IEEE Transactions on Aerospace and Electronics Systems*, AES-11(4):465–473, July 1975.

[Clark, 1978a] R. N. Clark. Instrument fault detection. *IEEE Transactions on Aerospace and Electronics Systems*, AES-14(3):456–465, May 1978.

[Clark, 1978b] R. N. Clark. A simplified instrument failure detection scheme. *IEEE Transactions on Aerospace and Electronics Systems*, AES-14(4):558–568, 1978.

[Clarke, 1983] D. W. Clarke. PID algorithms and their computer implementation. OUEL Report 1482/83, Department of Engineering Science, University of Oxford, 1983.

[Cohn and Ott, 1971] M. Cohn and G. Ott. Design of adaptive procedures for fault detection and isolation. *IEEE Transactions on Reliability*, R-20(1):7–10, February 1971.

[Cook and Weisberg, 1982] R. D. Cook and S. Weisberg. *Residuals and Influence in Regression.* Chapman and Hall, New York, 1982.

[Corbin and Jones, 1990] M. J. Corbin and J. G. Jones. Method for monitoring faults in a computer using band-limiting filters. *IEE Proceedings, Part D*, 137(2):97–103, March 1990.

[D'Azzo and Houpis, 1966] J. J. D'Azzo and C. H. Houpis. *Feedback Control System Analysis and Synthesis.* McGraw-Hill, New York, 1966.

[de Lotto and Paglia, 1986] I. de Lotto and G. E. Paglia. Dithering improves A/D converter linearity. *IEEE Transactions on Instrumentation and Measurement*, IM-35(2):170–177, June 1986.

[Deckert *et al.*, 1977] J. C. Deckert, M. N. Desai, J. J. Deyst, and A. J. Willsky. F8-DFBW sensor failure identification using analytical redundancy. *IEEE Transactions on Automatic Control*, AC-22(5):795–803, October 1977.

[de Sá, 1988] D. de Sá. The evolution of the intelligent measurement. *Measurement and Control*, 21(5):142–144, June 1988.

[Doebelin, 1983] E. O. Doebelin. *Measurement Systems: Application and Design.* McGraw-Hill, London, third edition, 1983.

[El Madbouly and Frank, 1983] E. El Madbouly and P. M. Frank. Robust instrument failure detection via Luenberger observers in nuclear power plants. In *IFAC Symposium on Control Applications for Power System Sensitivity*, pages 1–6, Florence, 1983.

[Emami-Naeini *et al.*, 1988] A. Emami-Naeini, M. M. Akhter, and S. M. Rock. Effect of model uncertainty on failure detection: The threshold selector. *IEEE Transactions on Automatic Control*, 33(12):1106–1115, December 1988.

[Favennec, 1987] J. M. Favennec. Smart sensors in industry. *Journal of Physics E: Scientific Instruments*, 20(10):1087–1090, 1987.

[Fortescue *et al.*, 1981] T. R. Fortescue, L. S. Kershenbaum, and B. E. Ydstie. Implementation of self-tuning regulators with variable forgetting factors. *Automatica*, 17(6):831–835, 1981.

[Frank and Keller, 1980] P. M. Frank and L. Keller. Sensitivity discriminating observer for instrument failure detection. *IEEE Transactions on Aerospace and Electronics Systems*, AES-16:460–467, July 1980.

[Frank, 1990] P. M. Frank. Fault diagnosis in dynamic systems using analytical and knowledge-based redundancy — a survey and some new results. *Automatica*, 26(3):459–474, 1990.

[Franklin and Powell, 1980] G. F. Franklin and J. D. Powell. *Digital Control of Dynamic Systems.* Addison-Wesley, Massachusetts, 1980.

[Friedlander, 1982] B. Friedlander. A modified prefilter for some recursive parameter estimation algorithms. *IEEE Transactions on Automatic Control*, AC-27(1):232–235, 1982.

[Fuchs, 1987] J. J. Fuchs. On estimating the order of an ARMA processes. *Automatica*, 23(6):779–782, 1987.

[Ge and Fang, 1988] W. Ge and C.-Z. Fang. Detection of faulty components via robust observation. *International Journal of Control*, 47(2):581–599, 1988.

[Gertler and Chang, 1986] J. Gertler and H.-S. Chang. An instability indicator for expert control. *IEEE Control Systems Magazine*, pages 14–17, August 1986.

[Gertler and Luo, 1989] J. Gertler and Q. Luo. Robust isolable models for failure diagnosis. *AIChE Journal*, 35(11):1856–1868, November 1989.

[Gertler *et al.*, 1990] J. Gertler, Q. Luo, K. Anderson, and X. Fang. Diagnosis of plant failures using orthogonal parity equations. In *IFAC 11th World Congress*, volume 8, pages 62–67, Tallinn, Estonia, August 1990.

[Gertler, 1988] J. Gertler. Survey of model-based failure detection and isolation in complex plants. *IEEE Control Systems Magazine*, 8(6):3–11, December 1988.

[Goff, 1966] K. W. Goff. Dynamics in direct digital control 1: Estimation characteristics and effects of noisy signals. *ISA Journal*, pages 45–49, November 1966.

[Goodwin and Sin, 1984] G. C. Goodwin and K. S. Sin. *Adaptive Filtering, Prediction and Control.* Prentice-Hall, New Jersey, 1984.

[Graupe *et al.*, 1975] D. Graupe, D. J. Krause, and J. B. Moore. Identification of autoregressive moving-average parameters of time series. *IEEE Transactions on Automatic Control*, AC-20(1):104–107, February 1975.

[Gunnarsson, 1988] S. Gunnarsson. Frequency domain aspects of modeling and control in adaptive systems. Dissertations 194, Linköping Studies in Science and Technology, Linköping University, 1988.

[Hägglund, 1983] T. Hägglund. The problem of forgetting old data in recursive estimation. In *IFAC Adaptive Systems in Control and Signal Processing*, pages 213–214, San Francisco, 1983.

[Halme and Selkäinaho, 1984] A. Halme and J. Selkäinaho. Instrument fault detection using an adaptive filtering method. In *IFAC 9th World Congress*, volume 3, pages 167–172, Budapest, Hungary, 1984.

[Hamming, 1983] R. W. Hamming. *Digital Filters.* Prentice-Hall, New Jersey, second edition, 1983.

[Hannan *et al.*, 1985] E. J. Hannan, P. R. Krishnaiah, and M. M. Rao, editors. *Time Series in Time Domain*, volume 5 of *Handbook of Statistics*. North-Holland, Amsterdam, 1985.

[Haykin, 1986] S. Haykin. *Adaptive Filter Theory*. Prentice-Hall, New Jersey, 1986.

[Henry and Clarke, 1991] M. P. Henry and D. W. Clarke. A standard interface for self-validating sensors. In *IFAC/IMC Symposium on Fault Detection, Supervision and Safety for Technical Processes (SAFEPROCESS 91)*, pages 405–412, Baden-Baden, September 1991.

[Himmelblau, 1978] D. M. Himmelblau. *Fault Detection and Diagnosis in Chemical and Petrochemical Process*. Elsevier Scientific, Amsterdam, 1978.

[Horowitz and Hill, 1980] P. Horowitz and W. Hill. *The Art of Electronics*. Cambridge University Press, Cambridge, 1980.

[Hoskins and Himmelblau, 1988] J. C. Hoskins and D. M. Himmelblau. Artificial neural network models of knowledge representation in chemical engineering. *Computers and Chemical Engineering*, 12(9/10):881–890, 1988.

[Hoskins *et al.*, 1991] J. C. Hoskins, K. M. Kaliyur, and D. M. Himmelblau. Fault diagnosis in complex chemical plants using artificial neural networks. *AIChE Journal*, 37(1):137–141, January 1991.

[Howell and Hamilton, 1990] S. K. Howell and T. D. S. Hamilton. Intelligent instrumentation. *Measurement Science and Technology*, 1(12):1265–1273, December 1990.

[Huber, 1981] P. Huber. *Robust Statistics*. John Wiley & Sons, New York, 1981.

[IEEE, 1979] IEEE Press. *Programs for Digital Signal Processing*, 1979.

[IEEE, 1981] *IEEE Spectrum*. A special issue on "reliability". 18(10), October 1981.

[Isermann, 1984] R. Isermann. Process fault detection based on modelling and estimation methods. *Automatica*, 20(4):387–404, 1984.

[Janik and Isermann, 1990] W. Janik and R. Isermann. Signal model based grinding chatter analysis. In *IFAC 11th World Congress*, volume 1, pages 130–134, Tallinn, Estonia, August 1990.

[Janßen and Frank, 1984] K. Janßen and P. M. Frank. Component failure detection via state estimation. In *IFAC 9th World Congress*, volume 1, pages 147–152, Budapest, Hungary, 1984.

[Jones and Corbin, 1988] J. G. Jones and M. J. Corbin. Analytical redundancy using band-limiting filters. *IEE Proceedings, Part D*, 135(4):257–267, July 1988.

[Jones, 1973] H. L. Jones. *Failure Detection in Linear Systems.* PhD thesis, M.I.T., Massachusetts, Cambridge, September 1973.

[Jones, 1977] B. E. Jones. *Instrumentation, Measurement and Feedback.* McGraw-Hill, Maidenhead, 1977.

[Jordan *et al.*, 1992] J. R. Jordan, S. Lytollis, and D. W. Kent. A fibre optically extended field bus. *Measurement Science and Technology*, 3(9):902–908, September 1992.

[Jordan, 1985] G. R. Jordan. Sensor technology of the future. *Journal of Physics E: Scientific Instruments*, 18(9):729–735, September 1985.

[Juhola *et al.*, 1991] M. Juhola, J. Katajainen, and T. Raita. Comparison of algorithms for standard median filtering. *IEEE Transactions on Signal Processing*, 39(1):204–208, January 1991.

[Kailath, 1970] T. Kailath. The innovations approach to detection and estimation theory. *Proceedings of IEEE*, 58(5):680–695, May 1970.

[Kay, 1988] S. M. Kay. *Modern Spectral Estimation: Theory and Application.* Prentice-Hall, New Jersey, 1988.

[Kendall, 1976] M. G. Kendall. *Time-Series.* Charles Griffin, London, second edition, 1976.

[Kerr, 1987] T. H. Kerr. Decentralized filtering and redundancy management for multisensor navigation. *IEEE Transactions on Aerospace and Electronics Systems*, AES-23(1):83–119, January 1987.

[Kerr, 1989] T. H. Kerr. A critique of several failure detection approaches for navigation systems. *IEEE Transactions on Automatic Control*, AC-34(7):791–792, July 1989.

[King and Gilles, 1990] R. King and E. D. Gilles. Multiple filter methods for detection of hazardous states in an industrial plant. *AIChE Journal*, 36(11):1697–1706, November 1990.

[Kitamura and Türkcan, 1985] M. Kitamura and E. Türkcan. Empirical modelling approach to fault detection and identification in nuclear power plant. In *IFAC Identification and System Parameter Estimation*, pages 693–698, York, 1985.

[Koscielny, 1986] J. M. Koscielny. Aims, tasks and method of on-line diagnosis of industrial control systems. In *IFAC Workshop on Reliability of Instrumentation Systems*, pages 131–136, Hague, 1986.

[Kosut and Walker, 1984] R. L. Kosut and R. A. Walker. Robust fault detection: The effect of model error. In *Proceedings of American Control Conference*, pages 1094–1096, 1984.

[Kulhavý, 1987] R. Kulhavý. Restricted exponential forgetting in real-time identification. *Automatica*, 23(5):589–600, 1987.

[Kwon and Goodwin, 1990] O.-K. Kwon and G. C. Goodwin. A fault detection method for uncertain systems with unmodelled dynamics linearization errors and noisy inputs. In *IFAC 11th World Congress*, volume 8, pages 68–73, Tallinn, Estonia, August 1990.

[Labfacility, 1986] Labfacility Limited, Middlesex. *Temperature Sensing with Thermocouples and Resistance Thermometers*, second edition, 1986.

[Leary and Gawthrop, 1987] J. J. Leary and P. J. Gawthrop. Process fault detection using constraint suspension. *IEE Proceedings, Part D*, 134(4):264–271, July 1987.

[Lees, 1973] F. P. Lees. Some data on the failure modes of instruments in the chemical plant environment. *Chemical Engineer*, (277):418–421, 1973.

[Lees, 1983] F. P. Lees. Process computer alarm and disturbance analysis: Review of the state of the art. *Computers and Chemical Engineering*, 7(6):669–694, 1983.

[Li *et al.*, 1989] S. Li, Y. Zhu, and B. W. Dickinson. A comparison of two linear methods of estimating the parameters of ARMA models. *IEEE Transactions on Automatic Control*, 34(8):915–917, August 1989.

[Liang and Dornfeld, 1989] S. Y. Liang and D. A. Dornfeld. Tool wear detection using time series analysis of acoustic emission. *Transactions of ASME, Journal of Engineering for Industry*, 111:199–205, August 1989.

[Ljung and Söderström, 1983] L. Ljung and T. Söderström. *Theory and Practice of Recursive Identification.* MIT Press, Massachusetts, 1983.

[Ljung, 1987] L. Ljung. *System Identification: Theory for the User.* Prentice-Hall, New Jersey, 1987.

[Ljung, 1989] L. Ljung. Choices of prefilters and forgetting factors in noise-free identification. In *Proceedings of American Control Conference*, pages 1409–1415, Pittsburgh, 1989.

[Lyon, 1987] R. H. Lyon. *Machinery Noise and Diagnostics.* Butterworths, Boston, 1987.

[Marple, 1987] S. L. Marple, Jr. *Digital Spectral Analysis with Application.* Prentice-Hall, New Jersey, 1987.

[Martin and Stubberud, 1974] W. C. Martin and A. R. Stubberud. An additional requirement for innovation testing in system identification. *IEEE Transactions on Automatic Control*, AC-19(5):583–584, October 1974.

[Martin *et al.*, 1992] H. R. Martin, F. Ismail, and A. Skuta. Algorithms for statistical moment evaluation for machine health monitoring. *Mechanical Systems and Signal Processing*, 6(4):317–327, July 1992.

[Martini *et al.*, 1987] R. A. Martini, R. W. Chylla, and A. Cinar. Fault tolerant computer control of a time-delayed system: Sensor failure tolerance by controller reconfiguration. *Computers and Chemical Engineering*, 11(5):481–488, 1987.

[Massoumnia *et al.*, 1989] M.-A. Massoumnia, G. C. Verghese, and A. S. Willsky. Failure detection and identification. *IEEE Transactions on Automatic Control*, AC-34(3):316–321, March 1989.

[Massoumnia, 1986] M.-A. Massoumnia. A geometric approach to the synthesis of failure detection filters. *IEEE Transactions on Automatic Control*, AC-31(9):839–846, September 1986.

[McMichael, 1988] D. W. McMichael. *On Line Fault Detection: A System-Nonspecific Approach.* D.Phil. thesis, Department of Engineering Science, University of Oxford, 1988.

[McMichael, 1990] D. W. McMichael. Robust recursive L_p estimation. *IEE Proceedings, Part D*, 137(2):67–76, March 1990.

[Mechefske and Mathew, 1992a] C. K. Mechefske and J. Mathew. Fault detection and diagnosis in low speed rolling element bearings Part I: The use of parametric spectra. *Mechanical Systems and Signal Processing*, 6(4):297–307, July 1992.

[Mechefske and Mathew, 1992b] C. K. Mechefske and J. Mathew. Fault detection and diagnosis in low speed rolling element bearings Part II: The use of nearest neighbour classification. *Mechanical Systems and Signal Processing*, 6(4):309–316, July 1992.

[Mehra and Peschon, 1971] R. K. Mehra and J. Peschon. An innovations approach to fault detection and diagnosis. *Automatica*, 7(5):637–640, 1971.

[Merrill *et al.*, 1988] W. C. Merrill, J. C. DeLatt, and W. M. Bruton. Advanced detection, isolation, and accommodation of sensor failures — real-time evaluation. *Journal of Guidance, Control, and Dynamics*, 11(6):517–526, November–December 1988.

[Metrabyte, 1986] Metrabyte Corporation, Massachusetts. *DASH–16/16F Manual*, 1986.

[Milito *et al.*, 1973] R. Milito, C. S. Padilla, R. A. Padilla, and D. Cadorin. An innovations approach to dual control. *IEEE Transactions on Automatic Control*, AC-27(1):132–137, February 1973.

[Milne, 1987] R. Milne. Artificial intelligence for online diagnosis. *IEE Proceedings, Part D*, 134(4):238–244, July 1987.

[Min, 1989a] P. S. Min. Diagnosis of on-board sensors in internal combustion (IC) engines. In *Proceedings of American Control Conference*, pages 1065–1070, Pittsburgh, 1989.

[Min, 1989b] P. S. Min. Robust application of Beard-Jones detection filter. In *Proceedings of American Control Conference*, pages 859–864, Pittsburgh, 1989.

[Mohanty, 1987] N. C. Mohanty. *Signal Processing: Signals, Filtering, and Detection.* Van Nostrand Reinhold, New York, 1987.

[Mohtadi, 1988] C. Mohtadi. On the role of prefiltering in parameter estimation and control. In *Workshop on Adaptive Strategies for Industrial Use*, Banff, Canada, 1988.

[Mulholland and Jones, 1983] H. Mulholland and C. R. Jones. *Fundamentals of Statistics.* Butterworths, London, 1983.

[Mylroi and Calvert, 1984] M. G. Mylroi and G. Calvert. *Measurement and Instrumentation for Control.* IEE Control Engineering Series 26. Peter Peregrinus, London, 1984.

[Naidu *et al.*, 1989] S. Naidu, E. Zafiriou, and T. J. McAvoy. Application of neural networks on the detection of sensor failure during the operation of a control system. In *Proceedings of American Control Conference*, pages 1336–1341, Pittsburgh, 1989.

[Naidu *et al.*, 1990] S. Naidu, E. Zafiriou, and T. J. McAvoy. Use of neural networks for sensor failure detection in a control system. *IEEE Control Systems Magazine*, 10:49–55, April 1990.

[Ono *et al.*, 1987] T. Ono, T. Kumamaru, A. Maeda, S. Sagara, and K. Kumamaru. Influence matrix approach to fault diagnosis of parameters in dynamical systems. *IEEE Transactions on Industrial Electronics*, IE-34(2):285–291, May 1987.

[Oppenheim *et al.*, 1983] A. V. Oppenheim, A. S. Willsky, and I. T. Young. *Signals and Systems.* Prentice-Hall, London, 1983.

[Owen, 1962] D. B. Owen. *Handbook of Statistical Tables.* Addison-Wesley, Massachusetts, 1962.

[Palowitch and Kramer, 1985] B. L. Palowitch, Jr. and M. A. Kramer. The application of a knowledge-based expert system to chemical plant fault diagnosis. In *Proceedings of American Control Conference*, pages 645–651, Boston, 1985.

[Papoulis, 1984] A. Papoulis. *Probability, Random Variables, and Stochastic Processes.* McGraw-Hill, New York, second edition, 1984.

[Parr, 1986] E. A. Parr. *Transducers*, volume 1 of *Industrial Control Handbook.* Collins, London, 1986.

[Patton *et al.*, 1986] R. J. Patton, S. W. Willcox, and S. J. Winter. A parameter insensitive technique for aircraft sensor fault analysis using eigenstructure assignment and analytical redundancy. In *AIAA Conference on Guidance, Navigation and Control*, pages 165–179, Williamsburg, Virginia, August 1986.

[Patton *et al.*, 1989] R. J. Patton, P. M. Frank, and R. N. Clark, editors. *Fault Diagnosis in Dynamic Systems.* Prentice-Hall, New Jersey, 1989.

[Pau, 1981] L. F. Pau. *Failure Diagnosis and Performance Monitoring.* Marcek Derrer, New York, 1981.

[Payne, 1983] P. A. Payne. Sensors and their applications. *Journal of Physics E: Scientific Instruments*, 16(10):947–951, October 1983.

[Pehrson, 1968] B. Pehrson. A non-linear digital filter for industrial measurements. Technical Paper TP 18.185, IBM Nordic Laboratory, Systems Development Division, Lidingö, Sweden, January 1968.

[Peterka, 1981] V. Peterka. Real-time parameter estimation and output prediction for ARMA type system models. *Kybernetika*, 17(6):526–533, 1981.

[Polenta *et al.*, 1988] H. P. Polenta, A. Ray, and J. A. Bernard. Microcomputer-based fault detection using redundant sensors. *IEEE Transactions on Industrial Applications*, IA-24(5):905–912, September/October 1988.

[Power and Simpson, 1978] H. M. Power and R. J. Simpson. *Introduction to Dynamics and Control.* McGraw-Hill, London, 1978.

[Press *et al.*, 1987] W. H. Press, B. P. Flannery, S. A. Teukolsky, and W. T. Vetterling. *Numerical Recipes.* Cambridge University Press, Cambridge, 1987.

[Rangwala and Dornfeld, 1990] S. Rangwala and D. Dornfeld. Sensor integration using neural networks for intelligent tool condition monitoring. *Transactions of ASME, Journal of Engineering for Industry*, 112:219–228, August 1990.

[Raven, 1961] F. H. Raven. *Automatic Control Engineering.* McGraw-Hill, New York, 1961.

[Ray *et al.*, 1983] A. Ray, M. Desai, and J. Deyst. Fault detection and isolation in a nuclear reactor. *Journal of Energy*, 7(1):79–85, 1983.

[Robinson and Clarke, 1991] B. D. Robinson and D. W. Clarke. Robustness effects of a prefilter on Generalized Predictive Control. *IEE Proceedings, Part D*, 138(1):2–8, 1991.

[Sato *et al.*, 1977] T. Sato, K. Sasaki, and Y. Nakamura. Real-time bispectral analysis of gear noise and its application to contactless diagnosis. *Journal of Acoustic Society of America*, 62(2):382–387, August 1977.

[Scarl *et al.*, 1987] E. A. Scarl, J. R. Jamieson, and C. I. Delaune. Diagnosis and sensor validation through knowledge structure and function. *IEEE Transactions on Systems, Man, and Cybernetics*, SMC-17(3):360–368, May/June 1987.

[Schuchman, 1964] L. Schuchman. Dither signals and their effect on quantization noise. *IEEE Transactions on Communications Technology*, pages 162–165, December 1964.

[Segen and Sanderson, 1980] J. Segen and A. C. Sanderson. Detecting changes in a time-series. *IEEE Transactions on Information Theory*, IT-26(2):249–255, March 1980.

[Selkäinaho and Halme, 1987] J. Selkäinaho and A. Halme. An intelligent fault tolerant control system. In *IFAC 10th World Congress*, volume 3, pages 69–73, Munich, 1987.

[Shinners, 1978] S. M. Shinners. *Modern Control System Theory and Application.* Addison-Wesley, Massachusetts, 1978.

[Smith, 1988] C. Smith. Loss prevention through process instrumentation — the continuous thermocouple. *Measurement and Control*, 21(10):297–301, December 1988.

[Söderström and Stoica, 1989] T. Söderström and P. Stoica. *System Identification.* Prentice-Hall, London, 1989.

[Sprent, 1989] P. Sprent. *Applied Nonparametric Statistical Methods.* Chapman and Hall, London, 1989.

[Sripada and Fisher, 1987] N. R. Sripada and D. G. Fisher. Improved least squares identification. *International Journal of Control*, 46(6):1889–1913, 1987.

[Stengel, 1991] R. F. Stengel. Intelligent failure-tolerant control. *IEEE Control Systems Magazine*, 11(4):14–23, June 1991.

[Strahle, 1988] W. C. Strahle. Adaptive nonlinear filter using fractal geometry. *Electronics Letters*, 24(19):1248–1249, September 1988.

[Sydenham, 1983] P. H. Sydenham, editor. *Practical Fundamentals*, volume 2 of *Handbook of Measurement Science.* John Wiley & Sons, Chichester, 1983.

[Tiao, 1985] G. C. Tiao. Autoregressive moving average models, intervention problems and outlier detection in time series. In E. J. Hannan, P. R. Krishnaiah, and M. M. Rao, editors, *Handbook of Statistics*, volume 5, pages 85–118. North-Holland, Amsterdam, 1985.

[Tsang, 1989] T. T. C. Tsang. *The Application of Predictive Control to Flexible Robot Arms.* D.Phil. thesis, Department of Engineering Science, University of Oxford, 1989.

[Unbehauen and Göhring, 1974] H. Unbehauen and B. Göhring. Tests for determining model order in parameter estimation. *Automatica*, 10(3):233–244, May 1974.

[Upadhyaya and Kerlin, 1978] B. R. Upadhyaya and T. W. Kerlin. Estimation of response time characteristics of platinum resistance thermometers by noise analysis technique. *ISA Transactions*, 17(4):21–38, 1978.

[Upadhyaya and Kitamura, 1981] B. R. Upadhyaya and M. Kitamura. Stability monitoring of boiling water reactors by time series analysis of neutron noise. *Nuclear Science and Engineering*, 77:480–492, 1981.

[Upadhyaya and Skorska, 1982] B. R. Upadhyaya and M. Skorska. A modular approach for the diagnostic analysis of dynamic systems using stochastic time-series models. *IEEESmc*, SMC-12(6):794–804, November/December 1982.

[Upadhyaya and Skorska, 1984] B. R. Upadhyaya and M. Skorska. Sensor fault analysis using decision theory and data-driven modeling of pressurized water reactor subsystems. *Nuclear Technology*, 64(1):70–77, 1984.

[Upadhyaya *et al.*, 1980] B. R. Upadhyaya, M. Kitamura, and T. W. Kerlin. Multivariate signal analysis algorithms for process monitoring and parameter estimation in nuclear reactors. *Annals of Nuclear Energy*, 7:1–11, 1980.

[Upadhyaya, 1985] B. R. Upadhyaya. Sensor failure detection and estimation. *Nuclear Safety*, 26(1):32–43, 1985.

[Usoro *et al.*, 1985] P. B. Usoro, I. C. Schick, and S. Negahdaripour. An innovation-based methodology for HVAC system fault detection. *Transactions of ASME, Journal of Dynamical Systems, Measurement and Control*, 107(4):284–289, December 1985.

[van den Enden and Verhoeckx, 1989] A. W. M. van den Enden and N. A. M. Verhoeckx. *Discrete-Time Signal Processing.* Prentice-Hall, London, 1989.

[Vanderkooy and Lipshitz, 1987] J. Vanderkooy and S. P. Lipshitz. Dither in digital audio. *Journal of Audio Engineering Society*, 35(12):966–975, December 1987.

[Vasudeva *et al.*, 1986] K. S. Vasudeva, A. Cubukcu, K. A. Loparo, M. R. Buchner, and R. Yoel. Application of an innovative process diagnosis algorithm to tube leak detection in a heat exchanger. In *IFAC Workshop on Reliability of instrumentation systems*, pages 143–148, Hague, 1986.

[Vostrý, 1975] Z. Vostrý. New algorithm for polynomial spectral factorization with quadratic convergence 1. *Kybernetika*, 11(6):415–422, 1975.

[Wagdy, 1989] M. F. Wagdy. Effect of various dither forms on quantization errors of ideal A/D converters. *IEEE Transactions on Instrumentation and Measurement*, 38(4):850–855, August 1989.

[Wahlberg and Ljung, 1986] B. Wahlberg and L. Ljung. Design variables for bias distribution in transfer function estimation. *IEEE Transactions on Automatic Control*, AC–31(2):134–144, 1986.

[Wahlberg and Ottersten, 1986] B. Wahlberg and B. Ottersten. ARMA estimation via model reduction. In *Proceedings of American Control Conference*, pages 1260–1266, Seattle, 1986.

[Wahlberg, 1990] B. Wahlberg. Robust frequency domain fault detection/diagnosis. In *IFAC 11th World Congress*, volume 8, pages 74–79, Tallinn, USSR, 1990.

[White and Speyer, 1987] J. E. White and J. L. Speyer. Detection filter design: Spectral theory and algorithms. *IEEE Transactions on Automatic Control*, AC-32:593–603, July 1987.

[Willsky and Jones, 1976] A. S. Willsky and H. L. Jones. A generalised likelihood ratio approach to detection and estimation of jumps in linear systems. *IEEE Transactions on Automatic Control*, AC-21(1):108–112, February 1976.

[Willsky *et al.*, 1980] A. S. Willsky, E. Y. Chow, S. B. Gershwin, C. S. Greene, P. K. Houpt, and A. L. Kurkjian. Dynamic model-based techniques for the detection of incidents on freeways. *IEEE Transactions on Automatic Control*, AC-25(3):347–360, June 1980.

[Willsky, 1976] A. S. Willsky. A survey of design methods for fault detection in dynamic systems. *Automatica*, 12(6):601–611, 1976.

[Willsky, 1980] A. S. Willsky. Failure detection in dynamic systems. In *AGARD Lecture Series*, No. 109, pages 2–1–14, 1980.

[Wood, 1988] G. G. Wood. International standards emerging for Fieldbus. *Control Engineering*, 2:22–25, October 1988.

[Wünnenberg and Frank, 1990] J. Wünnenberg and P. M. Frank. Dynamic model based incipient fault detection concept for robots. In *IFAC 11th World Congress*, volume 3, pages 76–81, Tallinn, Estonia, August 1990.

[Yoshimura *et al.*, 1979] T. Yoshimura, K. Watanabe, K. Konishi, and T. Soeda. A sequential failure detection approach and the identification of failure parameters. *International Journal of Systems Science*, 10(7):827–836, 1979.

[Yung and Clarke, 1989] S. K. Yung and D. W. Clarke. Local sensor validation. *Measurement and Control*, 22(5):132–141, June 1989.